



**HAL**  
open science

# Damage-Tolerant Modal Control Methods for Flexible Structures

Helói Francico Gentil Genari

► **To cite this version:**

Helói Francico Gentil Genari. Damage-Tolerant Modal Control Methods for Flexible Structures. Automatic. Ecole nationale supérieure d'arts et métiers - ENSAM; Universidade estadual de Campinas (Brésil), 2016. English. NNT : 2016ENAM0032 . tel-01416336v2

**HAL Id: tel-01416336**

**<https://hal.science/tel-01416336v2>**

Submitted on 17 Jan 2017

**HAL** is a multi-disciplinary open access archive for the deposit and dissemination of scientific research documents, whether they are published or not. The documents may come from teaching and research institutions in France or abroad, or from public or private research centers.

L'archive ouverte pluridisciplinaire **HAL**, est destinée au dépôt et à la diffusion de documents scientifiques de niveau recherche, publiés ou non, émanant des établissements d'enseignement et de recherche français ou étrangers, des laboratoires publics ou privés.



**UNIVERSIDADE ESTADUAL DE CAMPINAS**  
Faculdade de Engenharia Mecânica

**HELÓI FRANCISCO GENTIL GENARI**

**Damage-Tolerant Modal Control Methods for  
Flexible Structures**

**Métodos de Controle Modal Tolerante a  
Danos para Estruturas Flexíveis**

CAMPINAS  
2016

**PhD THESIS** in cotutelle  
To obtain the degree of  
**Docteur de**  
**l'École Nationale Supérieure d'Arts et Métiers**  
Spécialité "Automatique"  
École doctorale n° 432 : "Sciences des Métiers de l'ingénieur"  
**and**  
**Doutor na**  
**Universidade Estadual de Campinas**  
em "Engenharia Mecânica"  
Faculdade de Engenharia Mecânica

*Presented and defended publicly by*

**Helói Francisco Gentil GENARI**

September 15th, 2016

**Damage-Tolerant Modal Control Methods for Flexible Structures**

Co-Director of thesis: **Gérard COFFIGNAL**

Co-Director of thesis: **Eurípedes Guilherme de Oliveira NÓBREGA**

Co-supervisor of the thesis: **Nazih MECHBAL**

**Jury**

**Mme Valérie BUDINGER**, Associate Professor, DCAS, ISAE SUPAERO

**M. Volnei TITA**, Associate Professor, GEA, Universidade de São Paulo

**M. José Roberto de França ARRUDA**, Professor, DMC, Universidade Estadual de Campinas

**M. Pedro Luis Dias PERES**, Professor, DSE, Universidade Estadual de Campinas

**M. Jean-Christophe PONSART**, Professor, CRAN, Université de Lorraine

**M. Eurípedes Guilherme de Oliveira NÓBREGA**, Associate Professor, DMC, UNICAMP

**M. Gérard COFFIGNAL**, Professor, PIMM, Arts et Métiers ParisTech

**M. Nazih MECHBAL**, Associate Professor, PIMM, Arts et Métiers ParisTech

Reviewer

Reviewer

President

Examiner

Examiner

Examiner

Examiner

Examiner

HELÓI FRANCISCO GENTIL GENARI

# **Damage-Tolerant Modal Control Methods for Flexible Structures**

## **Métodos de Controle Modal Tolerante a Danos para Estruturas Flexíveis**

Thesis presented to the School of Mechanical Engineering of the University of Campinas in partial fulfillment of the requirements for the degree of Doctor in Mechanical Engineering in the area of Solid Mechanics and Mechanics Design and under the joint supervision agreement signed between UNICAMP and Arts et Métiers ParisTech.

Tese de Doutorado apresentada à Faculdade de Engenharia Mecânica da Universidade Estadual de Campinas como parte dos requisitos exigidos para obtenção do título de Doutor em Engenharia Mecânica na Área de Mecânica dos Sólidos e Projeto Mecânico no âmbito do acordo de cotutela firmado entre a UNICAMP e a Arts et Métiers ParisTech.

Orientador: Prof. Dr. Eurípedes Guilherme de Oliveira Nóbrega e Prof. Dr. Nazih Mechbal  
Coorientador: Prof. Dr. Gérard Maurice Henri Coffignal

ESTE EXEMPLAR CORRESPONDE À VERSÃO FINAL DA TESE DEFENDIDA PELO ALUNO HELÓI FRANCISCO GENTIL GENARI E ORIENTADO PELO PROF. DR. EURÍPEDES GUILHERME DE OLIVEIRA NÓBREGA E PELO PROF. DR. NAZIH MECHBAL.

.....  
ASSINATURA DO ORIENTADOR

CAMPINAS  
2016

Agência(s) de fomento e nº(s) de processo(s): CNPq, 141621/2012-5; CAPES, 12337/13-7

Ficha catalográfica  
Universidade Estadual de Campinas  
Biblioteca da Área de Engenharia e Arquitetura  
Luciana Pietrosanto Milla - CRB 8/8129

G285d Genari, Helói Francisco Gentil, 1985-  
Damage-tolerant modal control methods for flexible structures / Helói Francisco Gentil Genari – Campinas, SP: [s.n.], 2016.

Orientadores: Eurípedes Guilherme de Oliveira Nóbrega e Nazih Mechbal.

Coorientador: Gérard Maurice Henri Coffignal.

Tese (doutorado) – Universidade Estadual de Campinas, Faculdade de Engenharia Mecânica.

1. Vibração - controle. 2. Controle robusto. 3. Controle H [Infinito]. 4. Danos. 5. Estruturas flexíveis. I. Nóbrega, Eurípedes Guilherme de Oliveira, 1950-. II. Mechbal, Nazih. III. Coffignal, Gérard Maurice Henri. IV. Universidade Estadual de Campinas. Faculdade de Engenharia Mecânica. V. Título.

#### Informações para Biblioteca Digital

|                                   |   |
|-----------------------------------|---|
| <b>Título em outro idioma:</b>    | Métodos de controle modal tolerante a danos para estruturas flexíveis   |
| <b>Palavras-chave em inglês:</b>  | Vibration control; robust control; adaptive control systems; damage tolerance; structural health monitoring.  |
| <b>Área de concentração:</b>      | Mecânica dos Sólidos e Projeto Mecânico   |
| <b>Titulação:</b>                 | Doutor em Engenharia Mecânica   |
| <b>Banca examinadora:</b>         | Eurípedes Guilherme de Oliveira Nóbrega [Orientador], Nazih Mechbal [Orientador], Volnei Tita, José Roberto de França Arruda, Pedro Luis Dias Peres e Valérie Budinger. |
| <b>Data da defesa:</b>            | 15/09/2016  |
| <b>Programa de Pós-Graduação:</b> | Engenharia Mecânica   |

**UNIVERSIDADE ESTADUAL DE CAMPINAS  
FACULDADE DE ENGENHARIA MECÂNICA  
COMISSÃO DE PÓS-GRADUAÇÃO EM ENGENHARIA MECÂNICA  
DEPARTAMENTO DE MECÂNICA COMPUTACIONAL  
TESE DE DOUTORADO**

**Damage-Tolerant Modal Control Methods for  
Flexible Structures**

**Métodos de Controle Modal Tolerante a  
Danos para Estruturas Flexíveis**

Autor: Helói Francisco Gentil Genari

Orientador: Prof. Dr. Eurípedes Guilherme de Oliveira Nóbrega e Prof. Dr. Nazih Mechbal

Coorientador: Prof. Dr. Gérard Maurice Henri Coffignal

A Banca Examinadora composta pelos membros abaixo aprovou esta Tese:

Profa. Dra. Valérie Budinger  
DCAS, ISAE SUPAERO, França

Prof. Dr. Volnei Tita  
GEA, EESC/USP, Brasil

Prof. Dr. José Roberto de França Arruda  
DMC, FEM/UNICAMP, Brasil

Prof. Dr. Pedro Luis Dias Peres  
DSE, FEEC/UNICAMP, Brasil

Prof. Dr. Eurípedes Guilherme de Oliveira Nóbrega  
DMC, FEM/UNICAMP, Brasil

Prof. Dr. Nazih Mechbal  
PIMM, Arts et Métiers ParisTech, França

A Ata da defesa com as respectivas assinaturas dos membros encontra-se no processo de vida acadêmica do aluno.

Campinas, 15 de Setembro de 2016.

Dedicated to my parents, José and Terezinha, my brother Diogo, and my girlfriend,  
Fabíola.

## ACKNOWLEDGEMENTS

First, I would like to express my deepest gratitude to Prof. Dr. Eurípedes Guilherme de Oliveira Nóbrega, Prof. Dr. Nazih Mechbal, and Prof. Dr. Gérard Coffignal for their great supervision, friendly guidance, and encouragement throughout this study.

I am indebted to my family and my girlfriend for their endless love, care, and encouragement.

I wish to acknowledge the Department of Computational Mechanics and School of Mechanical Engineering of UNICAMP and the Laboratory of Process and Engineering in Mechanics and Materials of Arts et Métiers ParisTech to provide an excellent infrastructure to carry out my research.

I would also like to thank Prof. Dr. José Roberto de França Arruda, Prof. Dr. André Ricardo Fioravanti, and Prof. Dra. Grace S. Deaecto for their willing help and multiple suggestions for my research.

I wish to acknowledge the Prof. Dr. José Roberto de França Arruda, Profa. Dra. Valérie Budinger, Prof. Dr. Volnei Tita, Prof. Dr. Jean-Christophe Ponsart, and Prof. Dr. Pedro Luis Dias Peres to participate of the jury.

My sincere thanks to all my friends at UNICAMP and at Arts et Métiers ParisTech for their help, understanding, and motivations throughout this work.

I wish to acknowledge CNPQ (“Bolsista CNPq - Proc. n° 141621/2012-5”) and CAPES (“Bolsista da CAPES - Proc. n° 12337/13-7”) for my national and international research scholarships.



*"Todo caminho da gente é resvaloso.  
Mas também, cair não prejudica demais  
A gente levanta, a gente sobe, a gente volta! ...  
O correr da vida embrulha tudo, a vida é assim:  
Esquenta e esfria, aperta e daí afrouxa,  
Sossega e depois desinquieta.  
O que ela quer da gente é coragem."  
(João Guimarães Rosa)*

## ABSTRACT

Smart structures have increasingly become present in different industry applications and particularly in the fields of aeronautics and civil engineering. These structures have features that allow interactions with the environment, adapting their characteristics according to the needs (stiffness, damping, viscosity, etc.), monitoring their health or controlling their vibrations. Today, smart structure active control methods do not respond appropriately to damage, despite the capability of good rejection of external disturbances. Damage-tolerant active control (DTAC) is a recent research area that aims to develop integrated approaches to reduce vibrations while monitoring the structure integrity, identifying damage occurrence, and reconfiguring the control law of the adopted active vibration control method.

This thesis contributes to the DTAC area by proposing a novel modal control framework and some application strategies. The developed methods focus on noncollocated flexible structures, where multiple piezoelectric sensors and actuators are used to attenuate damaged structure vibration. The chapters present four main topics and the conclusions. Chapter 2 reviews the regular suboptimal  $H_\infty$  problem and its respective solution based on the linear matrix inequality approach, which is a fundamental tool for the development of subsequent topics. Chapter 3 introduces the modal  $H_\infty$ -norm-based method for vibration control, which reveals high modal selectivity, allowing control energy concentration on damage effects and presenting robustness to spillover and parameter variation. A new control strategy is developed in Chapter 4, taking into account existing knowledge about the structure stressed regions with high probability of damage occurrence, leading to specific requirements in the modal  $H_\infty$ -controller design. A structural health monitoring (SHM) technique assesses each damaged mode behaviour, which is used to design a preventive controller. Chapter 5 presents a novel modal double-loop control methodology to deal with the unpredictability of damage, nevertheless ensuring a good compromise between robustness and performance to both healthy and damaged structures. For this purpose, the first-loop modal controller is designed to comply with regular requirements for the healthy structure behaviour and the second-loop controller is reconfigured aiming to ensure satisfactory performance and robustness when and if damage occurs, based on a state observer and an SHM technique to adapt the controller online. In all these chapters, simulated (analytical- and finite-element-based) and/or experimental smart structures are used to examine the proposed methodology under the respective control strategies. The last chapter summarises

the achieved results for each different approach described in the previous chapters.

**Keywords:** Vibration control; robust control; adaptive control systems; damage tolerance; structural health monitoring.

## RESUMO

Estruturas inteligentes estão cada vez mais presentes em diferentes aplicações na indústria, em particular nas áreas de aeronáutica e engenharia civil. Essas estruturas possuem características que permitem interações com o ambiente, adaptando suas propriedades de acordo com as necessidades (rigidez, amortecimento, viscosidade, etc.), monitorando a própria integridade estrutural (SHM, de *Structural Health Monitoring*) ou controlando suas vibrações. Atualmente, os métodos ativos para controle de vibrações não respondem adequadamente a mudanças na dinâmica estrutural causada por dano, apesar da boa capacidade de rejeição a perturbações externas. O controle ativo tolerante a danos (DTAC, de *Damage-Tolerant Active Control*) é uma área recente de pesquisa que objetiva desenvolver métodos integrados para reduzir vibrações e, ao mesmo tempo, monitorar a integridade estrutural, sendo possível identificar a ocorrência de danos e, com isso, reconfigurar o controlador ativo de vibrações.

Esta tese contribui com a área de DTAC propondo uma nova abordagem de controle modal e algumas estratégias de aplicações. Os métodos propostos focam no controle de vibrações de estruturas flexíveis sujeitas a danos com múltiplos sensores e atuadores não colocados. Os capítulos apresentam quatro temas principais e as conclusões. O Capítulo 2 revisa o problema subótimo  $H_\infty$  e sua respectiva solução por meio da abordagem por desigualdades matriciais lineares, que é uma ferramenta fundamental para o desenvolvimento dos tópicos subsequentes. O Capítulo 3 introduz o método de controle modal de vibrações baseado na norma  $H_\infty$  modal, a qual revela elevada seletividade modal, permitindo a concentração de energia de controle sobre os efeitos do dano e apresentando robustez em relação ao *spillover* e à variação paramétrica. Uma nova estratégia de controle é desenvolvida no Capítulo 4, tendo em conta o conhecimento existente sobre as regiões da estrutura com alta probabilidade de sofrer danos, o que leva a requisitos específicos no projeto do controlador  $H_\infty$  modal. Uma técnica de SHM é usada para avaliar o efeito do dano em cada modo, dado que é usado para projetar um controlador preventivo. O Capítulo 5 apresenta uma metodologia modal de dupla malha que lida com a imprevisibilidade do dano, garantindo um bom compromisso entre robustez e desempenho para a estrutura saudável ou danificada. Para atingir esse objetivo, o controlador modal da primeira malha é projetado para atender os requisitos de desempenho para a estrutura íntegra. O controlador da segunda malha é reconfigurado objetivando assegurar robustez e um desempenho satisfatório quando, ou se, um dano ocorre. Essa lei de controle é baseada em um observador

de estados e em um algoritmo de SHM para reconfigurar o controlador *online*. Todas as técnicas propostas são testadas utilizando estruturas inteligentes criadas a partir de simulações (analíticas e de elementos finitos) e/ou experimentos. O último capítulo discute os principais resultados obtidos para cada abordagem descrita nos capítulos anteriores.

**Palavras-chave:** Vibração - controle; controle robusto; controle H [Infinito]; danos; estruturas flexíveis.

## RÉSUMÉ

Les structures intelligentes sont de plus en plus présentes dans différentes industries et notamment dans les domaines de l'aéronautique et du génie civil. Ces structures sont dotées de fonctions qui leur permettent d'interagir avec leur environnement, d'adapter leurs caractéristiques structurelles (raideur, amortissement, viscosité, etc.) selon les besoins ou de surveiller leur état de santé ou SHM (Structural Health Monitoring). Aujourd'hui, les performances des méthodes de contrôle actif peuvent être considérablement dégradées lors de l'apparition d'endommagement. Le contrôle actif tolérant aux dommages ou DTAC (Damage-Tolerant Active Control) est un champ de recherche récent qui s'intéresse à l'élaboration d'approches intégrées pour réduire les vibrations tout en surveillant l'intégrité de la structure, en identifiant les éventuels dommages, et en reconfigurant la loi de commande.

Cette thèse apporte une contribution au DTAC en proposant une approche originale basée sur la norme  $H_\infty$  modale. Les méthodes proposées se focalisent principalement sur le cas où plusieurs actionneurs et capteurs piézoélectriques non-collocalisés sont utilisés pour atténuer les vibrations des structures endommagées. Le manuscrit comprend quatre parties principales. Le chapitre 2 présente des rappels sur la commande  $H_\infty$  et sur sa solution sous optimale obtenue par une approche par inégalité matricielle linéaire, sur laquelle s'appuient les développements proposés dans ce travail. Le chapitre 3 décrit la norme  $H_\infty$  modale introduite pour le contrôle actif des vibrations. Cette commande présente une sélectivité modale élevée, permettant ainsi de se concentrer sur les effets du dommage tout en bénéficiant des propriétés de robustesse qu'offre la commande  $H_\infty$  vis-à-vis du spillover et des variations de paramètres. Une nouvelle stratégie de rejet des vibrations est proposée au chapitre 4. C'est une approche dite préventive où une prise en compte lors de l'élaboration de la commande  $H_\infty$  modale, des zones fortement contraintes de la structure, où le risque d'endommagement est élevé est réalisée. Un algorithme SHM est proposé afin d'évaluer la sévérité du dommage pour chaque mode. Le chapitre 5 propose une nouvelle approche modale à double boucle de commande pour faire face à des endommagements imprévisibles. Un premier correcteur est conçu dans ce but pour satisfaire les contraintes de performance et de robustesse sur la structure saine, tandis que le second a pour objectif de conserver un contrôle satisfaisant quand un dommage survient. La loi de commande s'appuie sur un observateur d'état et d'un algorithme SHM pour reconfigurer en ligne le correcteur. Toutes les approches DTAC proposées sont testées en utilisant des simulations

(analytiques et éléments finis) et/ou des expérimentations sur des structures intelligentes.

**Mots clés:** Contrôle actif tolérant au dommage; contrôle actif des vibrations; contrôle santé des structures; commande modal  $H_\infty$ ; robustesse.

## LIST OF FIGURES

|      |  |    |
|------|--|----|
| 2.1  | Block diagram of the $H_\infty$ control problem. . . . .   | 46 |
| 2.2  | Block diagram of the regular $H_\infty$ control problem. . . . .   | 51 |
| 2.3  | Experiment setup. . . . .  | 53 |
| 2.4  | Kanai-Tajimi spectra for three different earthquakes. . . . .  | 54 |
| 2.5  | Experimental signals used for system identification. . . . .   | 55 |
| 2.6  | Identified model. . . . .  | 56 |
| 2.7  | Frequency response comparison between the open-loop and the closed-loop systems. . . . .   | 56 |
| 2.8  | Signals used to analyse the controller performance. . . . .  | 57 |
| 2.9  | Frequency response of filter $F_u(s)$ . . . . .  | 58 |
| 2.10 | Frequency response comparison between open-loop and closed-loop systems. . . . .   | 58 |
| 2.11 | Simulated response when the disturbance is a chirp signal. . . . .   | 59 |
| 2.12 | Simulated response when the structure is excited in its natural frequency. . . . .   | 59 |
| 2.13 | Experimental response when the disturbance is a chirp signal. . . . .  | 60 |
| 2.14 | Experimental response when the structure is excited in its natural frequency. . . . .  | 60 |
|      |  |    |
| 3.1  | Block diagram of the modal $H_\infty$ control problem. . . . .   | 69 |
| 3.2  | Simulated structure. . . . .   | 70 |
| 3.3  | Simulated results of the healthy structure. . . . .  | 72 |
| 3.4  | Performance comparison between open loop (black line with points), RC (red solid line), and MC (blue dotted line) for the simulated structure. . . . . | 72 |
| 3.5  | Control signal comparison between RC (red solid line) and MC (blue dotted line) for the simulated structure. . . . .                                   | 73 |
| 3.6  | Experiment setup. . . . .  | 73 |
| 3.7  | Experimental and identified $P_{yu}$ and $P_{yw}$ . . . . .  | 75 |
| 3.8  | Transfer function comparison between full and reduced models. . . . .  | 75 |
| 3.9  | Healthy beam simulated signals. . . . .  | 76 |
| 3.10 | Frequency response comparison between healthy and damaged structures. . . . .  | 77 |
| 3.11 | Experimental output signals. . . . .   | 78 |
| 3.12 | Experimental control signals. . . . .  | 78 |
|      |  |    |
| 4.1  | Adopted DTAC strategy. . . . .   | 81 |



|      |   |     |
|------|---|-----|
| 4.2  | $T_{z,w}$ attenuation and peak values. . . . .  | 83  |
| 4.3  | Adopted aluminium structure with active elements. . . . .   | 86  |
| 4.4  | Detail A of Fig. 4.3(b): configuration of each couple of piezoceramic elements. . .   | 87  |
| 4.5  | Detail B of Fig. 4.3(b): modification of the boundary conditions to simulate a damage that models a crack of length $h$ . . . . . | 87  |
| 4.6  | Mode shapes of the nominal model. . . . .   | 87  |
| 4.7  | Transfer function comparison between complete and nominal models. . . . .   | 88  |
| 4.8  | Frequency response comparison between the healthy and the damaged structure (Damage 3). . . . .                                   | 89  |
| 4.9  | Modal distance estimation. . . . .  | 89  |
| 4.10 | Frequency response comparison between the uncontrolled and the controlled healthy structure. . . . .                              | 91  |
| 4.11 | Performance comparison between the uncontrolled and the controlled healthy structure. . . . .                                     | 91  |
| 4.12 | Control signal comparison between the MC and the RC in the healthy structure. . .   | 92  |
| 4.13 | Performance comparison of the controlled structure subjected to damage. . . . .   | 93  |
| 4.14 | Control signal comparison of the controlled structure subjected to damage. . . . .  | 94  |
| 5.1  | Single loop. . . . .  | 98  |
| 5.2  | Double loop. . . . .  | 98  |
| 5.3  | FTC framework. . . . .  | 99  |
| 5.4  | Proposed DTAC framework. . . . .  | 100 |
| 5.5  | Detailed block diagram of the proposed DTAC framework. . . . .  | 101 |
| 5.6  | Frequency response comparison between the uncontrolled and the controlled healthy structure. . . . .                              | 110 |
| 5.7  | Performance comparison between the uncontrolled and the controlled healthy structure. . . . .                                     | 110 |
| 5.8  | Control signal comparison between the MC and the RC in the healthy structure. . .   | 111 |
| 5.9  | Modal peak performance comparison of the controlled structure submitted to damage. .  | 113 |
| 5.10 | Control signal components of the MDLF. . . . .  | 114 |
| 5.11 | Adaptive gains of the damage compensator. . . . .   | 115 |
| A.1  | The angle between one-dimensional subspaces $S_1, S_2 \in \mathbb{R}^3$ . . . . .   | 133 |
| A.2  | Principal angles between two-dimensional subspaces $S_1, S_2 \in \mathbb{R}^3$ . . . . .  | 134 |

|      |  |     |
|------|--|-----|
| A.1  | Example of an active structure modelled with PLQP (DKT element, coarse mesh, $Z1$ area without piezoelectric pair, $Z2$ contains six areas with a piezoceramic pair (either an actuator or a sensor)). . . . . | 148 |
| A.2  | Configuration of each couple of piezoelectric layers (cross-section). . . . .  | 148 |
| B.1  | Dispositif expérimental. . . . .   | 162 |
| B.2  | Amplitudes expérimentales maximales de vibration de chaque mode. . . . .   | 163 |
| B.3  | Signaux de commande expérimentaux pour les structures saine et endommagée. . . . .   | 163 |
| B.4  | Atténuation de $T_{z,w}$ et les amplitudes de crête respectives. . . . .   | 165 |
| B.5  | Structure en aluminium possédant des éléments actifs, modélisée par éléments finis et maillée avec des éléments plaque triangulaires (éléments DKT) . . . . .  | 167 |
| B.6  | Distances modales en fonction du dommage. . . . .  | 167 |
| B.7  | Structure soumise au dommage 3: comparaison des réponses. . . . .  | 168 |
| B.8  | Comparaison de signaux de commande. . . . .  | 168 |
| B.9  | Le bloc-diagramme détaillé du système de DTAC. . . . .   | 170 |
| B.10 | Comparaison des amplitudes maximales des modes de la structure contrôlée. . . . .  | 175 |

## LIST OF TABLES

|     |  |     |
|-----|--|-----|
| 2.1 | Parameters to simulate the Kanai-Tajimi spectra. . . . .                                       | 54  |
| 4.1 | Structure mechanical properties. . . . .   | 87  |
| 4.2 | Mechanical and electrical properties of the piezoelectric elements (NOLIAC <sup>®</sup> ). . . | 87  |
| 4.3 | First natural frequencies of the healthy structure. . . . .                                    | 88  |
| 4.4 | Parameters of the weighing filters. . . . .  | 90  |
| 4.5 | Healthy beam modal responses with the regular controller. . . . .                              | 90  |
| 5.1 | Parameters of the bandpass filters. . . . .  | 111 |

## LIST OF ALGORITHMS

|     |  |     |
|-----|--|-----|
| 4.1 | Damage-tolerant controller design. . . . . | 84  |
| 5.1 | Nominal controller design. . . . .         | 108 |
| 5.2 | Damage compensator design. . . . .         | 108 |

## LIST OF ABBREVIATIONS AND ACRONYMS

|         |  |
|---------|--|
| AMD     | Active Mass Driver   |
| ATAC    | Adaptive Tolerant Active Control                                 |
| AVC     | Active Vibration Control   |
| DC      | Direct Current   |
| DMC     | Department of Computational Mechanics                            |
| DOF     | Degree Of Freedom  |
| DTAC    | Damage-Tolerant Active Control                                   |
| EDAC    | Evolving Damage Active Control                                   |
| EFR     | Experimental Frequency Response                                  |
| ENSAM   | École Nationale Supérieure d'Arts et Métiers                     |
| FDI     | Fault Detection and Isolation                                    |
| FE      | Finite Element   |
| FEM     | School of Mechanical Engineering                                 |
| FTC     | Fault-Tolerant Control   |
| IMSC    | Independent Modal Space Control                                  |
| LMI     | Linear Matrix Inequality   |
| MC      | Modal $H_\infty$ Controller                                      |
| MDLF    | Modal Double-Loop Framework                                      |
| MIMO    | Multiple-Input and Multiple-Output                               |
| PAC     | Preventive Active Control  |
| PIMM    | Laboratory of Process and Engineering in Mechanics and Materials |
| PWM     | Pulse-Width Modulation   |
| PZT     | Lead Zirconate Titanate  |
| RC      | Regular $H_\infty$ Controller                                    |
| SHM     | Structural Health Monitoring                                     |
| STAC    | Strictly Tolerant Active Control                                 |
| UNICAMP | University of Campinas   |

## LIST OF SYMBOLS

|                    |  |
|--------------------|--|
| $\mathbf{A}^T$     | transpose of matrix $\mathbf{A}$                   |
| $\mathbf{A}^*$     | complex conjugate transpose of matrix $\mathbf{A}$ |
| $t$                | time   |
| $\mathbf{w}(t)$    | disturbances                                       |
| $\mathbf{u}(t)$    | control signals                                    |
| $\mathbf{y}(t)$    | measured outputs                                   |
| $\mathbf{p}(t)$    | nodal displacements                                |
| $\mathbf{M}$       | mass matrix  |
| $\mathbf{D}$       | damping matrix                                     |
| $\mathbf{K}$       | stiffness matrix                                   |
| $\mathbf{B}_w$     | input matrix relative to $\mathbf{w}(t)$           |
| $\mathbf{B}_u$     | input matrix relative to $\mathbf{u}(t)$           |
| $\mathbf{C}_d$     | output matrix relative to $\mathbf{p}(t)$          |
| $\mathbf{C}_v$     | output matrix relative to $\dot{\mathbf{p}}(t)$    |
| $\mathbf{C}_w$     | output matrix relative to $\mathbf{w}(t)$          |
| $\mathbf{C}_u$     | output matrix relative to $\mathbf{u}(t)$          |
| $m$                | number of modes                                    |
| $\Phi$             | modal matrix                                       |
| $\mathbf{q}(t)$    | modal displacements                                |
| $\mathbf{M}_m$     | modal mass matrix                                  |
| $\mathbf{D}_m$     | modal damping matrix                               |
| $\mathbf{K}_m$     | modal stiffness matrix                             |
| $\mathbf{C}_{d_m}$ | modal displacement output matrix                   |
| $\mathbf{C}_{v_m}$ | modal velocity output matrix                       |
| $\Omega$           | matrix of natural frequencies                      |
| $\mathbf{Z}$       | matrix of modal damping coefficients               |
| $\mathbf{x}(t)$    | state vector                                       |
| $\mathbf{A}$       | modal dynamic matrix                               |

|  |  |
|--|--|
| $\mathbf{B}_1$   | matrix of disturbance inputs   |
| $\mathbf{B}_2$   | matrix of control inputs   |
| $\mathbf{C}_1$   | matrix of performance outputs  |
| $\mathbf{C}_2$   | matrix of measured outputs   |
| $\mathbf{D}_{11}, \mathbf{D}_{12}, \mathbf{D}_{21}, \mathbf{D}_{22}$ | direct transmission matrices   |
| $s$  | Laplace variable   |
| $\zeta(s)$   | Laplace transform of $\zeta(t)$  |
| $\mathbf{P}(s)$  | plant transfer matrix  |
| $\mathbf{K}(s)$  | controller transfer matrix   |
| $\mathbf{P}_{zw}(s)$   | transfer function matrix between $\mathbf{Z}(s)$ and $\mathbf{W}(s)$             |
| $\mathbf{P}_{zu}(s)$   | transfer function matrix between $\mathbf{Z}(s)$ and $\mathbf{U}(s)$             |
| $\mathbf{P}_{yw}(s)$   | transfer function matrix between $\mathbf{Y}(s)$ and $\mathbf{W}(s)$             |
| $\mathbf{P}_{yu}(s)$   | transfer matrix between $\mathbf{Y}(s)$ and $\mathbf{U}(s)$                      |
| $\mathbf{x}_c(t)$  | controller state vector  |
| $\mathbf{A}_c$   | controller dynamic matrix  |
| $\mathbf{B}_c$   | controller input matrix  |
| $\mathbf{C}_c$   | controller output matrix   |
| $\mathbf{D}_c$   | controller direct transmission matrix  |
| $\mathbf{T}_{uw}(s)$   | closed-loop transfer function matrix between $\mathbf{U}(s)$ and $\mathbf{W}(s)$ |
| $\mathbf{T}_{zw}(s)$   | closed-loop transfer function matrix between $\mathbf{Z}(s)$ and $\mathbf{W}(s)$ |
| $\ \cdot\ _\infty$   | infinity norm  |
| $\tilde{\mathbf{A}}$   | closed-loop dynamic matrix   |
| $\tilde{\mathbf{B}}$   | closed-loop input matrix   |
| $\tilde{\mathbf{C}}$   | closed-loop output matrix  |
| $\tilde{\mathbf{D}}$   | closed-loop direct transmission matrix   |
| $\mathbf{F}_u$   | weighing filter applied to $\mathbf{u}(t)$                                       |
| $\mathbf{F}_z$   | weighing filter applied to $\mathbf{z}(t)$                                       |
| $\omega_c$   | transition frequency between rejection band and passband                         |
| $k$  | filter order   |
| $M$  | gain at passband   |

|  |  |      |
|--|--|------|
| $\varepsilon$  | gain at rejection band   |      |
| $\mathbf{z}_u(t)$                                    | output of filter $\mathbf{F}_u$  |      |
| $\bar{\mathbf{z}}(t)$                                | output of filter $\mathbf{F}_z$  |      |
| $\mathbf{G}_n(s)$                                    | transfer function matrix of the nominal plant                                      |      |
| $\mathbf{G}_g(s)$                                    | transfer function matrix of the generalised plant                                  |      |
| $m_i$  | mass $i$   | kg   |
| $N_{sp}(s)$  | Kanai-Tajimi spectrum  |      |
| $\tilde{\mathbf{W}}_i(s)$                            | band $i$ disturbances in the frequency domain                                      |      |
| $\tilde{\mathbf{w}}_i(t)$                            | band $i$ disturbances in the time domain   |      |
| $\tilde{\mathbf{Y}}_i(s)$                            | responses in the frequency domain of band $i$                                      |      |
| $\tilde{\mathbf{y}}_i(t)$                            | responses in the time domain of band $i$   |      |
| $\mathbf{F}_i$                                       | ideal bandpass filter for band $i$   |      |
| $\mathbf{G}(s)$                                      | stable linear time-invariant transfer matrix                                       |      |
| sup  | supremum   |      |
| inf  | infimum  |      |
| $\bar{\mathbf{Y}}_i(s)$                              | responses in the frequency domain of mode $i$                                      |      |
| $\bar{\mathbf{y}}_i(t)$                              | responses in the time domain of mode $i$   |      |
| $\mathbf{Q}_i$                                       | diagonal matrix that weights mode $i$  |      |
| $\ \cdot\ _{\infty, \mathbf{Q}}$                     | weighted modal $H_\infty$ norm   |      |
| $diag(\cdot)$  | diagonal matrix  |      |
| $\mathbf{z}_p(t)$                                    | modal performance vector   |      |
| $\mathbf{\Gamma}, \mathbf{\Theta}, \mathbf{\Lambda}$ | matrices of modal performance vector   |      |
| $\mathbf{T}_{z_p w}(s)$                              | closed-loop transfer function matrix between $\mathbf{Z}_p(s)$ and $\mathbf{W}(s)$ |      |
| $k$  | stiffness coefficient  | N/m  |
| $d$  | damping coefficient  | Ns/m |
| $S_{aa}$   | power spectral density of $a(t)$   |      |
| $S_{ba}$   | cross power spectral density between $b(t)$ and $a(t)$                             |      |
| $M^{(\cdot)}$  | stable model   |      |
| $\mathcal{O}_\infty(M^{(\cdot)})$                    | infinite observability matrix of $M^{(\cdot)}$                                     |      |
| $\Delta(M^{(1)}, M^{(2)})$                           | distance between $M^{(1)}$ and $M^{(2)}$   |      |



|                                  |  |
|----------------------------------|--|
| $\theta_l$                       | $l^{th}$ principal angle between the subspace ranges $\mathcal{O}_\infty(M^{(1)})$ and $\mathcal{O}_\infty(M^{(2)})$               |
| $\mathcal{O}_\infty(M_i)$        | infinite observability matrix of a modal subsystem $M_i$   |
| $\Delta_i(M_i^{(1)}, M_i^{(2)})$ | distance between $M_i^{(1)}$ and $M_i^{(2)}$ for mode $i$  |
| $\bar{\mathbf{q}}$               | vector that balances the vibration reduction achieved by the $H_\infty$ controller and the relative effect of damage for each mode |
| $\alpha_i$                       | mode peak amplitude of the controlled structure  |
| $\phi_i$                         | mode peak reduction  |
| $\mathbf{q}$                     | linear transformation of vector $\bar{\mathbf{q}}$ into a reasonable range   |
| $h$                              | crack length   |
| $\mathbf{f}(t)$                  | fault signal   |
| $\mathbf{C}_1$                   | controller 1   |
| $\mathbf{C}_2$                   | controller 2   |
| $\varphi(t)$                     | bounded unknown signal that represents damage  |
| $\mathbf{u}_1(t)$                | control signal generated by the nominal controller   |
| $\mathbf{u}_2(t)$                | control signal generated by the damage compensator   |
| $\mathbf{x}_r(t)$                | reference state  |
| $\mathbf{e}_x(t)$                | residue  |
| $\hat{\mathbf{x}}(t)$            | state-vector estimation  |
| $\hat{\mathbf{y}}(t)$            | output-vector estimation   |
| $\mathbf{L}$                     | modal observer gain  |
| $\mathbf{e}(t)$                  | estimation error   |
| $J_{\varphi_e}$                  | performance index  |
| $V(\cdot)$                       | Lyapunov function  |
| $\mathbf{w}^*(t)$                | worst-case disturbance   |
| $\mathbf{K}_i$                   | mode $i$ gain vector   |
| $\mathbf{K}_{u_1}$               | gain vector over $\mathbf{u}_1$  |
| $\mathbf{A}_r$                   | reference dynamic matrix   |
| $\mathbf{B}_{1r}$                | reference matrix of disturbance inputs   |
| $\mathbf{B}_{2r}$                | reference matrix of control inputs   |
| $\hat{\mathbf{K}}_x(t)$          | estimation of $\mathbf{K}_x$   |

|  |  |
|--|--|
| $\hat{\mathbf{K}}_{\mathbf{u}_1}(t)$                                       | estimation of $\mathbf{K}_{\mathbf{u}_1}$                                      |
| $\Delta\mathbf{K}_{\mathbf{x}}^T(t), \Delta\mathbf{K}_{\mathbf{u}_1}^T(t)$ | gain estimation errors   |
| $\mathbf{T}_{\mathbf{x}}, \mathbf{T}_{\mathbf{u}_1}$                       | adaptation-rate matrices   |
| $\mathbf{T}_i$   | mode $i$ adaptation rate   |
| $tr(\cdot)$  | trace of a matrix  |
| $\omega_{c_1}$   | first cutoff frequency of the bandpass filter                                  |
| $\omega_{c_2}$   | second cutoff frequency of the bandpass filter                                 |
| $\mathbf{e}_{\mathbf{x}_i}(t)$   | residue relative to mode $i$   |
| $ \cdot $  | absolute value   |
| $[\mathbf{a}\angle\mathbf{b}]$   | angle between vectors $a$ and $b$  |
| $[\mathbf{A}\angle\mathbf{B}]$   | principal angles between $\text{row}(\mathbf{A})$ and $\text{row}(\mathbf{B})$ |
| $\cos$   | cosine   |
| $S$  | linear subspace  |
| $\text{rank}(\mathbf{A})$  | rank of matrix $\mathbf{A}$  |
| $\text{row}(\mathbf{A})$   | row space of matrix $\mathbf{A}$   |
| $\text{range}(\mathbf{A})$   | column space of matrix $\mathbf{A}$  |
| $\lambda(\mathbf{A})$  | eigenvalues of matrix $\mathbf{A}$   |
| $\max$   | maximum  |
| $\min$   | minimum  |

# CONTENTS

|          |  |           |
|----------|--|-----------|
| <b>1</b> | <b>INTRODUCTION</b>  | <b>29</b> |
| 1.1      | Motivations  | 29        |
| 1.2      | State of the art of the DTAC domains   | 30        |
| 1.2.1    | Smart structures   | 31        |
| 1.2.2    | Structural health monitoring   | 32        |
| 1.2.3    | Active vibration control   | 33        |
| 1.2.4    | Fault-tolerant control   | 35        |
| 1.2.5    | Damage-tolerant active control   | 36        |
| 1.3      | Objective of the thesis  | 38        |
| 1.4      | Organisation of the thesis   | 39        |
| 1.5      | Publications arising from this thesis  | 40        |
| <b>2</b> | <b>ACTIVE <math>H_\infty</math> CONTROLLER FOR VIBRATION REJECTION</b>           | <b>42</b> |
| 2.1      | Introduction   | 42        |
| 2.2      | State-space modal representation of flexible structures                          | 42        |
| 2.3      | $H_\infty$ control problem   | 45        |
| 2.4      | $H_\infty$ control solution using the LMI approach                               | 47        |
| 2.5      | Weighing filters   | 50        |
| 2.6      | Application: vibration control of a vertical structure subject to seismic events | 52        |
| 2.6.1    | Structure description and identification   | 53        |
| 2.6.2    | Controller design  | 56        |
| 2.6.3    | Experimental results   | 59        |
| 2.7      | Conclusion   | 60        |
| <b>3</b> | <b>A MODAL <math>H_\infty</math>-NORM APPROACH APPLIED TO DTAC</b>               | <b>62</b> |
| 3.1      | Introduction   | 62        |
| 3.2      | Modal norm definition  | 63        |
| 3.3      | Modal control problem  | 66        |
| 3.4      | Modal control solution   | 68        |
| 3.5      | Simulated and experimental results   | 69        |
| 3.5.1    | Simulated structure results  | 70        |

|          |  |           |
|----------|--|-----------|
| 3.5.2    | Experimental results . . . . .   | 73        |
| 3.5.2.1  | Healthy structure identification . . . . .   | 74        |
| 3.5.2.2  | Modal robust controller design . . . . .   | 75        |
| 3.5.2.3  | Control system experimental results . . . . .  | 77        |
| 3.6      | Conclusion . . . . .   | 79        |
| <b>4</b> | <b>A MODAL <math>H_\infty</math>-NORM PERFORMANCE REQUIREMENT FOR DTAC . . . . .</b> | <b>80</b> |
| 4.1      | Introduction . . . . .   | 80        |
| 4.2      | Assessing damage effects . . . . .   | 81        |
| 4.2.1    | Modal damage metric . . . . .  | 82        |
| 4.2.2    | Modal weighing matrices . . . . .  | 83        |
| 4.2.3    | Algorithm for the modal damage-tolerant controller design . . . . .                  | 84        |
| 4.3      | Simulated results with FE models . . . . .   | 85        |
| 4.3.1    | Simulated flexible structure . . . . .   | 85        |
| 4.3.2    | Damage simulation . . . . .  | 88        |
| 4.3.3    | Regular robust controller design . . . . .   | 89        |
| 4.3.4    | Modal robust controller design . . . . .   | 90        |
| 4.3.5    | Healthy structure responses . . . . .  | 91        |
| 4.3.6    | Controller responses under damage . . . . .  | 92        |
| 4.4      | Conclusion . . . . .   | 95        |
| <b>5</b> | <b>A MODAL DOUBLE-LOOP CONTROL FRAMEWORK FOR DTAC . . . . .</b>                      | <b>96</b> |
| 5.1      | Introduction . . . . .   | 96        |
| 5.2      | Adopted DTAC framework . . . . .   | 97        |
| 5.3      | Reconfigurable DTAC controller . . . . .   | 100       |
| 5.3.1    | Modal observer design . . . . .  | 101       |
| 5.3.2    | Reference model . . . . .  | 104       |
| 5.3.3    | Damage compensator . . . . .   | 105       |
| 5.3.4    | Reconfiguration mechanism . . . . .  | 106       |
| 5.3.5    | Modal double-loop controller design procedure . . . . .                              | 108       |
| 5.4      | Simulated results . . . . .  | 108       |
| 5.4.1    | Damage simulation . . . . .  | 109       |
| 5.4.2    | Nominal controller design . . . . .  | 109       |
| 5.4.3    | Damage compensator design . . . . .  | 111       |

|          |  |            |
|----------|--|------------|
| 5.4.4    | Controller responses under damage . . . . .  | 112        |
| 5.5      | Conclusion . . . . .   | 115        |
| <b>6</b> | <b>GENERAL CONCLUSIONS AND FUTURE PERSPECTIVES . . . . .</b>                             | <b>117</b> |
|          | <b>REFERENCES . . . . .</b>  | <b>120</b> |
|          | <b>APPENDIX A - THE PRINCIPAL ANGLES BETWEEN SUBSPACES . . . . .</b>                     | <b>133</b> |
| A.1      | The angles between two vectors . . . . .   | 133        |
| A.2      | Principal angles and directions . . . . .  | 134        |
| A.3      | The principal angles and respective directions as eigenvalues and eigenvectors . . . . . | 135        |
| A.4      | The cosines of the principal angles based on LQ decomposition . . . . .                  | 136        |
|          | <b>ANNEXE A - THE PRINCIPAL EQUATIONS OF THE PLQP SOFTWARE . . . . .</b>                 | <b>138</b> |
|          | <b>ANNEXE B - RÉSUMÉ ÉTENDU EN FRANÇAIS . . . . .</b>                                    | <b>156</b> |
| B.1      | Introduction . . . . .   | 156        |
| B.2      | Objectifs . . . . .  | 157        |
| B.3      | Modèle modal d'une structure intelligente . . . . .                                      | 157        |
| B.4      | Commande $H_\infty$ modale . . . . .   | 160        |
| B.4.1    | Résultats expérimentaux . . . . .  | 162        |
| B.5      | Prise en compte des effets des dommages dans la conception du correcteur modal . . . . . | 163        |
| B.5.1    | Métrique modale pour détecter les dommages et identifier leur sévérité. . . . .          | 164        |
| B.5.2    | Détermination des matrices de pondération modale . . . . .                               | 164        |
| B.5.3    | Résultats simulés . . . . .  | 166        |
| B.6      | Double boucle de commande . . . . .  | 169        |
| B.6.1    | Observateur modal . . . . .  | 169        |
| B.6.2    | Modèle de référence . . . . .  | 171        |
| B.6.3    | Compensation de dommage . . . . .  | 171        |
| B.6.4    | Mécanisme de reconfiguration . . . . .   | 172        |
| B.6.5    | Résultats simulés . . . . .  | 173        |
| B.7      | Conclusion . . . . .   | 174        |

# 1 INTRODUCTION

## 1.1 Motivations

Advances in materials and associated technologies have been conducting to larger, light-weight, and more flexible structures. Considering this trend, engineering systems like aerospace applications, robotic systems, and communication antennae (HU; NG, 2005) are more susceptible to disturbances caused by vibrations. This can lead these new structures to performance worsening, premature aging of materials, and eventually damage. In consequence, the interest in active vibration control has been increasing substantially and several different techniques have been developed along the last years (ZABIHOLLAH et al., 2007; KHOT et al., 2011; BRAGHIN et al., 2012; SHARMA et al., 2015).

Active Vibration Control (AVC) can be situated in the intersection between structural mechanics and automation research areas (BALAS, 1978). Recently, the evolution of micro-electronic and microcomputers, including also transducer integration, has conducted the development of active control methods applied to structures (GAWRONSKI, 2008; PREUMONT, 2011). Two preliminary steps are commonly necessary to design active vibration controllers. The first step is to model the structure using the Finite-Element (FE) method and/or experimentally identify the plant model, noticing that the respective transducers shall be in general included in the final model (KATAYAMA, 2005). Sometimes, an analytical model is available and is possible to adopt (MEIROVITCH, 1986). Considering the very high number of adopted modes, and the consequent number of equations, even for simple structures, the second step consists of reducing the model order aiming for a manageable model to design the controllers. The model order reduction may significantly affect the system performance and lead to instability. This phenomenon is known as spillover and must always be considered when designing active vibration controllers (BALAS, 1979).

A considerable variety of approaches to control flexible structures using robust active control may be found in the literature (SPENCER; NAGARAJAIAH, 2003; GAWRONSKI, 2008; CASCIATI et al., 2012). Considering the scope of this work, the following recent strategies deserve to be cited: adaptive control (HU; MA, 2006), fractional control (POMMIER-BUDINGER et al., 2008), fuzzy control (MARINAKI et al., 2010), decentralized control (JI-

ANG; LI, 2010), resonant control (PEREIRA et al., 2011), sliding mode control (HU; ZHU, 2012), modal control (CINQUEMANI et al., 2015), and finally  $H_2$  and  $H_\infty$  control in the classical approach (GAWRONSKI, 2004) and in the spatial approach (HALIM, 2002). However, considering these references and even most other publications, it may be affirmed that regular control methods do not take into account the possibility of damage, representing a new challenge to the active controller design.

The repeated exposition to loads and consequent vibration stress are responsible for accelerating the structure aging, which may change the material properties, usually leading to the occurrence of cracks. The reduction of vibration amplitude and its duration can provide an extension of the structure life, which represents a significant advantage for structures with vibration control mechanisms. The regular AVC consequence is to retard damage occurrence through the rejection of external disturbances. However, the model accuracy directly influences controlled robustness and performance, given that structural dynamics is sensitive to operational conditions, temperature, and structural damage (CHOMETTE et al., 2008; MECHBAL; NÓBREGA, 2015a). In most cases, operational condition changes included in the controller design can mitigate these effects. On the other hand, model changes due to structural damage are not easily incorporated into the control design because damage influence in the structure dynamics is difficult to predict. It is important to include the possibility of damage in the structural active control design, guaranteeing an acceptable performance (GENARI et al., 2015a). The structure active vibration control research area considering these requirements is referred to as Damage-Tolerant Active Control (DTAC) (MECHBAL; NÓBREGA, 2012). To include damage compensation as an effective controller design requirement, guaranteeing closed-loop performance before and after the damage occurrence, this thesis presents novel methods to design damage-tolerant active controllers.

## 1.2 State of the art of the DTAC domains

DTAC is a multidisciplinary engineering research area, involving concepts of smart structures, Structural Health Monitoring (SHM), AVC, and Fault-Tolerant Control (FTC). In order to discuss DTAC concepts, this section presents a short introduction to each of these domains, trying to focus on the main topics used to develop this work and presenting the adopted assump-

tions. After this, DTAC is introduced and some strategies to design the respective controllers are presented. In addition, the relation between FTC and DTAC is discussed, showing important particular differences between the control methods of each area.

### 1.2.1 Smart structures

Smart structures have becoming increasingly present in industrial products, especially in applications that require strict performance and safety such as aerospace and civil engineering areas. They can be defined as a structural system that responds to external stimuli using distributed transducers, often used to monitor the system condition, but that may also be used by control algorithms to change or adapt the structure itself or its dynamic behaviour. The development of the smart structure field is linked to the material science and the control fields. The material science is responsible for providing new materials for sensing and actuation, in an efficient and controlled manner, encompassing the effective integration of transducers in structures. The control techniques are responsible for analysing the structure response in order to produce actuating signals by adjusting structural characteristics such as shape, stiffness, or damping (FISCHER, 2013).

This thesis deals with the vibration attenuation of smart structures. These vibrations are caused by external disturbances such as wind, seismic events, loads, etc. The smart structures should be able to sense the vibrations and react through a control algorithm to attenuate them. There is a wide range of materials to be used as transducers, comprising piezoelectric, electrostrictive, magnetostrictive, carbon nanotubes, shape memory alloys, and others (SRINIVASAN; MCFARLAND, 2001). In this research, piezoelectric patches are adopted to work as sensors and/or actuators.

Piezoelectricity is an electromechanical interaction phenomenon, representing the coupling between mechanical deformations and electric fields in a material. In 1880, Pierre and Paul-Jacques Curie discovered the direct piezoelectric effect on various crystals such as tourmaline, Rochelle salt, and quartz. The researchers noted that these crystals generate electrical charges when they were mechanically strained in certain directions. In the following year, they also discovered that the crystals react to electric voltage with shape change. For this reason, the same piezoelectric patch can be used as actuator or sensor (HALIM, 2002).



In this research, PZT (lead zirconate titanate) ceramic patches are adopted. These are the most used in the industry due to strong electromechanical coupling, ability to produce large forces, short reaction time, high precision, durability, low costs, and the patches can be found in diverse forms. PZT ceramics are indeed capable of simultaneously measuring deformation and transmitting force to the structure. In addition, piezoelectric elements are light and may be easily glued on the structure body or incorporated inside composite materials.

### 1.2.2 Structural health monitoring

Structures are subject to aging from repetitive strain, friction, loads, and differences in temperatures and pressures. The combination of these agents contributes to structure deterioration. An efficient damage detection can prevent catastrophic failures and save maintenance costs (GENARI; NÓBREGA, 2012). Thereby, in the last decades, damage detection and SHM techniques have been investigated and several damage indicators have been proposed in the literature (MEVEL et al., 2003; FAN; QIAO, 2010; BAPTISTA et al., 2014; SARTORATO et al., 2017).

Damage may be defined as changes in the structure that adversely affect current or future performance. The damage concept makes sense by comparing two different substructure states: the initial state assumed as intact (or healthy) and the current state. There are several damage possibilities in smart structures, including damage in the respective transducers. For instance, the piezoelectric ceramic glued onto a structure may present the following damages: detachment of the ceramic, cracking of an electrode and/or a ceramic, disordering of a measuring cable, and breakdown of the piezoelectric material due to a high electric field. On the other hand, damage types in the structure body are several as well, depending on the structure material (metal alloys, composite materials, etc.). The most common damage types are cracks, debonding, deformations and material loss caused by impacts, and “nonmechanical” damage. The damage is called “nonmechanical” due to its origin, such as thermal, electrical, or pressure phenomena. In this thesis, DTAC-proposed methods are examined using metallic structures.

Some techniques for damage diagnosis using nondestructive evaluation methods are being developed, based on acoustic theory, magnetism, thermal science, x-ray, etc. These methods are usually applied to characterise the damage and to analyse the degree of severity but re-

quire previous knowledge of damage regions in structures (ZHENG; MITA, 2007). In addition, nondestructive methods commonly require system downtime and therefore an operating loss. Hence, the techniques for SHM in real time have been widely investigated. These new approaches have benefited from recent advances in smart materials, conducting to the deployment of new functions in smart structures.

There is a large number of approaches for designing SHM systems, in which it is possible to cite the following promising categories: classification problem (MECHBAL et al., 2015), electromechanical impedance (SELVA et al., 2013), acoustic emission (HOLFORD et al., 2009), Lamb waves (SOUZA; NÓBREGA, 2012), among others. However, structure vibration-based methods permit to detect, locate, and analyse the severity of damage from changes in vibration characteristics such as modal frequencies, mode shapes, and flexibility matrix (CARDEN; FANNING, 2004; HUMAR et al., 2006; SAEED et al., 2009a; MEDEIROS et al., 2016). This SHM approach usually provides valuable information about damage impacts on structural vibrations, which may be used to design and/or to reconfigure controllers to face the vibration changes. In this thesis, this SHM strategy is adopted to generate damage information used in the DTAC controller design.

### **1.2.3 Active vibration control**

Active control methods of structure vibrations adopt a reduced order model, as already mentioned, in which the active term is due to the use of an external energy source. Continuous mechanical structures have an infinite number of vibration modes, implying that there are always some neglected dynamics in the control system design. The order reduction is based on an effective frequency-of-interest band, which is determined based on control requirements and practical aspects. This causes the occurrence of the spillover phenomenon, corresponding to the excitation of out-of-interest-bandwidth natural frequencies, which may be considered the main active control limitation for real applications. Failure in properly considering spillover in the controller design usually leads to instability (BALAS, 1978; BALAS, 1979; MEIROVITCH; BARUH, 1985). Some proposed techniques render the problem manageable, adopting smart structures with a great number of collocated sensors and actuators (INMAN, 2001). The collocated approach corresponds to placing sensors and actuators on the same location on the struc-

ture. Considering the small range of realistic applications using collocated methods, the control technique development for noncollocated mechanical structures has been receiving the attention of the scientific community (MECHBAL et al., 2006; SCHRÖCK et al., 2011). However, noncollocated systems have more complex dynamics with non-minimum-phase zeros (GOSIEWSKI; KULESZA, 2013), making it difficult to achieve closed-loop robustness and good performance (PREUMONT, 2011). Despite the progress achieved so far, the noncollocated vibration control of structures remains challenging (MASTORY; CHALHOUB, 2014).

Several control methods have been proposed to mitigate structure vibrations with different success levels. Avoiding the spillover occurrence and instability caused by parameter variation may be considered the main issues to be solved in any control design method (MOHAMED et al., 2005; BOSSI et al., 2011). However, current techniques are generally inadequate to be applied to plants with dynamic uncertainties because they are very sensitive to model inaccuracy (TANG; CHEN, 2009).  $H_\infty$ -based control methods are able to handle both uncertainties and parameter variations, and have been successfully adopted to suppress low-order vibration modes (BOULET et al., 2001; HALIM, 2004; ROBU et al., 2010). Due to these characteristics,  $H_\infty$  methods have been used in active vibration control (NONAMI; SIVRIOGLU, 1996; ZHANG et al., 2009; GENARI et al., 2015). The  $H_\infty$  controller goal is to minimise the worst mode performance in the interest bandwidth, without excitation of the neglected dynamics. To achieve this effect, conveniently designed weighing filters are necessary to shape the desired frequency distribution (SERPA; NÓBREGA, 2005). The respective approach deals in general with low frequency bands as a whole, which prevents mode selectivity in terms of both amplitude and frequency in the interest bandwidth. This behaviour compromises the interest-bandwidth excitation relative to the control signal, as a result of the so-called water bed effect (ZHOU; DOYLE, 1997).

Early papers by Balas (1978) and Meirovitch et al. (1983) introduced the modal control aiming for specific structure modes. Meirovitch developed the Independent Modal Space Control (IMSC), where each mode is controlled separately. However, IMSC was very sensitive with respect to spillover and improvements were proposed to make the method more tolerant to this phenomenon (RESTA et al., 2010). For instance, Baz and Poh (1990) suggested the modified independent modal space control to overcome the spillover problem in the IMSC, adopting an optimal actuator placement technique. Fang et al. (2003) modified the IMSC algorithm for uncontrolled modes, considering the effects of residual modes and their connection with the controller to solve the spillover problem. Serra et al. (2013) proposed a new method called de-

pendent modal space controller, based on mode shape modifications by creating virtual nodes in desired locations. In parallel, other modal methods have been developed (INMAN, 2001; KIM et al., 2011; PEREIRA et al., 2011). Despite the evolution, the design of an efficient modal controller to face the spillover effects continues as an open problem (CINQUEMANI et al., 2015).

In all those analysed works on vibration control of flexible structures, the general strategy is to measure and to reduce the structure vibration at specific locations, adopting point-wise models. However, this strategy ignores the vibration effects on the rest of the structure, which may lead to performance loss if vibration attenuation over the entire structure is necessary. To overcome this limitation, the spatial  $H_2$  norm was proposed in (MOHEIMANI; FU, 1998) and the spatial  $H_\infty$  norm was proposed in (MOHEIMANI et al., 1997; MOHEIMANI et al., 1998), which are performance measures over the spatial domain. Both spatial norms can be seen as natural extensions of the regular  $H_2$  and  $H_\infty$  norms for spatially distributed systems (HALIM; MOHEIMANI, 2002b), leading to control problems that can be solved using regular approaches (HALIM; MOHEIMANI, 2002a). Successful experimental studies have been conducted by Halim (2002) and by Lee (2005) to test the spatial  $H_\infty$  approach.

#### 1.2.4 Fault-tolerant control

FTC is a control design methodology that can tolerate some system component faults, maintaining stability and an acceptable level of performance. These components are here understood as sensors, actuators, controllers, and plant parts. In general, the FTC system is designed with the ability to accommodate system faults automatically. During the last three decades, FTC has been applied to improve system reliability, maintainability, and survivability (ZHAO, 1999). Nowadays, FTC approaches have been increasingly used and researched in industrial and academic areas. Several survey papers have been published, using different approaches for different types of systems (FEKIH, 2009; KHELASSI et al., 2011; WANG et al., 2015).

Generally, there exist two approaches to FTC: passive and active. It is worth mentioning that this definition is completely different from the vibration control area, where the active and the passive terms are relative to the use or not of an external energy source.

In the FTC area, the passive techniques consist in designing fixed controllers, which are

not possible to change, based on a priori knowledge about component faults (HSIEH, 2002). These controlled systems must be robust with respect to the expected faults (JIANG; ZHAO, 2000). In this approach, fault tolerance is usually achieved by considering faults as uncertainties or external perturbations that the control systems should compensate. In general, the designer works with an adopted set of system-fault scenarios (ZHAO, 1999). However, the FTC system performance may not respond satisfactorily to an unexpected fault, eventually leading the plant to instability.

In the active approach, the FTC controller reacts to the system component fault, reconfiguring the controller parameters to maintain the system stability with desired performance. For this purpose, a real-time Fault Detection and Isolation (FDI) module is necessary to provide usable data about the plant state (KLINKHIEO, 2009). In this FTC strategy, the controlled system performance is related to the accuracy of the fault information and the robustness of the FDI to disturbances. The active FTC methods must be able to deal with several types of faults, including unexpected faults. There are several approaches to design FTC systems, of which some examples are given in (YANG et al., 2010). To conclude, (ZHANG; JIANG, 2008) shows a good review of active FTC methods.

### **1.2.5 Damage-tolerant active control**

The DTAC method development constitutes a recent research area that has intersections with both FTC and AVC areas. Specific FDI techniques are used by fault-tolerant controllers to provide online parameter adaptation aiming to maintain an adequate performance for controlled systems (ZHANG; JIANG, 2008; RODRIGUES et al., 2014; WANG et al., 2015). In the same way, DTAC methods use SHM techniques to design controllers presenting damage-tolerance (MECHBAL; NÓBREGA, 2012). DTAC methods may be considered an extension of FTC, focusing fundamentally on structural vibration control, aiming to expand the applicability of modern smart structures. However, adapting FTC methods to face damage-induced vibration in flexible structures leads to new challenges. The infinite number of structural vibration modes demands a controller robustness that is complicated by the dynamic changes due to damage perturbation (MECHBAL; NÓBREGA, 2015). The literature regarding vibration control of structures subject to damage is limited. For instance, Chattopadhyay et al. (2000) used a pole

placement technique together with a root mean square method to locate and to mitigate the damage caused by delamination in a composite plate. Umesh and Ganguli (2008) investigated the negative velocity feedback control algorithm to compensate the damage effects. Ripamonti et al. (2015) proposed an adaptive active vibration control to increase the structure life, emphasising the vibration reduction from the most damaging modes.

DTAC arises from intense investigation to bring more secure and efficient operations to flexible structures, aiming for extension of their life cycle as well (MECHBAL; NÓBREGA, 2015b). The first goal of DTAC methods is to achieve an adequate performance for healthy real-life structures. For this purpose, DTAC systems need to be able to solve the regular active control problem, which involves avoiding the spillover phenomenon (BALAS, 1978) and adopting noncollocated transducers on the mechanical structures (KIM; OH, 2013). In addition, as a second goal, the controlled system should prevent and/or retard damage occurrence. This basic DTAC idea corresponds to reducing the vibration. The third goal is that, in the event of structural damage, the controller should act to mitigate damage effects on structural vibrations, avoiding or delaying damage propagation (MECHBAL; NÓBREGA, 2015a).

DTAC strategies are based on the structure state condition, depending if the structure is healthy or damaged (MECHBAL; NÓBREGA, 2012). For the healthy structure condition, two strategies can be adopted (MECHBAL; NÓBREGA, 2015b):

- Strictly Tolerant Active Control (STAC);
- Preventive Active Control (PAC).

STAC represents a robust approach based on a nonreconfigurable controller, aiming to guarantee an acceptable performance for some types and severity levels of future damage. However, the compromise between robustness and performance may lead to unsatisfactory behaviour in damage absence, due to the natural opposition between these two features. To overcome this limitation, Genari et al. (2015b) proposed a robust modal approach that leads to a reasonable compromise between robustness and performance, in which both the healthy structure and the damaged structure have an adequate performance level with the same controller.

PAC is a preventive strategy aiming to avoid or to retard damage occurrence, consequently extending structure life. For instance, Chomette et al. (2010) designed a controller that attenuates the most damaging modes. Ambrosio et al. (2014) included material fatigue into a cost function, which is then minimised to obtain the PAC controller.

If damage occurs and is identified, two other possible strategies can be applied (MECHBAL; NÓBREGA, 2015b):

- Evolving Damage Active Control (EDAC);
- Adaptive Tolerant Active Control (ATAC).

The EDAC strategy admits that damage is detected, localised, and quantified. The controller is then designed to limit damage propagation, aiming to reduce vibration energy at the damage region. This strategy designs controllers that act over specific regions of the structure. For instance, it corresponds to the spatial  $H_\infty$  methodology applied to structural damage control that was investigated in (MECHBAL; NÓBREGA, 2015b). Ashokkumar (2015) proposed an actuator load to reduce vibration response magnitudes for damage growth control.

The ATAC strategy goal is to detect and then accommodate the damage, providing a satisfactory performance level for the controlled system in all circumstances. For this purpose, an SHM module and a reconfigurable controller are used to compose the control system. The SHM module must detect and analyse the damage and signal the controller to be reconfigured according to the SHM data. The ATAC strategy was used to design a damage-tolerant controller in (MECHBAL; NÓBREGA, 2015a) using a Lamb wave-based SHM module to localise damage. Then, the spatial  $H_\infty$  controller was reconfigured to reduce vibration energy flow in the detected damaged region.

### 1.3 Objective of the thesis

The thesis objective is the development of DTAC methods applied to vibration control of flexible structures subject to damage. First, in the regular AVC research area, a modal  $H_\infty$  technique is proposed and applied to vibration control of the healthy structure, based on a new modal  $H_\infty$  norm. Furthermore, considering the reasonable compromise between robustness and performance achieved with the proposed methodology, the modal technique is adopted as an STAC strategy for damage active tolerance.

Based on the results of the modal  $H_\infty$  approach to face damage, and considering that structural damage impact may be represented by a modal composition, a methodology to design the modal  $H_\infty$  controller including damage in the design requirements is proposed. For this purpose, a new damage indicator based on model subspace distance is also developed, in order to quantify modal damage effects. The modal  $H_\infty$  norm is computed based on the modal distances for simulated FE models, conducting to the damage-tolerant controller through the minimisa-

tion of the respective norm. This methodology configures a PAC strategy, but it may also be used as an EDAC one if the damage is already known.

As a final contribution, a double-loop control framework for the vibration attenuation of structures is proposed, performing the ATAC strategy. In this case, the controller in the first loop is designed to comply with the healthy structure requirements, based on the developed modal  $H_\infty$  control, and the second-loop controller is designed to compensate eventual damage effects. To achieve this goal, an online-reconfigurable technique is used in order to design the second controller, based on a modal state-tracking method to provide the updating of the controller parameters.

## 1.4 Organisation of the thesis

The thesis is organised into the following chapters:

### **Chapter 2: Active $H_\infty$ controller for vibration rejection**

The chapter introduces the  $H_\infty$  control technique to attenuate the vibrations in flexible structures, based on the LMI approach. This method is used to design regular vibration controllers but represents a fundamental step to design all the proposed damage compensators. The regular  $H_\infty$  controllers are used as the reference to assess the performance of the proposed controllers. Initially, the chapter presents a brief overview of the state-space representation to describe generic flexible structures, adopting a modal representation according to the proposed controller design methods. Moreover, the chapter presents an overview of the LMI approach to solve the  $H_\infty$  problem, including the weighting filters to impose the desired frequency response in the controller design. After that, this control technique is used to attenuate vibrations of a bench-scale structure that simulates a tall building subject to seismic loads. The controller is designed to reduce the vibration level considering the control input limit.

### **Chapter 3: A modal $H_\infty$ -norm approach applied to DTAC**

A new approach for vibration reduction of flexible structures subject to damage is presented in this chapter, based on the proposed modal  $H_\infty$  norm. Considering that structural damage provokes different effects on each vibration mode, the proposed method focus on the control action on specific modes that are indeed suffering the worst damage consequences. For this purpose, a new modal  $H_\infty$  norm is introduced, weighing each mode according to structural



convenience. Based on this norm, a regular  $H_\infty$  controller design is applied, using the LMI approach. Simulated and experimental results are presented to show the modal methodology applicability.

#### **Chapter 4: A modal $H_\infty$ -norm performance requirement for DTAC**

The modal  $H_\infty$  design is extended in this chapter to implement a PAC strategy. Considering the different damage effects, the proposed methodology adopts the modal  $H_\infty$  norm to include damage as a design requirement. The basic idea is to create an appropriate energy distribution over the frequency range of interest, aiming for specific vibration modes, guaranteeing robustness, damage tolerance, and an adequate overall performance. For this purpose, an SHM technique is applied to evaluate modal modifications caused by damage. This information is used to create modal weighing matrices, conducting to the modal  $H_\infty$  controller design. FE models are adopted for a case study structure, including crack simulation, in order to evaluate the proposed control strategy.

#### **Chapter 5: A modal double-loop control framework for DTAC**

This chapter presents an implementation of the ATAC strategy, designing two controllers to be used in a double loop, aiming for vibration reduction of flexible structures subject to damage. The two controller design methods are presented, with emphasis in the reconfigurable controller that faces the damage. To assess the proposed method, FE models including healthy and damaged conditions are simulated with different controllers. Results are compared to assess the efficiency of the proposed controller design method.

#### **Chapter 6: Conclusions**

The thesis is concluded by stating the main contributions of this research. Moreover, this chapter presents recommendations for further research in this area.

### **1.5 Publications arising from this thesis**

This work has been the subject of the following publications:

#### **Journal papers:**

- “Damage-Tolerant Active Control Using a Modal  $H_\infty$ -Norm-Based Methodology”, H. F. G. Genari and N. Mechbal and G. Coffignal and E. G. O. Nóbrega, Control

Engineering Practice, 2016, accepted with minor revision.

- “A Reconfigurable Damage-Tolerant Controller Based on a Modal Double-Loop Framework”, H. F. G. Genari and N. Mechbal and G. Coffignal and E. G. O. Nóbrega, Mechanical Systems and Signal Processing, 2016, under review.
- “A Modal  $H_\infty$ -Norm-Based Performance Requirement for Damage-Tolerant Active Controller Design”, H. F. G. Genari and N. Mechbal and G. Coffignal and E. G. O. Nóbrega, Journal of Sound and Vibration, 2016, under review.

#### **Conference papers:**

- “A Modal  $H_\infty$  Control Methodology for Damage-Tolerant Active Control”, H. F. G. Genari and N. Mechbal and G. Coffignal and E. G. O. Nóbrega, 9th IFAC Symposium on Fault Detection, Supervision and Safety for Technical Processes, Paris - France, 48(21), 664-669, 2015.
- “A Double-Loop Control Approach Applied to Damage-Tolerant Active Control”, H. F. G. Genari and N. Mechbal and G. Coffignal and E. G. O. Nóbrega, 23rd International Congress of Mechanical Engineering, Rio de Janeiro - Brazil, 1-8, 2015.
- “Robust Vibration Control of a Vertical Flexible Structure Subject to Seismic Events”, H. F. G. Genari and O. Oliveira Neto and E. G. O. Nóbrega and N. Mechbal and G. Coffignal, XVII International Symposium on Dynamic Problems of Mechanics, Natal - Brazil, 1-10, 2015.
- “Structural Damage Diagnosis Method Based on Subspace Identification Metric”, H. F. G. Genari and E. G. O. Nóbrega and N. Mechbal, 22nd International Congress of Mechanical Engineering, Ribeirão Preto - Brazil, 4200-4208, 2013.

## 2 ACTIVE $H_\infty$ CONTROLLER FOR VIBRATION REJECTION

The chapter goal is to present a brief overview of the LMI approach to solve the  $H_\infty$  problem, representing a fundamental step to design the damage controllers presented in the next chapters. A modal state-space model of a generic structure is introduced in the sequence. After that, the formulation and solution of the respective  $H_\infty$  problem are conducted. Finally, the robust control method is experimentally examined in a simulated tall building.

### 2.1 Introduction

The active controller design based on the  $H_\infty$  approach has been attracting attention due to its robustness to modelling errors and disturbance rejection capability. Usually, the  $H_\infty$  controllers are computed using two different approaches: Riccati equations and LMIs. The LMI approach has the advantage of easily including additional inequations while keeping its convexity, permitting to be solved by efficient algorithms (NESTEROV; NEMIROVSKI, 1994).

Considering that the  $H_\infty$  controller goal is to minimise the energy gain between the output and the disturbance in the interest bandwidth, without excitation of the neglected dynamics, conveniently designed weighing filters are adopted to ensure the desired frequency distribution (SERPA; NÓBREGA, 2005). The weighing filters shape the output responses and the control signals, obtaining a reasonable trade-off between performance and robustness and considering the frequency distribution based on the plant reduced model. The chapter presents a brief overview of the LMI approach to solve the  $H_\infty$  problem, including the weighing filters in the design procedure.

### 2.2 State-space modal representation of flexible structures

This section presents a brief overview of the modal state-space representation to describe a generic flexible structure, for the sake of completeness. This overview begins with a second-

order matrix differential equation, commonly used to represent structural dynamics by means of FE models. Then, the state-space model is defined from this differential equation, using a specific state-vector definition. To conclude, the transformation matrices to obtain different modal canonical representations are discussed.

A generic flexible structure can be modelled by the following second-order differential pair of equations:

$$\mathbf{M}\ddot{\mathbf{p}}(t) + \mathbf{D}\dot{\mathbf{p}}(t) + \mathbf{K}\mathbf{p}(t) = \mathbf{B}_w\mathbf{w}(t) + \mathbf{B}_u\mathbf{u}(t) \quad (2.1)$$

$$\mathbf{y}(t) = \mathbf{C}_d\mathbf{p}(t) + \mathbf{C}_v\dot{\mathbf{p}}(t) + \mathbf{C}_w\mathbf{w}(t) + \mathbf{C}_u\mathbf{u}(t), \quad (2.2)$$

in which  $\mathbf{p}(t)$  denotes the displacements,  $\mathbf{M}$  is the mass matrix,  $\mathbf{D}$  is the damping matrix,  $\mathbf{K}$  is the stiffness matrix,  $\mathbf{B}_w$  and  $\mathbf{B}_u$  are the respective input matrices, where  $\mathbf{w}(t)$  are the disturbance forces acting on the structure and  $\mathbf{u}(t)$  are the control forces, and  $\mathbf{y}(t)$  are the measured output signals modelled through the output matrices  $\mathbf{C}_d$ ,  $\mathbf{C}_v$ ,  $\mathbf{C}_w$ , and  $\mathbf{C}_u$ . In general, FE models generate high order models, which need to be reduced to represent the bandwidth of interest for the controller operation. Therefore, a model with  $m$  modes is considered, which leads to the following modal matrix:

$$\Phi = \begin{bmatrix} \phi_1 & \phi_2 & \dots & \phi_m \end{bmatrix},$$

where  $\phi_i$  is the  $i^{th}$  mode shape. A transformation into modal coordinates is obtained using  $\mathbf{p}(t) = \Phi\mathbf{q}(t)$ . Pre-multiplying Eq. (2.1) by  $\Phi^T$  and writing  $\mathbf{y}(t)$  in terms of  $\mathbf{q}(t)$  gives:

$$\Phi^T\mathbf{M}\Phi\ddot{\mathbf{q}}(t) + \Phi^T\mathbf{D}\Phi\dot{\mathbf{q}}(t) + \Phi^T\mathbf{K}\Phi\mathbf{q}(t) = \Phi^T\mathbf{B}_w\mathbf{w}(t) + \Phi^T\mathbf{B}_u\mathbf{u}(t)$$

$$\mathbf{y}(t) = \mathbf{C}_d\Phi\mathbf{q}(t) + \mathbf{C}_v\Phi\dot{\mathbf{q}}(t) + \mathbf{C}_w\mathbf{w}(t) + \mathbf{C}_u\mathbf{u}(t),$$

which may be written as:

$$\mathbf{M}_m\ddot{\mathbf{q}}(t) + \mathbf{D}_m\dot{\mathbf{q}}(t) + \mathbf{K}_m\mathbf{q}(t) = \mathbf{B}_{w_m}\mathbf{w}(t) + \mathbf{B}_{u_m}\mathbf{u}(t) \quad (2.3)$$

$$\mathbf{y}(t) = \mathbf{C}_{d_m}\mathbf{q}(t) + \mathbf{C}_{v_m}\dot{\mathbf{q}}(t) + \mathbf{C}_w\mathbf{w}(t) + \mathbf{C}_u\mathbf{u}(t), \quad (2.4)$$

where  $\mathbf{M}_m = \Phi^T\mathbf{M}\Phi$ ,  $\mathbf{D}_m = \Phi^T\mathbf{D}\Phi$ ,  $\mathbf{K}_m = \Phi^T\mathbf{K}\Phi$ ,  $\mathbf{B}_{w_m} = \Phi^T\mathbf{B}_w$ ,  $\mathbf{B}_{u_m} = \Phi^T\mathbf{B}_u$ ,  $\mathbf{C}_{d_m} = \mathbf{C}_d\Phi$ , and  $\mathbf{C}_{v_m} = \mathbf{C}_v\Phi$ . Matrices  $\mathbf{M}_m$  and  $\mathbf{K}_m$  are diagonal while  $\mathbf{D}_m$  is not necessarily diagonal. For analytical convenience, the damping matrix is commonly considered as a

linear combination of the stiffness and mass matrices,  $\mathbf{D} = \alpha\mathbf{M} + \beta\mathbf{K}$  for  $\alpha, \beta \geq 0$  (GAWRONSKI, 2004). This is a reasonable and usual assumption, considering that flexible structures have small damping factors.

Assuming that the matrix  $\mathbf{M}_m$  is nonsingular, Eq. (2.3) can be written as:

$$\ddot{\mathbf{q}}(t) + \mathbf{M}_m^{-1}\mathbf{D}_m\dot{\mathbf{q}}(t) + \mathbf{M}_m^{-1}\mathbf{K}_m\mathbf{q}(t) = \mathbf{M}_m^{-1}\mathbf{B}_{w_m}\mathbf{w}(t) + \mathbf{M}_m^{-1}\mathbf{B}_{u_m}\mathbf{u}(t), \quad (2.5)$$

and equivalently:

$$\ddot{\mathbf{q}}(t) + 2\mathbf{Z}\mathbf{\Omega}\dot{\mathbf{q}}(t) + \mathbf{\Omega}^2\mathbf{q}(t) = \mathbf{M}_m^{-1}\mathbf{B}_{w_m}\mathbf{w}(t) + \mathbf{M}_m^{-1}\mathbf{B}_{u_m}\mathbf{u}(t),$$

in which  $\mathbf{\Omega}^2 = \mathbf{M}_m^{-1}\mathbf{K}_m$ ,  $\mathbf{Z} = 0.5\mathbf{M}_m^{-1}\mathbf{D}_m\mathbf{\Omega}^{-1}$ ,  $\mathbf{B}_m = \mathbf{M}_m^{-1}\mathbf{\Phi}^T\mathbf{B}_0$ , and  $\mathbf{q}(t)$  represents the modal displacement vector. Moreover,  $\mathbf{\Omega}$  is the matrix of natural frequencies and  $\mathbf{Z}$  is the modal damping matrix, both defined as:

$$\mathbf{\Omega} = \begin{bmatrix} \omega_1 & 0 & \cdots & 0 \\ 0 & \omega_2 & \cdots & 0 \\ \vdots & \cdots & \ddots & \vdots \\ 0 & 0 & \cdots & \omega_m \end{bmatrix} \quad \text{and} \quad \mathbf{Z} = \begin{bmatrix} \zeta_1 & 0 & \cdots & 0 \\ 0 & \zeta_2 & \cdots & 0 \\ \vdots & \vdots & \ddots & \vdots \\ 0 & 0 & \cdots & \zeta_m \end{bmatrix},$$

where  $\omega_i$  and  $\zeta_i$  are respectively the natural frequency and damping relative to mode  $i$ .

Adopting the state-vector definition as  $\mathbf{x}(t) = [\mathbf{x}_1^T(t) \ \mathbf{x}_2^T(t)]^T = [\mathbf{q}^T(t) \ \dot{\mathbf{q}}^T(t)]^T$ , Eq. (2.4) and Eq. (2.5) can be transformed into:

$$\begin{aligned} \dot{\mathbf{x}}_1(t) &= \mathbf{x}_2(t) \\ \dot{\mathbf{x}}_2(t) &= -\mathbf{M}_m^{-1}\mathbf{K}_m\mathbf{x}_1(t) - \mathbf{M}_m^{-1}\mathbf{D}_m\mathbf{x}_2(t) + \mathbf{M}_m^{-1}\mathbf{B}_{w_m}\mathbf{w}(t) + \mathbf{M}_m^{-1}\mathbf{B}_{u_m}\mathbf{u}(t) \\ \mathbf{y}(t) &= \mathbf{C}_{d_m}\mathbf{x}_1(t) + \mathbf{C}_{v_m}\mathbf{x}_2(t) + \mathbf{C}_w\mathbf{w}(t) + \mathbf{C}_u\mathbf{u}(t), \end{aligned}$$

leading to the following state-space representation:

$$\begin{aligned} \dot{\bar{\mathbf{x}}}(t) &= \bar{\mathbf{A}}\bar{\mathbf{x}}(t) + \bar{\mathbf{B}}_1\mathbf{w}(t) + \bar{\mathbf{B}}_2\mathbf{u}(t) \\ \mathbf{y}(t) &= \bar{\mathbf{C}}_2\bar{\mathbf{x}}(t) + \mathbf{D}_{21}\mathbf{w}(t) + \mathbf{D}_{22}\mathbf{u}(t), \end{aligned}$$

in which  $\bar{\mathbf{C}}_2 = [\mathbf{C}_{d_m} \ \mathbf{C}_{v_m}]$ ,  $\mathbf{D}_{21} = \mathbf{C}_w$ , and  $\mathbf{D}_{22} = \mathbf{C}_u$ . Matrices  $\bar{\mathbf{A}}$ ,  $\bar{\mathbf{B}}_1$ , and  $\bar{\mathbf{B}}_2$  are obtained

using:

$$\bar{\mathbf{A}} = \begin{bmatrix} \mathbf{0} & \mathbf{I} \\ -\mathbf{M}_m^{-1}\mathbf{K}_m & -\mathbf{M}_m^{-1}\mathbf{D}_m \end{bmatrix}, \bar{\mathbf{B}}_1 = \begin{bmatrix} \mathbf{0} \\ \mathbf{M}_m^{-1}\mathbf{B}_{w_m} \end{bmatrix}, \text{ and } \bar{\mathbf{B}}_2 = \begin{bmatrix} \mathbf{0} \\ \mathbf{M}_m^{-1}\mathbf{B}_{u_m} \end{bmatrix}.$$

Finally, this model can be written into modal canonical representations using transformation matrices (GAWRONSKI, 2004). For the purpose of the thesis approach, the following state-space model structure is adopted:

$$\mathbf{A} = \begin{bmatrix} \mathbf{A}_1 & \mathbf{0} & \cdots & \mathbf{0} \\ \mathbf{0} & \mathbf{A}_2 & \cdots & \mathbf{0} \\ \vdots & \vdots & \ddots & \vdots \\ \mathbf{0} & \mathbf{0} & \cdots & \mathbf{A}_m \end{bmatrix}, \mathbf{B}_1 = \begin{bmatrix} \mathbf{b}_{11} \\ \mathbf{b}_{12} \\ \vdots \\ \mathbf{b}_{1m} \end{bmatrix}, \mathbf{B}_2 = \begin{bmatrix} \mathbf{b}_{21} \\ \mathbf{b}_{22} \\ \vdots \\ \mathbf{b}_{2m} \end{bmatrix}, \text{ and } \mathbf{C}_2 = \begin{bmatrix} \mathbf{c}_{21}^T \\ \mathbf{c}_{22}^T \\ \vdots \\ \mathbf{c}_{2m}^T \end{bmatrix}^T, \quad (2.6)$$

where it is possible to see that the system matrix has a block diagonal structure where each  $\mathbf{A}_i$  is a  $2 \times 2$  matrix for  $i = 1, \dots, m$ , therefore isolating each mode.

### 2.3 $H_\infty$ control problem

According to the optimal controller design framework, a performance indicator is introduced as an output vector  $\mathbf{z}(t)$ , leading to the following state-space equations:

$$\begin{aligned} \dot{\mathbf{x}}(t) &= \mathbf{A}\mathbf{x}(t) + \mathbf{B}_1\mathbf{w}(t) + \mathbf{B}_2\mathbf{u}(t) \\ \mathbf{z}(t) &= \mathbf{C}_1\mathbf{x}(t) + \mathbf{D}_{11}\mathbf{w}(t) + \mathbf{D}_{12}\mathbf{u}(t) \\ \mathbf{y}(t) &= \mathbf{C}_2\mathbf{x}(t) + \mathbf{D}_{21}\mathbf{w}(t) + \mathbf{D}_{22}\mathbf{u}(t), \end{aligned} \quad (2.7)$$

in which matrices  $\mathbf{C}_1$ ,  $\mathbf{D}_{11}$ , and  $\mathbf{D}_{12}$  are chosen to define the desired performance vector. All vectors and matrices have appropriate dimensions related to the number of inputs and outputs and to the model order.

The  $H_\infty$  control problem can be summarised in the block diagram of Fig. 2.1. In this figure,  $\mathbf{y}(t)$  is the output vector measured from the structural response,  $\mathbf{z}(t)$  is the performance vector,  $\mathbf{u}(t)$  are the control signals, and  $\mathbf{w}(t)$  represents the external disturbances. The structure

and the controller are respectively represented by transfer matrices  $\mathbf{P}(s)$  and  $\mathbf{K}_c(s)$ , where the dynamic controller  $\mathbf{K}_c$  is adopted with the following state-space representation:

$$\begin{aligned}\dot{\mathbf{x}}_c(t) &= \mathbf{A}_c \mathbf{x}_c(t) + \mathbf{B}_c \mathbf{y}(t) \\ \mathbf{u}(t) &= \mathbf{C}_c \mathbf{x}_c(t) + \mathbf{D}_c \mathbf{y}(t).\end{aligned}\quad (2.8)$$

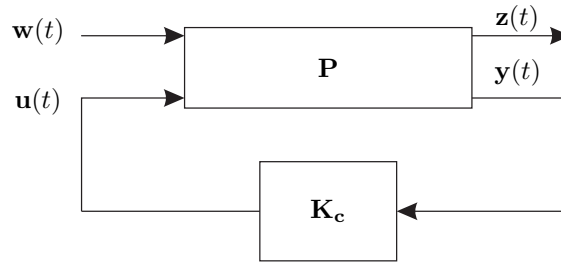


Figure 2.1 - Block diagram of the  $H_\infty$  control problem.

From Fig. 2.1, it is possible to write the following expression:

$$\begin{aligned}\begin{bmatrix} \mathbf{Z}(s) \\ \mathbf{Y}(s) \end{bmatrix} &= \mathbf{P}(s) \begin{bmatrix} \mathbf{W}(s) \\ \mathbf{U}(s) \end{bmatrix} \\ &= \begin{bmatrix} \mathbf{P}_{zw} & \mathbf{P}_{zu} \\ \mathbf{P}_{yw} & \mathbf{P}_{yu} \end{bmatrix} \begin{bmatrix} \mathbf{W}(s) \\ \mathbf{U}(s) \end{bmatrix},\end{aligned}\quad (2.9)$$

in which  $\mathbf{Z}(s)$ ,  $\mathbf{Y}(s)$ ,  $\mathbf{W}(s)$ , and  $\mathbf{U}(s)$  are respectively the Laplace transform of  $\mathbf{z}(t)$ ,  $\mathbf{y}(t)$ ,  $\mathbf{w}(t)$ , and  $\mathbf{u}(t)$ .

Considering Eq. (2.9) and the control effort given by  $\mathbf{U}(s) = \mathbf{K}_c(s)\mathbf{Y}(s)$ , it leads to:

$$\mathbf{Y}(s) = (\mathbf{I} - \mathbf{P}_{yu}(s)\mathbf{K}_c(s))^{-1}\mathbf{P}_{yw}(s)\mathbf{W}(s),$$

where the control effort can be written as:

$$\mathbf{U}(s) = \mathbf{K}_c(s)(\mathbf{I} - \mathbf{P}_{yu}(s)\mathbf{K}_c(s))^{-1}\mathbf{P}_{yw}(s)\mathbf{W}(s),\quad (2.10)$$

in which  $[\mathbf{K}_c(s)(\mathbf{I} - \mathbf{P}_{yu}(s)\mathbf{K}_c(s))^{-1}\mathbf{P}_{yw}(s)]$  is the transfer matrix between  $\mathbf{u}(t)$  and  $\mathbf{w}(t)$ , defined as  $\mathbf{T}_{uw}(s)$ .

In relation to  $\mathbf{Z}(s)$ , it is possible to write the following equation from Eq. (2.9):

$$\mathbf{Z}(s) = \mathbf{P}_{zw}(s)\mathbf{W}(s) + \mathbf{P}_{zu}(s)\mathbf{U}(s),$$

in which the following expression is obtained by considering Eq. (2.10):

$$\mathbf{Z}(s) = [\mathbf{P}_{zw}(s) + \mathbf{P}_{zu}(s)\mathbf{K}_c(s)(\mathbf{I} - \mathbf{P}_{yu}(s)\mathbf{K}_c(s))^{-1}\mathbf{P}_{yw}(s)]\mathbf{W}(s),$$

where  $[\mathbf{P}_{zw}(s) + \mathbf{P}_{zu}(s)\mathbf{K}_c(s)(\mathbf{I} - \mathbf{P}_{yu}(s)\mathbf{K}_c(s))^{-1}\mathbf{P}_{yw}(s)]$  represents the transfer matrix between  $\mathbf{z}(t)$  and  $\mathbf{w}(t)$ , defined as  $\mathbf{T}_{zw}(s)$ . Therefore:

$$\mathbf{Z}(s) = \mathbf{T}_{zw}(s)\mathbf{W}(s).$$

The optimal  $H_\infty$  problem consists in finding a controller  $\mathbf{K}_c(s)$  that minimises  $\|\mathbf{T}_{zw}\|_\infty$ . However, optimal  $H_\infty$  controllers are generally not unique for MIMO systems. Usually, to find an optimal  $H_\infty$  controller is often both numerically and theoretically complicated (ZHOU; DOYLE, 1997). One way to address this problem is to consider a feasible limit  $\gamma > 0$ , where a suboptimal approach is adopted to minimise  $\|\mathbf{T}_{zw}\|_\infty$ . The approach is based on successive iterations to find the controller  $\mathbf{K}_c(s)$  such that  $\|\mathbf{T}_{zw}\|_\infty < \gamma$ .

## 2.4 $H_\infty$ control solution using the LMI approach

Considering the controller given in Eq. (2.8) and the plant model described by Eq. (2.7), initially with  $\mathbf{D}_{22} = \mathbf{0}$  to facilitate the formulation, the closed-loop system is defined as:

$$\begin{aligned}\dot{\tilde{\mathbf{x}}}(t) &= \tilde{\mathbf{A}}\tilde{\mathbf{x}}(t) + \tilde{\mathbf{B}}\mathbf{w}(t) \\ \mathbf{z}(t) &= \tilde{\mathbf{C}}\tilde{\mathbf{x}}(t) + \tilde{\mathbf{D}}\mathbf{w}(t),\end{aligned}$$

in which

$$\begin{aligned}\tilde{\mathbf{A}} &= \begin{bmatrix} \mathbf{A} + \mathbf{B}_2\mathbf{D}_c\mathbf{C}_2 & \mathbf{B}_2\mathbf{C}_c \\ \mathbf{B}_c\mathbf{C}_2 & \mathbf{A}_c \end{bmatrix}, \tilde{\mathbf{B}} = \begin{bmatrix} \mathbf{B}_1 + \mathbf{B}_2\mathbf{D}_c\mathbf{D}_{21} \\ \mathbf{B}_c\mathbf{D}_{21} \end{bmatrix}, \\ \tilde{\mathbf{C}} &= \begin{bmatrix} \mathbf{C}_1 + \mathbf{D}_{12}\mathbf{D}_c\mathbf{C}_2 & \mathbf{D}_{12}\mathbf{C}_c \end{bmatrix}, \text{ and} \\ \tilde{\mathbf{D}} &= \mathbf{D}_{11} + \mathbf{D}_{12}\mathbf{D}_c\mathbf{D}_{21}.\end{aligned}$$

The standard  $H_\infty$  problem can be transformed into an optimisation problem with the



constraint in the LMI form as (BOYD et al., 1994; SCHERER et al., 1997):

$$\begin{aligned}
 & \text{minimise} \quad \|\mathbf{T}_{zw}\|_{\infty} \text{ until } \|\mathbf{T}_{zw}\|_{\infty} < \gamma \\
 & \text{subject to:} \quad \begin{bmatrix} \tilde{\mathbf{A}}^T \tilde{\mathbf{P}} + \tilde{\mathbf{P}} \tilde{\mathbf{A}} & \tilde{\mathbf{P}} \tilde{\mathbf{B}} & \tilde{\mathbf{C}}^T \\ \tilde{\mathbf{B}}^T \tilde{\mathbf{P}} & -\mathbf{I} & \tilde{\mathbf{D}}^T \\ \tilde{\mathbf{C}} & \tilde{\mathbf{D}} & -\gamma \mathbf{I} \end{bmatrix} < 0, \tilde{\mathbf{P}} > 0.
 \end{aligned} \tag{2.11}$$

Considering the decision variables of the problem, i.e., the state-space matrices of the controller realisation, there are nonlinear terms in (2.11). It is necessary to use an appropriate transformation of variables to eliminate them. These variable manipulations are fundamental for the problem in an LMI-based solution. For this purpose, a symmetric matrix  $\tilde{\mathbf{P}}$  is defined as:

$$\tilde{\mathbf{P}} = \begin{bmatrix} \mathbf{X} & \mathbf{U}^T \\ \mathbf{U} & \hat{\mathbf{X}} \end{bmatrix} \text{ and } \tilde{\mathbf{P}}^{-1} = \begin{bmatrix} \mathbf{Y} & \mathbf{V}^T \\ \mathbf{V} & \hat{\mathbf{Y}} \end{bmatrix},$$

in which  $\mathbf{X}$  and  $\mathbf{Y}$  are symmetric,  $\mathbf{V}\mathbf{U}^T = \mathbf{I} - \mathbf{X}\mathbf{Y}$ , and  $\tilde{\mathbf{P}}\tilde{\mathbf{P}}^{-1} = \tilde{\mathbf{P}}^{-1}\tilde{\mathbf{P}} = \mathbf{I}$ .

Let  $\mathbf{T}$  be a transformation matrix defined as:

$$\mathbf{T} = \begin{bmatrix} \mathbf{Y} & \mathbf{I} \\ \mathbf{V} & \mathbf{0} \end{bmatrix},$$

then the result of the congruence transformation applied to the constraint  $\tilde{\mathbf{P}} > 0$  is given by:

$$\mathbf{T}^T \tilde{\mathbf{P}} \mathbf{T} = \begin{bmatrix} \mathbf{Y} & \mathbf{I} \\ \mathbf{I} & \mathbf{X} \end{bmatrix} > 0.$$

The application of the following congruence matrix transformation into constraint (2.11) leads to:

$$\begin{aligned}
 & \begin{bmatrix} \mathbf{T}^T & \mathbf{0} & \mathbf{0} \\ \mathbf{0} & \mathbf{I} & \mathbf{0} \\ \mathbf{0} & \mathbf{0} & \mathbf{I} \end{bmatrix} \begin{bmatrix} \tilde{\mathbf{A}}^T \tilde{\mathbf{P}} + \tilde{\mathbf{P}} \tilde{\mathbf{A}} & \tilde{\mathbf{P}} \tilde{\mathbf{B}} & \tilde{\mathbf{C}}^T \\ \tilde{\mathbf{B}}^T \tilde{\mathbf{P}} & -\mathbf{I} & \tilde{\mathbf{D}}^T \\ \tilde{\mathbf{C}} & \tilde{\mathbf{D}} & -\gamma \mathbf{I} \end{bmatrix} \begin{bmatrix} \mathbf{T} & \mathbf{0} & \mathbf{0} \\ \mathbf{0} & \mathbf{I} & \mathbf{0} \\ \mathbf{0} & \mathbf{0} & \mathbf{I} \end{bmatrix} < 0 \\
 & \begin{bmatrix} \mathbf{T}^T (\tilde{\mathbf{A}}^T \tilde{\mathbf{P}} + \tilde{\mathbf{P}} \tilde{\mathbf{A}}) \mathbf{T} & \mathbf{T}^T \tilde{\mathbf{P}} \tilde{\mathbf{B}} & \mathbf{T}^T \tilde{\mathbf{C}}^T \\ \tilde{\mathbf{B}}^T \tilde{\mathbf{P}} \mathbf{T} & -\mathbf{I} & \tilde{\mathbf{D}}^T \\ \tilde{\mathbf{C}} \mathbf{T} & \tilde{\mathbf{D}} & -\gamma \mathbf{I} \end{bmatrix} < 0,
 \end{aligned}$$

where it is easy to obtain the following identities:

$$\begin{aligned}\tilde{\mathbf{C}}\mathbf{T} &= \begin{bmatrix} \mathbf{C}_1\mathbf{Y} + \mathbf{D}_{12}\mathbf{F} & \mathbf{C}_1 + \mathbf{D}_{12}\mathbf{D}_c\mathbf{C}_2 \end{bmatrix} \\ \tilde{\mathbf{B}}^T\tilde{\mathbf{P}}\mathbf{T} &= \begin{bmatrix} \mathbf{B}_1^T + \mathbf{D}_{21}^T\mathbf{D}_c^T\mathbf{B}_2^T & \mathbf{B}_1^T\mathbf{X} + \mathbf{D}_{21}^T\mathbf{L}^T \end{bmatrix} \\ \mathbf{T}^T\tilde{\mathbf{P}}\tilde{\mathbf{A}}\mathbf{T} &= \begin{bmatrix} \mathbf{A}\mathbf{Y} + \mathbf{B}_2\mathbf{F} & \mathbf{A} + \mathbf{B}_2\mathbf{D}_c\mathbf{C}_2 \\ \mathbf{M} & \mathbf{X}\mathbf{A} + \mathbf{L}\mathbf{C}_2 \end{bmatrix},\end{aligned}$$

in which  $\mathbf{F} = \mathbf{D}_c\mathbf{C}_2\mathbf{Y} + \mathbf{C}_c\mathbf{V}$ ,  $\mathbf{L} = \mathbf{X}\mathbf{B}_2\mathbf{D}_c + \mathbf{U}^T\mathbf{B}_c$ , and  $\mathbf{M} = \mathbf{X}\mathbf{A}\mathbf{Y} + \mathbf{X}\mathbf{B}_2\mathbf{F} + \mathbf{U}^T\mathbf{B}_c\mathbf{C}_2\mathbf{Y} + \mathbf{U}^T\mathbf{A}_c\mathbf{V}$ .

Thus, the standard  $H_\infty$  problem can be formulated as the following optimisation problem:

$$\begin{aligned} & \text{minimise} \quad \|\mathbf{T}_{zw}\|_\infty \text{ until } \|\mathbf{T}_{zw}\|_\infty < \gamma \\ & \text{subject to:} \quad \begin{bmatrix} \mathbf{R}_1 & \mathbf{R}_2 & \mathbf{R}_3 \\ \mathbf{R}_2^T & -\mathbf{I} & \mathbf{R}_4 \\ \mathbf{R}_3^T & \mathbf{R}_4^T & -\gamma\mathbf{I} \end{bmatrix} < 0 \\ & \quad \quad \quad \begin{bmatrix} \mathbf{Y} & \mathbf{I} \\ \mathbf{I} & \mathbf{X} \end{bmatrix} > 0, \end{aligned} \quad (2.12)$$

in which the optimisation variables are  $\gamma$ ,  $\mathbf{X}$ ,  $\mathbf{Y}$ ,  $\mathbf{F}$ ,  $\mathbf{L}$ ,  $\mathbf{M}$ , and  $\mathbf{D}_c$ . Moreover:

$$\begin{aligned}\mathbf{R}_1 &= \begin{bmatrix} \mathbf{Y}\mathbf{A}^T + \mathbf{F}^T\mathbf{B}_2^T & \mathbf{M}^T \\ \mathbf{A}^T + \mathbf{C}_2^T\mathbf{D}_c^T\mathbf{B}_2^T & \mathbf{A}^T\mathbf{X} + \mathbf{C}_2^T\mathbf{L}^T \end{bmatrix} + \begin{bmatrix} \mathbf{A}\mathbf{Y} + \mathbf{B}_2\mathbf{F} & \mathbf{A} + \mathbf{B}_2\mathbf{D}_c\mathbf{C}_2 \\ \mathbf{M} & \mathbf{X}\mathbf{A} + \mathbf{L}\mathbf{C}_2 \end{bmatrix}, \\ \mathbf{R}_2 &= \begin{bmatrix} \mathbf{B}_1 + \mathbf{B}_2\mathbf{D}_c\mathbf{D}_{21} \\ \mathbf{X}\mathbf{B}_1 + \mathbf{L}\mathbf{D}_{21} \end{bmatrix}, \mathbf{R}_3 = \begin{bmatrix} \mathbf{Y}\mathbf{C}_1^T + \mathbf{F}^T\mathbf{D}_{12}^T \\ \mathbf{C}_1^T + \mathbf{C}_2^T\mathbf{D}_c^T\mathbf{D}_{12}^T \end{bmatrix}, \text{ and} \\ \mathbf{R}_4 &= \mathbf{D}_{11}^T + \mathbf{D}_{21}^T\mathbf{D}_c^T\mathbf{D}_{12}^T.\end{aligned}$$

The controller for  $\mathbf{D}_{22} = \mathbf{0}$  is given by:

$$\begin{aligned}\dot{\mathbf{x}}_c(t) &= \hat{\mathbf{A}}_c\mathbf{x}_c(t) + \hat{\mathbf{B}}_c\hat{\mathbf{y}}(t), \\ \mathbf{u}(t) &= \hat{\mathbf{C}}_c\mathbf{x}_c(t) + \hat{\mathbf{D}}_c\hat{\mathbf{y}}(t),\end{aligned} \quad (2.13)$$

where  $\hat{\mathbf{A}}_c = (\mathbf{U}^T)^{-1}(\mathbf{M} - \mathbf{X}\mathbf{A}\mathbf{Y} - \mathbf{X}\mathbf{B}_2\mathbf{F} - \mathbf{U}^T\mathbf{B}_c\mathbf{C}_2\mathbf{Y})\mathbf{V}^{-1}$ ,  $\hat{\mathbf{B}}_c = (\mathbf{U}^T)^{-1}(\mathbf{L} - \mathbf{X}^T\mathbf{B}_2\mathbf{D}_c)$ , and  $\hat{\mathbf{C}}_c = (\mathbf{F} - \mathbf{D}_c\mathbf{C}_2\mathbf{Y})\mathbf{V}^{-1}$ .

From the controller given in Eq. (2.13), it is possible to extend the controller for  $\mathbf{D}_{22} \neq \mathbf{0}$ . The relation between  $\hat{\mathbf{y}}(t)$  and  $\mathbf{y}(t)$  is given by:

$$\hat{\mathbf{y}}(t) = \mathbf{y}(t) - \mathbf{D}_{22}\mathbf{u}(t). \quad (2.14)$$

Substituting Eq. (2.14) into Eq. (2.13), it results in:

$$\dot{\mathbf{x}}_c(t) = \hat{\mathbf{A}}_c\mathbf{x}_c(t) + \hat{\mathbf{B}}_c\mathbf{y}(t) - \hat{\mathbf{B}}_c\mathbf{D}_{22}\mathbf{u}(t) \quad (2.15)$$

$$\mathbf{u}(t) = (\mathbf{I} + \hat{\mathbf{D}}_c\mathbf{D}_{22})^{-1}\hat{\mathbf{C}}_c\mathbf{x}_c(t) + (\mathbf{I} + \hat{\mathbf{D}}_c\mathbf{D}_{22})^{-1}\hat{\mathbf{D}}_c\mathbf{y}(t). \quad (2.16)$$

Finally, substituting Eq. (2.16) into Eq. (2.15), it gives:

$$\dot{\mathbf{x}}_c(t) = [\hat{\mathbf{A}}_c - \hat{\mathbf{B}}_c\mathbf{D}_{22}(\mathbf{I} + \hat{\mathbf{D}}_c\mathbf{D}_{22})^{-1}\hat{\mathbf{C}}_c]\mathbf{x}_c(t) + [\hat{\mathbf{B}}_c - \hat{\mathbf{B}}_c\mathbf{D}_{22}(\mathbf{I} + \hat{\mathbf{D}}_c\mathbf{D}_{22})^{-1}\hat{\mathbf{D}}_c]\mathbf{y}(t).$$

Therefore, the controller matrices considering the full plant are given by:

$$\begin{aligned} \mathbf{A}_c &= \hat{\mathbf{A}}_c - \hat{\mathbf{B}}_c\mathbf{D}_{22}(\mathbf{I} + \hat{\mathbf{D}}_c\mathbf{D}_{22})^{-1}\hat{\mathbf{C}}_c, \\ \mathbf{B}_c &= \hat{\mathbf{B}}_c - \hat{\mathbf{B}}_c\mathbf{D}_{22}(\mathbf{I} + \hat{\mathbf{D}}_c\mathbf{D}_{22})^{-1}\hat{\mathbf{D}}_c, \\ \mathbf{C}_c &= (\mathbf{I} + \hat{\mathbf{D}}_c\mathbf{D}_{22})^{-1}\hat{\mathbf{C}}_c, \text{ and} \\ \mathbf{D}_c &= (\mathbf{I} + \hat{\mathbf{D}}_c\mathbf{D}_{22})^{-1}\hat{\mathbf{D}}_c. \end{aligned}$$

## 2.5 Weighing filters

The weighing filters may be applied to the input and/or the output of the plant in the controller design step. These filters have the objective of specifying a frequency band in which the controller is going to act, aiming to explore some characteristics such as bounding the control signals, obtaining a reasonable trade-off between performance and robustness, and designing controllers based on the reduced-order model.

Figure 2.2 presents the block diagram of the  $H_\infty$  control problem. In this figure, the filters  $\mathbf{F}_u$  and  $\mathbf{F}_z$  are applied to the control signal vector  $\mathbf{u}(t)$  and the performance vector  $\mathbf{z}(t)$ , generating respectively  $\mathbf{z}_u(t)$  and  $\bar{\mathbf{z}}(t)$ . The nominal plant is denoted by  $\mathbf{G}_n(s)$  and the generalised plant is  $\mathbf{G}_g(s)$ .

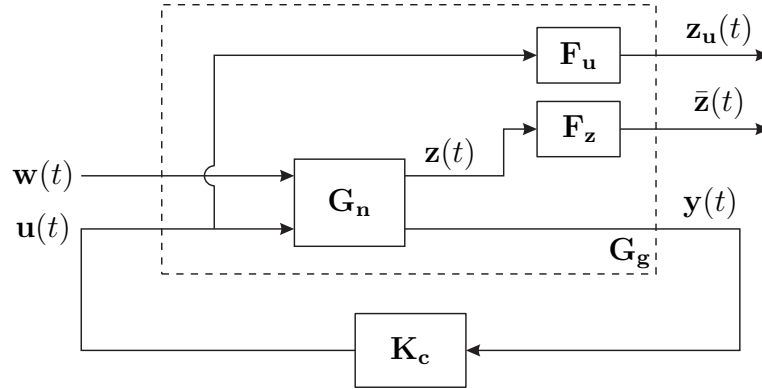


Figure 2.2 - Block diagram of the regular  $H_\infty$  control problem.

Considering a state space realisation of  $G_n(s)$  given by:

$$\begin{aligned}\dot{\mathbf{x}}_p(t) &= \mathbf{A}_p \mathbf{x}_p(t) + \mathbf{B}_{1p} \mathbf{w}(t) + \mathbf{B}_{2p} \mathbf{u}(t) \\ \mathbf{z}(t) &= \mathbf{C}_{1p} \mathbf{x}_p(t) + \mathbf{D}_{11p} \mathbf{w}(t) + \mathbf{D}_{12p} \mathbf{u}(t) \\ \mathbf{y}(t) &= \mathbf{C}_{2p} \mathbf{x}_p(t) + \mathbf{D}_{21p} \mathbf{w}(t) + \mathbf{D}_{22p} \mathbf{u}(t),\end{aligned}$$

and the state-space model of  $F_z$  as:

$$\begin{aligned}\dot{\mathbf{x}}_z(t) &= \mathbf{A}_z \mathbf{x}_z(t) + \mathbf{B}_z \mathbf{z}(t) \\ \bar{\mathbf{z}}(t) &= \mathbf{C}_z \mathbf{x}_z(t) + \mathbf{D}_z \mathbf{z}(t),\end{aligned}$$

it is possible to write the following pair of equations:

$$\begin{aligned}\dot{\mathbf{x}}_z(t) &= \mathbf{A}_z \mathbf{x}_z(t) + \mathbf{B}_z \mathbf{C}_{1p} \mathbf{x}_p(t) + \mathbf{B}_z \mathbf{D}_{11p} \mathbf{w}(t) + \mathbf{B}_z \mathbf{D}_{12p} \mathbf{u}(t) \\ \bar{\mathbf{z}}(t) &= \mathbf{C}_z \mathbf{x}_z(t) + \mathbf{D}_z \mathbf{C}_{1p} \mathbf{x}_p(t) + \mathbf{D}_z \mathbf{D}_{11p} \mathbf{w}(t) + \mathbf{D}_z \mathbf{D}_{12p} \mathbf{u}(t).\end{aligned}$$

Let the state-space model of  $F_u$  be defined as:

$$\begin{aligned}\dot{\mathbf{x}}_u(t) &= \mathbf{A}_u \mathbf{x}_u(t) + \mathbf{B}_u \mathbf{u}(t) \\ \mathbf{z}_u(t) &= \mathbf{C}_u \mathbf{x}_u(t) + \mathbf{D}_u \mathbf{u}(t),\end{aligned}$$

and let the controller signal input be given by:

$$\mathbf{y}(t) = \mathbf{C}_{2p} \mathbf{x}_p(t) + \mathbf{D}_{21p} \mathbf{w}(t) + \mathbf{D}_{22p} \mathbf{u}(t),$$

then it is possible to write the extended plant as:

$$\begin{aligned}
\begin{bmatrix} \dot{\mathbf{x}}_p(t) \\ \dot{\mathbf{x}}_u(t) \\ \dot{\mathbf{x}}_z(t) \end{bmatrix} &= \begin{bmatrix} \mathbf{A}_p & \mathbf{0} & \mathbf{0} \\ \mathbf{0} & \mathbf{A}_u & \mathbf{0} \\ \mathbf{B}_z \mathbf{C}_{1p} & \mathbf{0} & \mathbf{A}_z \end{bmatrix} \begin{bmatrix} \mathbf{x}_p(t) \\ \mathbf{x}_u(t) \\ \mathbf{x}_z(t) \end{bmatrix} + \begin{bmatrix} \mathbf{B}_{1p} \\ \mathbf{0} \\ \mathbf{B}_z \mathbf{D}_{11p} \end{bmatrix} \mathbf{w}(t) + \begin{bmatrix} \mathbf{B}_{2p} \\ \mathbf{B}_u \\ \mathbf{B}_z \mathbf{D}_{12p} \end{bmatrix} \mathbf{u}(t) \\
\begin{bmatrix} \bar{\mathbf{z}} \\ \mathbf{z}_u \end{bmatrix} &= \begin{bmatrix} \mathbf{D}_z \mathbf{C}_{1p} & \mathbf{0} & \mathbf{C}_z \\ \mathbf{0} & \mathbf{C}_u & \mathbf{0} \end{bmatrix} \begin{bmatrix} \mathbf{x}_p(t) \\ \mathbf{x}_u(t) \\ \mathbf{x}_z(t) \end{bmatrix} + \begin{bmatrix} \mathbf{D}_z \mathbf{D}_{11p} \\ \mathbf{0} \end{bmatrix} \mathbf{w}(t) + \begin{bmatrix} \mathbf{D}_z \mathbf{D}_{12p} \\ \mathbf{D}_u \end{bmatrix} \mathbf{u}(t) \\
\mathbf{y}(t) &= \begin{bmatrix} \mathbf{C}_{2p} & \mathbf{0} & \mathbf{0} \end{bmatrix} \begin{bmatrix} \mathbf{x}_p(t) \\ \mathbf{x}_u(t) \\ \mathbf{x}_z(t) \end{bmatrix} + \mathbf{D}_{21p} \mathbf{w}(t) + \mathbf{D}_{22p} \mathbf{u}(t). \tag{2.17}
\end{aligned}$$

Comparing the model given in Eq. (2.17) with the extended model given in Eq. (2.7), commonly used to design  $H_\infty$  controllers, it is possible to write the standard model with filter as:

$$\begin{aligned}
\mathbf{A} &= \begin{bmatrix} \mathbf{A}_p & \mathbf{0} & \mathbf{0} \\ \mathbf{0} & \mathbf{A}_u & \mathbf{0} \\ \mathbf{B}_z \mathbf{C}_{1p} & \mathbf{0} & \mathbf{A}_z \end{bmatrix}, \mathbf{B}_1 = \begin{bmatrix} \mathbf{B}_{1p} \\ \mathbf{0} \\ \mathbf{B}_z \mathbf{D}_{11p} \end{bmatrix}, \mathbf{B}_2 = \begin{bmatrix} \mathbf{B}_{2p} \\ \mathbf{B}_u \\ \mathbf{B}_z \mathbf{D}_{12p} \end{bmatrix}, \\
\mathbf{C}_1 &= \begin{bmatrix} \mathbf{D}_z \mathbf{C}_{1p} & \mathbf{0} & \mathbf{C}_z \\ \mathbf{0} & \mathbf{C}_u & \mathbf{0} \end{bmatrix}, \mathbf{D}_{11} = \begin{bmatrix} \mathbf{D}_z \mathbf{D}_{11p} \\ \mathbf{0} \end{bmatrix}, \mathbf{D}_{12} = \begin{bmatrix} \mathbf{D}_z \mathbf{D}_{12p} \\ \mathbf{D}_u \end{bmatrix}, \\
\mathbf{C}_2 &= \begin{bmatrix} \mathbf{C}_{2p} & \mathbf{0} & \mathbf{0} \end{bmatrix}, \mathbf{D}_{21} = \mathbf{D}_{21p}, \text{ and } \mathbf{D}_{22} = \mathbf{D}_{22p}.
\end{aligned}$$

## 2.6 Application: vibration control of a vertical structure subject to seismic events

This section presents experimental and analytical results concerning the structure identification and the active robust control. Initially, a specific test bench simulating a tall building equipped with an Active Mass Driver (AMD) is presented. After that, the state-space model of the flexible structure is identified using experimental data. To conclude, the  $H_\infty$  controller is designed, tested through simulations, and examined experimentally, following the procedure presented in this chapter.

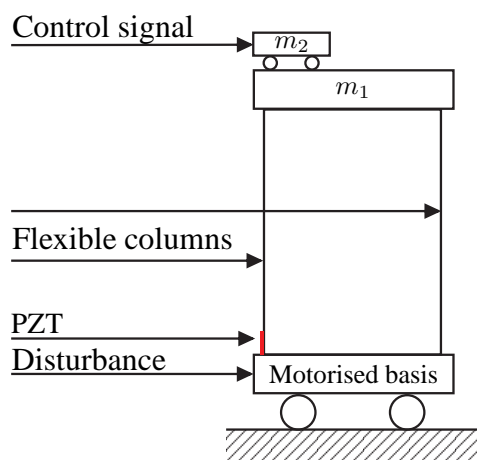
### 2.6.1 Structure description and identification

The vertical structure with a total mass of 16 kg and height of 824 mm is presented in Fig. 2.3(a) and can be divided into three main parts: basis, flexible system that simulates a tall building, and the AMD. The basis comprises a lead-screw mechanism coupled to the mechanical structure. Thus, the rotational movements of a DC motor of 35 W and 5500 rpm are converted into linear movements of the basis. The structure comprises mass  $m_1$  supported by four aluminium columns attached to the basis and there is a piezoelectric element, with dimensions of 0.5 mm  $\times$  20 mm  $\times$  20 mm, glued onto one column to measure lateral vibration. The active mass  $m_2$  is linearly moved by another DC motor by using a similar lead screw mechanism. Furthermore, movements of the basis and of the mass  $m_2$  are measured using two similar encoders of 2500 pulses per revolution and the DC motors are activated by power drives based on PWM signals.

The control system is designed to minimise vibrations caused by the basis movement. For this purpose, a control signal is used to create a specific movement of the AMD to compensate perturbations. Thus, the dynamic force produced by  $m_2$  displacement over the structure is responsible for vibration attenuation. Figure 2.3(b) shows the block diagram that describes the structure with the main input/output signals. Furthermore, a dSPACE<sup>®</sup> board model DS 1104 and ControlDesk<sup>®</sup> software are used for data acquisition, signal generation, and data processing.



(a) Vertical Structure.



(b) Block diagram.

Figure 2.3 - Experiment setup.

One of the main steps of the control design is to develop an accurate mathematical model of the system. There are several methods to elaborate the dynamical model. The identification strategy is adopted, based on relations between inputs and outputs. To collect high-quality input/output data, it is necessary to know the structure operation conditions (DYKE et al., 1996). In this work, the goal is to control a vertical flexible structure subject to seismic events. Thus, it is needed to know the frequency bands of these events that produce the highest vibrational effects in the structures. For this purpose, the earthquake parameters obtained from (SPENCER et al., 1994) about the San Jose N59E and the Kern County N90E earthquakes and from (ABREU; LOPES JR., 2010) about the Scaled El Centro earthquake are used to determine the frequency region for identification. The earthquake frequency spectrum can be simulated using the following equation, which is the well-known Kanai-Tajimi spectrum (ABREU; LOPES JR., 2010):

$$N_{sp}(s) = \sqrt{S} \frac{(2\zeta_{sp}\omega_{sp}s + \omega_{sp}^2)}{(s^2 + 2\zeta_{sp}\omega_{sp}s + \omega_{sp}^2)},$$

where  $N_{sp}(s)$  has been simulated for three different earthquakes. The used parameters and the acquired spectra are present respectively in Table 2.1 and Fig. 2.4

Table 2.1 - Parameters to simulate the Kanai-Tajimi spectra.

| Parameters            | San Jose N59E        | County N90E          | Scaled El Centro |
|-----------------------|----------------------|----------------------|------------------|
| $\omega_{sp}$ (rad/s) | 31.12                | 10.516               | 15               |
| $\zeta_{sp}$          | 0.064                | 0.317                | 0.5              |
| $S$                   | $4.5 \times 10^{-4}$ | $4.5 \times 10^{-4}$ | 0.005            |

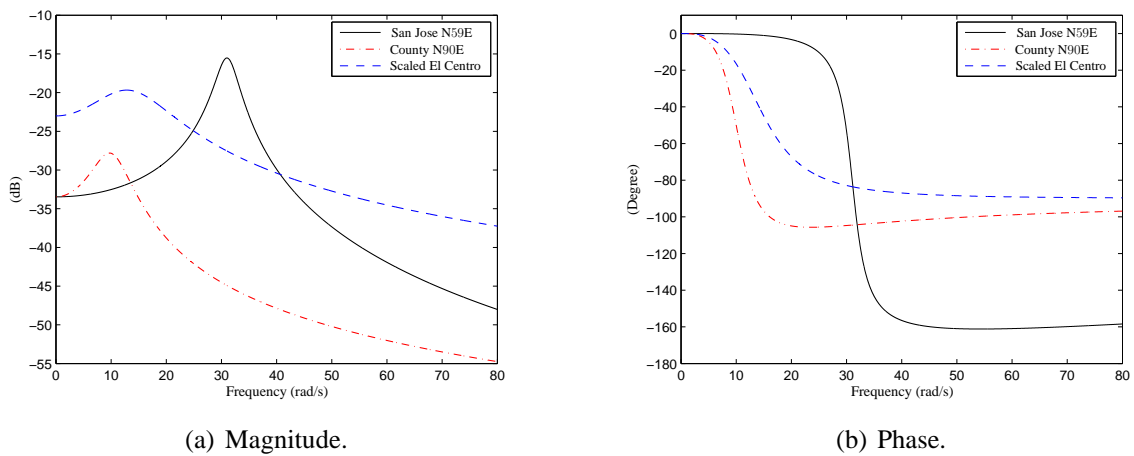


Figure 2.4 - Kanai-Tajimi spectra for three different earthquakes.

Considering the three spectra shown in Fig. 2.4, great part of the energy of real earthquakes is concentrated between 0 and 38 rad/s. Thus, the flexible structure should be identified

in this frequency region. For this purpose, a deterministic Schroeder signal with band between 0 and 38 rad/s, duration of 20 seconds, and sampled at 100 Hz is used as the input signal (see Fig. 2.5(a)). To determine the relation between the control signal and the structure response, the Schroeder signal is applied as a control signal and the disturbance is set to zero (the basis is stopped). To determine the relation between the disturbance and the PZT signal, the Schroeder signal is applied as a disturbance and the control signal is set to zero (the AMD is stopped). These experimental signals are shown in Fig. 2.5.

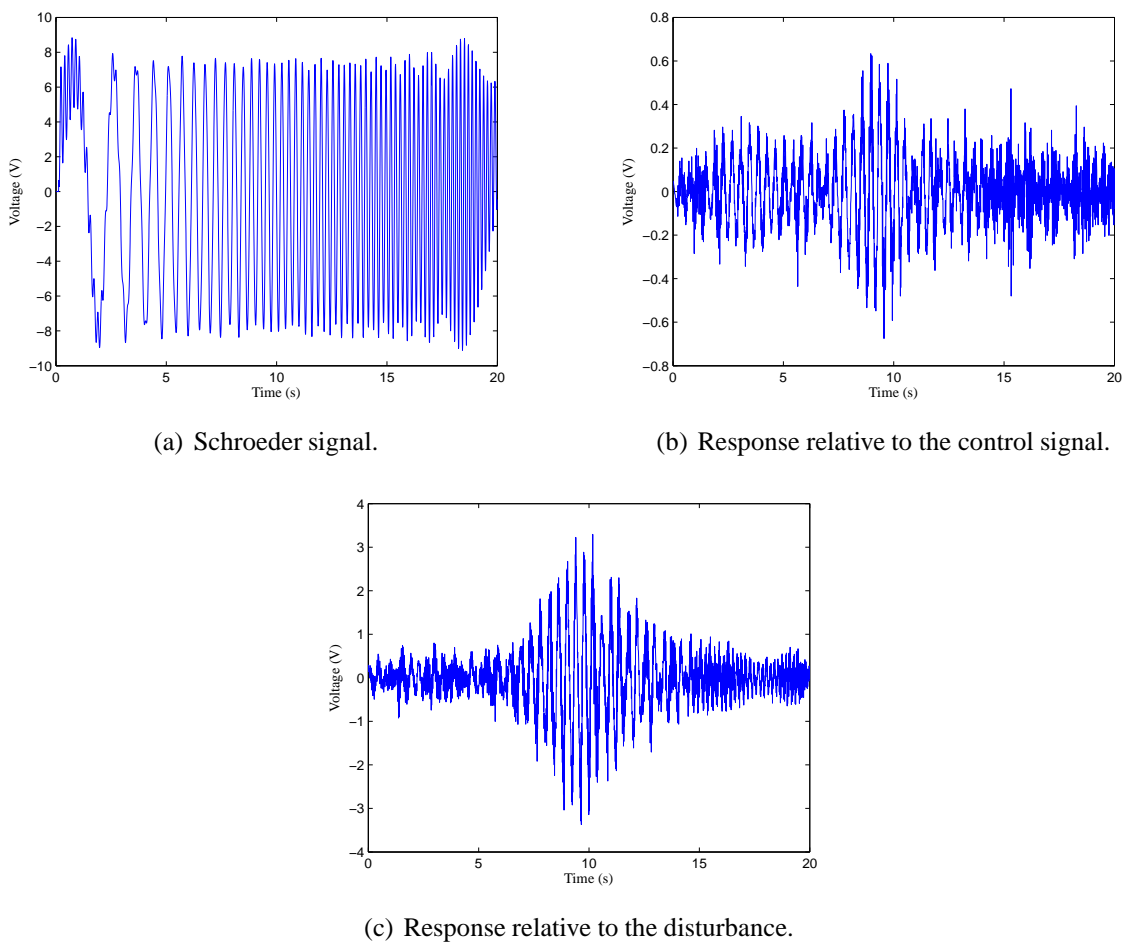


Figure 2.5 - Experimental signals used for system identification.

The transfer function between the PZT signal and the control signal is defined by  $P_{yu}$ , and  $P_{yw}$  is the transfer function between the PZT response and the disturbance signal. Thus,  $P_{yu}$  and  $P_{yw}$  are determined from the signals of Fig. 2.5 using the *tfestimate* MATLAB<sup>®</sup> function. Furthermore, the *ssest* function is used to identify the state-space model of the flexible structure. The identified model has order three, with two states representing one mode of the structure and one state describing the dynamics of the two similar DC motors. The experimental  $P_{yu}$  and  $P_{yw}$  and the respective model are presented and compared in Fig. 2.6.



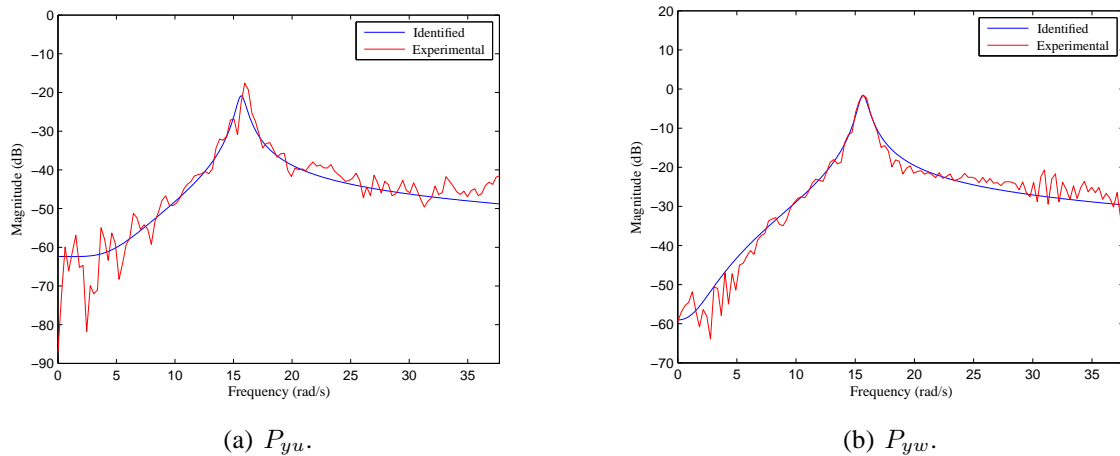


Figure 2.6 - Identified model.

### 2.6.2 Controller design

The robust controller is designed using the function *mincx* of MATLAB<sup>®</sup> to solve the optimisation problem given in (2.12). Figure 2.7 compares the frequency response of the open-loop and closed-loop systems.

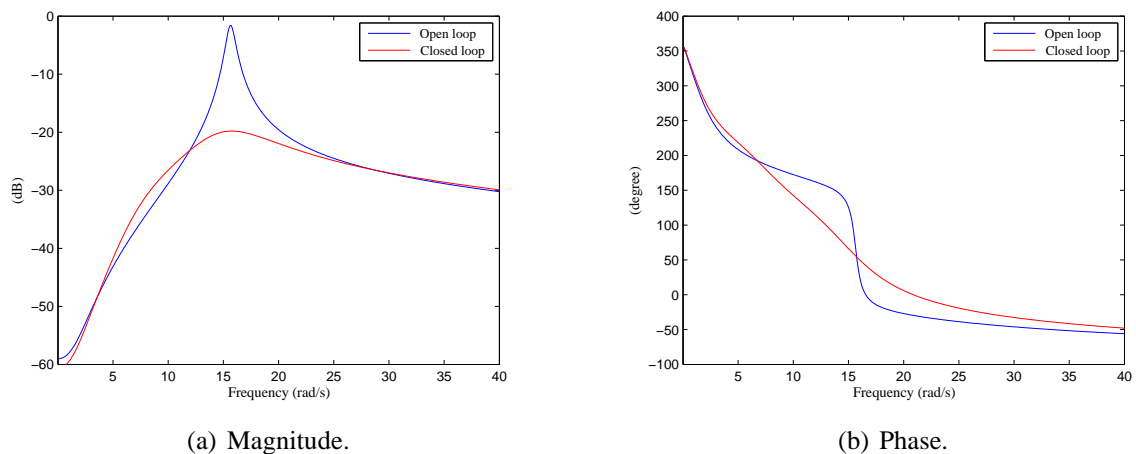


Figure 2.7 - Frequency response comparison between the open-loop and the closed-loop systems.

To analyse the control performance, a chirp signal presented in Fig. 2.8(a) with frequency band between 0 and 38 rad/s, an amplitude of 4 V, duration of 20 seconds, and sampled at 100 Hz is used as the disturbance signal. The structure response in open loop and in closed loop is compared in Fig. 2.8(b). The controller reduced vibrations by almost 78%, generating

a control signal that has values between 34 V and -34 V, as shown in Fig. 2.8(c). However, the control signal must be between -15 V and 15 V due to the bench-scale structure characteristic. Thus, the controller design is refined considering the control input limit.

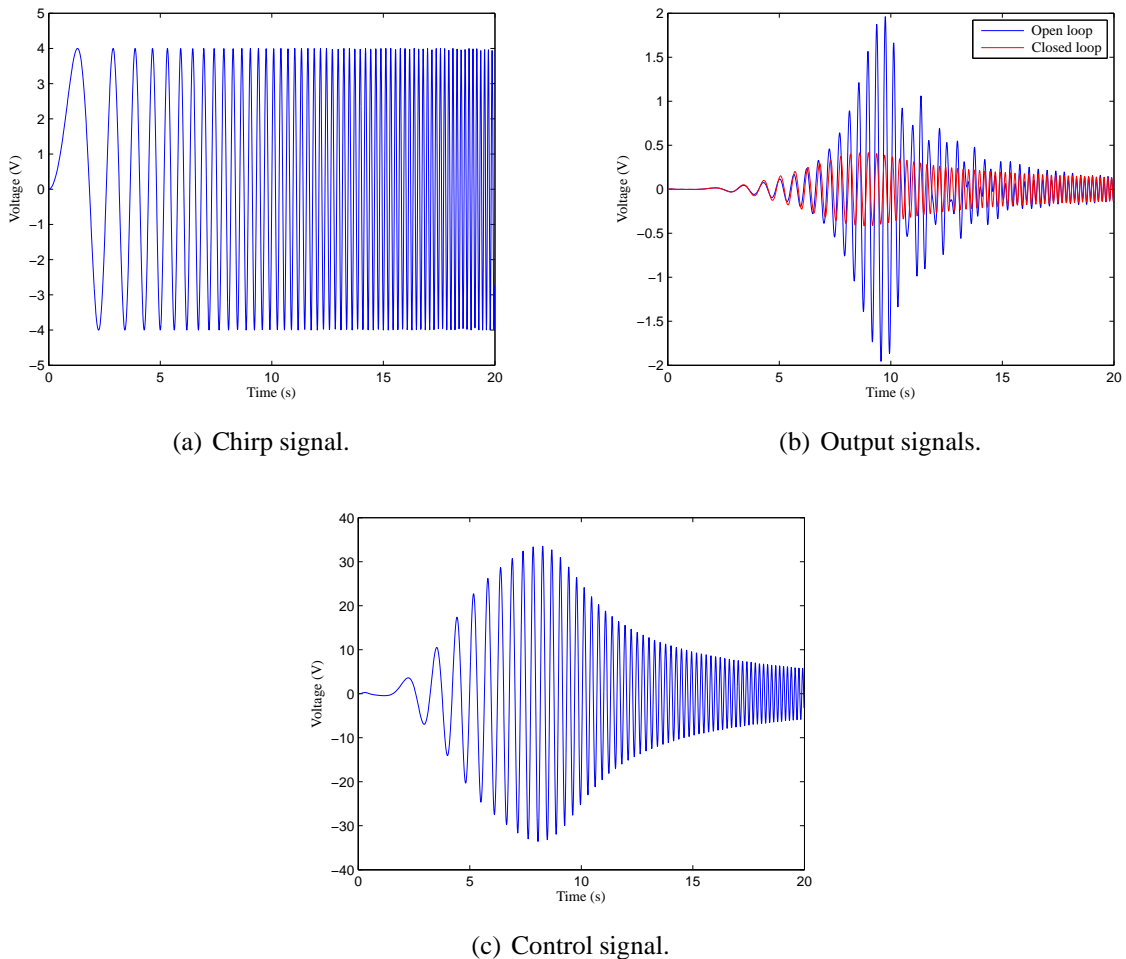


Figure 2.8 - Signals used to analyse the controller performance.

A weighting function is used to reduce the control signal. This function should reduce the control signal in the interest band and does not produce any significant control signal outside it, in order to avoid the spillover phenomenon. The weighting function is given by (ZHOU; DOYLE, 1997):

$$F_{\mathbf{u}}(s) = \left( \frac{s + \frac{\omega_c}{kM}}{s \sqrt[k]{\varepsilon} + \omega_c} \right)^k,$$

in which  $\omega_c$ ,  $k$ ,  $\varepsilon$ , and  $M$  determine the transition frequency between rejection band and pass-band, the filter order, the gain at passband, and the gain at rejection band, respectively. For this application, the weighting function parameters are selected as:  $\omega_c = 125$  rad/s,  $\varepsilon = 0.09$ ,  $M = 17$ , and  $k = 2$ . The frequency response of  $F_{\mathbf{u}}(s)$  is presented in Fig. 2.9. It is worth noting that the weighing is small in the interest frequency band to ensure the desired control signal and

the weighing is large outside the interest band to avoid the spillover effect.

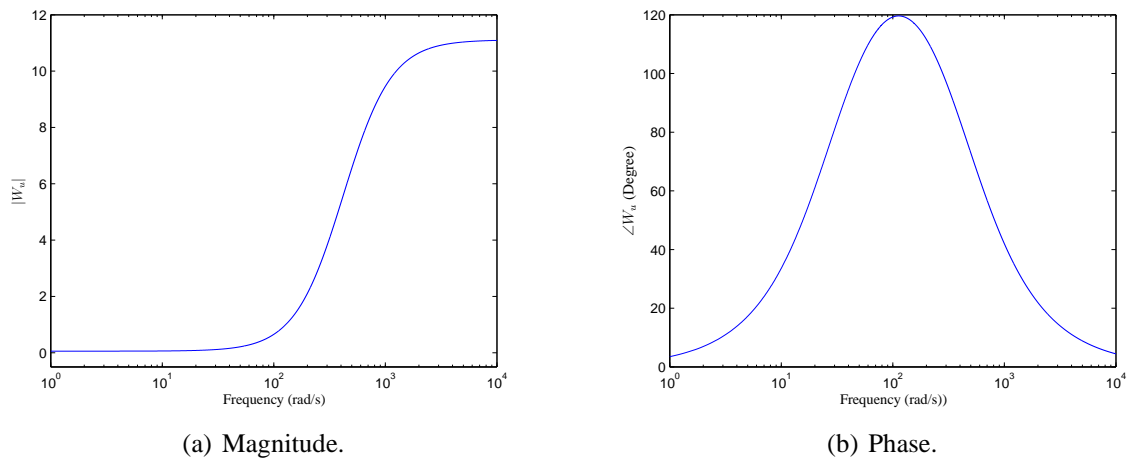


Figure 2.9 - Frequency response of filter  $F_u(s)$ .

The new controller is designed using the generalised plant, where the frequency response comparison between the open-loop and the closed-loop systems is presented in Fig. 2.10. These results are clearer when the time response is analysed. Figure 2.11(a) compares the vibration response of the uncontrolled and the controlled structure when the disturbance is the chirp signal of Fig. 2.8(a). For this case, the vibration attenuation is 27% and the control signal is within the limits of -15 V and 15 V, as can be seen in Fig. 2.11(b). Additionally, to test the control system efficiency when the structure is excited in the natural frequency of 15.6 rad/s, a sinusoid with 3 V of amplitude and frequency of 15.6 rad/s is used. Figure 2.12 shows the vibration reduction when the sinusoid is applied as the disturbance. The vibration reduction in this case is 48% and the control signal is within the stipulated limit.

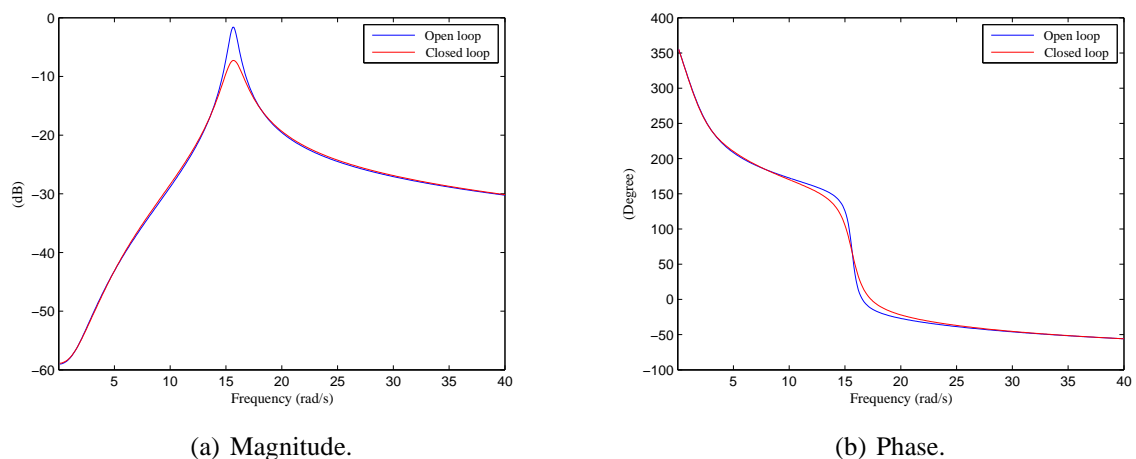
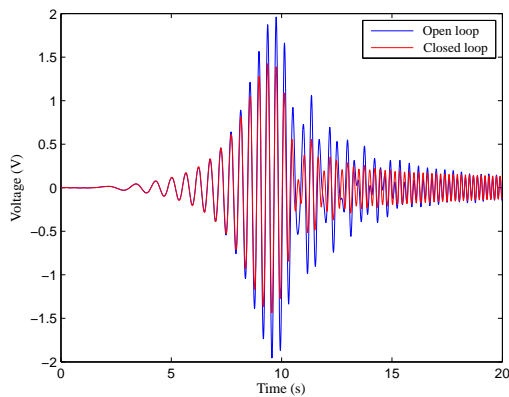
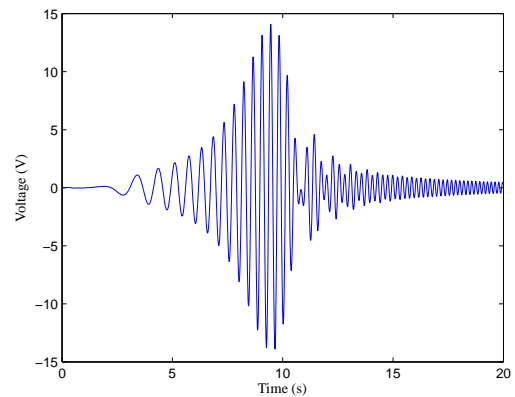


Figure 2.10 - Frequency response comparison between open-loop and closed-loop systems.

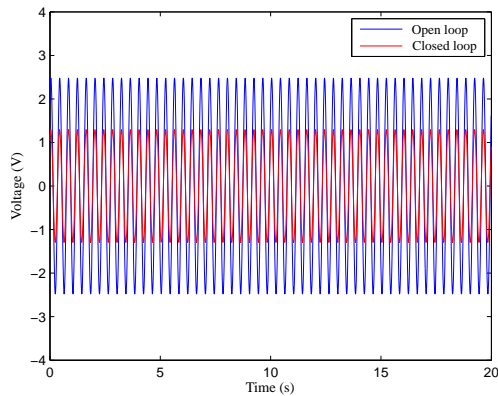


(a) Output signals.

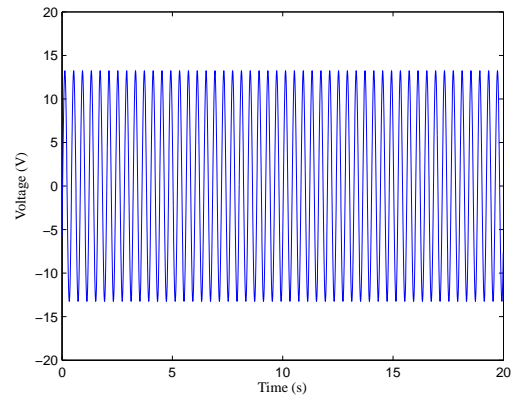


(b) Control signal.

Figure 2.11 - Simulated response when the disturbance is a chirp signal.



(a) Output signals.



(b) Control signal.

Figure 2.12 - Simulated response when the structure is excited in its natural frequency.

### 2.6.3 Experimental results

The controller is experimentally tested using the structure presented in Fig. 2.3. Initially, the chirp signal of Fig. 2.8(a) is created and applied as a disturbance in the vertical structure. The experimental vibration reduction is 36%, as depicted in Fig. 2.13, an increase of 9% compared to simulation. This increase is expected due to the small difference between the experimental frequency response and the model, as shown in Fig. 2.6(a). Furthermore, the control signals are similar in the experiment and in the simulation. To complete the experimentation, a sinusoid used in the simulated case is created and applied in the structure as a disturbance. The experimental vibration reduction for this case is almost 48% and is similar to the simulated case,

as can be seen in Fig. 2.14(a). Moreover, the control signals generated to counterbalance the vibration effects caused by perturbations are similar in the simulated and experimental cases, as can be noted in Fig. 2.14(b).

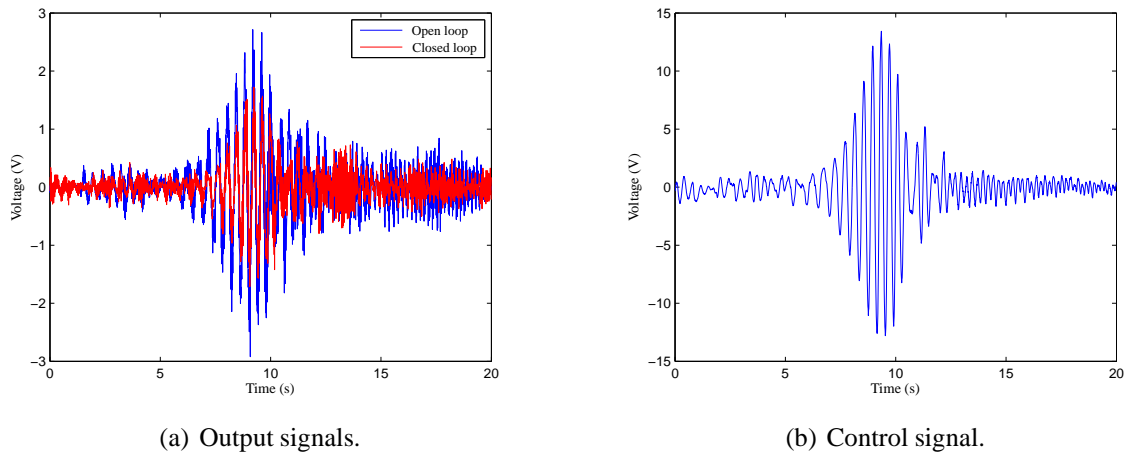


Figure 2.13 - Experimental response when the disturbance is a chirp signal.

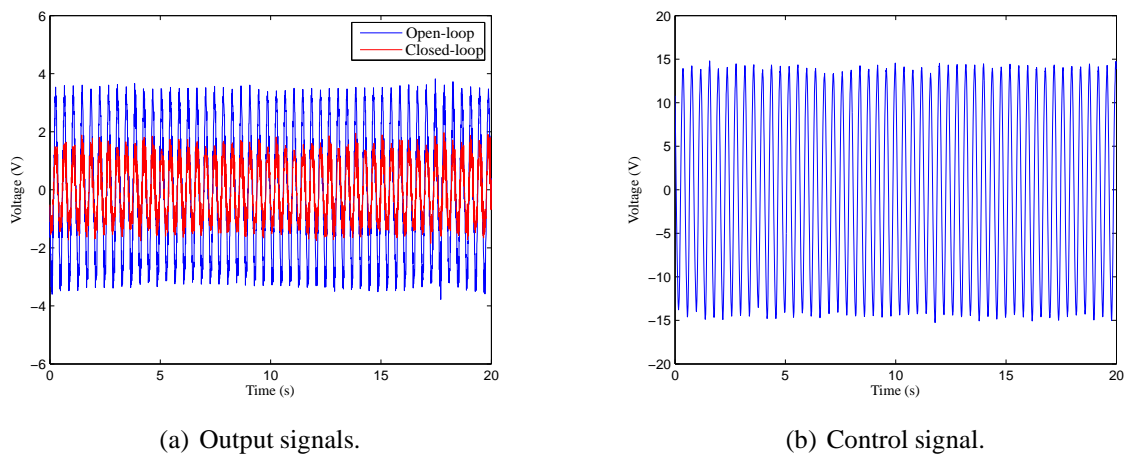


Figure 2.14 - Experimental response when the structure is excited in its natural frequency.

## 2.7 Conclusion

The regular  $H_\infty$  approach to attenuate vibrations in flexible structures is presented in this chapter, including weighing filters to impose the desired frequency response. Initially, a brief overview of the flexible structure modelling is presented, adopting a specific modal representation. After that, the control  $H_\infty$  problem is introduced and solved through a suboptimal

approach, based on the LMI method. Finally, the  $H_\infty$  control methodology is used to attenuate the vibrations of a bench-scale structure that simulates a tall building subject to seismic loads. Simulated and experimental results show that the proposed controller reduces significantly the vibration level of the vertical structure.

### 3 A MODAL $H_\infty$ -NORM APPROACH APPLIED TO DTAC

The objective of this chapter is to further explore the modal  $H_\infty$  methodology for the vibration control of flexible structures subject to damage, in order to develop a basic controller to implement the STAC strategy. The modal  $H_\infty$  norm is initially presented, followed by the description of the modal control problem, based on the introduced norm. The solution of the proposed problem is then developed, adapted from a regular  $H_\infty$  control LMI solution. Experimental and analytical examples are presented, followed by the result analysis.

#### 3.1 Introduction

A modal method has already been proposed to prevent damage caused by fatigue in (CHOMETTE et al., 2010). However, the goal in this thesis is more general because the modal  $H_\infty$  methodology is investigated to ensure an adequate performance even after damage occurrence. The proposed technique is based on the  $H_\infty$  methodology to support parameter variations. To ensure robustness is not enough to face damage because the increase of robustness usually leads to performance loss. Thereby, the adopted DTAC strategy aims at increasing the vibration reduction of each mode while minimising the damage effects on the global vibration result.

The proposed method merges the features of both modal and  $H_\infty$  controls, based on a novel modal  $H_\infty$  norm. Thus, the modal selection ability of modal techniques may be incorporated with robustness to spillover and to parametric variation of the  $H_\infty$  method. In addition, it presents the capability to be applied to multiple-transducer noncollocated systems. The modal  $H_\infty$  norm conveniently weights each mode, considering the intended modes to be reduced and conducting to modal control selectivity. The problem is then solved as a regular  $H_\infty$  design, using the LMI approach.

The proposed methodology is analysed and compared with regular  $H_\infty$  control cases, based on experiments and simulations with different levels of complexity. A simulated structure is built using four masses connected by springs and dampers, where damage is induced by changes in these parameters. This example is mainly for illustration purposes, allowing easy

analysis of the Modal  $H_\infty$  Controller (MC) performance for DTAC applications and easy reproducibility. Then, the methodology is experimentally examined on two similar aluminium cantilever beams with noncollocated piezoelectric transducers. One beam is considered healthy and the other is defined as damaged. A regular  $H_\infty$  controller is designed, whose performance is used as a reference. Afterward, the MCs are designed with different weights in their modes in order to show the reduction of the global vibration. Results indicate the effectiveness of the methodology along with performance improvement compared to a regular  $H_\infty$  controller for damage and health conditions.

### 3.2 Modal norm definition

This section introduces the new modal  $H_\infty$  norm. Initially, the relation between the  $H_\infty$  norm of a linear time-invariant system and the respective modal behaviour is presented. Then the involved concepts are used to propose the modal  $H_\infty$  norm.

Consider a stable linear time-invariant system with distinct natural frequencies represented by the transfer matrix  $\mathbf{G}(s)$ , where  $s$  is the Laplace variable. Assuming a disturbance  $\mathbf{W}(s)$ , the respective system output is given by  $\mathbf{Y}(s) = \mathbf{G}(s)\mathbf{W}(s)$ . Dividing the system frequency response into  $m$  bands, with only one mode of the reduced model in each band, leads to:

$$\mathbf{Y}(s) = \sum_{i=1}^m \tilde{\mathbf{Y}}_i(s) = \sum_{i=1}^m \mathbf{G}(s)\mathbf{W}_i(s) = \sum_{i=1}^m \mathbf{G}(s)\mathbf{F}_i[\mathbf{W}(s)], \quad (3.1)$$

where  $\mathbf{F}_i$  is an ideal bandpass filter and  $\mathbf{W}_i(s)$  is the disturbance at band  $i$ .

The induced  $H_\infty$  norm of  $\mathbf{G}(s)$  may be written as:

$$\|\mathbf{G}(s)\|_\infty^2 = \sup_{\mathbf{w} \neq 0, \mathbf{w} \in \mathcal{L}_2[0, \infty[} \frac{\int_0^\infty \mathbf{y}^T(t)\mathbf{y}(t)dt}{\int_0^\infty \mathbf{w}^T(t)\mathbf{w}(t)dt}, \quad (3.2)$$

where  $\mathbf{y}(t)$  and  $\mathbf{w}(t)$  are respectively the output and the input of  $\mathbf{G}(s)$  in the time domain. Equation (3.2) may be written as:

$$\|\mathbf{G}(s)\|_\infty^2 = \sup_{\mathbf{w} \neq 0, \mathbf{w} \in \mathcal{L}_2[0, \infty[} \frac{\int_0^\infty (\sum_{i=1}^m \tilde{\mathbf{y}}_i(t))^T (\sum_{j=1}^m \tilde{\mathbf{y}}_j(t)) dt}{\int_0^\infty (\sum_{i=1}^m \mathbf{w}_i(t))^T (\sum_{j=1}^m \mathbf{w}_j(t)) dt}.$$



Or, introducing  $\delta_{\tilde{\mathbf{y}}}$  and  $\delta_{\mathbf{w}}$  to represent the cross terms for  $i \neq j$ , it leads to:

$$\|\mathbf{G}(s)\|_{\infty}^2 = \sup_{\mathbf{w} \neq 0, \mathbf{w} \in \mathcal{L}_2[0, \infty[} \frac{\int_0^{\infty} (\sum_{i=1}^m \tilde{\mathbf{y}}_i^T(t) \tilde{\mathbf{y}}_i(t) + \delta_{\tilde{\mathbf{y}}}) dt}{\int_0^{\infty} (\sum_{i=1}^m \mathbf{w}_i^T(t) \mathbf{w}_i(t) + \delta_{\mathbf{w}}) dt}.$$

The following theorem has the objective of proving that the contribution of these cross terms can be disregarded, aiming for a norm representation that is more suitable to achieve an  $H_{\infty}$  controller design.

**Theorem 3.1.** *Given a scalar  $\gamma > 0$  and a stable linear time-invariant system with distinct natural frequencies represented by the transfer matrix  $\mathbf{G}(s)$ , where the output signal vector  $\mathbf{y}(t)$  is decomposed into  $m$  frequency bands according to Eq. (3.1), if*

$$\sup_{\mathbf{w} \neq 0, \mathbf{w} \in \mathcal{L}_2[0, \infty[} \frac{\int_0^{\infty} \mathbf{y}^T(t) \mathbf{y}(t) dt}{\int_0^{\infty} \mathbf{w}^T(t) \mathbf{w}(t) dt} < \gamma^2,$$

then

$$\sup_{\mathbf{w} \neq 0, \mathbf{w} \in \mathcal{L}_2[0, \infty[} \frac{\sum_{i=1}^m \int_0^{\infty} \tilde{\mathbf{y}}_i^T(t) \tilde{\mathbf{y}}_i(t) dt}{\sum_{i=1}^m \int_0^{\infty} \mathbf{w}_i^T(t) \mathbf{w}_i(t) dt} < \gamma^2.$$

*Proof.* The  $H_{\infty}$ -norm definition in Eq. (3.2) bounded by the scalar  $\gamma$  may be written as:

$$\|\mathbf{G}(s)\|_{\infty}^2 = \sup_{\mathbf{w} \neq 0, \mathbf{w} \in \mathcal{L}_2[0, \infty[} \frac{\int_0^{\infty} \mathbf{y}^T(t) \mathbf{y}(t) dt}{\int_0^{\infty} \mathbf{w}^T(t) \mathbf{w}(t) dt} < \gamma^2.$$

Considering the Parseval's theorem, it is possible to write the following expression:

$$\begin{aligned} \sum_{i=1}^m \int_0^{\infty} \tilde{\mathbf{y}}_i^T(t) \tilde{\mathbf{y}}_i(t) dt &= \frac{1}{2\pi} \sum_{i=1}^m \int_{-\infty}^{\infty} \tilde{\mathbf{Y}}_i^*(j\omega) \tilde{\mathbf{Y}}_i(j\omega) d\omega \\ &= \frac{1}{2\pi} \sum_{i=1}^m \int_{-\infty}^{\infty} \mathbf{W}_i^*(j\omega) \mathbf{G}^*(j\omega) \mathbf{G}(j\omega) \mathbf{W}_i(j\omega) d\omega \\ &\leq \|\mathbf{G}(s)\|_{\infty}^2 \frac{1}{2\pi} \sum_{i=1}^m \int_{-\infty}^{\infty} \mathbf{W}_i^*(j\omega) \mathbf{W}_i(j\omega) d\omega \\ \sum_{i=1}^m \int_0^{\infty} \tilde{\mathbf{y}}_i^T(t) \tilde{\mathbf{y}}_i(t) dt &\leq \|\mathbf{G}(s)\|_{\infty}^2 \sum_{i=1}^m \int_0^{\infty} \mathbf{w}_i^T(t) \mathbf{w}_i(t) dt. \end{aligned}$$

This leads to:

$$\|\mathbf{G}(s)\|_{\infty}^2 \geq \sup_{\mathbf{w} \neq 0, \mathbf{w} \in \mathcal{L}_2[0, \infty[} \frac{\sum_{i=1}^m \int_0^{\infty} \tilde{\mathbf{y}}_i^T(t) \tilde{\mathbf{y}}_i(t) dt}{\sum_{i=1}^m \int_0^{\infty} \mathbf{w}_i^T(t) \mathbf{w}_i(t) dt}.$$

Considering that  $\|\mathbf{G}(s)\|_\infty^2 < \gamma^2$ , it is possible to conclude:

$$\sup_{\mathbf{w} \neq 0, \mathbf{w} \in \mathcal{L}_2[0, \infty[} \frac{\sum_{i=1}^m \int_0^\infty \tilde{\mathbf{y}}_i^T(t) \tilde{\mathbf{y}}_i(t) dt}{\sum_{i=1}^m \int_0^\infty \mathbf{w}_i^T(t) \mathbf{w}_i(t) dt} < \gamma^2.$$

This proves the theorem.  $\square$

Theorem 3.1 relates the  $H_\infty$  norm to a truncated decomposition of the linear system as a summation of bandpass components. Applying the modal expansion theorem (INMAN, 1989), the system output may be decomposed into a summation of modal responses such as:

$$\mathbf{Y}(s) = \sum_{i=1}^m \bar{\mathbf{Y}}_i(s) = \sum_{i=1}^m \mathbf{G}_i(s) \mathbf{W}(s),$$

where  $\mathbf{G}_i(s)$  is the mode  $i$  submatrix that composes  $\mathbf{G}(s)$ .

The output  $\tilde{\mathbf{Y}}_i(s)$  is the system response due to all modes in the region of mode  $i$  and  $\bar{\mathbf{Y}}_i(s)$  corresponds to the response of only mode  $i$  in the same region. For each frequency band, the main contribution to the amplitude of  $\tilde{\mathbf{Y}}_i(s)$  is due to the amplitude of the resonant frequency response in the band, with the addition of all the other mode responses in the same band (GAWRONSKI, 2008). Taking into account that the  $H_\infty$  norm is an intrinsic characteristic of the system, it does not depend on the excitation. In particular, the response to the summation of the modal excitations is bounded by the  $H_\infty$  norm (GAWRONSKI, 2004). So, it is possible to write:

$$\sup_{\mathbf{w} \neq 0, \mathbf{w} \in \mathcal{L}_2[0, \infty[} \frac{\sum_{i=1}^m \int_0^\infty \bar{\mathbf{y}}_i^T(t) \bar{\mathbf{y}}_i(t) dt}{\sum_{i=1}^m \int_0^\infty \mathbf{w}_i^T(t) \mathbf{w}_i(t) dt} < \gamma^2. \quad (3.3)$$

Based on statement (3.3), it is possible to define a weighted norm to balance the contribution of each mode.

**Proposition 3.1.** *The weighted modal  $H_\infty$  norm of a stable linear time-invariant system  $G(s)$  with distinct natural frequencies is proposed as:*

$$\begin{aligned} \|\mathbf{G}(s)\|_{\infty, \mathbf{Q}}^2 &= \sup_{\mathbf{w} \neq 0, \mathbf{w} \in \mathcal{L}_2[0, \infty[} \frac{\sum_{i=1}^m \int_0^\infty \bar{\mathbf{y}}_i^T(t) \mathbf{Q}_i \bar{\mathbf{y}}_i(t) dt}{\sum_{i=1}^m \int_0^\infty \mathbf{w}_i^T(t) \mathbf{w}_i(t) dt} \\ &= \sup_{\mathbf{w} \neq 0, \mathbf{w} \in \mathcal{L}_2[0, \infty[} \frac{\int_0^\infty \hat{\mathbf{y}}^T(t) \mathbf{Q} \hat{\mathbf{y}}(t) dt}{\int_0^\infty \hat{\mathbf{w}}^T(t) \hat{\mathbf{w}}(t) dt} \\ &= \sup_{\mathbf{w} \neq 0, \mathbf{w} \in \mathcal{L}_2[0, \infty[} \frac{\|\hat{\mathbf{y}}(t)\|_{2, \mathbf{Q}}^2}{\|\hat{\mathbf{w}}(t)\|_2^2}, \end{aligned}$$

in which  $\hat{\mathbf{y}}^T(t) = [\bar{\mathbf{y}}_1^T(t) \ \bar{\mathbf{y}}_2^T(t) \ \cdots \ \bar{\mathbf{y}}_m^T(t)]$ ,  $\hat{\mathbf{w}}^T(t) = [\mathbf{w}_1^T(t) \ \mathbf{w}_2^T(t) \ \cdots \ \mathbf{w}_m^T(t)]$ ,  $\mathbf{Q}_i > 0$  is a diagonal matrix, and  $\mathbf{Q} = \text{diag}(\mathbf{Q}_1, \mathbf{Q}_2, \dots, \mathbf{Q}_m)$ .

### 3.3 Modal control problem

The  $H_\infty$  control problem is to find a controller  $\mathbf{K}_c$  to the plant given in Eq. (2.7), if there is one, stated as:

$$\begin{aligned}\dot{\mathbf{x}}_c(t) &= \mathbf{A}_c \mathbf{x}_c(t) + \mathbf{B}_c \mathbf{y}(t) \\ \mathbf{u}(t) &= \mathbf{C}_c \mathbf{x}_c(t) + \mathbf{D}_c \mathbf{y}(t),\end{aligned}\tag{3.4}$$

such that, for the closed-loop system and given a  $\gamma > 0$ ,

$$\underbrace{\inf}_{\mathbf{K}_c \in V} \underbrace{\sup}_{\mathbf{w} \neq 0, \mathbf{w} \in \mathcal{L}_2[0, \infty[} \frac{\int_0^\infty \mathbf{z}^T(t) \mathbf{z}(t) dt}{\int_0^\infty \mathbf{w}^T(t) \mathbf{w}(t) dt} < \gamma^2,$$

in which  $V$  represents the set of all controllers that stabilises the plant.

By defining a new modal performance output, the following theorem provides conditions to transform the modal  $H_\infty$  problem into a regular  $H_\infty$  problem.

**Theorem 3.2** (Modal  $H_\infty$  theorem). *Consider the  $H_\infty$  problem of designing a controller  $\mathbf{K}_c$  given in Eq. (3.4) for a structure according to Eq. (2.7) with the modal state matrix according to Eq. (2.6) and the following performance output:*

$$\mathbf{z}_p(t) = \mathbf{\Gamma} \mathbf{x}(t) + \mathbf{\Theta} \mathbf{w}(t) + \mathbf{\Lambda} \mathbf{u}(t),\tag{3.5}$$

with

$$\begin{aligned}\mathbf{\Gamma} &= \left[ \mathbf{Q}_1^{\frac{1}{2}} \mathbf{C}_{1_1} \quad \mathbf{Q}_2^{\frac{1}{2}} \mathbf{C}_{1_2} \quad \cdots \quad \mathbf{Q}_m^{\frac{1}{2}} \mathbf{C}_{1_m} \right], \\ \mathbf{\Theta} &= (\mathbf{Q}_1^{\frac{1}{2}} \mathbf{D}_{11_1} + \cdots + \mathbf{Q}_m^{\frac{1}{2}} \mathbf{D}_{11_m}), \\ \mathbf{\Lambda} &= (\mathbf{Q}_1^{\frac{1}{2}} \mathbf{D}_{12_1} + \cdots + \mathbf{Q}_m^{\frac{1}{2}} \mathbf{D}_{12_m}),\end{aligned}$$

where the diagonal matrix  $\mathbf{Q}_i > 0$  weights mode  $i$  and  $\mathbf{C}_{1_i}$ ,  $\mathbf{D}_{11_i}$ , and  $\mathbf{D}_{12_i}$  correspond to the

respective mode  $i$  submatrices in  $\mathbf{C}_1$ ,  $\mathbf{D}_{11}$ , and  $\mathbf{D}_{12}$ .

Then, given a scalar  $\gamma > 0$ , a controller that solves the respective  $H_\infty$  problem

$$\|\mathbf{T}_{\mathbf{z}_p \mathbf{w}}(s)\|_\infty < \gamma,$$

also guarantees that

$$\|\mathbf{T}_{\mathbf{z}_w}(s)\|_{\infty, \mathbf{Q}} < \gamma,$$

where  $\mathbf{T}_{\mathbf{z}_p \mathbf{w}}(s)$  and  $\mathbf{T}_{\mathbf{z}_w}(s)$  are the closed-loop transfer matrices.

*Proof.* Solving the respective  $H_\infty$  problem implies that:

$$\sup_{\mathbf{w} \neq 0, \mathbf{w} \in \mathcal{L}_2[0, \infty[} \frac{\int_0^\infty \mathbf{z}_p^T(t) \mathbf{z}_p(t) dt}{\int_0^\infty \mathbf{w}^T(t) \mathbf{w}(t) dt} < \gamma^2.$$

Considering the decomposition of  $\mathbf{z}_p(t)$  into modal components such as  $\mathbf{z}_p(t) = \sum_{i=1}^m \mathbf{z}_{p_i}(t)$  for  $i = 1 \dots m$ , then  $\mathbf{z}_{p_i}(t)$  can be defined as:

$$\mathbf{z}_{p_i}(t) = \mathbf{\Gamma}_i \mathbf{X}_i(t) + \mathbf{\Theta}_i \mathbf{w}(t) + \mathbf{\Lambda}_i \mathbf{u}(t),$$

in which  $\mathbf{X}_i(t)$  represents the state vector of mode  $i$  and  $\mathbf{\Gamma}_i$ ,  $\mathbf{\Theta}_i$ , and  $\mathbf{\Lambda}_i$  are respectively the submatrix of  $\mathbf{\Gamma}$ ,  $\mathbf{\Theta}$ , and  $\mathbf{\Lambda}$  relative to mode  $i$ .

Writing  $\mathbf{\Gamma}_i$ ,  $\mathbf{\Theta}_i$ , and  $\mathbf{\Lambda}_i$  as:

$$\begin{aligned} \mathbf{\Gamma}_i &= \mathbf{Q}_i^{\frac{1}{2}} \mathbf{C}_{1_i}, \\ \mathbf{\Theta}_i &= \mathbf{Q}_i^{\frac{1}{2}} \mathbf{D}_{11_i}, \\ \mathbf{\Lambda}_i &= \mathbf{Q}_i^{\frac{1}{2}} \mathbf{D}_{12_i}, \end{aligned}$$

where  $\mathbf{C}_{1_i}$ ,  $\mathbf{D}_{11_i}$ , and  $\mathbf{D}_{12_i}$  are the modal submatrices relative to mode  $i$  of the performance vector based on  $\mathbf{z}(t)$  according to Eq. (2.7). Then, the modal submatrices can be used to reconstruct the full modal performance vector as:

$$\begin{aligned} \mathbf{z}_p(t) &= \sum_{i=1}^m (\mathbf{\Gamma}_i \mathbf{X}_i(t) + \mathbf{\Theta}_i \mathbf{w}(t) + \mathbf{\Lambda}_i \mathbf{u}(t)) \\ &= \begin{bmatrix} \mathbf{Q}_1^{\frac{1}{2}} \mathbf{C}_{1_1} & \mathbf{Q}_2^{\frac{1}{2}} \mathbf{C}_{1_2} & \cdots & \mathbf{Q}_m^{\frac{1}{2}} \mathbf{C}_{1_m} \end{bmatrix} \mathbf{x}(t) + (\mathbf{Q}_1^{\frac{1}{2}} \mathbf{D}_{11_1} + \cdots + \mathbf{Q}_m^{\frac{1}{2}} \mathbf{D}_{11_m}) \mathbf{w}(t) + \\ &+ (\mathbf{Q}_1^{\frac{1}{2}} \mathbf{D}_{12_1} + \cdots + \mathbf{Q}_m^{\frac{1}{2}} \mathbf{D}_{12_m}) \mathbf{u}(t). \end{aligned}$$

Consequently, the product  $\mathbf{z}_{\mathbf{p}_i}^T(t)\mathbf{z}_{\mathbf{p}_i}(t)$  is given by:

$$\mathbf{z}_{\mathbf{p}_i}^T(t)\mathbf{z}_{\mathbf{p}_i}(t) = \begin{bmatrix} \mathbf{X}_i^T(t) & \mathbf{w}^T(t) & \mathbf{u}^T(t) \end{bmatrix} \begin{bmatrix} \mathbf{C}_{1_i}^T \\ \mathbf{D}_{11_i}^T \\ \mathbf{D}_{12_i}^T \end{bmatrix} \mathbf{Q}_i \begin{bmatrix} \mathbf{C}_{1_i} & \mathbf{D}_{11_i} & \mathbf{D}_{12_i} \end{bmatrix} \begin{bmatrix} \mathbf{X}_i(t) \\ \mathbf{w}(t) \\ \mathbf{u}(t) \end{bmatrix},$$

which leads to:

$$\mathbf{z}_{\mathbf{p}_i}^T(t)\mathbf{z}_{\mathbf{p}_i}(t) = \mathbf{z}_i^T(t)\mathbf{Q}_i\mathbf{z}_i(t). \quad (3.6)$$

Based on Theorem 3.1 and statement (3.6), it follows that:

$$\underbrace{\sup}_{\mathbf{w} \neq 0, \mathbf{w} \in \mathcal{L}_2[0, \infty[} \frac{\sum_{i=1}^m \int_0^\infty \mathbf{z}_{\mathbf{p}_i}^T(t)\mathbf{z}_{\mathbf{p}_i}(t)dt}{\sum_{i=1}^m \int_0^\infty \mathbf{w}_i^T(t)\mathbf{w}_i(t)dt} = \underbrace{\sup}_{\mathbf{w} \neq 0, \mathbf{w} \in \mathcal{L}_2[0, \infty[} \frac{\sum_{i=1}^m \int_0^\infty \mathbf{z}_i^T(t)\mathbf{Q}_i\mathbf{z}_i(t)dt}{\sum_{i=1}^m \int_0^\infty \mathbf{w}_i^T(t)\mathbf{w}_i(t)dt} < \gamma^2,$$

which comes to:

$$\|\mathbf{T}_{\mathbf{zw}}(s)\|_{\infty, \mathbf{Q}} < \gamma.$$

This proves the theorem. □

The proposed modal  $H_\infty$  technique allows that the control system designer prioritises a specific mode vibration reduction by changing only its respective weighing matrix. For instance, when a structure is submitted to severe stress conditions due to the external excitation of a mode. The excitation persistency may affect the life cycle of structures, potentially causing damage that may result in vibration increase. This cycle may contribute to damage severity increase, leading to undesirable consequences such as catastrophic failure. Thus, an adequate modal control is needed to mitigate this undesired cycle.

### 3.4 Modal control solution

The modal  $H_\infty$  problem is formulated in this section as a regular  $H_\infty$  problem, which can be summarised in the block diagram of Fig. 3.1. In this figure, the filters  $F_u$  and  $F_z$  are applied to the control signal vector  $\mathbf{u}(t)$  and the performance vector  $\mathbf{z}_p(t)$ , generating respectively  $\mathbf{z}_u(t)$  and  $\bar{\mathbf{z}}_p(t)$ .

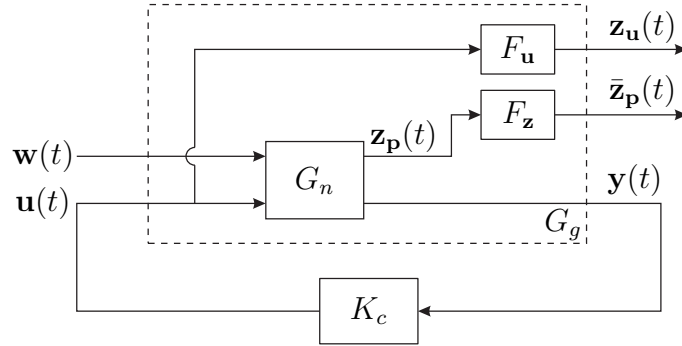


Figure 3.1 - Block diagram of the modal  $H_\infty$  control problem.

The weighing filters are key elements in the controller design process and often involve many iterations and fine tuning. To obtain a good trade-off between performance and robustness,  $F_z(s)$  is designed as a low-pass weighing filter. To avoid the spillover phenomenon,  $F_u(s)$  is designed as a high-pass weighing filter. In general, the weighing filters are designed as (ZHOU; DOYLE, 1997):

$$F_z(s) = \left( \frac{\frac{s}{\sqrt[k]{M}} + \omega_c}{s + \omega_c \sqrt[k]{\varepsilon}} \right)^k \quad \text{and} \quad F_u(s) = \left( \frac{s + \frac{\omega_c}{\sqrt[k]{M}}}{s \sqrt[k]{\varepsilon} + \omega_c} \right)^k, \quad (3.7)$$

in which  $\omega_c$ ,  $k$ ,  $\varepsilon$ , and  $M$  are the transition frequency between rejection band and passband, the filter order, the gain at passband, and the gain at rejection band, respectively.

The  $H_\infty$  norm of the transfer function between the disturbance  $w(t)$  and the performance output  $\hat{z}(t) = \begin{bmatrix} \bar{z}_p^T(t) & z_u^T(t) \end{bmatrix}^T$  is designated by  $\|\mathbf{T}_{\hat{z}w}\|_\infty$ . Thus, the modal  $H_\infty$  controller design consists in finding a central controller  $\mathbf{K}_c$  that minimises  $\|\mathbf{T}_{\hat{z}w}\|_\infty$ . It is usual to solve a suboptimal problem that minimises  $\|\mathbf{T}_{\hat{z}w}\|_\infty$  through iterations, as presented in Chapter 2.

### 3.5 Simulated and experimental results

This section presents experimental and analytical results concerning DTAC. Initially, the modal  $H_\infty$  control methodology is examined in a simple structure with four masses connected by springs and dampers, and damage is simulated through changes in these parameters. This structure is used to examine the proposed technique for different locations and damage severities. After that, the methodology is experimentally tested using two similar aluminium beams, one integer and the second with a simulated damage, both with cantilever boundary conditions and noncollocated piezoelectric transducers.

### 3.5.1 Simulated structure results

The structure for analysis is presented in Fig. 3.2. This example is used for illustration purposes, allowing easy reproducibility and easy DTAC application analysis. Mass, stiffness, and damping coefficients are represented respectively by  $m_e$ ,  $k_e$ , and  $d_e$  for  $e = 1, \dots, 4$ . The signal  $w(t)$  represents the disturbance signal acting on mass  $m_1$ , and  $u(t)$  is the control signal acting on mass  $m_4$ . The outputs  $y_1(t)$  and  $y_2(t)$  are the displacements of masses  $m_2$  and  $m_3$ , respectively.

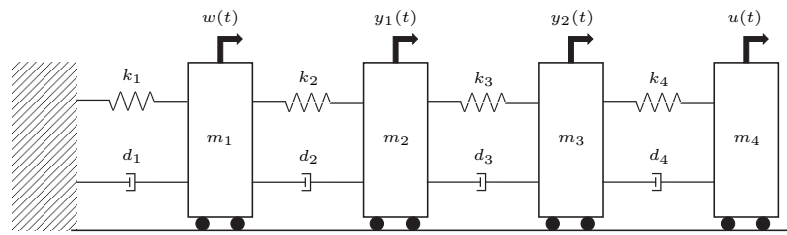


Figure 3.2 - Simulated structure.

This simple structure can be modelled by Eq. (2.1):

$$\mathbf{M}\ddot{\mathbf{p}}(t) + \mathbf{D}\dot{\mathbf{p}}(t) + \mathbf{K}\mathbf{p}(t) = \begin{bmatrix} \mathbf{B}_w & \mathbf{B}_u \end{bmatrix} \begin{bmatrix} w(t) \\ u(t) \end{bmatrix},$$

where

$$\mathbf{M} = \begin{bmatrix} m_1 & 0 & 0 & 0 \\ 0 & m_2 & 0 & 0 \\ 0 & 0 & m_3 & 0 \\ 0 & 0 & 0 & m_4 \end{bmatrix}, \mathbf{D} = \begin{bmatrix} d_1 + d_2 & -d_2 & 0 & 0 \\ -d_2 & d_2 + d_3 & -d_3 & 0 \\ 0 & -d_3 & d_3 + d_4 & -d_4 \\ 0 & 0 & -d_4 & d_4 \end{bmatrix}, \mathbf{B}_w = \begin{bmatrix} 1 \\ 0 \\ 0 \\ 0 \end{bmatrix},$$

$$\mathbf{K} = \begin{bmatrix} k_1 + k_2 & -k_2 & 0 & 0 \\ -k_2 & k_2 + k_3 & -k_3 & 0 \\ 0 & -k_3 & k_3 + k_4 & -k_4 \\ 0 & 0 & -k_4 & k_4 \end{bmatrix}, \text{ and } \mathbf{B}_u = \begin{bmatrix} 0 \\ 0 \\ 0 \\ 1 \end{bmatrix}.$$

The control objective is to reduce the vibration of masses  $m_2$  and  $m_3$  caused by disturbance  $w(t)$  on mass  $m_1$ . Thus, to design the regular  $H_\infty$  controller, it is necessary to transform

the model into the state-space form:

$$\bar{\mathbf{A}} = \begin{bmatrix} \mathbf{0} & \mathbf{I} \\ -\mathbf{M}^{-1}\mathbf{K} & -\mathbf{M}^{-1}\mathbf{D} \end{bmatrix}, \bar{\mathbf{B}}_1 = \begin{bmatrix} \mathbf{0} \\ \mathbf{M}^{-1}\tilde{\mathbf{B}}_1 \end{bmatrix}, \bar{\mathbf{B}}_2 = \begin{bmatrix} \mathbf{0} \\ \mathbf{M}^{-1}\tilde{\mathbf{B}}_2 \end{bmatrix},$$

$$\bar{\mathbf{C}}_1 = \begin{bmatrix} 0 & 1 & 0 & 0 & 0 & 0 & 0 & 0 \\ 0 & 0 & 1 & 0 & 0 & 0 & 0 & 0 \end{bmatrix}, \bar{\mathbf{C}}_1 = \bar{\mathbf{C}}_2, \text{ and } \bar{\mathbf{D}}_{11} = \bar{\mathbf{D}}_{12} = \bar{\mathbf{D}}_{21} = \bar{\mathbf{D}}_{22} = \begin{bmatrix} 0 \\ 0 \end{bmatrix}.$$

To simulate this simple structure, mass and stiffness values are selected as  $m_1 = 3$  kg,  $m_2 = 2$  kg,  $m_3 = 2$  kg,  $m_4 = 3$  kg,  $k_1 = 4800$  N/m,  $k_2 = 2200$  N/m,  $k_3 = 1200$  N/m, and  $k_4 = 500$  N/m. The damping matrix is defined proportionally to the stiffness and mass matrices:  $\mathbf{D} = 0.0005\mathbf{K} + 0.001\mathbf{M}$ . The modal model Eq. (2.7) is obtained using the function *canon* and the  $H_\infty$  controllers are designed using *mincx*, both functions of MATLAB<sup>®</sup>. The open-loop and closed-loop results are shown in Fig. 3.3. The Regular  $H_\infty$  Controller (RC) reduces peak vibration in the four modes, but it is still possible to increase performance by using the Modal  $H_\infty$  Controller (MC). Analysing  $T_{z_1w}$  presented in Fig. 3.3(a), the greatest reductions correspond to the first modes. Thus, to increase the control performance, modes 2, 3, and 4 should be weighted, focusing on modes 3 and 4 due to the small vibration reduction using the RC. The weights for modes 1, 2, 3, and 4 are chosen as 0.6, 1.3, 1.6, and 1.6, respectively. The RC performance is analogous to  $T_{z_2w}$ . However, the vibration reduction should be increased in modes 2 and 3 because mode 4 has a small magnitude, as can be seen in Fig. 3.3(b). For  $T_{z_2w}$ , the weights are respectively 1, 1.6, 1.4, and 0.6 for modes 1, 2, 3, and 4. Thereby, the weighing matrices are depicted as:

$$\mathbf{Q}_1^{\frac{1}{2}} = \begin{bmatrix} 0.6 & 0 \\ 0 & 1 \end{bmatrix}, \mathbf{Q}_2^{\frac{1}{2}} = \begin{bmatrix} 1.3 & 0 \\ 0 & 1.6 \end{bmatrix}, \mathbf{Q}_3^{\frac{1}{2}} = \begin{bmatrix} 1.6 & 0 \\ 0 & 1.4 \end{bmatrix}, \text{ and } \mathbf{Q}_4^{\frac{1}{2}} = \begin{bmatrix} 1.6 & 0 \\ 0 & 0.6 \end{bmatrix}.$$

Figure 3.3 presents the comparison between the open-loop and closed-loop systems, demonstrating the performance increase in the weighted modes. To test the effectiveness of the MC for DTAC applications, damage is simulated in the structure through changes in its mass and stiffness values, causing natural frequency shift and changes in damping for the structure modes. For this purpose, four configurations are induced sequentially to simulate damage severity increase:

1. Healthy: no changes in mass or stiffness (reference model);
2. Damage 1: reduction in masses  $m_2$  and  $m_3$  of 10 % relative to the reference model;



3. Damage 2: reduction in stiffness coefficients  $k_1$  and  $k_4$  of 10 % relative to configuration 2;
4. Damage 3: reduction in stiffness coefficients  $k_2$  and  $k_3$  of 20 % relative to configuration 3.

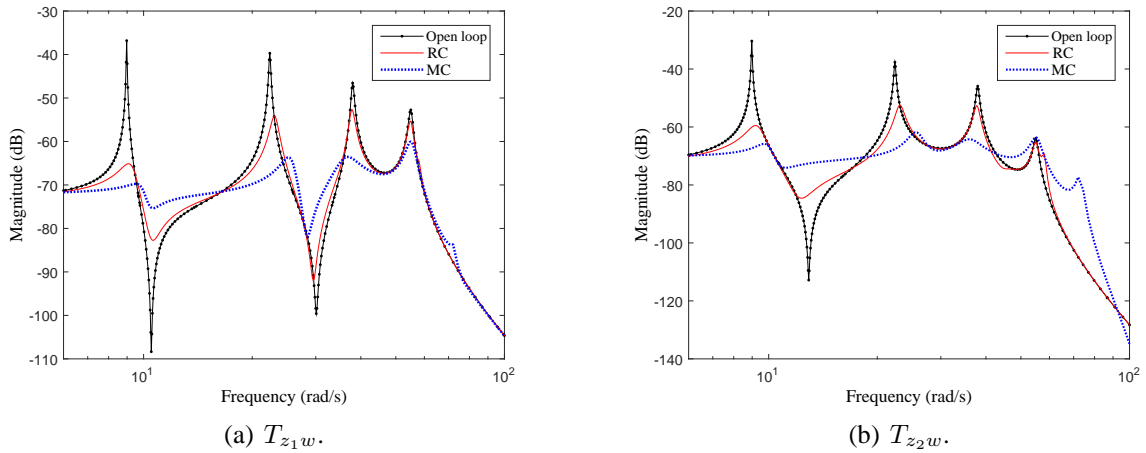


Figure 3.3 - Simulated results of the healthy structure.

The MC and the RC designed for the healthy structure are examined for DTAC using the models of configurations 2 to 4. The performance comparison between the RC and the MC is presented in Fig. 3.4. For all configurations, the MC is more effective in vibration reduction than the RC, as can be noted by analysing the frequency responses presented in Fig. 3.4(a) and Fig. 3.4(b). These results demonstrate that an appropriate vibration reduction in each mode decreases damage effects in the controlled system performance. However, this performance increase generally implies an increase in the control effort, as can be seen in Fig. 3.5.

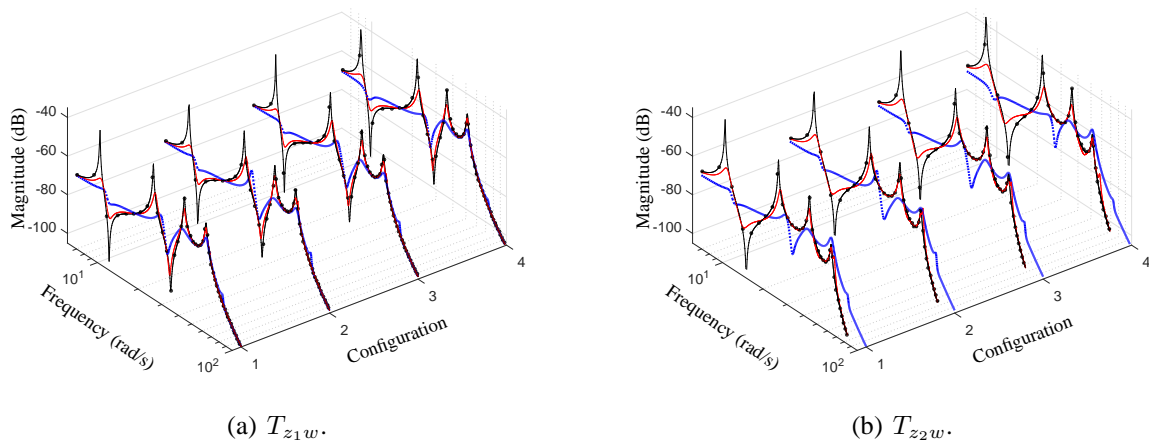


Figure 3.4 - Performance comparison between open loop (black line with points), RC (red solid line), and MC (blue dotted line) for the simulated structure.

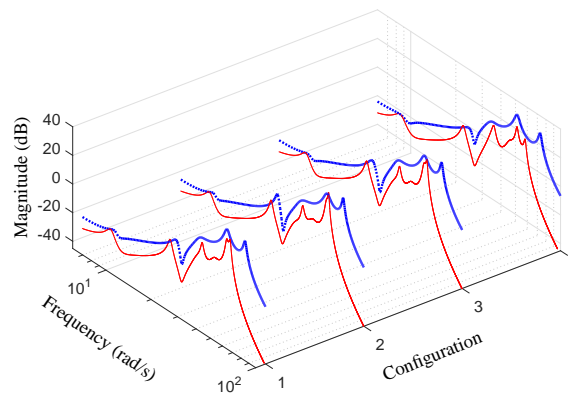
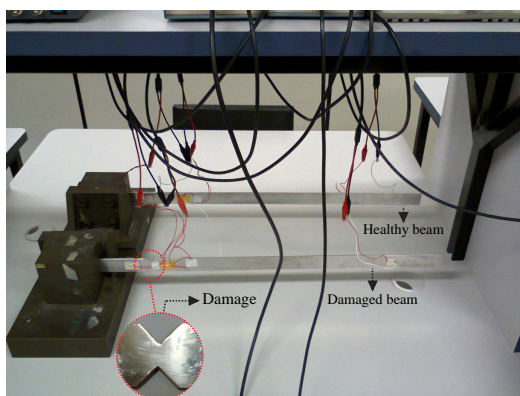


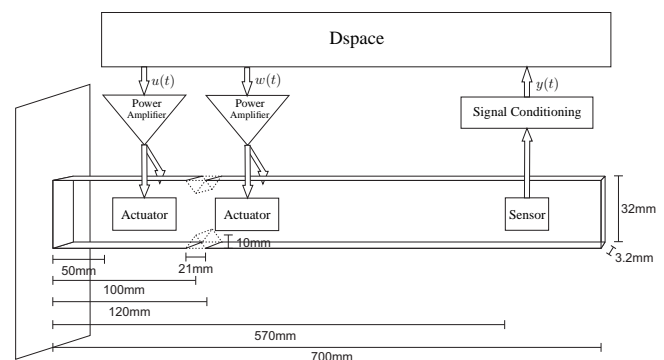
Figure 3.5 - Control signal comparison between RC (red solid line) and MC (blue dotted line) for the simulated structure.

### 3.5.2 Experimental results

The experimental setup consists of two similar aluminium beams of 700 mm with cantilever boundary conditions and rectangular cross sections of 3.2 mm  $\times$  32 mm. In each side of the beams, a PZT element with dimensions of 0.3 mm  $\times$  20 mm  $\times$  30 mm is glued 50 mm away from the origin and is used as an actuator. To apply the disturbance signal, PZTs with dimensions of 0.2 mm  $\times$  20 mm  $\times$  30 mm are glued to both sides of the beams 120 mm far from the origin. As a sensor, a PZT with dimensions of 0.5 mm  $\times$  20 mm  $\times$  20 mm is glued 110 mm away from the end on one side of each beam. The beams are presented in Fig. 3.6(a).



(a) Aluminium beams.



(b) Block diagram.

Figure 3.6 - Experiment setup.

The block diagram used to illustrate the experimental configuration for DTAC purpose is shown in Fig. 3.6(b). In this illustration, the dotted triangular prism represents completely removed material to act as the induced damage. The signal generation, data acquisition, and the controller are implemented using a dSPACE<sup>®</sup> board model DS1104 and ControlDesk<sup>®</sup> software. The control signal  $u(t)$  and the disturbance signal  $w(t)$  are generated, amplified by 20 times, and applied to their respective transducers. The vibration signal  $y(t)$  is captured by a PZT sensor, then it is conditioned and transmitted to the acquisition.

### 3.5.2.1 Healthy structure identification

The Experimental Frequency Responses (EFRs) are estimated using the deterministic Schroeder signal as excitation, sampled at 4 kHz and with frequency band between 0 Hz and 500 Hz. An EFR can be written as (PINTELON; SCHOUKENS, 2001):

$$P_{ba} = \frac{S_{ba}}{S_{aa}},$$

in which  $a(t)$  represents the input signal ( $u(t)$  or  $w(t)$ ), and  $b(t)$  is the output signal ( $y(t)$ ).  $S_{aa}$  is the power spectral density of  $a(t)$ , and  $S_{ba}$  is the cross power spectral density between  $b(t)$  and  $a(t)$ .

To determine  $P_{yu}$ , the Schroeder signal is applied to the piezoelectric actuator and the disturbance signal is set to zero. Similarly,  $P_{yw}$  is determined when the Schroeder signal is considered as disturbance and the signal  $u(t)$  is set to zero. Furthermore, forty periods of the Schroeder signal are used to estimate each EFR. The experimental estimation of  $P_{yu}$  and  $P_{yw}$  is presented in Fig. 3.7, showing that  $P_{yu}$  and  $P_{yw}$  have five different modes. However, the first peak of  $P_{yw}$  is much smaller than the other four peaks. Thus, as the objective is to reduce the structure vibrations when there is some disturbance, the first mode can be ignored in the identification. Therefore, using the *ssest* function of MATLAB<sup>®</sup>, the structure model is identified in the state-space form as a multiple-input-single-output system considering four main modes of vibration. The identification results can be compared with the EFRs in Fig. 3.7. It is possible to notice that the identified model is a reasonable estimation of the structure in the frequency band of interest.

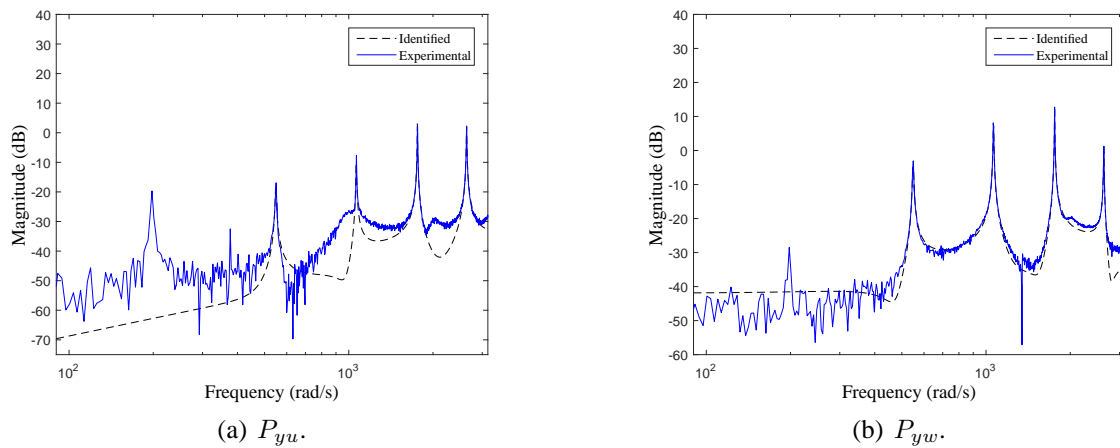


Figure 3.7 - Experimental and identified  $P_{yu}$  and  $P_{yw}$ .

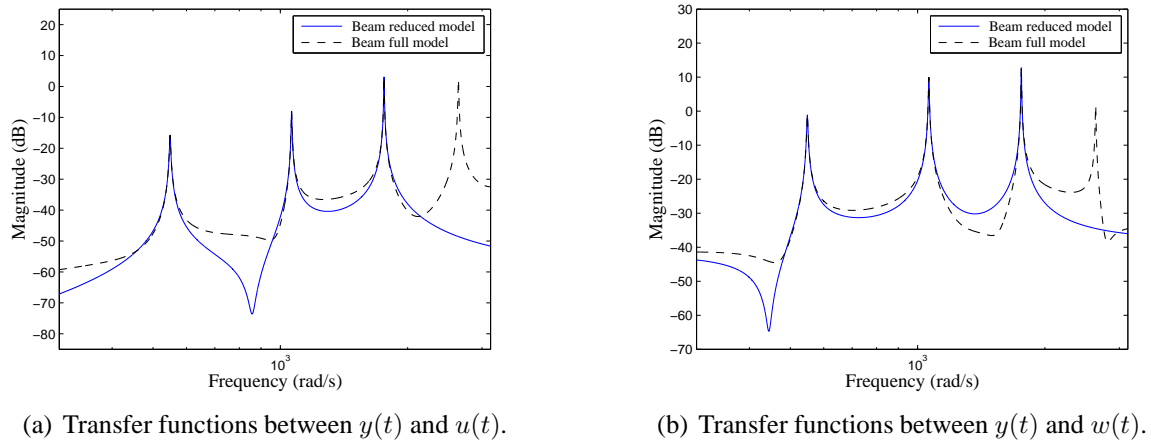


Figure 3.8 - Transfer function comparison between full and reduced models.

### 3.5.2.2 Modal robust controller design

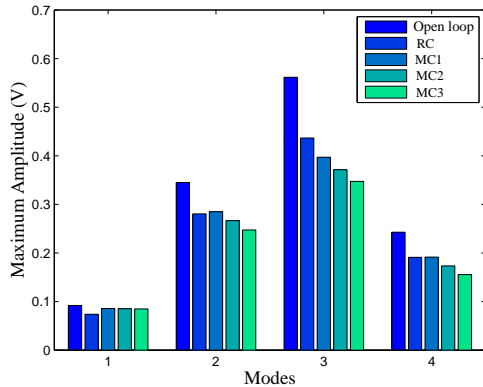
The control design criterion of this work is to suppress vibration in the first three recognised modes of the flexible beam subject to damage. Thus, the model is directly truncated, including only the first three modes, as can be seen in Fig. 3.8. The lost information by the model truncation may affect the dynamics and bring undesirable effects such as spillover. Thus, to avoid this effect, both weighing functions of Eq. (3.7) are designed with the following parameters:  $M = 255$ ,  $k = 1$ ,  $\varepsilon = 0.1$ , and  $w_c = 1800$  rad/s. The plant model is built in the state-space form with matrices  $(\mathbf{A}, \mathbf{B}_1, \mathbf{B}_2, \mathbf{C}_2, \mathbf{D}_{21}, \mathbf{D}_{22})$  obtained directly from the truncation of the identified model. Moreover, the performance matrices are defined as  $\mathbf{C}_1 = \mathbf{C}_2$  and

$D_{11} = D_{12} = 0$ . In the tests, the chirp signal with band between 78 Hz and 500 Hz, duration of 5.4 seconds, and amplitude of 0.5 V is considered as a disturbance, focusing on identified modes.

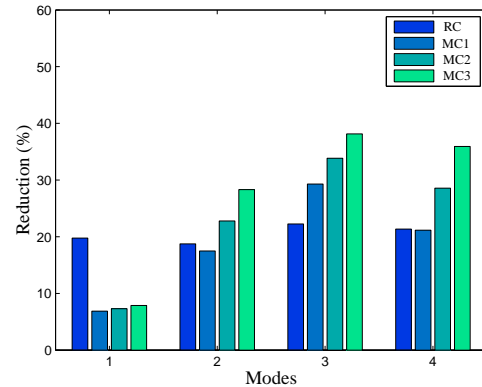
The RC is initially designed and its performance is used as the reference. The RC reduces the vibration level over the four modes, three modes in the interest band and one out, as can be seen in Fig. 3.9. To analyse the weighing effects in the modes, three configurations are created:

1. MC1:  $[Q_1^{1/2} \ Q_2^{1/2} \ Q_3^{1/2}] = [0.5 \ 1.0 \ 1.2]$ ;
2. MC2:  $[Q_1^{1/2} \ Q_2^{1/2} \ Q_3^{1/2}] = [0.5 \ 1.2 \ 1.4]$ ;
3. MC3:  $[Q_1^{1/2} \ Q_2^{1/2} \ Q_3^{1/2}] = [0.5 \ 1.4 \ 1.6]$ .

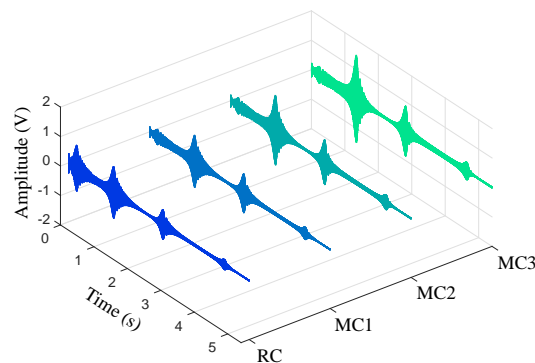
Figure 3.9(a) shows the modal peak vibration of the healthy structure. The modal vibration reduction is optimised by increasing the mode weighing. Also, the MCs are more effective in reducing vibration than the RC. These results are demonstrated more clearly by analysing the percentage reduction in Fig. 3.9(b), computed in relation to the open-loop response of the healthy structure. Moreover, the control signal amplitude increases with the mode weights, as can be seen in Fig. 3.9(c).



(a) Peak vibration of each mode.



(b) Percentage reduction.



(c) Control signals.

Figure 3.9 - Healthy beam simulated signals.

### 3.5.2.3 Control system experimental results

To examine the modal  $H_\infty$  control methodology for regular vibration control and for DTAC purpose, the controllers designed for the healthy beam are experimentally examined in the healthy beam and in the damaged beam. Figure 3.10 shows the open-loop frequency response comparison of the healthy and the damaged structures. It is possible to notice that damage produces natural frequency shifts in all modes. Moreover, damage provokes amplitude increase in almost all modes, decreasing only in the last mode of  $P_{yw}$ , which is outside the interest band.

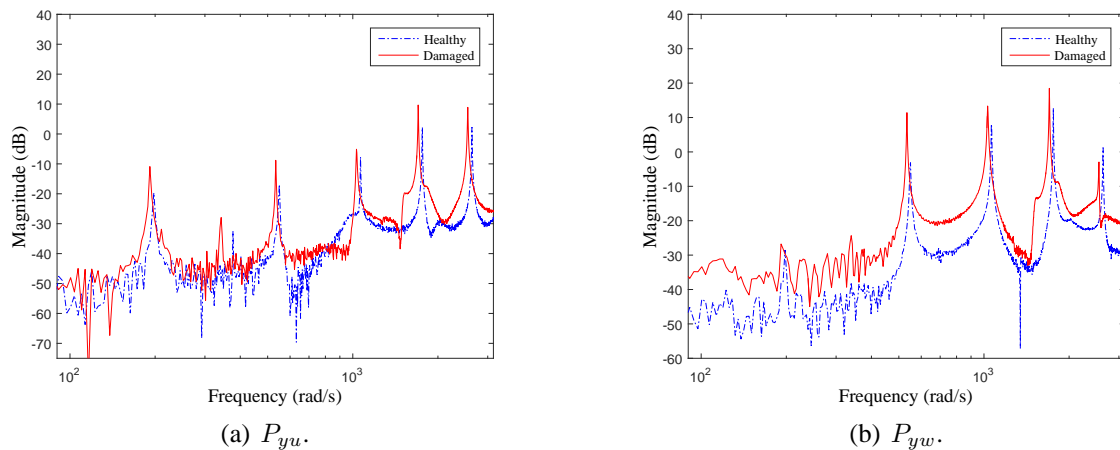


Figure 3.10 - Frequency response comparison between healthy and damaged structures.

The experimental data analysis starts with the healthy beam experimental vibration signals, whose peak vibration of each mode is shown in Fig. 3.11(a). Moreover, the relative vibration reduction is presented in Fig. 3.11(b), adopting the open-loop response of the healthy structure as the reference. Similarly to the simulated case, the RC reduces the global vibration in the interest band. For MCs, the vibration reduction in each mode is enhanced by the increasing mode weight. For instance, the third mode weight is continuously increased and its vibration is continuously reduced. For mode 1, the RC is causing the greatest vibration reduction. This result is expected because the MCs have a low weight in this mode. For mode 2, the MC1 does not change its weight, so it has a response similar to the RC. For mode 4, which is outside the interest band, the amplitude is attenuated in relation to the open-loop response, considering all tested controllers. Analogously to the simulated results, the weighing increases the experimental control signal, as can be seen in Fig. 3.12(a).

The peak vibration and the relative vibration reduction of the damaged structure are shown

respectively in Fig. 3.11(a) and Fig. 3.11(b), adopting the open-loop response of the damaged structure as the reference to compute the percentage of vibration reduction. However, all controllers showed to be effective in reducing vibrations. The modal controllers also continue with superior performance in relation to the RC, but this performance difference between the MCs and the RC is increased when compared with the results of the healthy beam. Moreover, the MC3 reduces substantially mode 3 peak vibration in the damaged beam, reaching similar values of the best results of the closed-loop healthy beam. Mode 2 has a slighter performance because this mode is less weighted. For mode 4, which is outside the interest band, the attenuation is more effective for the damaged beam, considering that damage itself provokes vibration attenuation in this mode. Figure 3.12(b) shows that the increase in weights also implies a rise in the control signal. As a final analysis, these experimental results show that an adequate control of the selected modes produces better results than the RC when the structure undergoes damage.

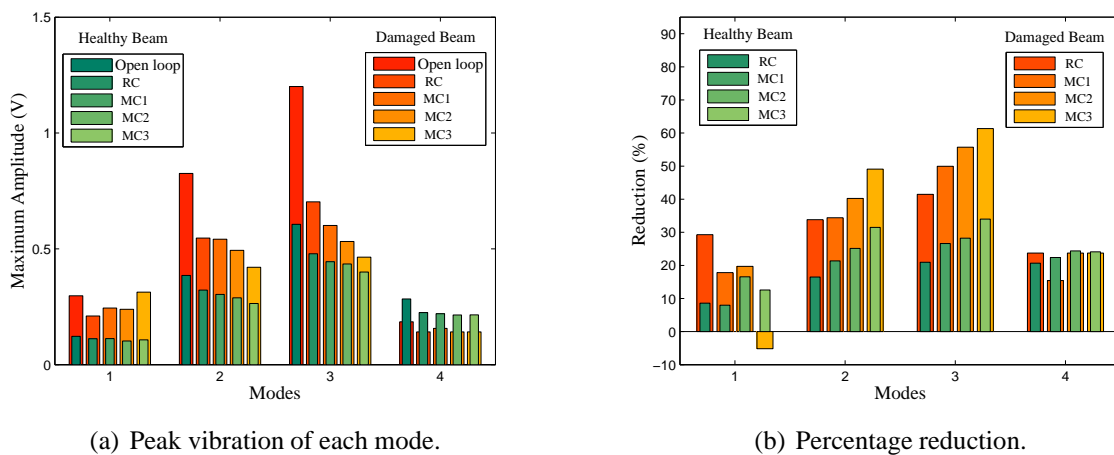


Figure 3.11 - Experimental output signals.

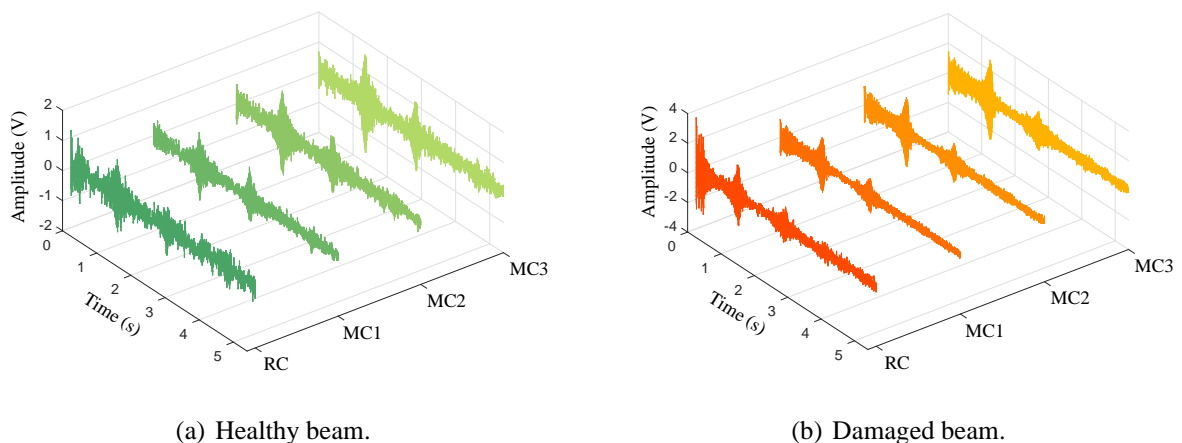


Figure 3.12 - Experimental control signals.

### 3.6 Conclusion

This chapter presented a novel modal  $H_\infty$  control methodology applied to DTAC. The technique provides appropriate control energy distribution over selected modes to reduce damage effects. For this purpose, a weighted modal  $H_\infty$  norm is proposed, where modal weighing leads to the design of  $H_\infty$  controllers presenting a high modal selectivity property. Therefore, the adopted strategy links the modal control with robust control. The methodology effectiveness is examined through applications with different levels of difficulty. Initially, the technique is analysed in a simulated system created with four masses connected by springs and dampers, and damage is included by changes in these parameters. Then, the methodology is experimentally tested using two similar cantilever aluminium beams and damage is created by material removal. Results show that the modal  $H_\infty$  approach is more effective than the regular  $H_\infty$  technique in suppressing structural vibration in the analysed cases, unfolding the possibility of selectivity and effective modal control.



## 4 A MODAL $H_\infty$ -NORM PERFORMANCE REQUIREMENT FOR DTAC

This chapter presents a novel methodology to include damage as a design requirement in the modal  $H_\infty$  control technique. For this purpose, the proposed modal SHM technique to assess the damage effects on each mode is initially detailed. Then, a new method is presented to convert the modal damage information into modal weighing matrices, conducting to design the respective DTAC controllers. Simulated results with FE models are analysed, considering different damage severities.

### 4.1 Introduction

Chapter 3 presented a new control method associating modal control and  $H_\infty$  control concepts, aiming to achieve good performance through modal selectivity. The control strategy is to design a modal robust controller that achieves an adequate performance through vibration reduction of high energy modes, controlling each mode independently. However, modes with lower energy may also be affected by damage, eventually leading to significant vibration increase of the controlled structure. To overcome this limitation, the strategy proposed in this chapter is based on the measure of the distance between the healthy and damaged structure models, in order to create an appropriate energy distribution over the vibration modes, taking into account the damage effect on each mode.

The adopted strategy considers that flexible structures are often submitted to repetitive disturbances, with some critical regions more affected than others. The repeating cycle eventually leads to damage in these regions due to a fatigue process, which demands an SHM technique to be adopted to prevent failure. The proposed DTAC methodology retards damage occurrence and limits its propagation in these critical regions, combining PAC and EDAC strategies to design a nonreconfigurable controller. Figure 4.1 illustrates the adopted strategy framework. Piezoelectric transducers constitute the sensor and actuator network in the critical regions. Simulations of damage situations provide damage impact on modes, based on preliminary knowledge from structure analysis, fatigue tests, and maintenance history. An SHM module assesses the damage severity on each mode. Considering the expected damage information, modal weighing matrices

are built and used to design the modal controller, based on the modal  $H_\infty$  control approach of Chapter 3. The proposed strategy is evaluated in terms of robustness and vibration rejection and is compared to the regular  $H_\infty$  control technique. The studied structure is a flexible beam with noncollocated piezoelectric transducers, modelled through the FE method. An increasing severity damage is simulated to test and compare the controller performances.

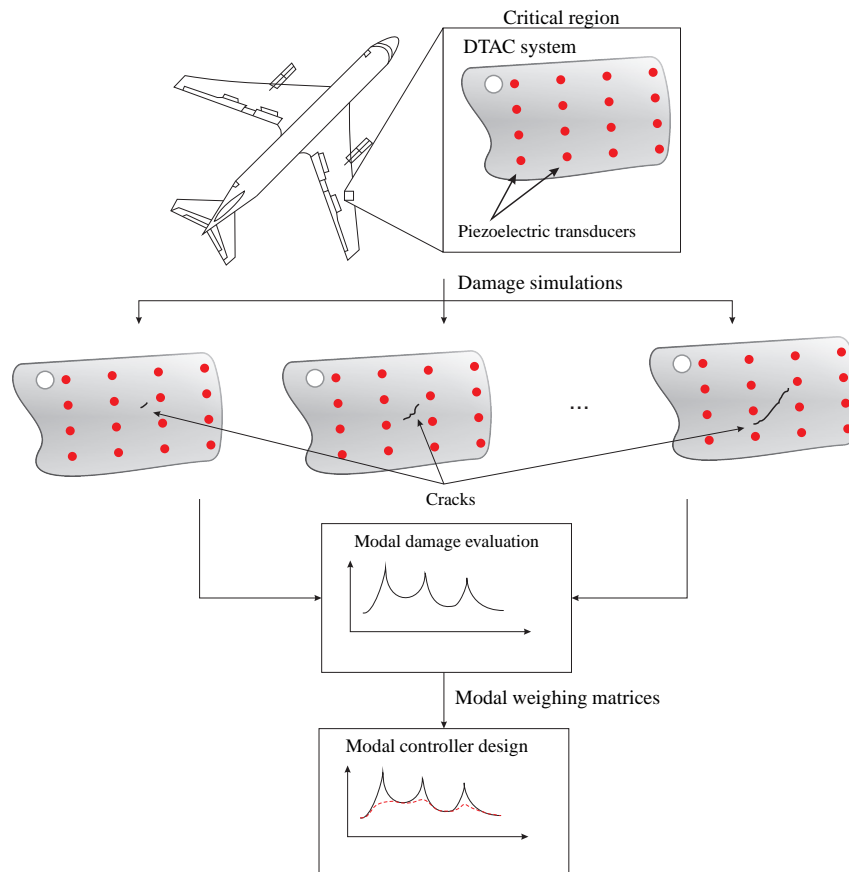


Figure 4.1 - Adopted DTAC strategy.

## 4.2 Assessing damage effects

A subspace metric to quantify damage effects on structure modes is proposed to enable the inclusion of damage as a controller design requirement. The regular approach for this metric is the assessment of the distance between subspaces representing a healthy model and a damaged model, based on dynamic response changes as damage indicators. For instance, Zheng and Mita (2008) applied a subspace metric to monitor the structural health of a simulated structure with five storeys subject to ambient and seismic excitations. Genari et al. (2013) investigated the

metric for detection, severity analysis, and location of damage experimentally, considering a medium frequency range. However, these metric applications do not provide information about damage effects on each mode. To overcome this limitation, the subspace metric is modified to provide modal damage effects, based on the adopted state-space modal model. Using this data, the modal weighing matrices are then estimated in order to compensate each affected mode.

#### 4.2.1 Modal damage metric

The infinite observability matrix for the flexible structure  $\mathbf{M}$  described by Eq. (2.7) is defined as:

$$\mathcal{O}_\infty(\mathbf{M}) = \left[ (\mathbf{C}_2)^T \quad (\mathbf{C}_2\mathbf{A})^T \quad (\mathbf{C}_2\mathbf{A}^2)^T \quad \dots \right]^T.$$

Assuming that  $\mathbf{M}^{(1)}$  and  $\mathbf{M}^{(2)}$  are two stable models with order  $2m$ , the respective observability matrices are  $\mathcal{O}_\infty(\mathbf{M}_1)$  and  $\mathcal{O}_\infty(\mathbf{M}_2)$ . The distance between  $\mathbf{M}^{(1)}$  and  $\mathbf{M}^{(2)}$  can be calculated in terms of the principal angles between the subspace ranges  $\mathcal{O}_\infty(\mathbf{M}_1)$  and  $\mathcal{O}_\infty(\mathbf{M}_2)$  (see Appendix A for details). Thus, the distance between  $\mathbf{M}^{(1)}$  and  $\mathbf{M}^{(2)}$  is given by (DE COCK; DE MOOR, 2002):

$$\Delta(\mathbf{M}^{(1)}, \mathbf{M}^{(2)})^2 = \log \left( \prod_{l=1}^{2m} \frac{1}{\cos^2 \theta_l} \right), \quad (4.1)$$

in which  $\theta_l$  is the  $l^{th}$  principal angle between the subspace ranges  $\mathcal{O}_\infty(\mathbf{M}^{(1)})$  and  $\mathcal{O}_\infty(\mathbf{M}^{(2)})$ .

The distance computed by Eq. (4.1) is a scalar indicator, which does not take into account modal effects. To get a modal indicator, the metric is modified to calculate damage impact on each vibration mode. Decomposing  $\mathbf{M}$  into  $m$  modal subsystems, the infinite observability matrix of a modal subsystem  $\mathbf{M}_i$  is defined as:

$$\mathcal{O}_\infty(\mathbf{M}_i) = \left[ (\mathbf{C}_{2_i})^T \quad (\mathbf{C}_{2_i}\mathbf{A}_i)^T \quad (\mathbf{C}_{2_i}\mathbf{A}_i^2)^T \quad \dots \right]^T, \quad (4.2)$$

where  $\mathbf{C}_{2_i}$  and  $\mathbf{A}_i$  represent respectively the elements of  $\mathbf{C}_2$  and  $\mathbf{A}$  relative to mode  $i$ . The distance between  $\mathbf{M}_i^{(1)}$  and  $\mathbf{M}_i^{(2)}$  for mode  $i$  is then proposed as:

$$\Delta_i(\mathbf{M}_i^{(1)}, \mathbf{M}_i^{(2)})^2 = \log \left( \prod_{j=1}^2 \frac{1}{\cos^2 \theta_j} \right). \quad (4.3)$$

## 4.2.2 Modal weighing matrices

Considering the above definition of modal distances, this subsection presents an original approach that allows inserting damage information into the modal  $H_\infty$  controller design, using the modal weighing matrices. Structural damage may lead to modal vibration increase or reduction, depending on several factors. The modal distance technique permits to evaluate damage effects in the modes, but it is not able to distinguish if its vibration amplitude is increasing or reducing.

To overcome this limitation, the proposed method assesses the effect of a regular  $H_\infty$  controller on the healthy structure. The idea is to use, for each mode of the healthy structure, its closed-loop attenuation and the respective peak values. By associating these two values to the modal damage effects on the structure, i.e., the modal distances between the open-loop response of the healthy and of the damaged structure, it gives an indication of the amplitude variation and also of the respective importance of each mode. With these data, it is possible to obtain a relation to provide the modal damage amplitude weighing that can be used to design the damage-tolerant controller.

Considering  $p$  different performance signals, Fig. 4.2 shows the open-loop amplitude frequency response of the healthy structure and also the closed-loop response using the regular  $H_\infty$  controller, between the performance signal  $\mathbf{z}_l(t)$  for  $l = 1, \dots, p$  and the disturbance  $\mathbf{w}(t)$ . The following indicator balances the vibration reduction achieved by the controller and the relative effect of the damage for each mode:

$$\bar{\mathbf{q}}_l = \left[ \left( \frac{\alpha_{l1} \Delta_1}{\phi_{l1}} \right) \quad \left( \frac{\alpha_{l2} \Delta_2}{\phi_{l2}} \right) \quad \dots \quad \left( \frac{\alpha_{lm} \Delta_m}{\phi_{lm}} \right) \right], \quad (4.4)$$

in which  $\Delta_i$  is the calculated modal distance,  $\alpha_{li}$  is the modal peak amplitude of the controlled structure and  $\phi_{li}$  is the modal peak reduction, for  $i = 1, \dots, m$ .

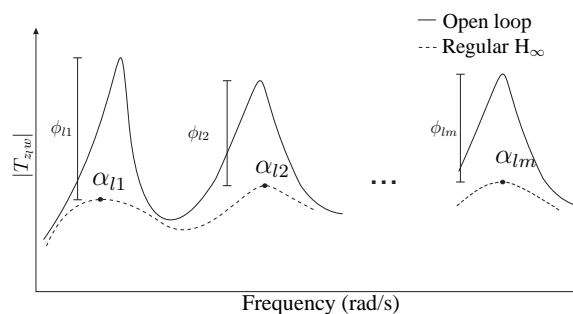


Figure 4.2 -  $T_{\mathbf{z}_l \mathbf{w}}$  attenuation and peak values.

One can notice that each factor in Eq. (4.4) shall correspond to an element of the modal weighing matrices. However, considering the relative values of these parameters, it is possible to have very small or very large numbers. To limit these numbers, it is convenient to establish an amplitude transformation, taking into account the minimum and the maximum values of the vector given by Eq. (4.4). Attributing two new values for these numbers, the adopted transformation is the line equation formed by these two points in a plane. The new values must conduct the parameters to a reasonable range, chosen based on practical aspects, e.g., maximum output voltage. The new consistent vector is now:

$$\mathbf{q}_l = \begin{bmatrix} \beta_{l1} & \beta_{l2} & \cdots & \beta_{lm} \end{bmatrix}, \quad (4.5)$$

which leads to the following modal weighing matrices that distribute the control energy among the modes, conducting to modal selectivity:

$$\mathbf{Q}_1^{\frac{1}{2}} = \begin{bmatrix} \beta_{11} & 0 & 0 & 0 \\ 0 & \beta_{21} & 0 & 0 \\ \vdots & \vdots & \ddots & \vdots \\ 0 & 0 & 0 & \beta_{p1} \end{bmatrix}, \dots, \mathbf{Q}_m^{\frac{1}{2}} = \begin{bmatrix} \beta_{1m} & 0 & 0 & 0 \\ 0 & \beta_{2m} & 0 & 0 \\ \vdots & \vdots & \ddots & \vdots \\ 0 & 0 & 0 & \beta_{pm} \end{bmatrix}. \quad (4.6)$$

### 4.2.3 Algorithm for the modal damage-tolerant controller design

The following algorithm summarises the steps to design the damage-tolerant controller.

---

#### **Algorithm 4.1** Damage-tolerant controller design.

---

- 1: Determine the modal state-space model of the healthy plant (Eq. (2.7)) and the respective observability matrices (Eq. (4.2));
  - 2: Estimate the observability matrices for the damaged plant and calculate the subspace angles for each mode;
  - 3: Design the regular  $H_\infty$  controller by solving the respective optimisation problem (2.12);
  - 4: Compute the subspace distances for each mode between the healthy and damaged models (Eq. (4.3));
  - 5: Compute the raw indicator of each mode considering the amplitude variation due to damage (Eq. (4.4)) and transform them into consistent values (Eq. (4.5));
  - 6: Build the modal weighing matrices (Eq. (4.6));
  - 7: Design the modal  $H_\infty$  controller by solving the respective optimisation problem (Theorem (3.2)).
-

### 4.3 Simulated results with FE models

This section presents details of the healthy and the damaged structure, using FE models. In the sequence, a Regular  $H_\infty$  Controller (RC) and a Modal  $H_\infty$  Controller (MC) are designed to reduce the structural vibration caused by disturbance. Recall that only the MC design uses the damage information through the weighing matrices, as already described. Then, the simulated controller performances are analysed and compared.

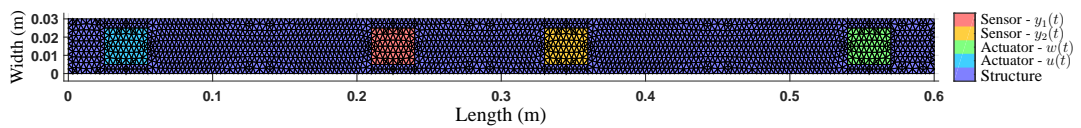
#### 4.3.1 Simulated flexible structure

Considering the classical approach of linear constitutive relations for the materials with small mechanical and electrical perturbations (BATOZ et al., 1980; PREUMONT, 2002), the proposed method is general and does not rely on a particular shape or boundary conditions of the controlled structure. The only requirement is that the structure can be modelled by means of a theory that leads to Eq. (2.1) and Eq. (2.2). Using a dedicated software, the FE method gives a general frame to get such equations, linking the idealisation of any physical structure, which may provide accurate models with a high number of degrees of freedom.

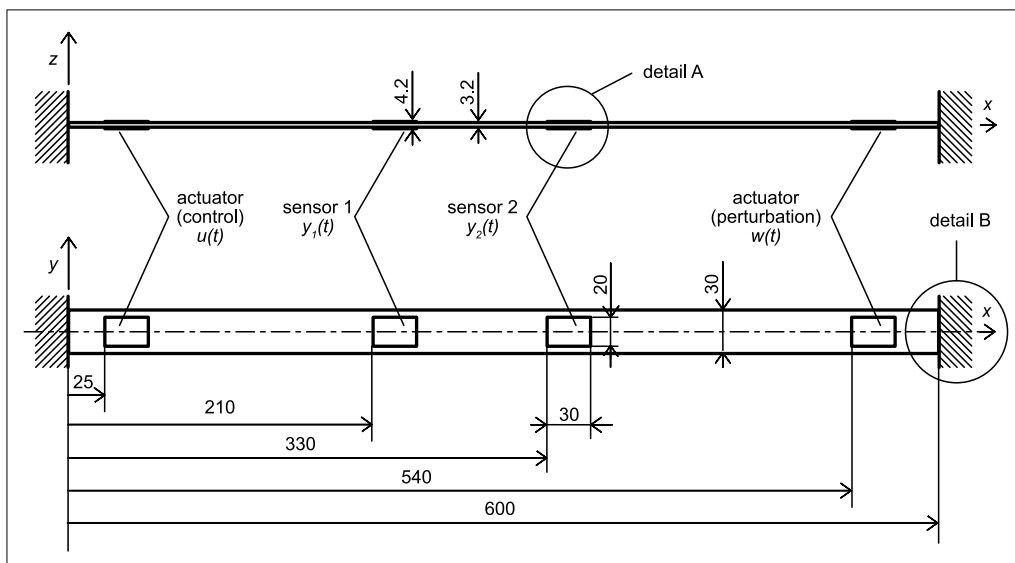
The example of an active aluminium structure chosen to demonstrate the application of the proposed modal  $H_\infty$  technique is shown in Fig. 4.3(a), according to the guidelines presented in Fig. 4.3(b) and to the material properties of the structure in Table 4.1. This structure is a  $600 \text{ mm} \times 30 \text{ mm}$  uniform aluminium plate, equipped with four pairs of piezoelectric ceramic elements bonded on its upper and lower faces, as shown in Fig. 4.4. The respective thicknesses are 3.2 mm for the plate and 0.5 mm for each piezoelectric ceramic element, whose properties are given in Table 4.2. The control signal  $u(t)$  and the disturbance  $w(t)$  are applied to the actuators, where the sensors generate respectively the signals  $y_1(t)$  and  $y_2(t)$ . The structure is simulated using a dedicated FE software, named PLQP and developed at the PIMM Laboratory to test control strategies on plates. The FE model mesh contains 3939 discrete Kirchhoff triangular plate elements (BATOZ et al., 1980), considering 472 ones to model the four areas where the piezoelectric transducers are placed. Moreover, 2186 nodes are used, considering three mechanical DOFs per node, which represent three generalised displacements, i.e., one translation and

two rotations. Thus, it leads to 6558 mechanical DOFs and four electrical DOFs, which describe the potential electric difference  $p_j(t)$  applied to each external electrode of ceramics couples, for  $j = 1, \dots, 4$ . The electric potential is constant and orthogonal to the plane  $(x,y)$  in each piezoelectric layer. These ceramics have an isotropic behaviour in the plane  $(x,y)$ , the direction of polarisation is  $z$ , and they are covered with electrodes. The aluminium core imposes the same potential of reference (0) to the electrodes at  $z = \pm 1.6$  mm and the electric connections imply equal potentials  $p_j^+(t) = p_j^-(t) = p_j(t)$  on the external electrodes ( $z = \pm 1.85$  mm). More details about the PLQP software can be seen in Annexe A.

When the perfect boundary conditions in  $x = 0$  and  $x = 600$  mm are considered, the aspect ratio allows to model this active structure as a clamped-clamped beam if the model aims to represent only the first modes of vibration. However, due to the consideration of a “damaged” clamping at  $x = 600$  mm, this assumption cannot be done and the structure is modelled as a Kirchhoff plate. The choice of a symmetric structure with respect to the plane  $(x,y)$  induces an uncoupling of the membrane and bending modes. The chosen electric connections lead to control signals that do not induce membrane deformations.



(a) Flexible structure.



(b) Schematic diagram in mm.

Figure 4.3 - Adopted aluminium structure with active elements.

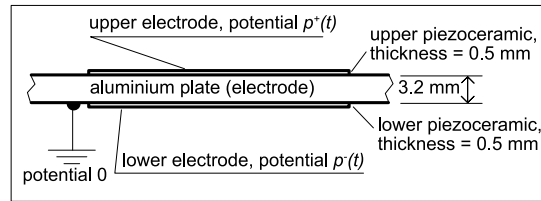


Figure 4.4 - Detail A of Fig. 4.3(b): configuration of each couple of piezoceramic elements.

Table 4.1 - Structure mechanical properties.

| Dimension (mm) | $\rho$ (kg/m <sup>3</sup> ) | $E$ (GPa) | $\nu$ |
|----------------|-----------------------------|-----------|-------|
| 30×600×3.2     | 2700                        | 70        | 0.33  |

Table 4.2 - Mechanical and electrical properties of the piezoelectric elements (NOLIAC<sup>®</sup>).

| Dimension (mm) | $\rho$ (kg/m <sup>3</sup> ) | $E_{11}$ (GPa) | $E_{33}$ (GPa) | $\nu_{12}$ | $d_{31}$ (pC/N) | $d_{33}$ (pC/N) |
|----------------|-----------------------------|----------------|----------------|------------|-----------------|-----------------|
| 20×30×0.5      | 7600                        | 62.50          | 52.63          | 0.38       | -195            | 460             |

Damage is simulated by a partial clamping at  $x = 600$  mm as shown in Fig. 4.5; it is a common damage in clamped structures. The length  $h$  of the free boundary governs the severity of this damage. It can be interpreted as the model of a crack of length  $h$  in the linking of the beam to the rigid frame.

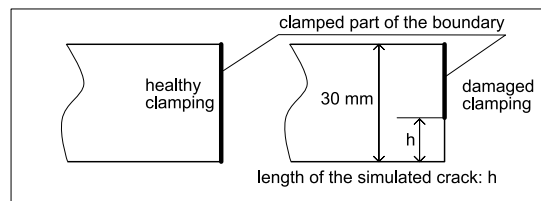


Figure 4.5 - Detail B of Fig. 4.3(b): modification of the boundary conditions to simulate a damage that models a crack of length  $h$ .

The nominal plant model used to design the controllers is reduced to four modes. Another model with ten modes, referred here as the complete model, is adopted to analyse the controller performance in order to verify that the controller is effectively avoiding spillover. A comparison of the open-loop transfer functions for both models is presented in Fig. 4.7. The respective vibration modes and natural frequencies are presented in Table 4.3 and the mode shapes of the nominal model are shown in Fig. 4.6.



Figure 4.6 - Mode shapes of the nominal model.



Table 4.3 - First natural frequencies of the healthy structure.

| Mode | Frequency (rad/s) | Deformation | Mode | Frequency (rad/s) | Deformation |
|------|-------------------|-------------|------|-------------------|-------------|
| 1    | 295.69            | Bending     | 6    | 3861.10           | Bending     |
| 2    | 816.72            | Bending     | 7    | 5360.21           | Bending     |
| 3    | 1590.10           | Bending     | 8    | 7173.37           | Bending     |
| 4    | 2574.19           | Bending     | 9    | 7630.50           | Torsion     |
| 5    | 3683.19           | Torsion     | 10   | 9267.03           | Bending     |

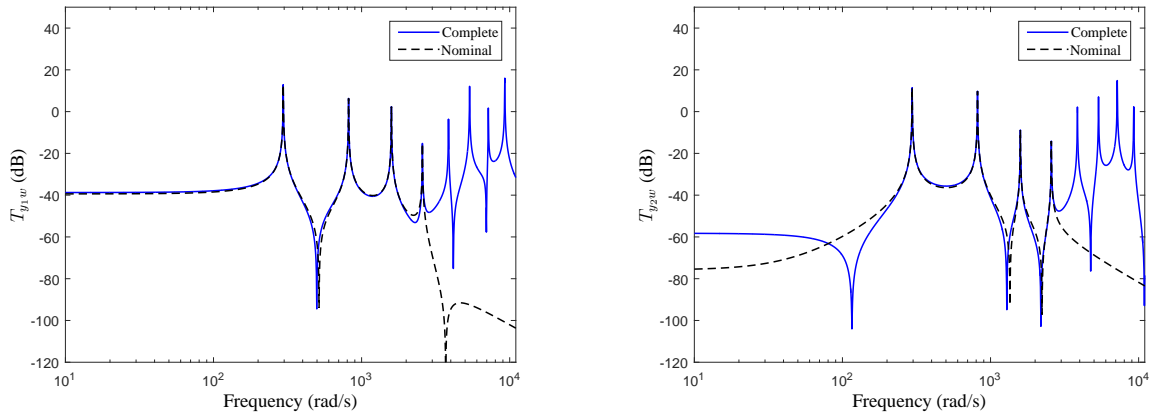


Figure 4.7 - Transfer function comparison between complete and nominal models.

### 4.3.2 Damage simulation

Damage is simulated as a crack with different severities depending on its length  $h$ . For this purpose, three different severities are simulated:

- No damage:  $h = 0$ ;
- Damage 1:  $h = 10$  mm;
- Damage 2:  $h = 15$  mm;
- Damage 3:  $h = 20$  mm.

Damage may induce different effects on each mode of vibration, because the crack changes the boundary conditions, thus changing mode shapes. This can be seen in Fig. 4.8, which shows the frequency responses from the healthy structure and the damaged structure, for damage 3. It is possible to notice natural frequency shifts in all modes and amplitude changes, larger in modes 3 and 4, which belong to the frequency range of interest. In mode 3, damage reduces the amplitude of vibrations while in mode 4 damage leads to a larger amplitude. Damage effects on the natural frequencies and modal amplitudes can be summarised in a single value for

each vibration mode, using a modal damage metric. Figure 4.9 presents the modal distances for the three damage cases, in which their increase with damage severity can be easily seen. These results also verify the proposed modal metric as a tool to assess damage severity.

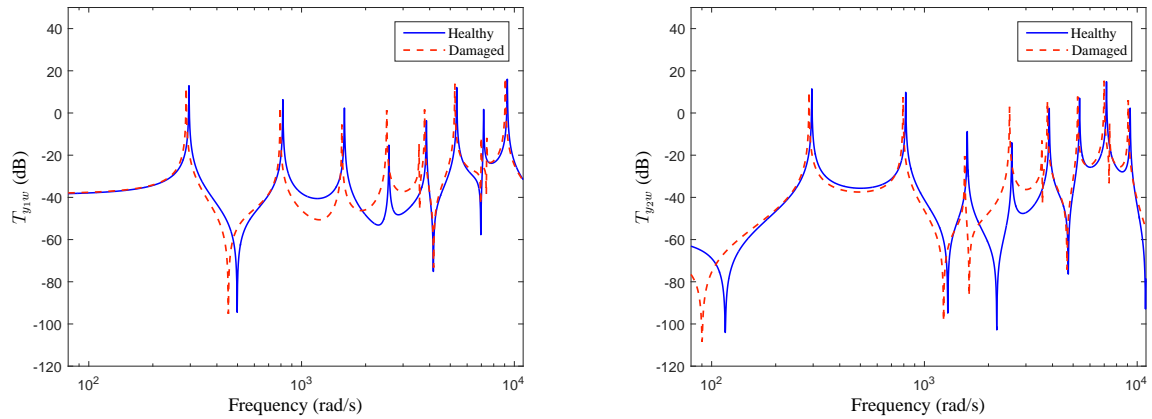


Figure 4.8 - Frequency response comparison between the healthy and the damaged structure (Damage 3).

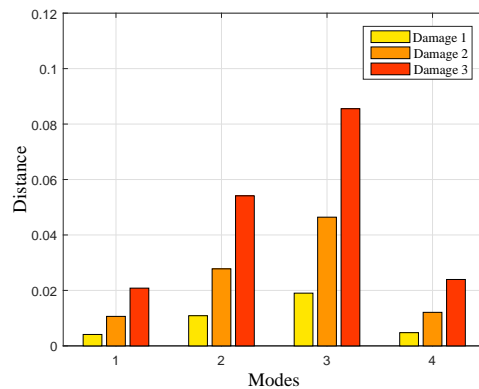


Figure 4.9 - Modal distance estimation.

### 4.3.3 Regular robust controller design

Regular robust controllers are commonly used to reduce vibrations effects caused by disturbance. The regular controller is designed based on the nominal model of the healthy structure, according to Eq. (2.7). The performance matrices are defined as  $C_1 = C_2$  and  $D_{11} = D_{12} = [0 \ 0]^T$ . A chirp signal with band between 0 Hz and 500 Hz, duration of 20 seconds, and amplitude of 4 V is considered as the disturbance to examine the controller performance. The complete model is employed to close the loop. The spillover-avoiding capab-

ility is achieved by using the weighing filters of Eq. (3.7), designed with the parameters present in Table 4.4.

Table 4.4 - Parameters of the weighing filters.

| weighing filters | $\omega_c$ | $k$ | $M$ | $\varepsilon$ |
|------------------|------------|-----|-----|---------------|
| $F_u$            | 2320       | 2   | 65  | 0.07          |
| $F_z$            | 2320       | 1   | 65  | 0.07          |

Frequency and time responses for the open-loop and closed-loop healthy structure are shown in Fig. 4.10 and Fig. 4.11, which also show results for the modal controller presented in the next subsection. Figure 4.10 presents frequency responses for the two performance outputs in the interest band. It can be seen the vibration reduction for all modes, with mode 4 presenting the lowest reduction. Table 4.5 details the vibration attenuation for each mode.

Table 4.5 - Healthy beam modal responses with the regular controller.

| Modal vibration reduction (dB; $ \phi $ )    |               |               |               |               |
|--|---------------|---------------|---------------|---------------|
| Transfer function                            | Mode 1        | Mode 2        | Mode 3        | Mode 4        |
| $T_{z_1w}$                                   | 44.6; 169.82  | 34.0; 050.12  | 34.8; 55.95   | 4.2; 1.62     |
| $T_{z_2w}$                                   | 47.0; 223.87  | 43.4; 147.91  | 27.5; 23.71   | 4.2; 1.62     |
| Controlled structure peaks (dB; $ T_{zw} $ ) |               |               |               |               |
| $T_{z_1w}$                                   | -31.5; 0.0266 | -28.1; 0.0394 | -31.6; 0.0266 | -19.2; 0.1096 |
| $T_{z_2w}$                                   | -35.5; 0.0168 | -33.5; 0.0211 | -35.9; 0.0160 | -18.1; 0.1245 |

#### 4.3.4 Modal robust controller design

The same controller structure with the same filters is adopted for the modal robust controller design, adding the modal weighing matrices and the respective performance outputs. These matrices are determined based on modal distances calculated between the open-loop healthy and damaged structures (damage 3), and using data contained in Table 4.5, according to Eq. (4.4). The minimum weighing value is 0.6 and the maximum value is 4.5. Based on these parameters, the following modal weighing matrices are calculated:

$$\mathbf{Q}_1^{\frac{1}{2}} = \begin{bmatrix} 0.6 & 0 \\ 0 & 0.6 \end{bmatrix}, \mathbf{Q}_2^{\frac{1}{2}} = \begin{bmatrix} 0.7 & 0 \\ 0 & 0.6 \end{bmatrix}, \mathbf{Q}_3^{\frac{1}{2}} = \begin{bmatrix} 0.7 & 0 \\ 0 & 0.7 \end{bmatrix}, \text{ and } \mathbf{Q}_4^{\frac{1}{2}} = \begin{bmatrix} 4.5 & 0 \\ 0 & 4.5 \end{bmatrix}.$$

These values imply that vibration mode 4 has the highest desired weighing factor. Notice that similar modal weighing matrices are obtained using the modal distances considering damage 1

or damage 2.

### 4.3.5 Healthy structure responses

The performance of both controllers are initially compared for the healthy structure. Frequency and time responses are presented in Fig. 4.10 and Fig. 4.11, respectively. It can be seen in both figures that, for mode 1, the controllers have similar performance. For modes 2 and 3, the RC performance is slightly better than the MC performance. These results are expected because the MC has a low weight in these modes. For mode 4, the MC performance is better than the RC one, due to the modal weighing increase in this mode. Figure 4.11 also shows that there is no spillover excitation.

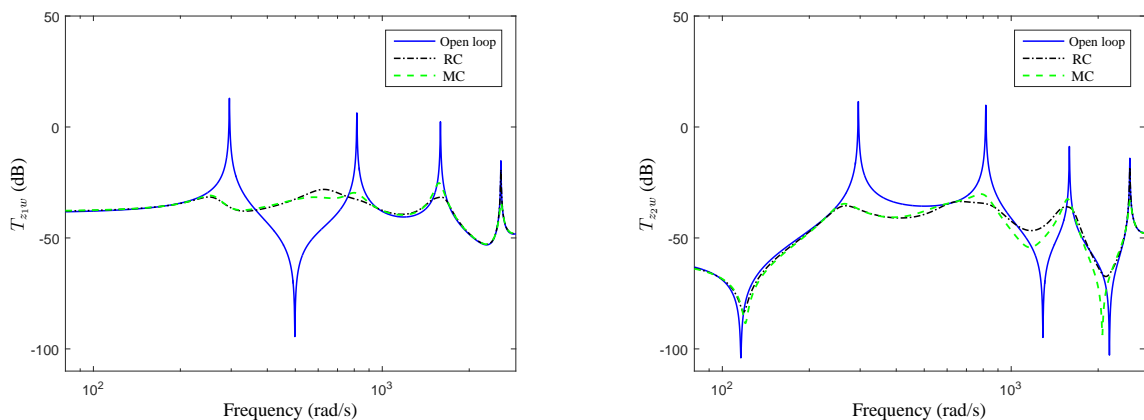


Figure 4.10 - Frequency response comparison between the uncontrolled and the controlled healthy structure.

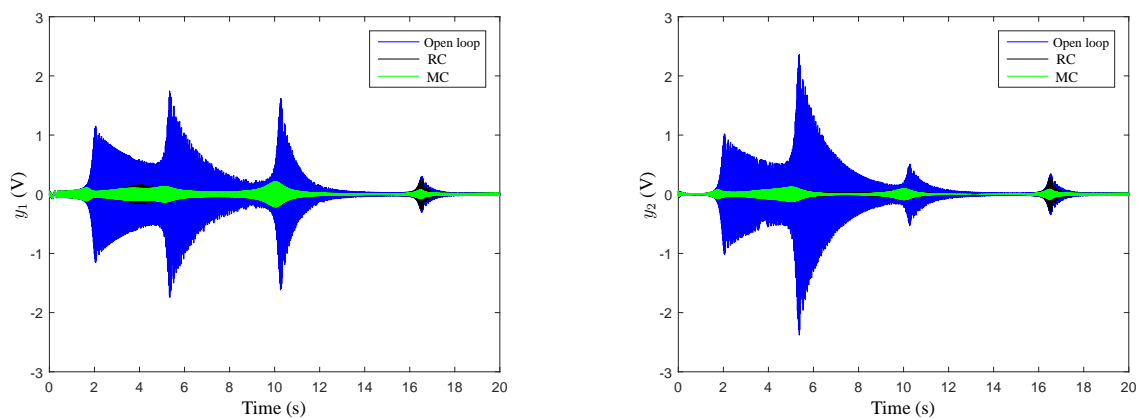


Figure 4.11 - Performance comparison between the uncontrolled and the controlled healthy structure.

Figure 4.12 permits to compare the RC and MC control signals, where the colour superposition changes in order to clarify the relative amplitudes. It can be seen that the MC presents a better energy distribution, due to the relative specified modal weighing. Comparing with the RC, the MC control signal has its amplitude reduced in mode 2, is equivalent in mode 3 and is amplified in mode 4, but its amplitude is low compared to mode 2. It can be affirmed that both controllers achieves satisfactory performance in the healthy structure vibration reduction.

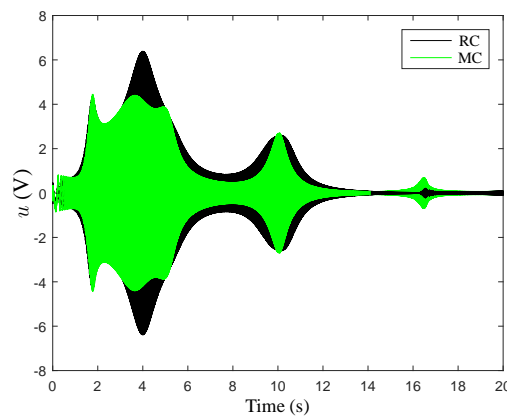
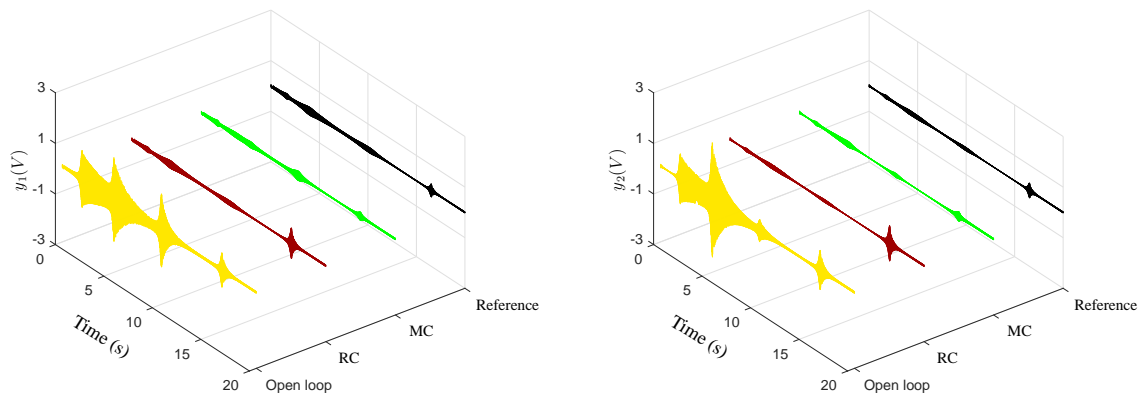


Figure 4.12 - Control signal comparison between the MC and the RC in the healthy structure.

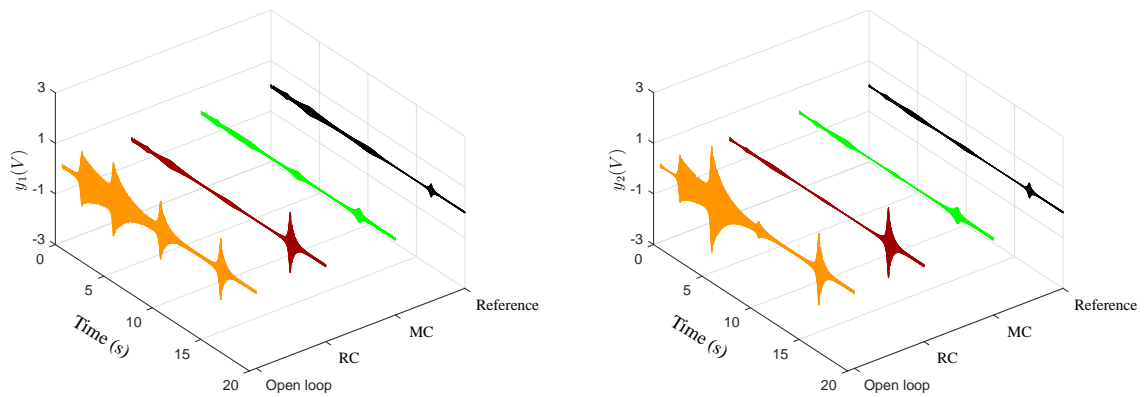
#### 4.3.6 Controller responses under damage

The adopted DTAC strategy aims to focus the control action on modes that are indeed suffering the worst damage consequences. For this purpose, the MC is designed to provide an appropriate energy distribution to mitigate damage effects, besides controlling the healthy structure, too. The MC is now examined under the three different damage conditions and it is compared to the RC behaviour. Time domain performance signals are presented in Fig. 4.13, in which the RC performance of the healthy structure is used as the reference.

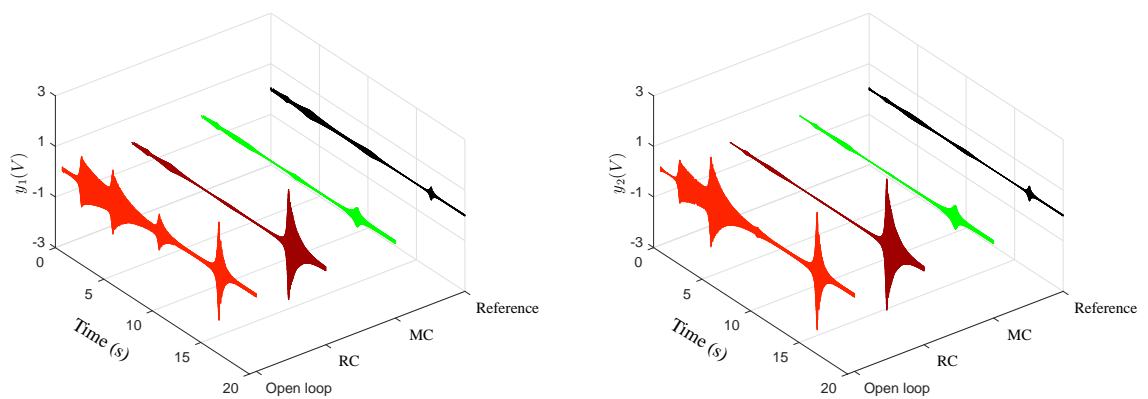
It can be seen in Fig. 4.13 that the modes 1, 2, and 3 are slightly affected by damage even for the higher severity case, with both controllers presenting similar performance, also close to the reference. Recall that for the uncontrolled structure this also occurs, but it is possible to notice that there are performance differences for the mode 4, which increase significantly the vibration peak under the RC, getting even higher than the open-loop vibration peaks. However, the MC maintains the mode 4 close to the reference and significantly smaller than the open-loop behaviour.



(a) Structure submitted to damage 1.



(b) Structure submitted to damage 2.



(c) Structure submitted to damage 3.

Figure 4.13 - Performance comparison of the controlled structure subjected to damage.

Figure 4.14 shows the control signal behaviour for the two tested controllers, where the colour superposition changes in order to clarify the relative amplitudes. Comparing the control signal evolution among the three severity cases, their amplitudes decrease for both controllers for the first three modes, which are less affected by the damage, and increase for the fourth

mode, as the severity progresses. However, it can be seen that the MC amplitude for the mode 4 increases substantially, leading to the high attenuation seen in Fig. 4.13. The general result is an energy migration from the first three modes to the fourth, but it is more efficient with the MC.

It is also interesting to note that both controllers concentrate the energy for the attenuation in the first and second modes, which present the highest open-loop amplitude. The damage effect in the analysed cases increases significantly the open-loop vibrations of the fourth mode, which presents a low amplitude when compared to the first modes. Healthy mechanical structures usually behave as low-pass systems, but the damage renders the fourth-mode amplitude higher than the other modes, as seen in Fig. 4.13(c). The proposed method permits to foresee this effect and to design a controller that, being effective for the healthy structure, can present the damage-tolerant capability, which, as seen in the results, does not occur for a regular-designed controller.

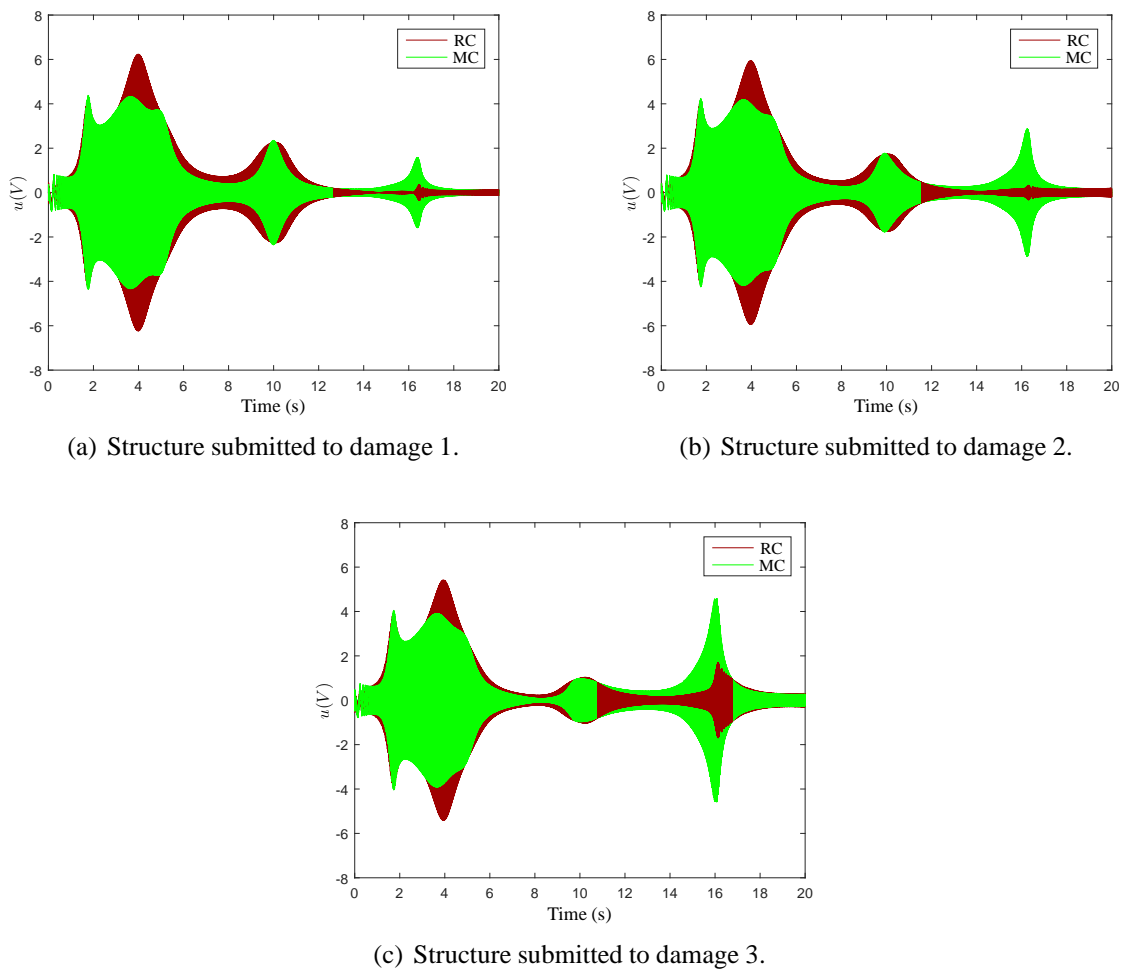


Figure 4.14 - Control signal comparison of the controlled structure subjected to damage.

#### 4.4 Conclusion

An investigation of the damage-tolerant controller design based on a modal  $H_\infty$  norm was conducted. The proposed methodology allows to design an effective control system for a healthy structure, which can also face damage effects. The adopted approach considers foreseen study results that can point the most stressed regions and, therefore, the most probable ones where a damage could occur. The same controller can achieve an adequate performance to the healthy and damaged structures, avoiding the necessity of a reconfigurable controller design process. As a consequence of these characteristics, the proposed method can also extend the operational life of the structures.

The damage controller achieves these goals by specifying modal weighing matrices in order to provide an adequate control signal energy distribution to mitigate damage effects. The adopted approach considers that structural damage impact is represented by a composition of damage effects on each mode, which may be quantified using a damage indicator based on a proposed modal distance. The modal damage indicator is used to build modal weighing matrices, used as a design requirement to provide an appropriate damage-tolerant controller. A transformation of the performance output vector of the RC design includes these modal constraints, leading to an optimisation problem that may be efficiently solved by known LMI methods.

The proposed methodology is tested using the FE modelling of a clamped-clamped beam, where the controller response to three different damage severities is simulated. The performance results of the MC are shown to be more effective against damage impacts, compared to the RC, due to the achieved modal selectivity. This feature is responsible for concentrating the control energy on the modes that are mostly affected by damage. Moreover, the performance of the damage-tolerant controller is also adequate to the healthy structure, which yields the conclusion that the proposed modal approach can protect the structure, retarding damage occurrence.



## 5 A MODAL DOUBLE-LOOP CONTROL FRAMEWORK FOR DTAC

This chapter shows a novel modal double-loop control framework to face damage effects on structure vibrations. Initially, the adopted framework describing the double loop and its modules is presented, where the first loop is based on a modal controller and the second aims to compensate damage dynamic changes of the plant. A detailed description of the damage compensator follows, which is based on a new SHM module and a reconfiguration mechanism to adapt the controller parameters. The simulated results are the subject of the next section, and then the final conclusions are presented balancing the observed behaviour of the proposed method.

### 5.1 Introduction

Smart structures may present a sophisticated computational level, allowing real-time functions like SHM and AVC. Many techniques have been developed for SHM (ISERMANN, 2006; SAEED et al., 2009b; GENARI; NÓBREGA, 2012; FENDZI et al., 2015) and for AVC (HALIM, 2004; GAWRONSKI, 2008; PREUMONT, 2011; PEREIRA; SERPA, 2015), focusing on damage detection and diagnosis, or adequate performance and robustness for controlled systems. However, SHM and AVC methods are independently designed in general, despite the fact that damage may significantly affect the AVC performance. Aiming to overcome the controller performance decline due to damage, this chapter presents a framework to design damage-tolerant active controllers, based on a novel double-loop modal controller, which may be adaptively reconfigured in real time.

The double-loop robust control concept was proposed by Zhou and Ren (2001) to solve the conflict between performance and robustness for the regular feedback controller. The key idea is to use two controllers, where the first controller is designed to provide performance and the other is designed to guarantee stability and robustness. This control idea has been successfully used as an FTC strategy (CIESLAK et al., 2008; ALVES JR. et al., 2009; QIU et al., 2011). A new double-loop methodology is presented in this chapter, based on the application of the modal  $H_\infty$  norm proposed in Chapter 3 to control flexible structures subject to damage.

In this case, the first controller is designed to comply with performance and robustness requirements for the healthy structure. The second controller aims to ensure satisfactory closed-loop performance and robustness including damage effects. An online reconfigurable technique is adopted to design the second controller, based on a modal state-tracking method to provide the update of the controller parameters. FE models of a case study structure are adopted, considering the health condition and some levels of damage conditions, in order to test the proposed double-loop control methodology.

## 5.2 Adopted DTAC framework

Regular controllers are designed in order to ensure a specified level of performance and robustness for the closed-loop system. However, both properties are directly influenced by structural model accuracy (CHOMETTE et al., 2008). Mechanical structure dynamics is highly sensitive to damage, which may increase the vibration of both the open-loop and the closed-loop structures. On the other hand, damage effects over system dynamics is difficult to predict, hindering to incorporate structural damage information into the controller design. Simply trying to increase the robustness, expecting to accommodate the large model variation due to damage effects, may lead to significant performance loss in the closed-loop system for the healthy structure. Notwithstanding, it does not guarantee acceptable performance if a damage occurs.

To include damage as a control design requirement, the closed-loop system should be able to comply with previously defined performance and robustness requirements for the healthy plant, and also to ensure that, despite the damage dynamic effects, the system maintains an adequate performance level. A methodology for AVC based on the modal double-loop controller for DTAC applications is proposed in this chapter, which satisfies these requirements. Several strategies and approaches are possible for DTAC, similar to existing solutions for FTC. The simple approach is to design just a robust controller in a single loop, as mentioned in the previous paragraph. This strategy is depicted in Fig. 5.1, where a robust controller  $C_1$  is designed to reduce the structural vibration  $y(t)$  caused by the disturbance forces  $w(t)$ , satisfying a performance index vector  $z(t)$ . However, the unpredictability of the damage effects implies that a good performance is not guaranteed. A better approach is used in Chapter 4, where the key idea is to use previous knowledge acquired from similar structures to predict future damage most likely

effects, and design a nonreconfigurable controller to face this probable damage, if and when it happens.

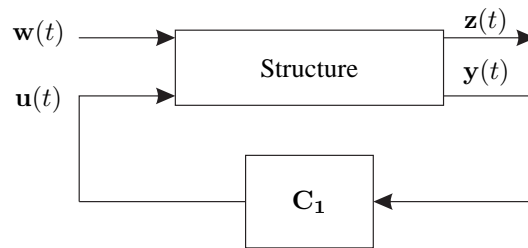


Figure 5.1 - Single loop.

Zhou and Ren (2001) proposed the double-loop scheme in Fig. 5.2 to be used for robustness increase and also for FTC applications. Comparing with the scheme in Fig. 5.1, a residue generator and a second controller  $C_2$  are included. The controller  $C_2$  acts over the residue signal, which is due to the plant dynamic changes. An application of this configuration is for nonlinear systems, which may be linearised at an operation point, and the second controller compensates any significant variation of this operating point. These two strategies are based on fixed parameter controllers, which is called in the FTC area a *passive* strategy. However, a more general solution is to design an automatically reconfigurable controller, with the ability to characterise the damage-caused dynamic changes on the plant and adapt the controller online, without the intervention of a human operator. The double-loop scheme is adopted in this chapter as a reconfigurable DTAC, considering its simple way to compensate big model changes. In the present case, a linear time-invariant controller is chosen for the first controller, called the nominal controller, and a reconfigurable controller is adopted as the damage compensator.

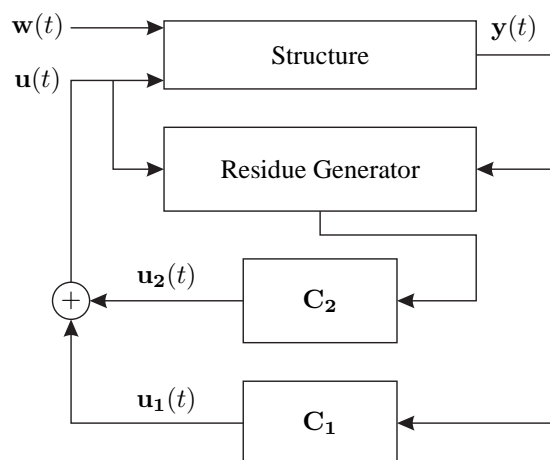


Figure 5.2 - Double loop.

Figure 5.3 presents the well known FTC reconfigurable framework (ZHANG; JIANG, 2008) for a regulator controller, which is in general based on a single-loop controller with vari-

able parameters. A residue generator block receives in parallel with the plant both the control input signal and the real-time measurement output. This block embeds an implicit plant model used to generate the respective residue signal resulting from the processing of these two input signals. Several FDI techniques may be used to estimate the fault effects, represented by the signal  $f(t)$ . In the mechanical structure area, the SHM has similarities in relation to the FDI, with the corresponding differences due to the particularities of the structural behaviour. Considering that smart structures embed transducers, damage may also impact on the transducer behaviour, rendering the DTAC a more complex problem. However, in both areas, the residue signals need to present the capability to conduct the reconfiguration of the controller. In order to do this, the reconfiguration mechanism, another functional block that can be seen in Fig. 5.3, uses the residue to compute online the new controller parameters.

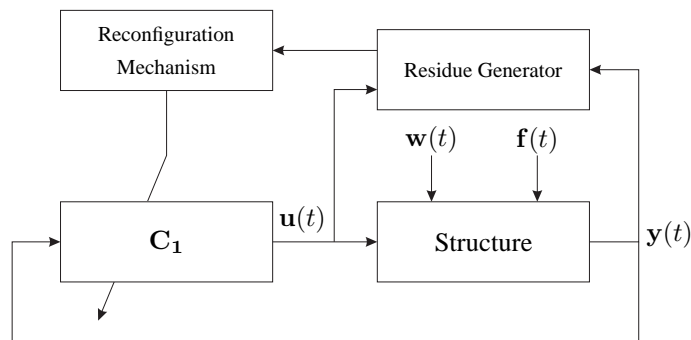


Figure 5.3 - FTC framework.

The proposed DTAC framework is presented in Fig. 5.4. It shows two different controllers, the nominal controller and the damage compensator, which cooperate in order to control the vibrations of flexible structures subject to damage. The nominal controller parameters are set in the design phase to provide the disturbance rejection and they are not updated. The damage compensator parameters are reconfigured online to face the damage consequences on the plant behaviour. The modal  $H_\infty$  approach is adopted to design the nominal controller. The modal approach provides high authority over the control energy distribution among the modes, reflecting a designer-chosen compromise to guarantee a good performance for the healthy structure (see Chapter 3 for more details). As such, this healthy closed-loop model is also adopted as the reference to generate the desired performance output. This means that the damage compensator goal is to maintain the same performance that was present in the plant before the damage occurrence. The damage effects are assumed as a bounded unknown input signal  $\varphi(t)$ . To design the reconfigurable damage compensator, a state-tracking strategy is modified, based on a model reference adaptive control approach (LAVRETSKY; WISE, 2013), which includes the modal

behaviour as a design requirement. The estimated state vector is compared to the reference state vector, generating a residue vector which the reconfiguration mechanism uses to adapt the damage compensator parameters. In the next sections, the proposed DTAC methodology is detailed, in order to explain how the double-loop approach may be used to implement a reconfigurable controller.

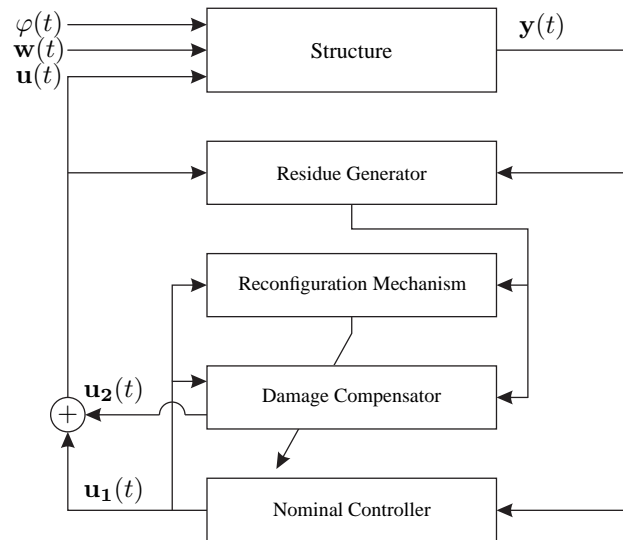


Figure 5.4 - Proposed DTAC framework.

### 5.3 Reconfigurable DTAC controller

Figure 5.5 shows the detailed block diagram of the DTAC framework, including the plant and five constitutive modules, respectively the nominal controller, the modal observer, the reference model, the reconfiguration mechanism, and the damage compensator. The nominal controller generates the control signal  $\mathbf{u}_1(t)$  and is already proposed in the previous section. The damage compensator generates the control signal  $\mathbf{u}_2(t)$ , based on the updated parameters provided by the reconfiguration mechanism. An SHM module encompasses a modal-state observer and a reference model block, whose output  $\mathbf{x}_r(t)$  is compared to the observed state  $\hat{\mathbf{x}}(t)$  to generate the residue  $\mathbf{e}_x(t) = \hat{\mathbf{x}}(t) - \mathbf{x}_r(t)$ . The residue is essential for the parameter reconfiguration. These modules are detailed in the next subsections.

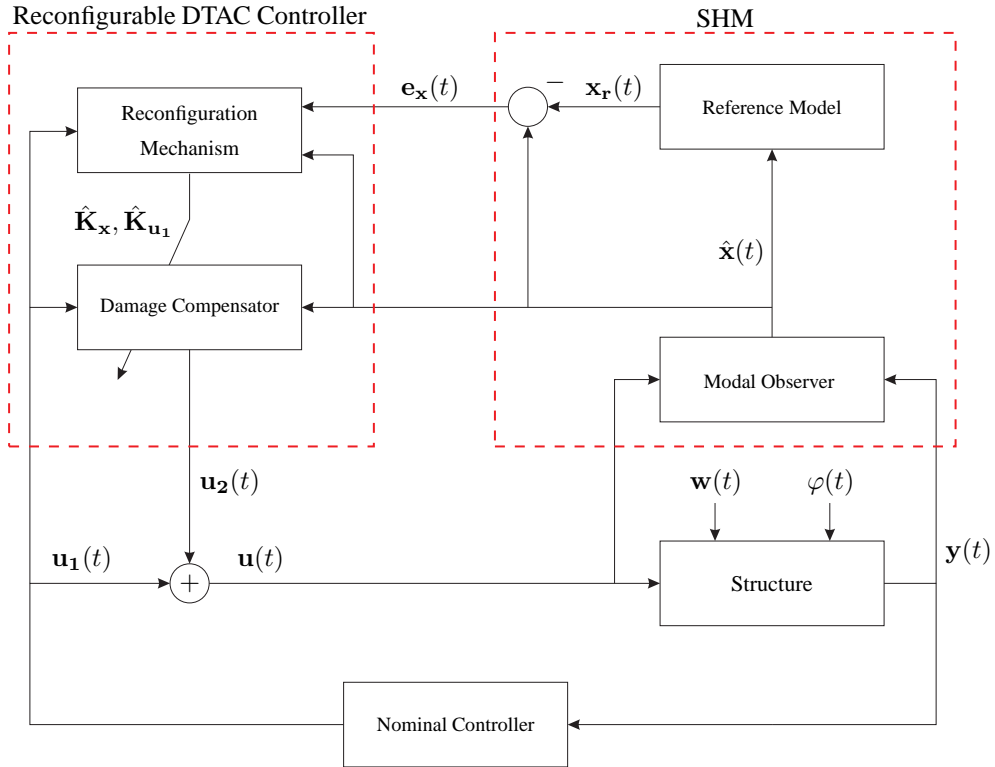


Figure 5.5 - Detailed block diagram of the proposed DTAC framework.

### 5.3.1 Modal observer design

The modal state vector  $\mathbf{x}(t)$  is estimated online based on the measured output signal  $\mathbf{y}(t)$  and the control signal  $\mathbf{u}(t)$ , which contain the respective damage information. The following representation is adopted to include damage in the state-space model:

$$\begin{aligned}\dot{\mathbf{x}}(t) &= \mathbf{A}\mathbf{x}(t) + \mathbf{B}_1\mathbf{w}(t) + \mathbf{B}_2\mathbf{u}(t) + \mathbf{B}_3\varphi(t) \\ \mathbf{y}(t) &= \mathbf{C}_2\mathbf{x}(t) + \mathbf{D}_{21}\mathbf{w}(t),\end{aligned}$$

where  $\varphi \in \mathcal{L}_2$  represents the unknown damage signal and  $\mathbf{B}_3$  is responsible for balancing the damage in each mode. Considering that the controller objective is to compensate the modal vibration in terms of the modal  $H_\infty$  norm and respective assumed weights, the control transducer position implies that it guarantees the authority to do so. Therefore, for the sake of simplicity, it is possible to admit that  $\mathbf{B}_3 = \mathbf{B}_2$ , without generality loss. Moreover, the pair  $(\mathbf{A}, \mathbf{C}_2)$  is assumed observable and  $\mathbf{D}_{22} = \mathbf{0}$ .

The following traditional Luenberger observer is adopted to estimate the modal states:

$$\begin{aligned}\dot{\hat{\mathbf{x}}}(t) &= \mathbf{A}\hat{\mathbf{x}}(t) + \mathbf{B}_2\mathbf{u}(t) + \mathbf{L}(\mathbf{y}(t) - \hat{\mathbf{y}}(t)) \\ \hat{\mathbf{y}}(t) &= \mathbf{C}_2\hat{\mathbf{x}}(t),\end{aligned}$$

in which  $\hat{\mathbf{x}}(t)$  and  $\hat{\mathbf{y}}(t)$  are the estimations of the state and the output vectors. The gain  $\mathbf{L}$  is chosen so that  $\hat{\mathbf{x}}(t)$  converges to  $\mathbf{x}(t)$ . The estimation error dynamics,  $\dot{\mathbf{e}}(t) = \dot{\mathbf{x}}(t) - \dot{\hat{\mathbf{x}}}(t)$ , is given by:

$$\begin{aligned}\dot{\mathbf{e}}(t) &= \mathbf{A}\mathbf{x}(t) + \mathbf{B}_1\mathbf{w}(t) + \mathbf{B}_2\mathbf{u}(t) - \mathbf{A}\hat{\mathbf{x}}(t) - \mathbf{B}_2\mathbf{u}(t) - \mathbf{L}(\mathbf{y}(t) - \mathbf{C}_2\hat{\mathbf{x}}(t)) + \mathbf{B}_2\varphi(t) \\ &= \mathbf{N}\mathbf{e}(t) + \mathbf{E}\mathbf{w}(t) + \mathbf{B}_2\varphi(t),\end{aligned}\quad (5.1)$$

in which  $\mathbf{N} = \mathbf{A} - \mathbf{L}\mathbf{C}_2$  and  $\mathbf{E} = \mathbf{B}_1 - \mathbf{L}\mathbf{D}_{21}$ .

The observer gain  $\mathbf{L}$  is computed in order to ensure the stability of the estimation error dynamics and to attenuate the influence of damage and disturbance in the state estimation. The following theorem is proposed to give an observer solution based on an LMI approach.

**Theorem 5.1.** *The estimation error dynamics given in Eq. (5.1) is globally stable if there exist matrices  $\bar{\mathbf{P}} = \bar{\mathbf{P}}^T \geq 0$ ,  $\Theta$ , and scalars  $\rho, \nu, \alpha > 0$  that satisfy  $\|\mathbf{e}(t)\|_2 \leq \rho\|\varphi(t)\|_2$ ,  $\|\mathbf{w}(t)\|_2 \leq \nu$ , and the following LMI:*

$$\begin{bmatrix} \mathbf{A}^T\bar{\mathbf{P}} - \mathbf{C}_2^T\Theta^T + \bar{\mathbf{P}}\mathbf{A} - \Theta\mathbf{C}_2 + \mathbf{I} + \alpha\mathbf{I} & \bar{\mathbf{P}}\mathbf{B}_2 & \bar{\mathbf{P}}\mathbf{B}_1 - \Theta\mathbf{D}_{21} \\ \mathbf{B}_2^T\bar{\mathbf{P}} & -\mu\mathbf{I} & \mathbf{0} \\ \mathbf{B}_1^T\bar{\mathbf{P}} - \mathbf{D}_{21}^T\Theta^T & \mathbf{0} & -\frac{1}{\beta}\mathbf{I} \end{bmatrix} < 0, \quad (5.2)$$

in which  $\mu = \rho^2$ ,  $\beta = \alpha^{-1}\nu^2$ , and the observer gain is computed as  $\mathbf{L} = \bar{\mathbf{P}}^{-1}\Theta$ .

*Proof.* The  $\mathcal{L}_2$ -induced norm from  $\varphi(t)$  to  $\mathbf{e}(t)$  considering  $\rho > 0$  is given by:

$$\int_0^\infty \mathbf{e}^T(t)\mathbf{e}(t) dt < \rho^2 \int_0^\infty \varphi^T(t)\varphi(t) dt. \quad (5.3)$$

The performance index  $J_{\varphi_e}$  is defined from the inequality (5.3) as:

$$J_{\varphi_e} = \int_0^\infty \{\mathbf{e}^T(t)\mathbf{e}(t) - \rho^2\varphi^T(t)\varphi(t)\} dt.$$

Considering the Lyapunov candidate function  $V(\mathbf{e}(t))$  and that the boundary conditions

are null, i.e.,  $V(\mathbf{e}(t))|_{t=0} = 0$  and  $V(\mathbf{e}(t))|_{t \rightarrow \infty} \rightarrow 0$ , then:

$$\begin{aligned} J_{\varphi_e} &= \int_0^{\infty} \left\{ \mathbf{e}^T(t)\mathbf{e}(t) - \rho^2 \varphi^T(t)\varphi(t) + \dot{V}(\mathbf{e}(t)) - \dot{V}(\mathbf{e}(t)) \right\} dt \\ &= \int_0^{\infty} \left\{ \mathbf{e}^T(t)\mathbf{e}(t) - \rho^2 \varphi^T(t)\varphi(t) + \dot{V}(\mathbf{e}(t)) \right\} dt. \end{aligned} \quad (5.4)$$

The Lyapunov quadratic function is chosen as  $V(\mathbf{e}(t)) = \mathbf{e}^T(t)\bar{\mathbf{P}}\mathbf{e}(t)$ . Thus, the derivative of  $V(\mathbf{e}(t))$  along Eq. (5.1) is given by:

$$\dot{V}(\mathbf{e}(t)) = \mathbf{e}^T(t)(\mathbf{N}^T\bar{\mathbf{P}} + \bar{\mathbf{P}}\mathbf{N})\mathbf{e}(t) + 2\mathbf{e}^T(t)\bar{\mathbf{P}}\mathbf{E}\mathbf{w}(t) + \varphi^T(t)\mathbf{B}_2^T\bar{\mathbf{P}}\mathbf{e}(t) + \mathbf{e}^T(t)\bar{\mathbf{P}}\mathbf{B}_2\varphi(t).$$

For  $\|\mathbf{w}(t)\|_2 \leq \nu$ , it follows that:

$$\dot{V}(\mathbf{e}(t)) < \mathbf{e}^T(t)(\mathbf{N}^T\bar{\mathbf{P}} + \bar{\mathbf{P}}\mathbf{N})\mathbf{e}(t) + 2\nu\|\mathbf{e}^T(t)\bar{\mathbf{P}}\mathbf{E}\|_2 + \varphi^T(t)\mathbf{B}_2^T\bar{\mathbf{P}}\mathbf{e}(t) + \mathbf{e}^T(t)\bar{\mathbf{P}}\mathbf{B}_2\varphi(t),$$

where, for a scalar  $\alpha > 0$ , then  $(2\nu\|\mathbf{e}^T(t)\bar{\mathbf{P}}\mathbf{E}\|_2 \leq \alpha^{-1}\nu^2\|\mathbf{e}(t)^T\bar{\mathbf{P}}\mathbf{E}\|_2^2 + \alpha)^1$ , which leads to:

$$\dot{V}(\mathbf{e}(t)) < \mathbf{e}^T(t)(\mathbf{N}^T\bar{\mathbf{P}} + \bar{\mathbf{P}}\mathbf{N})\mathbf{e}(t) + \beta\|\mathbf{e}^T(t)\bar{\mathbf{P}}\mathbf{E}\|_2^2 + \alpha + \varphi^T(t)\mathbf{B}_2^T\bar{\mathbf{P}}\mathbf{e}(t) + \mathbf{e}^T(t)\bar{\mathbf{P}}\mathbf{B}_2\varphi(t), \quad (5.5)$$

in which  $\beta = \alpha^{-1}\nu^2$ . Substituting inequality (5.5) into Eq. (5.4), the performance index is then given by (HAMDI et al., 2012):

$$J_{\varphi_e} = \int_0^{\infty} \begin{bmatrix} \mathbf{e}^T(t) & \varphi^T(t) \end{bmatrix} \begin{bmatrix} \mathbf{N}^T\bar{\mathbf{P}} + \bar{\mathbf{P}}\mathbf{N} + \beta\bar{\mathbf{P}}\mathbf{E}\mathbf{E}^T\bar{\mathbf{P}} + \mathbf{I} + \alpha\mathbf{I} & \bar{\mathbf{P}}\mathbf{B}_2 \\ \mathbf{B}_2^T\bar{\mathbf{P}} & -\rho^2\mathbf{I} \end{bmatrix} \begin{bmatrix} \mathbf{e}(t) \\ \varphi(t) \end{bmatrix} dt.$$

The condition to satisfy the inequality (5.3) is  $J_{\varphi_e} < 0$ , leading to:

$$\begin{bmatrix} \mathbf{N}^T\bar{\mathbf{P}} + \bar{\mathbf{P}}\mathbf{N} + \beta\bar{\mathbf{P}}\mathbf{E}\mathbf{E}^T\bar{\mathbf{P}} + \mathbf{I} + \alpha\mathbf{I} & \bar{\mathbf{P}}\mathbf{B}_2 \\ \mathbf{B}_2^T\bar{\mathbf{P}} & -\rho^2\mathbf{I} \end{bmatrix} < 0. \quad (5.6)$$

Considering the Schur complement (BOYD et al., 1994), inequality (5.6) becomes:

$$\begin{bmatrix} \mathbf{N}^T\bar{\mathbf{P}} + \bar{\mathbf{P}}\mathbf{N} + \mathbf{I} + \alpha\mathbf{I} & \bar{\mathbf{P}}\mathbf{B}_2 & \bar{\mathbf{P}}\mathbf{E} \\ \mathbf{B}_2^T\bar{\mathbf{P}} & -\rho^2\mathbf{I} & \mathbf{0} \\ \mathbf{E}^T\bar{\mathbf{P}} & \mathbf{0} & -\frac{1}{\beta}\mathbf{I} \end{bmatrix} < 0. \quad (5.7)$$

<sup>1</sup>Based on the tautology that for two real scalars  $a$  and  $b$ ,  $(a - b)^2 \geq 0$ .



A new matrix  $\Theta = \bar{\mathbf{P}}\mathbf{L}$  together with  $\mathbf{N} = \mathbf{A} - \mathbf{L}\mathbf{C}_2$ ,  $\mathbf{E} = \mathbf{B}_1 - \mathbf{L}\mathbf{D}_{21}$ , and  $\mu = \rho^2$  is used in order to eliminate the quadratic terms in (5.7):

$$\begin{bmatrix} \mathbf{A}^T\bar{\mathbf{P}} - \mathbf{C}_2^T\Theta^T + \bar{\mathbf{P}}\mathbf{A} - \Theta\mathbf{C}_2 + \mathbf{I} + \alpha\mathbf{I} & \bar{\mathbf{P}}\mathbf{B}_2 & \bar{\mathbf{P}}\mathbf{B}_1 - \Theta\mathbf{D}_{21} \\ & \mathbf{B}_2^T\bar{\mathbf{P}} & -\mu\mathbf{I} & \mathbf{0} \\ & \mathbf{B}_1^T\bar{\mathbf{P}} - \mathbf{D}_{21}^T\Theta^T & \mathbf{0} & -\frac{1}{\beta}\mathbf{I} \end{bmatrix} < 0,$$

where  $\mu$ ,  $\bar{\mathbf{P}}$ , and  $\Theta$  are the variables to be computed via the numerical solution of LMI. This completes the proof.  $\square$

The proposed modal observer is based on the reduced model order. However, the sensor outputs may be affected by residual modes through the observation spillover (CASCIATI et al., 2006), which may introduce an additive noise in the state-vector estimation. To avoid this effect, the state pair of each mode is filtered using a bandpass filter focused on the resonant frequency.

### 5.3.2 Reference model

As already mentioned, the reference model uses the closed loop of the healthy structure model given in Eq. (2.7) under the nominal controller represented in Eq. (2.8). The reference model module continuously generates the desired vector state  $\mathbf{x}_r(t)$ , i.e., without the damage influence. For this purpose, the disturbance input should be known in order to be used to excite the reference model. Usually, it is difficult to estimate online the disturbance forces acting on practical structures. To overcome this limitation, an estimation of the worst-case disturbance is used instead, according to the following equation:

$$\mathbf{w}^*(t) = (\gamma^2\mathbf{I} - \tilde{\mathbf{D}}^T\tilde{\mathbf{D}})^{-1}(\tilde{\mathbf{B}}^T\tilde{\mathbf{P}} + \tilde{\mathbf{D}}^T\tilde{\mathbf{C}})\hat{\mathbf{x}}(t),$$

where this equation is based on the solution of the nominal controller problem, represented here by the set of LMIs (2.12) (see (ZHOU et al., 1995) for more details). Notice that, using the worst-case disturbance, the residue vector is the largest possible. Finally, it is worth to mention that a plant model with additional high-order modes may be adopted in order to build a more precise reference model, without impact on the controller design.

### 5.3.3 Damage compensator

The damage compensator is designed to minimise the residue vector  $\mathbf{e}_x(t)$ , based on the modal adaptive strategy. Considering the model given in Eq (2.7) and the control signal  $\mathbf{u}(t)$  formed by the output signals of both controllers, it is possible to write the following equation:

$$\dot{\mathbf{x}}(t) = \mathbf{A}\mathbf{x}(t) + \mathbf{B}_1\mathbf{w}(t) + \mathbf{B}_2\mathbf{u}_1(t) + \mathbf{B}_2\mathbf{u}_2(t),$$

where the pair  $(\mathbf{A}, \mathbf{B}_2)$  is assumed controllable.

Assuming an ideal fixed-gain control law for the damage compensator as:

$$\begin{aligned} \mathbf{u}_2(t) &= \begin{bmatrix} \mathbf{K}_1^T & \cdots & \mathbf{K}_m^T \end{bmatrix} \begin{bmatrix} \mathbf{X}_1(t) \\ \vdots \\ \mathbf{X}_m(t) \end{bmatrix} + \mathbf{K}_{\mathbf{u}_1}^T \mathbf{u}_1(t) \\ &= \mathbf{K}_x^T \mathbf{x}(t) + \mathbf{K}_{\mathbf{u}_1}^T \mathbf{u}_1(t), \end{aligned} \quad (5.8)$$

in which  $\mathbf{K}_i$  is the gain vector and  $\mathbf{X}_i(t)$  is the state vector, both relative to mode  $i$ , for  $i = 1, \dots, m$ . Then, the closed-loop system with this controller is given by:

$$\dot{\mathbf{x}}(t) = (\mathbf{A} + \mathbf{B}_2\mathbf{K}_x^T)\mathbf{x}(t) + \mathbf{B}_1\mathbf{w}(t) + (\mathbf{B}_2 + \mathbf{B}_2\mathbf{K}_{\mathbf{u}_1}^T)\mathbf{u}_1(t). \quad (5.9)$$

The damage compensator goal is to track asymptotically the reference model state to mitigate damage effects. The state-space model of the healthy structure is defined as:

$$\dot{\mathbf{x}}_r(t) = \mathbf{A}_r\mathbf{x}_r(t) + \mathbf{B}_{1r}\mathbf{w}(t) + \mathbf{B}_{2r}\mathbf{u}_1(t), \quad (5.10)$$

in which the matching conditions can be obtained by comparing Eq. (5.9) to Eq. (5.10):

$$\mathbf{A}_r = \mathbf{A} + \mathbf{B}_2\mathbf{K}_x^T, \mathbf{B}_{1r} = \mathbf{B}_1, \text{ and } \mathbf{B}_{2r} = \mathbf{B}_2 + \mathbf{B}_2\mathbf{K}_{\mathbf{u}_1}^T.$$

Based on Eq. (5.8) and the state-estimation results, the following real control law is proposed for the damage compensator:

$$\mathbf{u}_2(t) = \hat{\mathbf{K}}_x^T(t)\hat{\mathbf{x}}(t) + \hat{\mathbf{K}}_{\mathbf{u}_1}^T(t)\mathbf{u}_1(t), \quad (5.11)$$

where  $\hat{\mathbf{K}}_{\mathbf{x}}(t)$ ,  $\hat{\mathbf{K}}_{\mathbf{u}_1}(t)$ , and  $\hat{\mathbf{x}}(t)$  are respectively the online estimations of  $\mathbf{K}_{\mathbf{x}}$ ,  $\mathbf{K}_{\mathbf{u}_1}$ , and  $\mathbf{x}(t)$ . Then, the closed loop with these new gains is given by:

$$\dot{\hat{\mathbf{x}}}(t) = (\mathbf{A} + \mathbf{B}_2 \hat{\mathbf{K}}_{\mathbf{x}}^T(t)) \hat{\mathbf{x}}(t) + \mathbf{B}_1 \mathbf{w}(t) + (\mathbf{B}_2 + \mathbf{B}_2 \hat{\mathbf{K}}_{\mathbf{u}_1}^T(t)) \mathbf{u}_1(t). \quad (5.12)$$

The next subsection presents the adopted reconfiguration mechanism to estimate the parameters  $\hat{\mathbf{K}}_{\mathbf{x}}(t)$  and  $\hat{\mathbf{K}}_{\mathbf{u}_1}(t)$  online, which are responsible for reconfiguring the compensator to face damage effects, considering the stability of the control system.

### 5.3.4 Reconfiguration mechanism

The reconfiguration mechanism goal is to provide the estimation of  $\hat{\mathbf{K}}_{\mathbf{x}}(t)$  and  $\hat{\mathbf{K}}_{\mathbf{u}_1}(t)$ . For this purpose, the state-tracking error dynamics is defined as  $\dot{\mathbf{e}}_{\mathbf{x}}(t) = \dot{\hat{\mathbf{x}}}(t) - \dot{\mathbf{x}}_r(t)$ . Substituting from Eq. (5.10) and Eq. (5.12), and using the matching conditions, it leads to:

$$\begin{aligned} \dot{\mathbf{e}}_{\mathbf{x}}(t) &= (\mathbf{A} + \mathbf{B}_2 \hat{\mathbf{K}}_{\mathbf{x}}^T(t)) \hat{\mathbf{x}}(t) + \mathbf{B}_1 \mathbf{w}(t) + (\mathbf{B}_2 + \mathbf{B}_2 \hat{\mathbf{K}}_{\mathbf{u}_1}^T(t)) \mathbf{u}_1(t) - \mathbf{A}_r \mathbf{x}_r(t) \\ &\quad - \mathbf{B}_{1r} \mathbf{w}(t) - \mathbf{B}_{2r} \mathbf{u}_1(t) \\ &= \mathbf{A}_r \hat{\mathbf{x}}(t) + \mathbf{B}_2 \Delta \mathbf{K}_{\mathbf{x}}^T(t) \hat{\mathbf{x}}(t) + \mathbf{B}_2 \Delta \mathbf{K}_{\mathbf{u}_1}^T(t) \mathbf{u}_1(t) - \mathbf{A}_r \mathbf{x}_r(t) \\ &= \mathbf{A}_r \mathbf{e}_{\mathbf{x}}(t) + \mathbf{B}_2 \Delta \mathbf{K}_{\mathbf{x}}^T(t) \hat{\mathbf{x}}(t) + \mathbf{B}_2 \Delta \mathbf{K}_{\mathbf{u}_1}^T(t) \mathbf{u}_1(t), \end{aligned} \quad (5.13)$$

in which  $\Delta \mathbf{K}_{\mathbf{x}}^T(t) = (\hat{\mathbf{K}}_{\mathbf{x}}^T(t) - \mathbf{K}_{\mathbf{x}}^T)$  and  $\Delta \mathbf{K}_{\mathbf{u}_1}^T(t) = (\hat{\mathbf{K}}_{\mathbf{u}_1}^T(t) - \mathbf{K}_{\mathbf{u}_1}^T)$  are the gain estimation errors.

The adaptive gains  $\hat{\mathbf{K}}_{\mathbf{x}}(t)$  and  $\hat{\mathbf{K}}_{\mathbf{u}_1}(t)$  must be adequately estimated in order to ensure the stability of the tracking error dynamics, aiming for the tracking error  $\mathbf{e}_{\mathbf{x}}(t)$  to tend asymptotically to zero. To achieve these goals, the following theorem provides an online estimation of the controller gains.

**Theorem 5.2.** *The state-tracking error dynamics given in Eq. (5.13) is stable for the following adaptive gain laws:*

$$\dot{\hat{\mathbf{K}}}_{\mathbf{x}}(t) = -\mathbf{T}_{\mathbf{x}} \hat{\mathbf{x}}(t) \mathbf{e}_{\mathbf{x}}^T(t) \mathbf{P} \mathbf{B}_2, \quad (5.14)$$

$$\dot{\hat{\mathbf{K}}}_{\mathbf{u}_1}(t) = -\mathbf{T}_{\mathbf{u}_1} \mathbf{u}_1(t) \mathbf{e}_{\mathbf{x}}^T(t) \mathbf{P} \mathbf{B}_2, \quad (5.15)$$

in which for  $\mathbf{R} = \mathbf{R}^T > 0$ ,  $\mathbf{P} = \mathbf{P}^T > 0$  satisfies the following algebraic Lyapunov equation:

$$\mathbf{P}\mathbf{A}_r + \mathbf{A}_r^T\mathbf{P} = -\mathbf{R}. \quad (5.16)$$

Moreover,  $\mathbf{T}_x > 0$  and  $\mathbf{T}_{u_1} > 0$  are diagonal matrices that determine adaptation rates. Matrix  $\mathbf{T}_x$  is a function of the modal adaptation-rate submatrices:

$$\mathbf{T}_x = \text{diag}(\mathbf{T}_1, \mathbf{T}_2, \dots, \mathbf{T}_m), \quad (5.17)$$

where the  $2 \times 2$  matrix  $\mathbf{T}_i$  determines the adaptation rate of mode  $i$ .

*Proof.* The following quadratic Lyapunov candidate function is chosen to analyse the stability of the state-tracking error dynamics:

$$\begin{aligned} V(\mathbf{e}_x(t), \Delta\mathbf{K}_x(t), \Delta\mathbf{K}_{u_1}(t)) &= \mathbf{e}_x^T(t)\mathbf{P}\mathbf{e}_x(t) + \text{tr}([\Delta\mathbf{K}_x^T(t)\mathbf{T}_x^{-1}\Delta\mathbf{K}_x(t)] + \\ &\quad + \text{tr}([\Delta\mathbf{K}_{u_1}^T(t)\mathbf{T}_{u_1}^{-1}\Delta\mathbf{K}_{u_1}(t)]), \end{aligned}$$

in which  $\text{tr}$  represents the trace of a matrix.

The derivative of  $V(\mathbf{e}_x(t), \Delta\mathbf{K}_x(t), \Delta\mathbf{K}_{u_1}(t))$ , evaluated using Eq. (5.13), is given by:

$$\begin{aligned} \dot{V}(\mathbf{e}_x(t), \Delta\mathbf{K}_x(t), \Delta\mathbf{K}_{u_1}(t)) &= \dot{\mathbf{e}}_x^T(t)\mathbf{P}\mathbf{e}_x(t) + \mathbf{e}_x^T(t)\mathbf{P}\dot{\mathbf{e}}_x(t) + 2\text{tr}([\Delta\mathbf{K}_x^T(t)\mathbf{T}_x^{-1}\dot{\hat{\mathbf{K}}}_x(t)]) \\ &\quad + 2\text{tr}([\Delta\mathbf{K}_{u_1}^T(t)\mathbf{T}_{u_1}^{-1}\dot{\hat{\mathbf{K}}}_{u_1}(t)]) \\ &= \mathbf{e}_x^T(t)(\mathbf{A}_r^T\mathbf{P} + \mathbf{P}\mathbf{A}_r)\mathbf{e}_x(t) + 2\mathbf{e}_x^T(t)\mathbf{P}\mathbf{B}_2\Delta\mathbf{K}_x^T(t)\hat{\mathbf{x}}(t) \\ &\quad + 2\text{tr}([\Delta\mathbf{K}_x^T(t)\mathbf{T}_x^{-1}\dot{\hat{\mathbf{K}}}_x(t)]) + 2\mathbf{e}_x^T(t)\mathbf{P}\mathbf{B}_2\Delta\mathbf{K}_{u_1}^T(t)\mathbf{u}_1(t) \\ &\quad + 2\text{tr}([\Delta\mathbf{K}_{u_1}^T(t)\mathbf{T}_{u_1}^{-1}\dot{\hat{\mathbf{K}}}_{u_1}(t)]) \\ &= -\mathbf{e}_x^T(t)\mathbf{R}\mathbf{e}_x(t) + 2\text{tr}(\Delta\mathbf{K}_x^T(t)[\hat{\mathbf{x}}(t)\mathbf{e}_x^T(t)\mathbf{P}\mathbf{B}_2 + \mathbf{T}_x^{-1}\dot{\hat{\mathbf{K}}}_x(t)]) \\ &\quad + 2\text{tr}(\Delta\mathbf{K}_{u_1}^T(t)[\mathbf{u}_1(t)\mathbf{e}_x^T(t)\mathbf{P}\mathbf{B}_2 + \mathbf{T}_{u_1}^{-1}\dot{\hat{\mathbf{K}}}_{u_1}(t)]). \end{aligned}$$

If the adaptive laws are selected as:

$$\dot{\hat{\mathbf{K}}}_x(t) = -\mathbf{T}_x\hat{\mathbf{x}}(t)\mathbf{e}_x^T(t)\mathbf{P}\mathbf{B}_2 \text{ and } \dot{\hat{\mathbf{K}}}_{u_1}(t) = -\mathbf{T}_{u_1}\mathbf{u}_1(t)\mathbf{e}_x^T(t)\mathbf{P}\mathbf{B}_2,$$

then  $\dot{V}(\mathbf{e}_x(t), \Delta\mathbf{K}_x(t), \Delta\mathbf{K}_{u_1}(t)) = -\mathbf{e}_x^T(t)\mathbf{R}\mathbf{e}_x(t) \leq 0$ . Therefore, the state-tracking error tends asymptotically to zero, i.e.,  $\lim_{t \rightarrow \infty} \|\hat{\mathbf{x}}(t) - \mathbf{x}_r(t)\| = 0$ . This proves the theorem.  $\square$

### 5.3.5 Modal double-loop controller design procedure

The procedure to design the modal double-loop controller can be divided into two parts: the nominal controller design given in Algorithm 5.1 and the damage compensator design given in Algorithm 5.2.

---

#### Algorithm 5.1 Nominal controller design.

---

- 1: Determine the modal state-space model of the healthy plant using Eq. (2.6) and Eq. (2.7);
  - 2: Design a standard  $H_\infty$  controller using the traditional approach. Then, adjust the weighing filters, based on Eq. (3.7);
  - 3: Choose the modes to act upon, based on the modal performance of the standard  $H_\infty$  controller; build the modal weighing matrices; and build the respective modal performance indicator vector (Eq. (3.5));
  - 4: Solve the modal  $H_\infty$  problem.
- 

---

#### Algorithm 5.2 Damage compensator design.

---

- 1: Design the modal observer by solving the respective LMI (5.2);
  - 2: Design the bandpass filters;
  - 3: Build the reference model, using the closed loop of the healthy structure model given in Eq. (2.7) under the nominal controller represented in Eq. (2.8);
  - 4: Determine matrix  $\mathbf{R} > 0$ . After that, compute matrix  $\mathbf{P}$  by solving the algebraic Lyapunov equation given in Eq. (5.16);
  - 5: Define the matrix  $\mathbf{T}_{u_1}$  and the modal matrices  $\mathbf{T}_i$  to build  $\mathbf{T}_x$ , following Eq. (5.17);
  - 6: Build the adaptive gain laws (Eq. (5.14) and Eq. (5.15));
  - 7: Build the control law (Eq. 5.11).
- 

## 5.4 Simulated results

This section shows results that test the proposed methodology, considering the flexible structure given in Fig. 4.3 of Chapter 4. An MC and a modal adaptive controller are designed to compose the Modal Double-Loop Framework (MDLF). An RC is also designed to be included in the evaluation of the proposed methodology. The performances of the regular controller and the nominal controller, both in single loop, are compared and analysed with the modal double-loop controller.

Moreover, the nominal plant model used to design the controllers and the observer is

reduced to four modes. Another model with ten modes, referred here as the complete model, is also adopted to analyse the controller performance, in order to verify that the methodology is effective in avoiding the spillover.

#### 5.4.1 Damage simulation

The same crack of Chapter 4 of length  $h$  localised at the beam extremity is here adopted, considering two different lengths:

- Damage 2:  $h = 15$  mm;
- Damage 3:  $h = 20$  mm.

#### 5.4.2 Nominal controller design

The nominal controller is designed based on the nominal model of the healthy structure, where the performance matrices are defined as  $\mathbf{C}_1 = \mathbf{C}_2$  and  $\mathbf{D}_{11} = \mathbf{D}_{12} = [0 \ 0]^T$ . A chirp signal, with bandwidth from 0 Hz to 500 Hz, duration of 20 seconds, and amplitude of 4 V, is considered as a disturbance in order to examine the controller performance. To balance the control signals and the relation between disturbance and performance signals, the weighing filters are designed with the parameters presented in Table 4.4.

The RC is initially designed to reduce the vibration of the healthy structure and uses the same filters of the nominal controller in order to have an acceptable comparison base. This controller is used to provide reference performances to be compared with the other control techniques. Frequency and time responses for the open-loop and the closed-loop healthy structure are shown in Fig. 5.6 and Fig. 5.7, which also show results for the MC presented next. It is possible to see that the regular controller reduces the peak vibration for all modes, with modes 1 and 2 presenting the largest reduction.

The nominal controller is designed based on the modal approach and with the same controller structure of the RC, adding the respective performance outputs. These matrices are built considering the low peak vibration attenuation of mode 4, obtained by the RC. Thus, the fol-

lowing weighing matrices are adopted:

$$\mathbf{Q}_1^{\frac{1}{2}} = \begin{bmatrix} 0.7 & 0 \\ 0 & 0.7 \end{bmatrix}, \mathbf{Q}_2^{\frac{1}{2}} = \begin{bmatrix} 0.7 & 0 \\ 0 & 0.7 \end{bmatrix}, \mathbf{Q}_3^{\frac{1}{2}} = \begin{bmatrix} 0.9 & 0 \\ 0 & 0.9 \end{bmatrix}, \text{ and } \mathbf{Q}_4^{\frac{1}{2}} = \begin{bmatrix} 1.6 & 0 \\ 0 & 1.6 \end{bmatrix}.$$

The performance of both single-loop controllers for the healthy structure is compared in Fig. 5.6 and Fig. 5.7. Considering modes 1 and 2, the RC performance is slightly better than the MC performance, due to the low weight of the MC. For mode 3, both controllers have similar performances due to the small change of the respective modal weighing matrix. However, the MC performance is better than the RC one for mode 4, due to the respective modal weighing increase. Figure 5.8 permits to analyse the modal control energy distribution of both controllers, where the colour superposition changes in order to clarify the relative amplitudes. Comparing with the RC, the MC control signal has its amplitude reduced in mode 2, does not change in modes 1 and 3, and is amplified in mode 4. It is possible to affirm that both controllers have a satisfactory performance considering the healthy structure vibration attenuation.

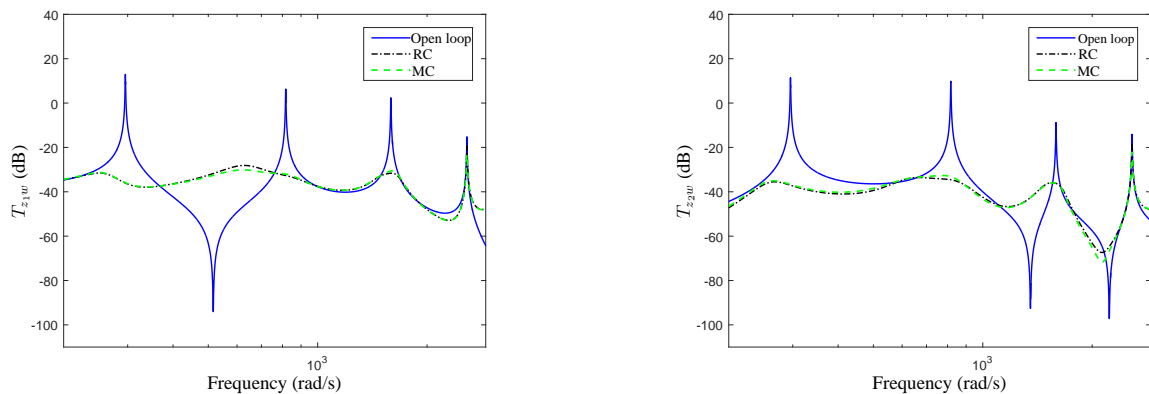


Figure 5.6 - Frequency response comparison between the uncontrolled and the controlled healthy structure.

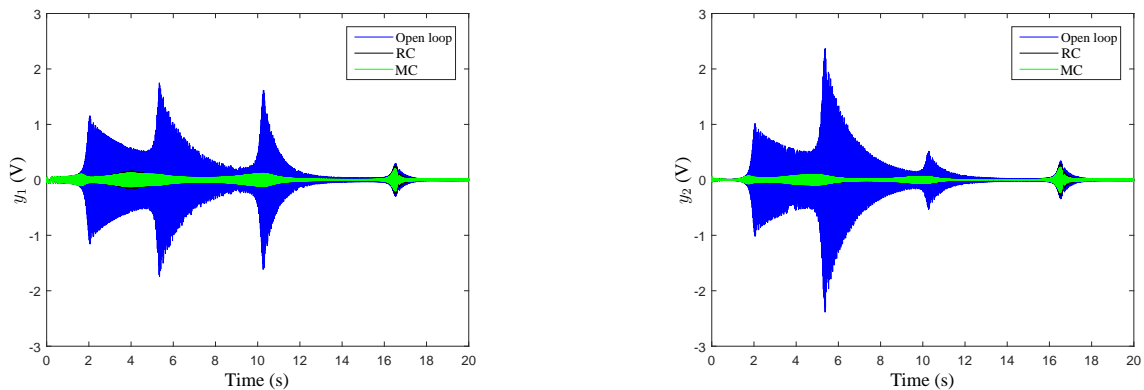


Figure 5.7 - Performance comparison between the uncontrolled and the controlled healthy structure.

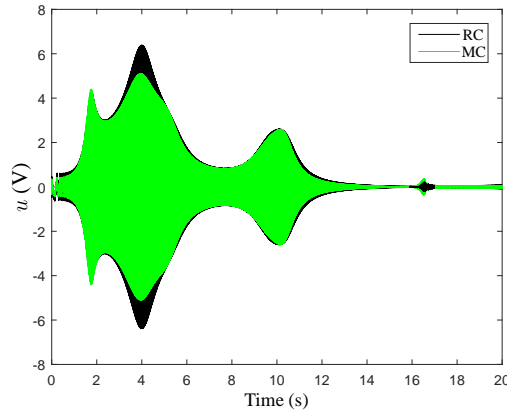


Figure 5.8 - Control signal comparison between the MC and the RC in the healthy structure.

### 5.4.3 Damage compensator design

Following the Algorithm 5.2 to design the damage compensator, the first step is to design the modal observer, solving the LMI (5.2), where it is adopted  $\nu = 5$  and  $\alpha = 5$ . A Butterworth approach is considered for the bandpass filters, according to the parameters presented in Table 5.1.

Table 5.1 - Parameters of the bandpass filters.

| Cutoff frequency (rad/s) | Mode 1 | Mode 2 | Mode 3 | Mode 4 |
|--------------------------|--------|--------|--------|--------|
| $\omega_{c1}$            | 0      | 400    | 1200   | 1900   |
| $\omega_{c2}$            | 400    | 1200   | 1900   | 2700   |

Matrix  $\mathbf{R}$  and the modal adaptation-rate matrices are chosen with the highest gains over the modes 3 and 4, due to the low vibration attenuations achieved with the RC. Thus, the following matrices are adopted:

$$\mathbf{R} = \text{diag}(0.01; 0.01; 0.01; 0.01; 0.1; 0.1; 1; 1),$$

$$\mathbf{T}_1 = \begin{bmatrix} 50 & 0 \\ 0 & 50 \end{bmatrix}, \mathbf{T}_2 = \begin{bmatrix} 50 & 0 \\ 0 & 50 \end{bmatrix}, \mathbf{T}_3 = \begin{bmatrix} 500 & 0 \\ 0 & 500 \end{bmatrix},$$

$$\mathbf{T}_4 = \begin{bmatrix} 2000 & 0 \\ 0 & 2000 \end{bmatrix}, \text{ and } \mathbf{T}_{u_1} = 0.001.$$

The adaptive controller struggles to track the reference model state vector by estimating



the gains  $\mathbf{K}_x$  and  $\mathbf{K}_{u_1}$ . The control effort may generate high amplitude signals, leading even to actuator saturation, however producing a small reduction of the state-tracking error. A threshold is adopted to interrupt the iteration process, setting the gains to the previous value. This procedure is described by the following rule:

$$\hat{\mathbf{K}}_i(t) = \begin{cases} \text{Eq. (5.14)}, & \text{if } \|\mathbf{e}_{x_i}\| > \varepsilon_i, \text{ measured during a } \Delta(t) \\ \text{last value}, & \text{otherwise,} \end{cases}$$

where  $\Delta(t)$  is a specific time period and  $\mathbf{K}_i$ ,  $\mathbf{X}_i$ , and  $\mathbf{e}_{x_i}$  represent respectively the gain, the state vector, and the state-vector difference relative to mode  $i$ .

#### 5.4.4 Controller responses under damage

The same chirp signal adopted before is used to simulate the disturbance for three cycles of twelve repetitions of the signal. Each cycle corresponds to one condition of the structure: healthy plant, plant with damage 2, and plant with damage 3, as described before. Three controller methodologies are examined in these different situations: single-loop RC, single-loop MC, and the MDLF formed by the composition of the MC and the adaptive controller.

Figure 5.9 shows the behaviour of each mode in twelve separate panels. Modal peak amplitudes from the open-loop response and also the closed-loop response for the output signals  $y_1(t)$  and  $y_2(t)$ , for each one of the three adopted controllers, and the three respective control signals  $u(t)$  may be seen in the panels.

It is possible to see that the damage occurrence reduces the amplitude of modes 1 to 3 of the uncontrolled structure, as previously discussed. However, damage does not change the controller performances in modes 1 to 3, for both levels of damage severity. Regarding the control signals, the peak amplitudes are similar to all controllers for modes 1 and 3. For mode 2, it may be seen that the control signal amplitude for the RC controller is higher than those for both modal controllers. This shows modal controllers efficiency over the RC. Regarding mode 4, the open-loop vibration amplitude increases with damage severity and the controllers have distinct performances. The respective modal vibration increases significantly under the RC, getting even higher than the open-loop respective peak. The MC presents a better performance than the RC, however the modal vibrations also increase with damage severity. For damage 2, the

MDLF initially responds similar to the MC but the adaptive adjustment of its parameters gradually reduces the peak amplitude. For damage 3, the response is much better since the beginning of the damage occurrence. The control signal amplitudes increase for all the controllers to face damage, however the MDLF amplitude is the highest, which leads to the efficient attenuation of the mode.

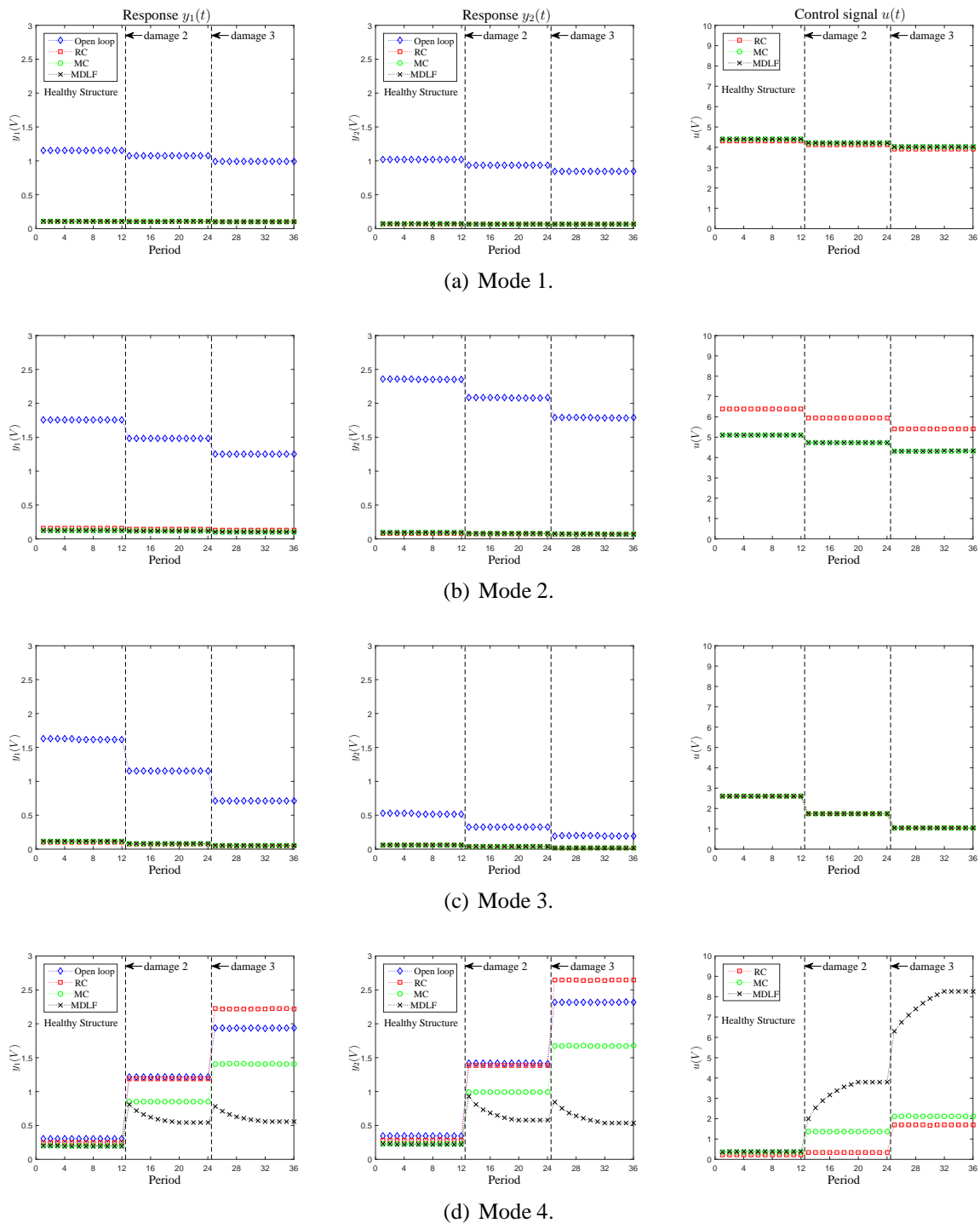


Figure 5.9 - Modal peak performance comparison of the controlled structure submitted to damage.

Figure 5.10 presents the modal peak amplitudes of the two control signals  $u_1(t)$  and  $u_2(t)$ ,

aiming to analyse the contribution of the nominal controller and the damage compensator to the general performance of the MDLF. It may be seen that  $u_1(t)$ , generated by the nominal controller, is the main responsible for attenuating the vibrations of the first three modes, presenting a similar performance for the three plant conditions while maintaining  $u_2(t)$  very small. Regarding mode 4, this behaviour is inverted and the main contribution for the control signal is now from  $u_2(t)$ . It may be seen that the control signal of the nominal controller increases a little with damage but the high level of  $u_2(t)$  dominates over these signals. Considering the overall performance for all modes, it is possible to affirm that both controllers cooperate to achieve a satisfactory performance.

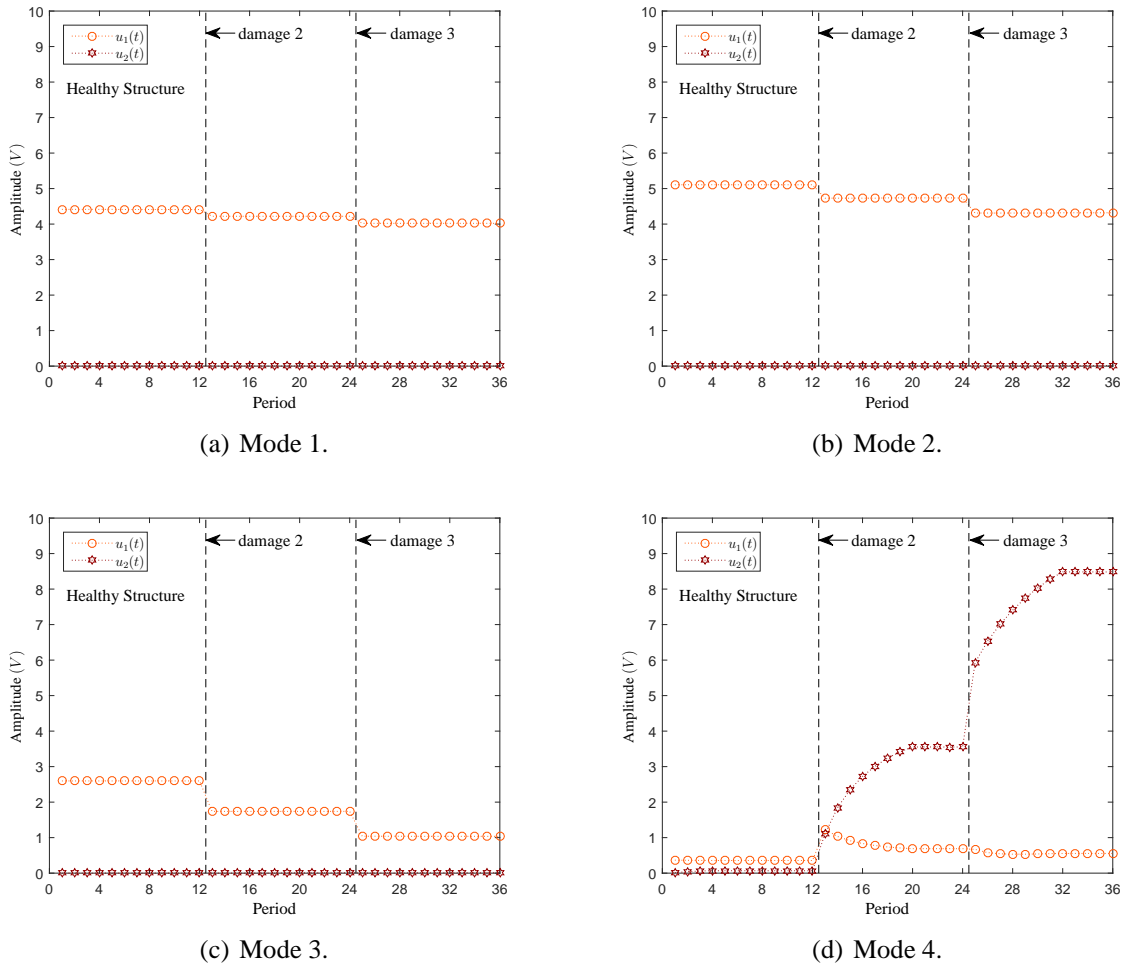


Figure 5.10 - Control signal components of the MDLF.

Considering that the damage compensator has two parameters, in which the first is the modal gain vector that multiplies the state vector and the second is a scalar that weighs the nominal control signal, the adaptive evolution of these parameters is analysed based on the signals represented in Fig. 5.11. It may be seen that, despite the fact that the gains of mode 3 are

larger than mode 2 gains, which are also larger than mode 1 gains, reacting to damage severity, all these values are very small compared to mode 4 gains. One can notice the difference in the vertical scales of these figures. To conclude, Fig. 5.11(e) shows that the contribution of the gain  $\hat{\mathbf{K}}_{u_1}$  to the composition of  $u_2(t)$  is very small.

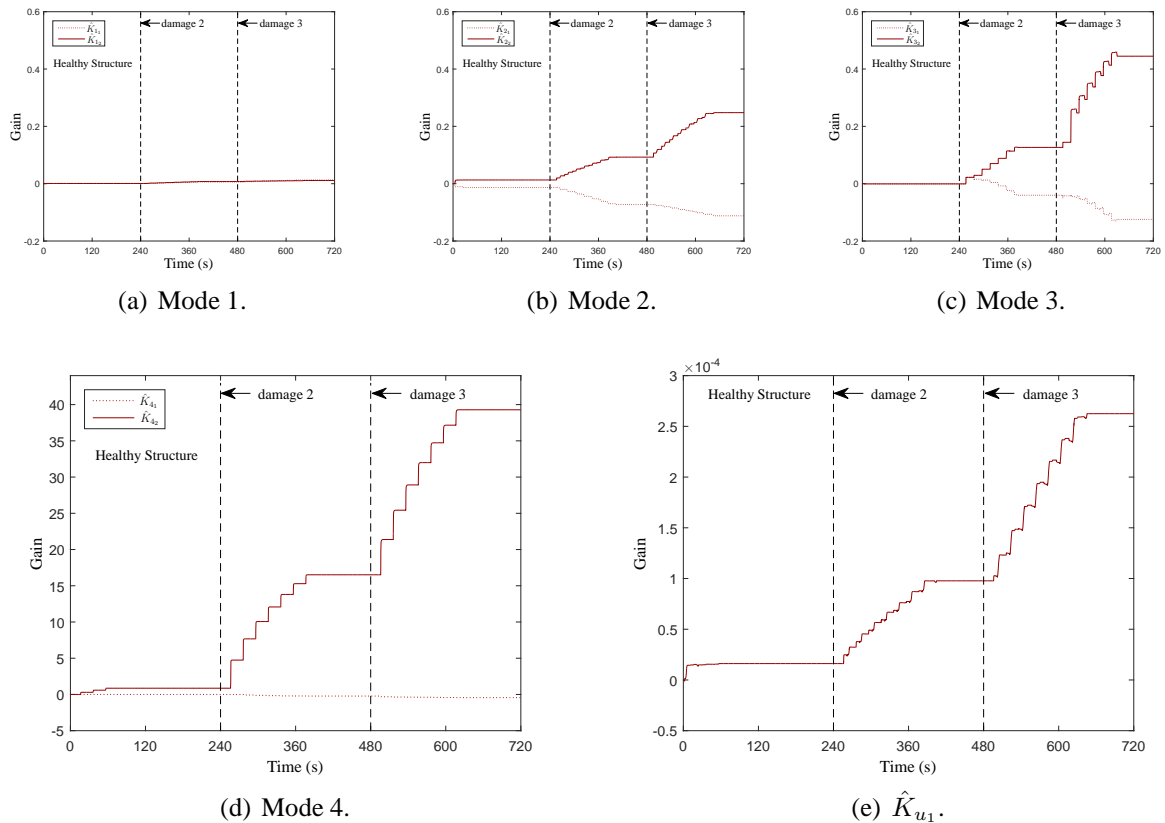


Figure 5.11 - Adaptive gains of the damage compensator.

## 5.5 Conclusion

A new control methodology for damage-tolerant active control is presented in this chapter, based on a modal double-loop control framework. In the outer loop, a modal  $H_\infty$  controller is designed to comply with performance and robustness requirements for the healthy structure. The second modal controller, reconfigured online, has the objective of mitigating damage effects through parameter adaptation laws, based on the output of a modal observer. The damage compensator objective is to reduce the state-tracking error between the healthy and the damage structure, aiming to mitigate the vibration increase caused by damage.

The proposed methodology was examined using the FE modelling of a clamped-clamped structure, where the controller responses for two different damage severities were simulated. The structure was sequentially submitted to two damages, simulating two damage severity levels. A regular  $H_\infty$  controller, a single-loop modal  $H_\infty$  controller, and the modal double-loop framework are examined and compared in facing damage. Performance results show that the double-loop methodology is more effective in mitigating the harmful damage effects on structural vibrations. Moreover, the proposed framework had an adequate performance for the healthy structure, with the result coming from the modal  $H_\infty$  controller, designed to comply with the design requirements of the healthy plant. Furthermore, the proposed methodology acts to retard damage caused by vibration persistency. In the damage case, the methodology acts to mitigate the respective effects on structural vibrations. As a consequence of these characteristics, the proposed modal double-loop framework can extend the structural operational life.

## 6 GENERAL CONCLUSIONS AND FUTURE PERSPECTIVES

Damage-tolerant active control methods are a response to the demand of extending the new flexible structures integrity and the quality of operation. DTAC controllers aim to attenuate structure vibrations due to disturbances even if damage occurs, acting, in this case, to contain or to delay damage evolution providing additional structure life. This thesis contributes to the DTAC area proposing new methods to design damage-tolerant controllers, which are viable to implement the strategies presented in the introduction.

Three different controller design methods are developed, where the proposed modal  $H_\infty$  norm represents an important base. The first method is a robust modal controller that exhibits better performance for the healthy and the damaged structures than the regular  $H_\infty$  controllers. The second method is a preventive modal controller, using previous knowledge about the most stressed regions of the structure, and so the most probable future damaged regions, in order to estimate damage consequences and so design the controller, including the desired performance in the requirements. Results show that the modal selectivity on the energy distribution permits to concentrate the controller efforts on the most affected vibration peaks. The third method is an online reconfigurable controller, associated to a modal controller in a double loop, that detects, estimates, and responds to damage occurrence in order to compensate damage effects. Its results show the effectiveness of this methodology comparing to single-loop controllers to face damage effects, enabling the method to be used to face unexpected damage occurrence.

Considering the several modules necessary to configure the proposed controllers, techniques in SHM, state-tracking reference modelling, and adaptive control were also developed. The main contributions of this work may be listed as follows:

- (i) A method for the modal control of flexible structures is proposed, based on a new modal  $H_\infty$  norm. Considering the compromise between robustness and performance achieved with modal robust controllers, the methodology to design STAC controllers adopting this method is investigated, obtaining promising experimental and simulated results. Moreover, these results show that an adequate control of the damaging modes produces better performance than the regular  $H_\infty$  approach to face damage.
- (ii) The modal  $H_\infty$  approach is extended to include damage as a design requirement,

assuming knowledge of the stressed structure regions. The estimated damage consequences of each mode are used to build the modal weighing matrices and the modal  $H_\infty$  norm, used to design the modal  $H_\infty$  controllers. A selective energy distribution over the frequency range of interest is achieved, implementing the PAC strategy. The method may also be used to implement the EDAC strategy.

- (iii) A modal damage indicator based on a model subspace distance measurement, between a healthy and a damaged model, is proposed and used to estimate damage impact on each structure mode. This information is used to create the modal weighing matrices, as a step to design the proposed PAC damage-tolerant controller.
- (iv) A modal double-loop framework for the vibration control of flexible structures subject to damage is proposed, adopting online reconfigurability of the damage compensator, which aims to attenuate the damage-caused structural vibrations. This ATAC controller has the reconfigurability based on a modal state-tracking approach, which achieved the same selectivity efficiency of the PAC controller and has the advantage of responding to damage without previous knowledge of the system.
- (v) The reference model state-tracking, used in the ATAC strategy, is an adaptation of a reference model output-tracking technique. The modified module uses the performance reference output to track its respective states, (through an observer, commented in the next item), where the reference is the healthy structure closed-loop model, adopting the developed STAC modal controller.
- (vi) A new modal observer technique is developed using the proposed modal  $H_\infty$  norm, and is adopted to estimate the reference model state vector, based on its outputs. This observer reflects the structure dynamics changes as a consequence of damage, permitting the online adaptation of the damage compensator parameters.

There exist many challenges to be faced to design DTAC applications, considering that research in this area is just beginning. However, as a consequence of this work some challenges should be investigated. Future research lines are given below:

- (i) Optimal placement investigation of actuators/sensors in flexible structures considering the possibility of damage occurrence. The regular methods deal with healthy

structures in general. However, as presented in this thesis, damage may change the dynamic characteristics of the structures, where an optimal placement for transducers in healthy structures may not be an optimal solution after damage occurrence.

- (ii) A different approach to avoid the spillover phenomenon considering the change in dynamics due to damage. In this case, the neglected dynamics can be included in the structure model as a modelling error, which may be inserted into the control system design using the modal  $H_\infty$  approach.
- (iii) Testing the modal damage indicator for real structure applications. This indicator showed to be effective in the detection and severity analysis of damage in simulated structures. However, it is interesting to test the proposed damage indicator experimentally, analysing its capability for detection, severity analysis, and localisation of damage, under the SHM scope.
- (iv) Also under the SHM scope, test the estimated subspace distance between the reference model state vector  $\mathbf{x}_r(t)$  and the estimation state vector  $\mathbf{x}(t)$  of the operational structure for detection, severity analysis, and localisation of the damage.
- (v) The implementation of the proposed DTAC methods for more complicated real-life structures. Experiments can be performed to examine the effectiveness of the modal controllers in controlling the vibration in industrial structures subject to damage.
- (vi) To study the active control that takes into account aspects of the material fatigue, introducing the criteria to reduce stress and the respective fatigue, using von Mises, for instance, as part of the performance cost function used to design the damage compensators.



## REFERENCES

- ABREU, G. L. C. M.; LOPES JR., V.  $H_2$  optimal control for earthquake excited structures. In: **VI Congresso Nacional de Engenharia Mecânica**. Campina Grande, Brazil.: [s.n.], 2010.
- ALVES JR., M.; NÓBREGA, E.; YONEYAMA, T. Adaptive neural control for a tolerant fault system. In: **7th IFAC Symposium on Fault Detection, Supervision and Safety for Technical Processes**. Barcelona, Spain: [s.n.], 2009. p. 137–142.
- AMBROSIO, P.; CAZZULANI, G.; RESTA, F.; RIPAMONTI, F. An optimal vibration control logic for minimising fatigue damage in flexible structures. **Journal of Sound and Vibration**, v. 333, n. 5, p. 1269–1280, 2014.
- ASHOKKUMAR, C. R. Vibration control for structural damage mitigation. **Journal of Vibration and Control**, v. 21, n. 15, p. 2995–3006, 2015.
- BALAS, M. J. Active control of flexible systems. **Journal of Optimization Theory and Applications**, v. 25, n. 3, p. 415–436, 1978.
- \_\_\_\_\_. Direct velocity feedback control of large space structures. **Journal of Guidance, Control, and Dynamics**, v. 2, n. 3, p. 252–253, 1979.
- BAPTISTA, F. G.; BUDOYA, D. E.; ALMEIDA, V. A. D.; ULSON, J. A. C. An experimental study on the effect of temperature on piezoelectric sensors for impedance-based structural health monitoring. **Sensors**, v. 1, n. 14, p. 1208–1227, 2014.
- BATOZ, J. L.; BATHE, K. J.; HO, L. W. A study of three-node triangular plate bending elements. **International Journal for Numerical Methods in Engineering**, v. 15, n. 12, p. 1771–1812, 1980.
- BAZ, A.; POH, S. Experimental implementation of the modified independent modal space control method. **Journal of Sound and Vibration**, v. 139, n. 1, p. 133–149, 1990.

BOSSI, L.; ROTTENBACHER, C.; MIMMI, G.; MAGNI, L. Multivariable predictive control for vibrating structures: An application. **Control Engineering Practice**, v. 19, n. 10, p. 1087–1098, 2011.

BOULET, B.; FRANCIS, B. A.; HUGHES, P. C.; HONG, T.  $\mu$  synthesis for a large flexible space structure experimental testbed. **Journal of Guidance, Control, and Dynamics**, v. 24, n. 5, p. 967–977, 2001.

BOYD, S.; EL GHAOUI, L.; FERON, E.; BALAKRISHNAN, V. **Linear Matrix Inequalities in Systems and Control Theory**. Philadelphia, PA: SIAM, 1994.

BRAGHIN, F.; CINQUEMANI, S.; RESTA, F. A new approach to the synthesis of modal control laws in active structural vibration control. **Journal of Vibration and Control**, p. 1–20, 2012.

CARDEN, E. P.; FANNING, P. Vibration based condition monitoring: A review. **Structural Health Monitoring**, v. 3, n. 4, p. 355–377, 2004.

CASCIATI, F.; MAGONETTE, G.; MARAZZI, F. **Technology of Semiactive Devices and Applications in Vibration Mitigation**. [S.l.]: Wiley, 2006.

CASCIATI, F.; RODELLAR, J.; YILDIRIM, U. Active and semi-active control of structures - theory and applications: A review of recent advances. **Journal of Intelligent Material Systems and Structures**, p. 1–15, 2012.

CHATTOPADHYAY, A.; NAM, C.; KIM, Y. Damage detection and vibration control of a delaminated smart composite plate. **Advanced Composites Letters**, v. 9, n. 1, p. 7–15, 2000.

CHOMETTE, B.; CHESNÉ, S.; RÉMOND, D.; GAUDILLER, L. Damage reduction of on-board structures using piezoelectric components and active modal control: Application to a printed circuit board. **Mechanical Systems and Signal Processing**, v. 24, n. 2, p. 352–364, 2010.

CHOMETTE, B.; RÉMOND, D.; CHESNÉ, S.; GAUDILLER, L. Semi-adaptive modal control of on-board electronic boards using an identification method. **Smart Materials and Structures**, v. 17, n. 6, p. 1–8, 2008.

CIESLAK, J.; HENRY, D.; ZOLGHADRI, A.; GOUPIL, P. Development of an active fault-tolerant flight control strategy. **Journal of Guidance, Control, and Dynamics**, v. 31, n. 1, p. 135–147, 2008.

CINQUEMANI, S.; FERRARI, D.; BAYATI, I. Reduction of spillover effects on independent modal space control through optimal placement of sensors and actuators. **Smart Materials and Structures**, v. 24, n. 8, p. 1–11, 2015.

DE COCK, K. **Principal Angles in System Theory, Information Theory and Signal Processing**. PhD Thesis — Katholieke Universiteit Leuven, 2002.

DE COCK, K.; DE MOOR, B. Subspace angles between ARMA models. **Systems & Control Letters**, v. 46, n. 4, p. 265–270, 2002.

DYKE, S. J.; SPENCER, B. F.; QUAST, P.; KASPARI, D. C.; SAIN, M. K. Implementation of an active mass driver using acceleration feedback control. **Computer-Aided Civil and Infrastructure Engineering**, v. 11, n. 5, p. 305–323, 1996.

FAN, W.; QIAO, P. Vibration-based damage identification methods: A review and comparative study. **Structural Health Monitoring**, p. 1–29, 2010.

FANG, J. Q.; LI, Q. S.; JEARY, A. P. Modified independent modal space control of m.d.o.f. systems. **Journal of Sound and Vibration**, v. 261, n. 3, p. 421 – 441, 2003.

FEKIH, A. A robust fault tolerant control strategy for aircraft systems. In: **18th IEEE International Conference on Control Applications**. Saint Petersburg: [s.n.], 2009. p. 1643–1648.

FENDZI, C.; MECHBAL, N.; RÉBILLAT, M.; GUSKOV, M.; COFFIGNAL, G. A general

bayesian framework for ellipse-based and hyperbola-based damage localization in anisotropic composite plates. **Journal of Intelligent Material Systems and Structures**, p. 1–25, 2015.

FISCHER, M. **Finite Element Based Simulation, Design and Control of Piezoelectric and Lightweight Smart Structures**. PhD Thesis — Technische Universität München, 2013.

GAWRONSKI, W. **Advanced Structural Dynamics and Active Control of Structures**. [S.l.]: Springer-Verlag, 2004.

\_\_\_\_\_. **Modeling and Control of Antennas and Telescopes**. [S.l.]: Springer, 2008.

GENARI, H. F. G.; MECHBAL, N.; COFFIGNAL, G.; NÓBREGA, E. G. O. A double-loop control approach applied to damage-tolerant active control. In: **23rd International Congress of Mechanical Engineering**. Rio de Janeiro, Brazil: [s.n.], 2015. p. 1–8.

\_\_\_\_\_. A modal  $H_\infty$  control methodology for damage-tolerant active control. In: **9th IFAC Symposium on Fault Detection, Supervision and Safety for Technical Processes**. Paris, France: [s.n.], 2015. p. 664–669.

GENARI, H. F. G.; NÓBREGA, E. G. O. A damage detection technique based on ARMA models distance estimation. In: **1st International Symposium on Uncertainty Quantification and Stochastic Modeling**. São Sebastião: [s.n.], 2012. p. 140–148.

GENARI, H. F. G.; NÓBREGA, E. G. O.; MECHBAL, N. Structural damage diagnosis method based on subspace identification metric. In: **22nd International Congress of Mechanical Engineering**. Ribeirão Preto, Brazil: [s.n.], 2013. p. 4200–4208.

GENARI, H. F. G.; OLIVEIRA NETO, O.; NÓBREGA, E. G. O.; MECHBAL, N.; COFFIGNAL, G. Robust vibration control of a vertical flexible structure subject to seismic events. In: **XVII International Symposium on Dynamic Problems of Mechanics - DINAME 2015**. Natal, Brazil: [s.n.], 2015. p. 1–10.

GOSIEWSKI, Z.; KULESZA, Z. Virtual collocation of sensors and actuators for a flexible

rotor supported by active magnetic bearings. In: **14th International Carpathian Control Conference**. Rytro: [s.n.], 2013. p. 94–99.

HALIM, D. **Vibration Analysis and Control of Smart Structures**. PhD Thesis — School of Electrical Engineering and Computer Science, University of Newcastle, Australia, 2002.

HALIM, D. Control of flexible structures with spatially varying disturbance: spatial  $H_\infty$  approach. In: **43rd IEEE Conference on Decision and Control**. Atlantis, Paradise Island, Bahamas: [s.n.], 2004. v. 5, p. 5065–5070.

HALIM, D.; MOHEIMANI, S. Experimental implementation of spatial  $H_\infty$  control on a piezoelectric-laminate beam. **IEEE/ASME Transactions on Mechatronics**, v. 7, n. 3, p. 346–356, 2002.

\_\_\_\_\_. Spatial  $H_2$  control of a piezoelectric laminate beam: experimental implementation. **IEEE Transactions on Control Systems Technology**, v. 10, n. 4, p. 533–546, 2002.

HAMDI, H.; RODRIGUES, M.; MECHMECHE, C.; BRAIEK, N. B. Robust fault detection and estimation for descriptor systems based on multi-models concept. **International Journal of Control, Automation and Systems**, v. 10, n. 6, p. 1260–1266, 2012.

HOLFORD, K. M. et al. Acoustic emission for monitoring aircraft structures. **Journal of Aerospace Engineering**, v. 223, n. 5, p. 525–532, 2009.

HSIEH, C. S. Performance gain margins of the two-stage lq reliable control. **Automatica**, v. 38, n. 11, p. 1985–1990, 2002.

HU, J.; ZHU, D. Vibration control of smart structure using sliding mode control with observer. **Journal of Computers**, v. 7, n. 2, p. 411–418, 2012.

HU, Q.; MA, G. Adaptive variable structure maneuvering control and vibration reduction of three-axis stabilized flexible spacecraft. **European Journal of Control**, v. 12, n. 6, p. 654–668, 2006.

HU, Y.; NG, A. Active robust vibration control of flexible structures. **Journal of Sound and Vibration**, v. 288, n. 1–2, p. 43–56, 2005.

HUMAR, J.; BAGCHI, A.; XU, H. Performance of vibration-based techniques for the identification of structural damage. **Structural Health Monitoring**, v. 5, n. 3, p. 215–241, 2006.

INMAN, D. J. **Vibration with Control, Measurement, and Stability**. [S.l.]: Prentice-Hall International Editions, 1989.

\_\_\_\_\_. Active modal control for smart structures. **Philosophical Transactions of the Royal Society of London**, v. 359, p. 205–219, 2001.

ISERMANN, R. **Fault-Diagnosis Systems: An Introduction from Fault Detection to Fault Tolerance**. [S.l.]: Springer, 2006.

JIANG, J.; LI, D. Decentralized guaranteed cost static output feedback vibration control for piezoelectric smart structures. **Smart Materials and Structures**, v. 19, n. 1, p. 1–9, 2010.

JIANG, J.; ZHAO, Q. Design of reliable control systems possessing actuator redundancies. **Journal of Guidance Control and Dynamics**, v. 23, n. 4, p. 709–718, 2000.

KATAYAMA, T. **Subspace Methods for System Identification**. [S.l.]: Springer, 2005.

KHELASSI, A.; THEILLIOL, D.; WEBER, P.; PONSART, J. Fault-tolerant control design with respect to actuator health degradation: An LMI approach. In: **IEEE International Conference on Control Applications**. Denver, CO: [s.n.], 2011. p. 983–988.

KHOT, S.; YELVE, N. P.; TOMAR, R.; DESAI, S.; VITTAL, S. Active vibration control of cantilever beam by using PID based output feedback controller. **Journal of Vibration and Control**, v. 18, n. 3, p. 366–372, 2011.

KIM, S.; OH, J. A modal filter approach to non-collocated vibration control of structures.

**Journal of Sound and Vibration**, v. 332, n. 9, p. 2207–2221, 2013.

KIM, S.; WANG, S.; BRENNAN, M. J. Comparison of negative and positive position feedback control of a flexible structure. **Smart Materials and Structures**, v. 20, n. 1, p. 1–10, 2011.

KLINKHIEO, S. **On-line Estimation Approaches to Fault-Tolerant Control of Uncertain Systems**. PhD Thesis — The University of Hull, England, 2009.

LAVRETSKY, E.; WISE, K. A. **Robust and Adaptive Control with Aerospace Applications**. [S.l.]: Springer, 2013.

LEE, Y. **Active Vibration Control of a Piezoelectric Laminate Plate Using Spatial Control Approach**. Master Thesis — Department of Mechanical Engineering, University of Adelaide, Australia, 2005.

MARINAKI, M.; MARINAKIS, Y.; STAVROULAKIS, G. E. Fuzzy control optimized by PSO for vibration suppression of beams. **Control Engineering Practice**, v. 18, n. 6, p. 618–629, 2010.

MASTORY, C. G.; CHALHOUB, N. G. Enhanced structural controllers for non-collocated systems. **Journal of Vibration and Control**, p. 1–17, 2014.

MECHBAL, N.; NÓBREGA, E. Spatial  $H_\infty$  approach to damage-tolerant active control. **Structural Control and Health Monitoring**, v. 22, n. 9, p. 1148–1172, 2015.

MECHBAL, N.; NÓBREGA, E. G. O. Damage tolerant active control: Concept and state of the art. In: **8th IFAC Symposium on Fault Detection, Supervision and Safety of Technical Processes**. Mexico City, Mexico: [s.n.], 2012. p. 63–71.

\_\_\_\_\_. Adaptive strategy to damage tolerant active control. In: **9th IFAC Symposium on Fault Detection, Supervision and Safety for Technical Processes**. Paris, France: [s.n.], 2015. p. 658–663.

\_\_\_\_\_. Spatial  $H_\infty$  approach to damage-tolerant active control. **Structural Control and Health Monitoring**, v. 22, n. 9, p. 1148–1172, 2015.

MECHBAL, N.; URIBE, J. S.; RÉBILLAT, M. A probabilistic multi-class classifier for structural health monitoring. **Mechanical Systems and Signal Processing**, v. 60-61, p. 106–123, 2015.

MECHBAL, N.; VERGÉ, M.; COFFIGNAL, G.; GANAPATHI, M. Application of a combined active control and fault detection scheme to an active composite flexible structure. **Mechatronics**, v. 16, n. 3-4, p. 193–208, 2006.

MEDEIROS, R.; SARTORATO, M.; VANDEPITTE, D.; TITA, V. A comparative assessment of different frequency based damage detection in unidirectional composite plates using MFC sensors. **Journal of Sound and Vibration**, v. 383, p. 171–190, 2016.

MEIROVITCH, L. **Elements of Vibration Analysis**. 2nd edition. ed. [S.l.]: McGraw-Hill, 1986.

MEIROVITCH, L.; BARUH, H. The implementation of modal filters for control of structures. **Journal of Guidance, Control, and Dynamics**, v. 8, n. 6, p. 707–716, 1985.

MEIROVITCH, L.; BARUH, H.; OZ, H. A comparison of control techniques for large flexible systems. **Journal of Guidance, Control, and Dynamics**, v. 6, n. 4, p. 302–310, 1983.

MEVEL, L.; GOURSAT, M.; BASSEVILL, M. Stochastic subspace-based structural identification and damage detection and localisation: application to the Z24 bridge benchmark. **Mechanical Systems and Signal Processing**, v. 17, n. 1, p. 143–151, 2003.

MOHAMED, Z.; MARTINS, J. M.; TOKHI, M. O.; Sá da Costa, J.; BOTTO, M. A. Vibration control of a very flexible manipulator system. **Control Engineering Practice**, v. 13, n. 3, p. 267–277, 2005.

MOHEIMANI, S.; H.R.POTA; PETERSEN, I. Spatial control for active vibration control of



piezoelectric laminates. In: **37th IEEE Conference on Decision and Control**. Tampa, Florida: [s.n.], 1998. p. 4308–4313.

MOHEIMANI, S.; POTA, H. R.; PETERSEN, I. R. Spatial balanced model reduction for flexible structures. In: **The 1997 American Control Conference**. Albuquerque, New Mexico: [s.n.], 1997. p. 3098–3102.

MOHEIMANI, S. O. R.; FU, M. Spatial  $H_2$  norm of flexible structures and its application in model order selection. In: **37th IEEE Conference on Decision and Control**. Tampa, Florida: [s.n.], 1998. p. 3623–3624.

NESTEROV, Y.; NEMIROVSKI, A. **Interior-Point Polynomial Algorithms in Convex Programming**. [S.l.]: SIAM Studies in Applied Theory Mathematics, 1994.

NONAMI, K.; SIVRIOGLU, S. Active vibration control using LMI-based mixed  $H_2/H_\infty$  state and output feedback control with nonlinearity. In: **35th IEEE Conference on Decision and Control**. Kobe: [s.n.], 1996. v. 1, p. 161–166.

PEREIRA, D.; SERPA, A. Bank of  $H_\infty$  filters for sensor fault isolation in active controlled flexible structures. **Mechanical Systems and Signal Processing**, v. 60-61, p. 678–694, 2015.

PEREIRA, E.; APHALE, S. S.; FELIU, V.; MOHEIMANI, S. O. R. Integral resonant control for vibration damping and precise tip-positioning of a single-link flexible manipulator. **IEEE/ASME Transactions on Mechatronics**, v. 16, n. 2, p. 232–240, 2011.

PINTELON, R.; SCHOUKENS, J. **System Identification: A Frequency Domain Approach**. [S.l.]: IEEE Press, 2001.

POMMIER-BUDINGER, V.; JANAT, Y.; NELSON-GRUEL, D.; LANUSSE, P.; OUSTALOUP, A. Fractional robust control with ISO-damping property. In: **American Control Conference**. Seattle, USA: [s.n.], 2008. p. 1–6.

PREUMONT, A. **Vibration Control of Active Structures: An Introduction**. [S.l.]: Kluwer

Academic Publishers, 2002.

\_\_\_\_\_. \_\_\_\_\_. 3rd edition. ed. [S.l.]: Springer, 2011.

QIU, J.; REN, Y. Z. M.; GUO, Y. Active fault-tolerant control for vehicle active suspension systems in finite-frequency domain. **IET Control Theory and Applications**, v. 5, n. 13, p. 1544–1550, 2011.

RESTA, F.; RIPAMONTI, F.; CAZZULANI, G.; FERRARI, M. Independent modal control for nonlinear flexible structures: An experimental test rig. **Journal of Sound and Vibration**, v. 329, n. 8, p. 961–972, 2010.

RIPAMONTI, F.; CAZZULANI, G.; CINQUEMANI, S.; RESTA, F.; TORTI, A. Adaptive active vibration control to improve the fatigue life of a carbon-epoxy smart structure. In: **Active and Passive Smart Structures and Integrated Systems**. San Diego, USA: [s.n.], 2015. p. 1–9.

ROBU, B.; BUDINGER, V.; BAUDOUIN, L.; PRIEUR, C.; ARZELIER, D. Simultaneous  $H_\infty$  vibration control of fluid/plate system via reduced-order controller. In: **49th IEEE Conference on Decision and Control**. Atlanta, GA: [s.n.], 2010. p. 3146–3151.

RODRIGUES, M.; HAMDI, H.; BRAIEK, N. B.; THEILLIOL, D. Observer-based fault tolerant control design for a class of LPV descriptor systems. **Journal of the Franklin Institute**, v. 351, n. 6, p. 3104–3125, 2014.

SAEED, K.; MECHBAL, N.; COFFIGNAL, G.; VERGÉ, M. Artificial neural network based structural damage diagnosis using non-parametric subspace residual. In: **7th International Workshop on Structural Health Monitoring**. Stanford, USA: [s.n.], 2009.

\_\_\_\_\_. Structural damage diagnosis using subspace based residual and artificial neural networks. In: **7th IFAC Symposium on Fault Detection, Supervision and Safety of Technical Processes**. Barcelona, Spain: [s.n.], 2009.

SARTORATO, M.; MEDEIROS, R.; VANDEPITTE, D.; TITA, V. Computational model for supporting SHM systems design: Damage identification via numerical analyses. **Mechanical Systems and Signal Processing**, v. 84, p. 445–461, 2017.

SCHERER, C.; GAHINET, P.; CHILALI, M. Multiobjective output-feedback control via LMI optimization. **IEEE Transactions on Automatic Control**, v. 42, n. 7, p. 896–911, 1997.

SCHRÖCK, J.; MEURER, T.; KUGI, A. Non-collocated feedback stabilization of a non-uniform euler-bernoulli beam with in-domain actuation. In: **50th IEEE Conference on Decision and Control and European Control Conference**. Orlando, FL: [s.n.], 2011. p. 2776–2781.

SELVA, P.; CHERRIER, O.; BUDINGER, V.; LACHAUD, F.; MORLIER, J. Smart monitoring of aeronautical composites plates based on electromechanical impedance measurements and artificial neural networks. **Engineering Structures**, v. 56, p. 794–804, 2013.

SERPA, A. L.; NÓBREGA, E. G. O.  $H_\infty$  control with pole placement constraints for flexible structures vibration reduction. In: **18th International Congress of Mechanical Engineering**. Ouro Preto, Brazil: [s.n.], 2005. p. 1–8.

SERRA, M.; RESTA, F.; RIPAMONTI, F. Dependent modal space control. **Smart Materials and Structures**, v. 22, n. 10, p. 1–11, 2013.

SHARMA, A.; KUMAR, R.; VAISH, R.; CHAUHAN, V. S. Experimental and numerical investigation of active vibration control over wide range of operating temperature. **Journal of Intelligent Material Systems and Structures**, p. 1–15, 2015.

SOUZA, P. R.; NÓBREGA, E. G. O. A fault location method using lamb waves and discrete wavelet transform. **Journal of the Brazilian Society of Mechanical Sciences and Engineering**, v. 34, n. 4, p. 515–524, 2012.

SPENCER, B.; NAGARAJIAH, S. State of the art of structural control. **Journal of**

**Structural Engineering**, v. 129, n. 7, p. 845–856, 2003.

SPENCER, B. F.; SUHARDJO, J.; SAIN, M. K. Frequency domain optimal control strategies for a seismic protection. **Journal of Engineering Mechanics**, v. 120, n. 1, p. 135–159, 1994.

SRINIVASAN, A. V.; MCFARLAND, D. M. **Smart Structures: Analysis and Design**. [S.l.]: Cambridge University Press, 2001.

TANG, X.; CHEN, I. Robust control of XYZ flexure-based micromanipulator with large motion. **Frontiers of Mechanical Engineering in China**, v. 4, n. 1, p. 25–34, 2009.

UMESH, K.; GANGULI, R. Shape and vibration control of a smart composite plate with matrix cracks. **Smart Materials and Structures**, v. 18, n. 2, p. 1–13, 2008.

WANG, T.; XIE, W.; ZHANG, Y. Sliding mode reconfigurable fault tolerant control for nonlinear aircraft systems. **Journal of Aerospace Engineering**, v. 28, n. 3, p. 1–11, 2015.

YANG, H.; JLANG, B.; COCQUENPOT, V. **Fault tolerant control design for hybrid systems**. [S.l.]: Lecture Notes in Control and Information Sciences, Springer Verlag, 2010.

ZABIHOLLAH, A.; SEDAGAHTI, R.; GANESAN, R. Active vibration suppression of smart laminated beams using layerwise theory and an optimal control strategy. **Smart Materials and Structures**, v. 16, n. 6, p. 2190–2201, 2007.

ZHANG, J.; HE, L.; WANG, E.; GAO, R. Robust active vibration control of flexible structures based on  $H_\infty$  control theorem. In: **International Workshop on Intelligent Systems and Applications**. Wuhan: [s.n.], 2009. p. 1–6.

ZHANG, Y.; JIANG, J. Bibliographical review on reconfigurable fault-tolerant control systems. **Annual Reviews in Control**, v. 32, n. 2, p. 229–252, 2008.

ZHAO, Q. **Fault tolerant control systmes design**. PhD Thesis — Western University, Canada, 1999.

ZHENG, H.; MITA, A. Two-stage damage diagnosis based on the distance between ARMA models and pre-whitening filters. **Smart Materials and Structures**, v. 16, p. 1829–1836, 2007.

\_\_\_\_\_. Damage indicator defined as the distance between ARMA models for structural health monitoring. **Structural Control and Health Monitoring**, v. 15, n. 7, p. 992–1005, 2008.

ZHOU, K.; DOYLE, J. C. **Essentials of Robust Control**. [S.l.]: Prentice Hall, 1997.

ZHOU, K.; DOYLE, J. C.; GLOVER, K. **Robust and Optimal Control**. [S.l.]: Prentice Hall, 1995.

ZHOU, K.; REN, Z. A new controller architecture for high performance, robust, and fault-tolerant control. **IEEE Transactions on Automatic Control**, v. 46, n. 10, p. 1613–1618, 2001.

## APPENDIX A - THE PRINCIPAL ANGLES BETWEEN SUBSPACES

In this appendix, the principal angles between subspaces are discussed, considering that these angles may be defined by the generalisation of angles between two vectors. Initially, the angles between two vectors are introduced. After that, the concept of principal angles and principal directions between two subspaces is presented. To conclude, some procedure to compute these angles are introduced. Moreover, this appendix is based on the results of (DE COCK, 2002).

### A.1 The angles between two vectors

Consider two vectors  $\mathbf{a}, \mathbf{b} \in \mathbb{R}^n$ . Based on Cauchy-Schwarz inequality, the cosine of the angle between  $\mathbf{a}$  and  $\mathbf{b}$  is defined as:

$$\cos[\mathbf{a} \angle \mathbf{b}] = \frac{|\mathbf{a}^T \mathbf{b}|}{\|\mathbf{a}\| \|\mathbf{b}\|},$$

in which  $\|\mathbf{a}\|$  is the Euclidean norm of  $\mathbf{a}$  and  $[\mathbf{a} \angle \mathbf{b}]$  represents the angle between the vectors, which belongs to the interval  $[0, \frac{\pi}{2}]$ . Figure A.1 shows the geometric representation of the angle between two vectors.

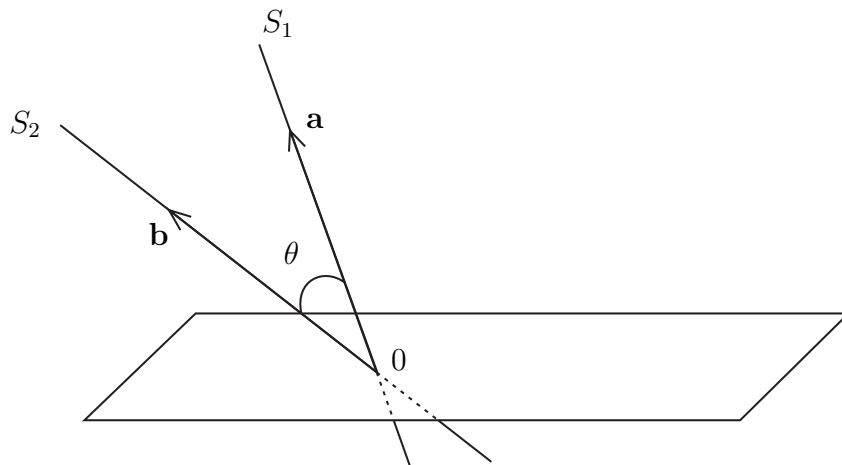


Figure A.1 - The angle between one-dimensional subspaces  $S_1, S_2 \in \mathbb{R}^3$ .

## A.2 Principal angles and directions

The concept of an angle between two one-dimensional subspaces can be extended to higher dimensional subspaces. Consider that there exist two linear subspaces  $S_1, S_2 \in \mathbb{R}^n$  of dimension  $d_1$  and  $d_2$ . Now, one chooses a unitary vector  $\mathbf{u}_1$  from  $S_1$  and another unitary vector  $\mathbf{v}_1$  from  $S_2$  such that the angle between  $\mathbf{u}_1$  and  $\mathbf{v}_1$  is minimised. Then, the vector  $\mathbf{u}_1$  and  $\mathbf{v}_1$  are the principal directions and the angle between them is the first principal angle  $\theta_1$ . This procedure continues for  $\min(d_1, d_2)$  angles and their respective principal directions. Figure A.2 illustrates this procedure for the first two steps.

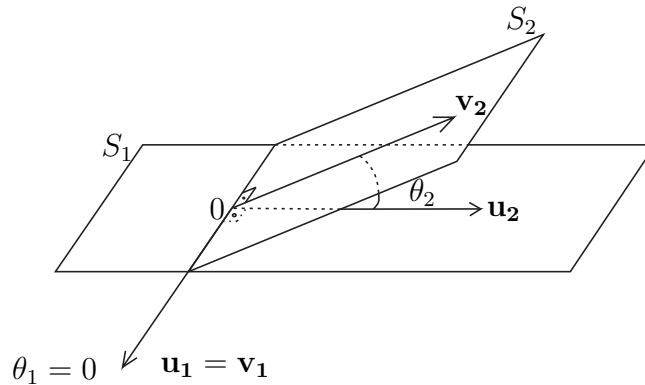


Figure A.2 - Principal angles between two-dimensional subspaces  $S_1, S_2 \in \mathbb{R}^3$ .

**Definition A.1** (Principal angles and directions). *The principal angles  $0 \leq \theta_1 \leq \theta_2 \leq \dots \leq \theta_{\min(d_1, d_2)} \leq \pi/2$  between the subspaces  $S_1$  and  $S_2$  of dimensions  $d_1$  and  $d_2$ , respectively, and the corresponding principal directions  $\mathbf{u}_i \in S_1$  and  $\mathbf{v}_i \in S_2$  are recursively defined as:*

$$\cos \theta_1 = \max_{\substack{\mathbf{u} \in S_1 \\ \mathbf{v} \in S_2}} \mathbf{u}^T \mathbf{v} = \mathbf{u}_1^T \mathbf{v}_1,$$

$$\cos \theta_k = \max_{\substack{\mathbf{u} \in S_1 \\ \mathbf{v} \in S_2}} \mathbf{u}^T \mathbf{v} = \mathbf{u}_k^T \mathbf{v}_k, \text{ for } k = 2, \dots, \min(d_1, d_2),$$

subject to:

$$\|\mathbf{u}\| = \|\mathbf{v}\| = 1,$$

and for  $k > 1$ :

$$\mathbf{u}^T \mathbf{u}_i = 0 \quad i = 1, \dots, k-1,$$

$$\mathbf{v}^T \mathbf{v}_i = 0 \quad i = 1, \dots, k-1.$$

Let  $\mathbf{A} \in \mathbb{R}^{p \times n}$  have rank  $r_a$  and  $\mathbf{B} \in \mathbb{R}^{q \times n}$  have rank  $r_b$ , then the principal angles between the row space of  $\mathbf{A}$  and  $\mathbf{B}$  are defined as:

$$(\theta_1, \theta_2, \dots, \theta_{\min(r_a, r_b)}) = [\mathbf{A} \triangleleft \mathbf{B}],$$

where three kinds of principal angles are:

1.  $n_0$  zero principal angles:  $\theta_1 = \dots = \theta_{n_0} = 0$ , where

$$n_0 = \dim(\text{row}(\mathbf{A}) \cap \text{row}(\mathbf{B})),$$

or

$$n_0 = \text{rank}(\mathbf{A}) + \text{rank}(\mathbf{B}) - \text{rank} \begin{pmatrix} \mathbf{A} \\ \mathbf{B} \end{pmatrix}.$$

2.  $(r_{ab} - n_0)$  acute principal angles:  $0 < \theta_{n_0+1} \leq \dots \leq \theta_{r_{ab}} < \frac{\pi}{2}$ , for  $r_{ab} = \text{rank}(\mathbf{A}\mathbf{B}^T)$ .
3.  $(\min(r_a, r_b) - r_{ab})$  right principal angles:  $\theta_{r_{ab}+1} = \dots = \theta_{\min(r_a, r_b)} = \frac{\pi}{2}$ .

### A.3 The principal angles and respective directions as eigenvalues and eigenvectors

For the matrices  $\mathbf{A} \in \mathbb{R}^{p \times n}$  and  $\mathbf{B} \in \mathbb{R}^{q \times n}$  with rank  $r_a$  and  $r_b$ , respectively, the principal angles between  $\text{row}(\mathbf{A})$  and  $\text{row}(\mathbf{B})$  and the respective directions follow from the symmetric generalised eigenvalue problem:

$$\begin{bmatrix} \mathbf{0} & \mathbf{A}\mathbf{B}^T \\ \mathbf{B}\mathbf{A}^T & \mathbf{0} \end{bmatrix} \begin{bmatrix} \mathbf{x} \\ \mathbf{y} \end{bmatrix} = \begin{bmatrix} \mathbf{A}\mathbf{A}^T & \mathbf{0} \\ \mathbf{0} & \mathbf{B}\mathbf{B}^T \end{bmatrix} \begin{bmatrix} \mathbf{x} \\ \mathbf{y} \end{bmatrix} \lambda, \quad (\text{A.1})$$

subject to  $\mathbf{x}^T \mathbf{A}\mathbf{A}^T \mathbf{x} = 1$  and  $\mathbf{y}^T \mathbf{B}\mathbf{B}^T \mathbf{y} = 1$ .

Considering that  $p + q$  eigenvalues  $\lambda_i$  are sorted as:

$$\lambda_1 \geq \dots \geq \lambda_{p+q},$$



then the vectors  $\mathbf{A}^T \mathbf{x}_i$  and  $\mathbf{B}^T \mathbf{y}_i$  for  $i = 1, \dots, \min(r_a, r_b)$  where  $\mathbf{x}_i$  and  $\mathbf{y}_i$  satisfy Eq. (A.1) with  $\lambda = \lambda_i$  are the principal directions relative to the principal angle  $\theta_i$ . Thus, if  $\mathbf{A}$  and  $\mathbf{B}$  have full row rank and  $p \leq q$ , the cosines of the principal angles between  $\text{row}(\mathbf{A})$  and  $\text{row}(\mathbf{B})$  are given by:

$$\cos[\mathbf{A} \angle \mathbf{B}] = \sqrt{\lambda((\mathbf{A}\mathbf{A}^T)^{-1}\mathbf{A}\mathbf{B}^T(\mathbf{B}\mathbf{B}^T)^{-1}\mathbf{B}\mathbf{A}^T)}.$$

#### A.4 The cosines of the principal angles based on LQ decomposition

The computation of the angles between larger subspaces may have high computational cost. To overcome this limitation, an efficient algorithm based on LQ decomposition is used. Initially, the LQ decomposition is introduced and then the algorithm is presented.

**Definition A.2.** *The LQ decomposition of a real matrix  $\mathbf{A} \in \mathbb{R}^{v \times n}$  is given by:*

$$\mathbf{A} = \mathbf{L}\mathbf{Q}^T, \quad (\text{A.2})$$

in which  $\mathbf{Q} \in \mathbb{R}^{n \times n}$  is orthogonal and  $\mathbf{L} \in \mathbb{R}^{v \times n}$  is lower triangular.

**Definition A.3** (The LR decomposition as a QR decomposition). *The LQ decomposition of a matrix  $\mathbf{A}$  is the QR decomposition of  $\mathbf{A}^T$ . If  $\mathbf{A}^T = \mathbf{Q}\mathbf{R}$ , where  $\mathbf{Q}$  is orthogonal and  $\mathbf{R}$  is upper triangular, then  $\mathbf{A} = \mathbf{R}^T\mathbf{Q}^T$  is the factorisation of  $\mathbf{A}$  into a lower triangular matrix and the transpose of an orthogonal matrix, as in the LQ decomposition.*

**Theorem A.1** (The computation of the angles between two subspaces based on LQ decomposition). *Consider the matrices  $\mathbf{A} \in \mathbb{R}^{p \times n}$  and  $\mathbf{B} \in \mathbb{R}^{q \times n}$  with full row rank,  $p \leq q$ , and  $(p + q) \leq n$ . The principal angles between  $\text{row}(\mathbf{A})$  and  $\text{row}(\mathbf{B})$  can be computed as:*

1. Compute the triangular part of the LQ decomposition of the matrix  $\begin{bmatrix} \mathbf{A} \\ \mathbf{B} \end{bmatrix}$ .

The triangular part is denoted by:

$$\begin{bmatrix} \mathbf{L}_{11} & \mathbf{0} \\ \mathbf{L}_{21} & \mathbf{L}_{22} \end{bmatrix} \in \mathbb{R}^{(p+q) \times (p+q)},$$

where  $\mathbf{L}_{11} \in \mathbb{R}^{p \times p}$ ,  $\mathbf{L}_{21} \in \mathbb{R}^{q \times p}$ , and  $\mathbf{L}_{22} \in \mathbb{R}^{q \times q}$ .

2. Compute the triangular part of the LQ decomposition of  $\begin{bmatrix} \mathbf{L}_{21} & \mathbf{L}_{22} \end{bmatrix}$ :

$$\begin{bmatrix} \mathbf{L}_{21} & \mathbf{L}_{22} \end{bmatrix} = \begin{bmatrix} \mathbf{S} & \mathbf{0} \end{bmatrix} \mathbf{T},$$

where matrix  $\mathbf{S} \in \mathbb{R}^{q \times q}$  is nonsingular.

3. The cosines of the principal angles between  $\text{row}(A)$  and  $\text{row}(B)$  are the singular values of  $\mathbf{S}^{-1}\mathbf{L}_{21}$ .

*Proof.* See (DE COCK, 2002).

□

## ANNEXE A - THE PRINCIPAL EQUATIONS OF THE PLQP SOFTWARE

This annexe presents a document with a brief theory that introduces the principal equations of the PLQP software developed by Prof. Dr. Gérard Coffignal at PIMM laboratory of Arts et Métiers ParisTech for testing control strategies applied to structures that can be modelled in plate bending using Kirchhoff's theory. This document has been created to present the theoretical aspects used in the respective software, aiming for a fast theory explanation for new users. As this document was created separated from the thesis, a different notation is considered, based on the traditional FE theory. This file has its own list of principal symbols, abbreviations, and acronyms, where the vectors are denoted by  $\{\cdot\}$  and the matrices by  $[\cdot]$  in order to allow the use of lower cases or capital letters for both vectors and matrices. This also allows to use the same notation for quantities that are different in this annexe and in the main part of this thesis, and therefore could be confusing.

|  |
|--|
| <h3>Finite Element Modelling<br/>of Active Piezoelectric Structures</h3> |
|--|

Note GC-2016-09

**Authors : Gérard Coffignal and Helói Genari**

PIMM, Arts et Métiers ParisTech

151 Bd de l'Hôpital, 75013 Paris, FRANCE

*gerard.coffignal@gmail.com*

– 6 june 2016 –

### List of Abbreviations and Acronyms

|      |  |
|------|--|
| BC   | Boundary Conditions  |
| DKT  | Discrete Kirchhoff Triangle                                      |
| DOF  | Degree of Freedom (mechanical and/or electrical)                 |
| DTAC | Damage-Tolerant Active Control                                   |
| FE   | Finite Element   |
| PIMM | Laboratory of Process and Engineering in Mechanics and Materials |
| PLQP | dedicated FE software developed at PIMM by G. Coffignal          |

## List of Principal Symbols

Only the principal symbols are listed next. Other symbols are described as they are introduced.

### Continuum (3D)

|  |   |
|--|---|
| $\{u\}$                                  | displacement vector   |
| $\phi$                                   | electric potential  |
| $\{T\}$                                  | components of the stress tensor   |
| $\{S\}$                                  | $= \nabla_s \{u\}$ , components of the strain tensor ( $\nabla_s = 1/2(\nabla + \nabla^T)$ )  |
| $\{E\}$                                  | $= -\nabla\phi$ , electric field  |
| $\{D\}$                                  | electric displacement   |
| $[c]$                                    | elastic stiffness matrix at constant $\{E\}$  |
| $[e]$                                    | piezoelectric matrix  |
| $[\epsilon]$                             | dielectric permittivity matrix at constant $\{S\}$  |
| $V, \partial V$                          | active structure domain and its boundary  |
| $V_p, \partial V_p$                      | piezoelectric domain and its boundary, where $V_p \subset V$  |
| $\partial_u V, \partial_F V$             | parts of the boundary $\partial V$ , where displacements are prescribed ( $\partial_u V$ ) and forces are prescribed ( $\partial_F V$ ), satisfying $\partial V = \partial_u V \cup \partial_F V$ and $\partial_u V \cap \partial_F V = \emptyset$                                    |
| $\partial_\phi V_p, \partial_\sigma V_p$ | parts of the boundary $\partial V_p$ , where the potentials are prescribed ( $\partial_\phi V_p$ ) and charges are prescribed ( $\partial_\sigma V_p$ ) with $\partial V_p = \partial_\phi V_p \cup \partial_\sigma V_p$ and $\partial_\phi V_p \cap \partial_\sigma V_p = \emptyset$ |

### Finite Elements

|                                   |   |
|-----------------------------------|---|
| $\{\tilde{U}_u\}$                 | vector of generalised displacements (mechanical DOFs)   |
| $[\tilde{N}_u]$                   | matrix of interpolation functions for $\{\tilde{U}_u\}$   |
| $\{\tilde{U}_\phi\}$              | vector of potentials (electrical DOFs)  |
| $[\tilde{N}_\phi]$                | matrix of interpolation functions for $\{\tilde{U}_\phi\}$  |
| $\{\bar{U}_u\}, \{\bar{U}_\phi\}$ | vectors of known DOFs (interpolation matrices: $[\bar{N}_u], [\bar{N}_\phi]$ )  |
| $\{U_u\}, \{U_\phi\}$             | vectors of unknown DOFs (interpolation matrices: $[N_u], [N_\phi]$ )  |
| $\{v\}$                           | vector of forcing functions, either known functions (the disturbance vector $w$ of control theory) or calculated by a controller (the control vector $u$ of control theory) |
| $[Q_u], [Q_\phi]$                 | matrices that links respectively FE generalised forces to $\{v\}$ and FE electric charges to $\{v\}$  |
| $[B]$                             | generic name of a matrix that links (generalised) strains to a vector of DOF  |
| $[M]$                             | generic name of a mass matrix   |
| $[K]$                             | generic name of a stiffness matrix  |

## Plates

|  |   |
|--|---|
| $\{\tilde{u}\}$                            | $= \begin{Bmatrix} u_z \\ \{\beta\} \end{Bmatrix}$ generalised displacement vector (Mindlin theory for transverse deformation)  |
| $u_z$                                      | transverse displacement   |
| $\{\beta\}$                                | $= \begin{Bmatrix} \beta_x \\ \beta_y \end{Bmatrix}$ rotations, where $\theta_x, \theta_y$ of the normal direction are given by $\theta_x = -\beta_y, \theta_y = \beta_x$   |
| $\{\bar{S}_0\}$                            | reference surface membrane strain   |
| $\{\kappa\}$                               | curvature change  |
| $\{N\}$                                    | membrane forces   |
| $\{M\}$                                    | moments   |
| $V_c$                                      | piezoelectric region $V_c \subset V$ , where a couple of piezoelectric layers are bonded, one on the upper face and the other on the lower one  |
| $\{\bar{\phi}\}, \{\bar{E}\}, \{\bar{D}\}$ | vectors of respective potentials, electric fields, and electric displacements in layers 1 and 3 of a piezoelectric area   |
| $\Sigma, \partial\Sigma$                   | trace of $V$ on the mid-plane $(x,y)$ of the plate, boundary of $\Sigma$ in $(x,y)$   |
| $\partial_u\Sigma, \partial_F\Sigma$       | parts of the boundary $\partial\Sigma$ , where the respective generalised displacements are prescribed ( $\partial_u\Sigma$ ) and generalised forces are prescribed ( $\partial_F\Sigma$ ), satisfying $\partial\Sigma = \partial_u\Sigma \cup \partial_F\Sigma$ and $\partial_u\Sigma \cap \partial_F\Sigma = \emptyset$ |
| $z^+$                                      | $z^+ = h_2/2 + h_3$ in a piezoelectric area, otherwise $z^+ = h_2/2$  |
| $z^-$                                      | $z^- = -h_2/2 - h_1$ in a piezoelectric area, otherwise $z^- = -h_2/2$  |

## Introduction

In DTAC area, it is recommended that the simulations of active structures are performed during the design of the controllers, aiming to test ideas and to demonstrate the applications of new proposed methods by means of numerical simulations. In order to achieve this goal, the numerical models of the structures, including damage simulations and modelling of its active elements, must be built. In the following, this is done for linear structures in an inertial frame. Damage modelling, as needed to assess DTAC methods, is not discussed here, considering that it may be simulated by several means in finite element solvers: by the modification of boundary conditions, by local stiffness reductions, or by introducing partial links between parts (crack simulation). To simplify, this document is written in the frame of the Rayleigh-Ritz approach (“displacement” approach) without entering in the description of operations at the element level

that can be found in (BATHE, 1982) or (BATOZ; DHATT, 1990).

### Finite element model of a continuum body including piezoelectric materials

This section is mainly based on the work of (ALLIK; HUGHES, 1970) and uses partially its notations to recall the main lines of the method, leading to the matrix equation Eq. (A.15), which is the starting point for the control side of DTAC analyses. The modelling of active structures based on piezoelectric sensors and actuators necessitates considering the following piezoelectric constitutive relations:

$$\{T\} = [c] \{S\} - [e]\{E\} \quad (\text{A.1a})$$

$$\{D\} = [e]^T\{S\} + [\epsilon]\{E\}, \quad (\text{A.1b})$$

in which  $\{T\}$  is the components of the stress tensor,  $\{S\}$  represents the components of the strain tensor,  $\{E\}$  is the electric field,  $\{D\}$  is the electric displacement,  $[c]$  represents the elastic stiffness matrix at  $\{E\}$ ,  $[e]$  is the piezoelectric matrix, and  $[\epsilon]$  is the dielectric permittivity matrix at  $\{S\}$ .

In a piezoelectric material, these relations couple the mechanical and electrical fields in the piezoelectric domain  $V_p \subset V$ . In the following,  $\{u_d\}$  and  $\phi_d$  are known functions and  $\{u\} = \{u_d\}$  on boundary  $\partial_u V$  and  $\phi = \phi_d$  on boundary  $\partial_\phi V_p$ . The principle of virtual work applied to a piezoelectric continuum gives a variational principle (ALLIK; HUGHES, 1970). This allows to incorporate the piezoelectric effect in a finite element (FE) formulation:

$$\int_V \left( \{\delta S\}^T \{T\} - \{\delta E\}^T \{D\} - \{\delta u\}^T \{f_d\} + \rho \{\delta u\}^T \{\ddot{u}\} \right) dV - \int_{\partial_F V} \{\delta u\}^T \{F_d\} d\Gamma + \int_{\partial_\sigma V_p} \delta\phi \sigma_d d\Gamma = 0, \quad (\text{A.2})$$

where  $\partial V = \partial_u V \cup \partial_F V$  and  $\partial V_p = \partial_\phi V_p \cup \partial_\sigma V_p$  are respectively the boundary of  $V$  and  $V_p$  for  $\{\delta u\} = \{0\}$  on  $\partial_u V$  and  $\delta\phi = 0$  on  $\partial_\phi V_p$ . Taking into account the constitutive relations given in Eq. (A.1a) and Eq. (A.1b), it leads to:

$$\int_V \left( \{\delta S\}^T [c] \{S\} - \{\delta S\}^T [e] \{E\} - \{\delta E\}^T [e]^T \{S\} - \{\delta E\}^T [\epsilon] \{E\} - \{\delta u\}^T \{f_d\} + \rho \{\delta u\}^T \{\ddot{u}\} \right) dV - \int_{\partial_F V} \{\delta u\}^T \{F_d\} d\Gamma + \int_{\partial_\sigma V_p} \delta\phi \sigma_d d\Gamma = 0. \quad (\text{A.3})$$

This formulation is given here when there are no body charges and when known surface

tractions  $\{F_d\}$  and surface charge  $\sigma_d$  are considered respectively on surfaces  $\partial_F V$  and  $\partial_\sigma V_p$  and known body forces  $\{f_d\}$  are considered in  $\partial_F V$ . The displacement  $\{u\}$  and the electric potential  $\phi$  are the independent variables in this approach. As stated before to simplify the notation,  $V_p \subset V$  denotes the piezoelectric part of  $V$ . In order to describe simply changes in the boundary conditions (BC), Eq. (A.2) and Eq. (A.3) are also written before taking into account these BC. This gives the equilibrium equations, Eq. (A.4) and Eq. (A.5), including the unknown surface tractions  $\{F\}$  on  $\partial_u V$  and unknown surface charges  $\sigma$  on  $\partial_\phi V_p$ . Once  $\partial_F V$ ,  $\partial_\sigma V_p$ ,  $\{F_d\}$ , and  $\sigma_d$  are given,  $\{F\} = \{F_d\}$  on  $\partial_F V$  and surface charges  $\sigma = \sigma_d$  on  $\partial_\sigma V_p$ .

Eq. (A.3) is obtained by taking  $\{\delta u\} = \{0\}$  on  $\partial_u V$  and  $\delta\phi = 0$  on  $\partial_\phi V_p$ , suppressing the presence of unknowns that are not independent variables and can be calculated once  $\{u\}$  and  $\phi$  are known in the formulation. A more general expression considers arbitrary values of  $\{\delta u\}$  and  $\delta\phi$  on the whole boundary  $\partial V$ , including unknown quantities  $\{F\}$  on  $\partial_u V$  and  $\sigma$  unknown on  $\partial_\phi V_p$ :

$$\int_V \left( \{\delta S\}^T \{T\} - \{\delta E\}^T \{D\} - \{\delta u\}^T \{f_d\} + \rho \{\delta u\}^T \{\ddot{u}\} \right) dV - \int_{\partial V} \{\delta u\}^T \{F\} d\Gamma + \int_{\partial V} \delta\phi \sigma d\Gamma = 0 \quad (\text{A.4})$$

$$\int_V \left( \{\delta S\}^T [c] \{S\} - \{\delta S\}^T [e] \{E\} - \{\delta E\}^T [e]^T \{S\} - \{\delta E\}^T [\epsilon] \{E\} - \{\delta u\}^T \{f_d\} + \rho \{\delta u\}^T \{\ddot{u}\} \right) dV - \int_{\partial V} \{\delta u\}^T \{F\} d\Gamma + \int_{\partial V_p} \delta\phi \sigma d\Gamma = 0. \quad (\text{A.5})$$

It must be noticed that  $\sigma = -\{D\}^T \{n\}$  on  $\partial V_p$  can be nonzero only if a conductor allows exchanges of electric charges with other points, such as an electrode. For this purpose, the electrodes that cover the two faces of piezoelectric ceramics play that role. If independent electrodes are denoted by  $\Gamma_i, i \in \{1, 2, 3, \dots\}$ , the only part of the boundary  $\partial V_p$  where  $\sigma$  is nonzero is defined as  $\cup_i \Gamma_i$ .

The FE formulation is obtained by approximating the continuous fields  $\{u\}$  and  $\phi$  via interpolation functions  $[\tilde{N}_u]$  and  $[\tilde{N}_\phi]$ , which are built in a systematic way. First, the domain  $V$  is partitioned into a finite number of elements with simple shapes. This meshing operation of  $V$  leads to a set of elements and to a set of nodes. Nodes usually include vertices of elements and nodes internal to element edges, faces, and volume. Interpolation functions are then built

at element level. Outside  $V_p$ , electric quantities ( $\phi$ ,  $\{E\}$ , and  $\{D\}$ ) are not considered and need not to be approximated. For the sake of simplicity, it is considered that  $V_p = V$ , then  $V_p$  is distinguished from  $V$  in the definition of matrix terms leading to the FE matrix system.

In a piezoelectric region, the FE approximation at point  $r = (x, y, z)$  and time  $t$  can be written as:

$$\{u\} = [\tilde{N}_u]\{\tilde{U}_u\} \quad \text{i.e.} \quad \{u(r, t)\} = [\tilde{N}_u(r)]\{\tilde{U}_u(t)\} \quad (\text{A.6a})$$

$$\phi = [\tilde{N}_\phi]\{\tilde{U}_\phi\} \quad \text{i.e.} \quad \phi(r, t) = [\tilde{N}_\phi(r)]\{\tilde{U}_\phi(t)\}, \quad (\text{A.6b})$$

in which  $\{\tilde{U}_u\}$  and  $\{\tilde{U}_\phi\}$  are respectively the mechanical and electrical vectors of degrees of freedom (DOFs). In the classical approach that is considered here, they contain respectively the displacements and potentials of the nodes. In order to shorten the presentation of equations, electric degrees of freedom are directly attached to an electrode when the corresponding node belongs to that electrode. Each electrode is assumed to be a perfect conductor, considering that its points have the same potential. This potential is thus one of the components of  $\{\tilde{U}_\phi\}$ . Other nodes in the piezoelectric domain have their own potential in  $\{\tilde{U}_\phi\}$ . This avoids an additional step in the solution process. From these expressions and from their definitions, the expressions of the strain and electric fields are given by:

$$\{S\} = [\tilde{B}_u]\{\tilde{U}_u\} \quad \text{with} \quad [\tilde{B}_u] = 1/2(\nabla[\tilde{N}_u] + \nabla^T[\tilde{N}_u]) \quad (\text{A.7a})$$

$$\{E\} = -[\tilde{B}_\phi]\{\tilde{U}_\phi\} \quad \text{with} \quad [\tilde{B}_\phi] = \nabla[\tilde{N}_\phi]. \quad (\text{A.7b})$$

If the known quantities that describe the BC are denoted by  $\{\bar{U}_u\}$  and  $\{\bar{U}_\phi\}$ , this makes partitions into “known” and “unknown” submatrices. Thus, if  $\{U_u\}$  and  $\{U_\phi\}$  denote the unknown DOFs in these partitions, it leads to:

$$\{u\} = [\bar{N}_u]\{\bar{U}_u\} + [N_u]\{U_u\} \quad \text{with} \quad [N_u] = [0] \quad \text{on} \quad \partial_u V$$

$$\phi = [\bar{N}_\phi]\{\bar{U}_\phi\} + [N_\phi]\{U_\phi\} \quad \text{with} \quad [N_\phi] = [0] \quad \text{on} \quad \partial_\phi V_p \subset \partial V_p$$

$$\{S\} = [\bar{B}_u]\{\bar{U}_u\} + [B_u]\{U_u\} \quad (\text{A.8a})$$

$$\{E\} = -[\bar{B}_\phi]\{\bar{U}_\phi\} - [B_\phi]\{U_\phi\}. \quad (\text{A.8b})$$

## FE equations

Considering  $\{\delta u\} = [N_u]\{\delta U_u\}$  and  $\delta\phi = [N_\phi]\{\delta U_\phi\}$  in Eq. (A.3) for all  $\{\delta U_u\}$  and



$\{\delta U_u\}$ , it leads to the following FE matrix equations:

$$\{\delta U_u\}^T \left( \int_V \rho [N_u]^T \{\ddot{u}\} dV + \int_V [B_u]^T [c] \{S\} dV - \int_V [B_u]^T [e] \{E\} dV - \int_V [N_u]^T \{f_d\} dV - \int_{\partial_{FV}} [N_u]^T \{F_d\} d\Gamma \right) = 0 \quad (\text{A.9a})$$

$$\{\delta U_\phi\}^T \left( \int_V [B_\phi]^T [e]^T \{S\} dV + \int_V [B_\phi]^T [e] \{E\} dV + \int_{\partial_\sigma V_p} [N_\phi]^T \sigma_d d\Gamma \right) = 0, \quad (\text{A.9b})$$

and thus:

$$\int_V \rho [N_u]^T \{\ddot{u}\} dV + \int_V [B_u]^T [c] \{S\} dV - \int_V [B_u]^T [e] \{E\} dV = \int_V [N_u]^T \{f_d\} dV + \int_{\partial_{FV}} [N_u]^T \{F_d\} d\Gamma \quad (\text{A.10})$$

$$\int_V [B_\phi]^T [e]^T \{S\} dV + \int_V [B_\phi]^T [e] \{E\} dV = - \int_{\partial_\sigma V_p} [N_\phi]^T \sigma_d d\Gamma. \quad (\text{A.11})$$

Considering  $V$  and  $V_p$  and introducing Eq. (A.8) into Eq. (A.10), it leads to the following terms:

$$\begin{aligned} \int_V [B_u]^T [c] \{S\} dV &= \underbrace{\int_V [B_u]^T [c] [B_u] dV}_{[K_{uu}]} \{U_u\} + \underbrace{\int_V [B_u]^T [c] [\bar{B}_u] dV}_{-\{F_{1u}\} = -[Q_{1u}]\{v\}} \{\bar{U}_u\} \\ - \int_V [B_u]^T [e] \{E\} dV &= \underbrace{\int_{V_p} [B_u]^T [e] [B_\phi] dV}_{[K_{u\phi}]} \{U_\phi\} + \underbrace{\int_{V_p} [B_u]^T [e] [\bar{B}_\phi] dV}_{-\{F_{2u}\} = -[Q_{2u}]\{v\}} \{\bar{U}_\phi\} \\ \int_V \rho [N_u]^T \{\ddot{u}\} dV &= \underbrace{\int_V \rho [N_u]^T [N_u] dV}_{[M] = [M_{uu}]} \{\ddot{U}_u\} + \underbrace{\int_V \rho [N_u]^T [\bar{N}_u] dV}_{-\{F_{3u}\} = -[Q_{3u}]\{v\}} \{\ddot{\bar{U}}_u\} \\ \int_V [N_u]^T \{f_d\} dV &= \{F_{4u}\} = [Q_{4u}]\{v\} \\ \int_{\partial_{FV}} [N_u]^T \{F_d\} d\Gamma &= \{F_{5u}\} = [Q_{5u}]\{v\}. \end{aligned}$$

Analogously, considering  $V$  and  $V_p$  and introducing Eq. (A.8) into Eq. (A.11):

$$\begin{aligned} \int_V [B_\phi]^T [e]^T \{S\} dV &= \underbrace{\int_{V_p} [B_\phi]^T [e]^T [B_u] dV}_{[K_{\phi u}] \{U_u\}} + \underbrace{\int_{V_p} [B_\phi]^T [e]^T [\bar{B}_u] dV}_{-\{F_{1\phi}\} = -[Q_{1\phi}] \{v\}} \{U_u\} \\ \int_V [B_\phi]^T [\epsilon] \{E\} dV &= - \underbrace{\int_{V_p} [B_\phi]^T [\epsilon] [B_\phi] dV}_{[K_{\phi\phi}] \{U_\phi\}} - \underbrace{\int_{V_p} [B_\phi]^T [\epsilon] [\bar{B}_\phi] dV}_{\{F_{2\phi}\} = [Q_{2\phi}] \{v\}} \{U_\phi\} \\ - \int_{\partial_\sigma V_p} [N_\phi]^T \sigma_d d\Gamma &= \{F_{3\phi}\} = [Q_{3\phi}] \{v\}. \end{aligned}$$

In this document, all the “known” quantities are linked to a set of functions  $v_i$  gathered in the vector  $\{v\}$ . As a matter of fact, in the control theory context,  $\{v\}$  contains all functions  $u_k$  (the components of the control vector) and  $w_\ell$  (the components of the disturbance vector). Reordering Eq. (A.10) and Eq. (A.11), it is possible to write the following pair of equations:

$$[M] \{\ddot{U}_u\} + [K_{uu}] \{U_u\} + [K_{u\phi}] \{U_\phi\} = [Q_u] \{v\} \quad (\text{A.12})$$

$$[K_{\phi u}] \{U_u\} + [K_{\phi\phi}] \{U_\phi\} = [Q_\phi] \{v\}, \quad (\text{A.13})$$

where if  $[K_{\phi\phi}]$  is nonsingular, then Eq. (A.13) allows to eliminate  $\{U_\phi\}$  in Eq. (A.12).  $[K_{\phi\phi}]$  is nonsingular if electrode potentials are all properly defined with respect to a unique and common potential of reference, which must be the case. This permits to eliminate  $\{U_\phi\}$ :

$$\{U_\phi\} = [K_{\phi\phi}]^{-1} [Q_\phi] \{v\} - [K_{\phi\phi}]^{-1} [K_{\phi u}] \{U_u\}, \quad (\text{A.14})$$

leading to:

$$[M] \{\ddot{U}_u\} + [K_{uu}] \{U_u\} + [K_{u\phi}] \left( [K_{\phi\phi}]^{-1} [Q_\phi] \{v\} - [K_{\phi\phi}]^{-1} [K_{\phi u}] \{U_u\} \right) = [Q_u] \{v\},$$

and finally:

$$[M] \{\ddot{U}(t)\} + [K] \{U(t)\} = [Q] \{v(t)\}, \quad (\text{A.15})$$

where  $\{U\} = \{U_u\}$ ,  $[K] = [K_{uu}] - [K_{u\phi}] [K_{\phi\phi}]^{-1} [K_{\phi u}]$ ,  $[Q_u] = \sum_{i=1}^5 [Q_{iu}]$ ,  $[Q_\phi] = \sum_{i=1}^3 [Q_{i\phi}]$ , and  $[Q] = [Q_u] - [K_{u\phi}] [K_{\phi\phi}]^{-1} [Q_\phi]$ .

To fit the notation in the context of control theory and ignoring the notation of this part,

the right hand side of Eq. (A.15) can be written as:

$$[Q]\{v(t)\} = [\mathbf{B}_w]\{w(t)\} + [\mathbf{B}_u]\{u(t)\}.$$

## Measures

In this section, it is shown how measures such as displacements, potentials, and charges are obtained by using an FE model. External connections of the electrodes of piezoelectric sensors govern the measure type that is obtained. For instance, a voltage sensor (no current in the external circuit due to its very high impedance) or a charge sensor (null voltage between electrodes in the external circuit imposed by a charge amplifier) can be obtained. Once the solution  $\{U_u(t)\} = \{U(t)\}$  of Eq. (A.15) is known at time  $t$ , Eq. (A.14) gives the unknown potentials  $\{U_\phi(t)\}$ . At this stage,  $\{\tilde{U}_u(t)\}$  and  $\{\tilde{U}_\phi(t)\}$  are thus known.

The measure of point  $r$  displacement at time  $t$ ,  $\{u(r,t)\}$ , is then simply given by the chosen FE approximation, i.e.,

$$\{u(r,t)\} = [\tilde{N}_u(r)]\{\tilde{U}_u(t)\}. \quad (\text{A.16})$$

The electric potential measure of an electrode covering  $\Gamma_i$  is given by its corresponding component in  $\{\tilde{U}_\phi(t)\}$ , as defined before. The electric charge measure of an electrode covering  $\Gamma_i \subset \partial_\phi V_p$  is given by its corresponding component in the vector  $\{\tilde{F}_\phi(t)\}$  of nodal (and electrode) charges, which is the conjugate of  $\{\tilde{U}_\phi(t)\}$ . Considering  $\delta\phi = [\tilde{N}_\phi]\{\delta\tilde{U}_\phi\}$  in the variational principle, it comes to:

$$\{\delta\tilde{U}_\phi\}^T \left( \int_V [\tilde{B}_\phi]^T [e]^T \{S\} dV + \int_V [\tilde{B}_\phi]^T [\epsilon] \{E\} dV + \int_{\partial_\sigma V_p} [\tilde{N}_\phi]^T \sigma d\Gamma \right) = 0, \quad (\text{A.17})$$

where  $\{\tilde{F}_\phi\}$  is defined as:

$$\{\tilde{F}_\phi\} = \int_{\partial V} [\tilde{N}_\phi]^T \sigma d\Gamma,$$

which can be computed by using Eq. (A.17) and Eq. (A.7) as:

$$\{\tilde{F}_\phi\} = - \int_V [\tilde{B}_\phi]^T [e]^T [\tilde{B}_u] dV \{\tilde{U}_u\} + \int_V [\tilde{B}_\phi]^T [\epsilon] [\tilde{B}_\phi] dV \{\tilde{U}_\phi\}. \quad (\text{A.18})$$

For an electrode, it must be noticed that the support of the matrix function  $[\tilde{B}_\phi]$  corresponds to the elements that are connected to this electrode, in which the only nonzero line in matrix  $[\tilde{B}_\phi]^T$  is the one corresponding to the electrode potential. Matrices that are factor of  $\{\tilde{U}_u\}$  and  $\{\tilde{U}_\phi\}$  have only one line and can be calculated only once. Thereby, the effort to compute the electric charge of an electrode is very small.

The relations given in Eq. (A.16) and in Eq. (A.18) allow to build up the vector  $\mathbf{y}$  (output signals) of the control theory as:

$$\mathbf{y}(t) = [\mathbf{C}_d] \{U(t)\} + [\mathbf{C}_v] \{\dot{U}(t)\} + [\mathbf{C}_w] \{w(t)\} + [\mathbf{C}_u] \{u(t)\}.$$

### **Flat shells with symmetric piezoelectric layers**

Continuum 3D models allow to describe complex geometries but lead to a very large number of DOFs. In order to test new methods and algorithms in DTAC, it is not necessary to consider such refined continuum models because the main work in the control area is done using a reduced modal basis. However, it is necessary that the dynamic behaviour described by the model is sufficiently complicated to check the method in the worst conditions. With this aim in mind, plate structures are interesting because they are easy to build and their FE models only need 2D meshes of the mid-plane. This leads to fewer DOFs than 3D models to get accurate results in a wide range of frequencies as far as the shell approximation can be done. Thus, the objective of this section is to prepare the very short description of the FE approach that is implemented in the PLQP software.

Flat thin shell theories can model structures whose domain is defined between two planes. The kinematic description of displacements is associated to the mid-plane, defined here as the plane  $(x,y)$ . The plate thickness is the distance between these two planes. The model can be used successfully if the thickness is piecewise continuous such as the case when sensors or actuators are bonded on a uniform plate, provided that each constant thickness area has dimensions large enough with respect to the thickness. This is the first requirement to use the theory. An example of this respective situation is given in Fig. A.1. In Fig. A.2, a cross section shows the two external layers that are added to the core layer in order to build each piezoelectric transducer (actuator or sensor).

For the sake of simplicity, only the main lines of the theory are given, considering also only the thin flat shells. In this case, the transverse shear can be neglected and Kirchhoff's theory can be applied for bending. A model of the electric potential distribution in the thickness

is chosen to complete the theory. This allows to build plate and shell FE including piezoelectric materials when the structure contains piezoelectric layers. Moreover, the constant thicknesses  $h_1 = h_3$  of piezoelectric laminae are assumed small compared to the whole thickness. They are bonded on the upper and lower faces of a homogeneous plate of constant thickness  $h_2$ . In an area where piezoelectric laminae are present,  $z^- = -h_3 - \frac{h_2}{2}$  and  $z^+ = \frac{h_2}{2} + h_3$ , elsewhere  $z^- = -\frac{h_2}{2}$  and  $z^+ = \frac{h_2}{2}$ . Materials are assumed orthotropic and their principal directions are  $(x, y, z)$ .

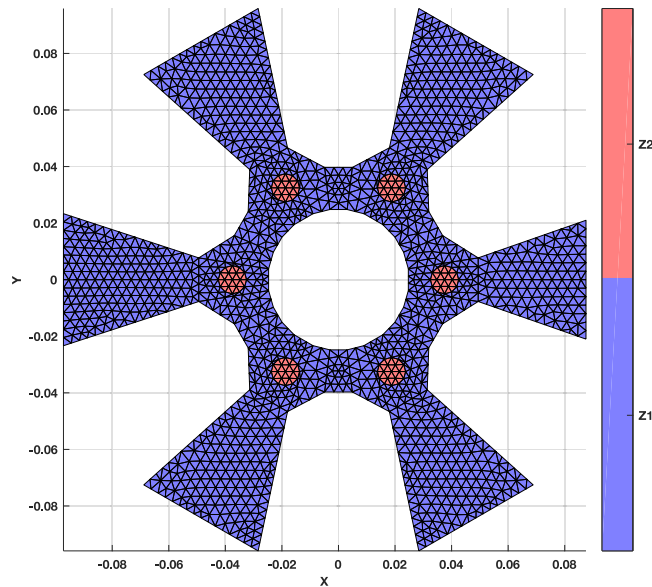


Figure A.1 - Example of an active structure modelled with PLQP (DKT element, coarse mesh,  $Z1$  area without piezoelectric pair,  $Z2$  contains six areas with a piezoceramic pair (either an actuator or a sensor)).

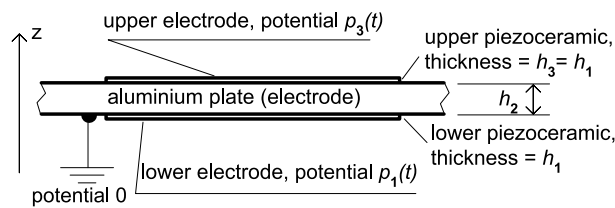


Figure A.2 - Configuration of each couple of piezoelectric layers (cross-section).

The main assumptions of Kirchhoff's theory are that a segment normal to the undeformed configuration remains normal to the deformed configuration. This permits to describe the displacement of each point of the plate by means of the mid-plane ( $z = 0$ ) displacements ( $\bar{u}_{0x} = u_x(x, y, 0)$ ,  $\bar{u}_{0y} = u_y(x, y, 0)$ , and  $\bar{u}_{0z} = u_z(x, y, 0)$ ) and by rotations of the segment described by the opposite of  $\bar{u}_z$  slopes (that implies zero transverse shear, i.e.,  $S_{xz} = S_{yz} = 0$ ):

$$\beta_x(x, y) = -\partial \bar{u}_z / \partial x \quad \text{and} \quad \beta_y(x, y) = -\partial \bar{u}_z / \partial y, \quad (\text{A.19})$$

thus leading to:

$$\begin{Bmatrix} \bar{u}_x \\ \bar{u}_y \end{Bmatrix} = \begin{Bmatrix} \bar{u}_{0x} \\ \bar{u}_{0y} \end{Bmatrix} + z \begin{Bmatrix} \beta_x \\ \beta_y \end{Bmatrix} \quad \text{i.e.} \quad \{\bar{u}\} = \{\bar{u}_0\} + z\{\beta\} \text{ for } \bar{u}_z = \bar{u}_{0z}. \quad (\text{A.20})$$

To get an accurate description of bending in conjunction with the kinematic model represented in Eq. (A.20), the theory assumes plane stress  $T_{zz} = 0$  in the planes parallel to  $(x,y)$ . In addition,  $\{\bar{T}\} = [T_x \ T_y \ T_{xy}]^T$  is considered for membrane and bending. Transverse stresses  $T_{xz}$  and  $T_{yz}$  are obtained by equilibrium considerations in the thickness.  $[\bar{c}]$ ,  $\{\bar{e}\}$ , and  $\bar{\epsilon}$  are deduced from Eq. (A.1a) and Eq. (A.1b) as constant in each layer. According to piezoelectric ceramics used in this work, the poling direction of a piezoelectric lamina  $\ell$  is  $z$ . In PLQP, the potential is assumed to vary linearly between its two electrodes. The electric field is thus constant and parallel to  $z$  ( $E_{x\ell} = E_{y\ell} = 0$ ), defined as:

$$E_{z\ell} = p_\ell/h_\ell, \quad (\text{A.21})$$

where  $p_\ell$  is the electric voltage between its upper and lower electrodes. In a piezoelectric area, the two electric fields (in layer 1 and layer 3) are defined as:

$$\begin{Bmatrix} E_{z1} \\ E_{z3} \end{Bmatrix} = \begin{bmatrix} 1/h_1 & 0 \\ 0 & 1/h_3 \end{bmatrix} \begin{Bmatrix} p_1 \\ p_3 \end{Bmatrix} \quad \text{with} \quad \begin{Bmatrix} p_1 \\ p_3 \end{Bmatrix} = \begin{bmatrix} -1 & 1 & 0 & 0 \\ 0 & 0 & -1 & 1 \end{bmatrix} \begin{Bmatrix} \phi_1^- \\ \phi_1^+ \\ \phi_3^- \\ \phi_3^+ \end{Bmatrix},$$

in which  $\phi_\ell^-$  and  $\phi_\ell^+$  denote respectively the potentials of the lower and upper electrodes in a piezoelectric layer  $\ell$  of the model. Thus, it is possible to write:

$$\begin{Bmatrix} E_{z1} \\ E_{z3} \end{Bmatrix} = \begin{bmatrix} -1/h_1 & 1/h_1 & 0 & 0 \\ 0 & 0 & -1/h_3 & 1/h_3 \end{bmatrix} \begin{Bmatrix} \phi_1^- \\ \phi_1^+ \\ \phi_3^- \\ \phi_3^+ \end{Bmatrix} \quad \text{i.e.} \quad \{\bar{E}\} = [\bar{B}_E]\{\bar{\phi}\},$$

and considering a piezoelectric area  $V_c = \Sigma_c \times [z^-, z^+]$  in which continuous electrodes and layer are present ( $\{\bar{E}(r,t)\} = \{\bar{E}_c(t)\}$ ) because  $[\bar{B}_E(r)] = [\bar{b}_c]$  is constant. The four potentials are denoted by  $\{\bar{\phi}_c\}$ :  $\{\bar{\phi}(t)\} = \{\bar{\phi}_c(t)\}$ .

The strain associated to the plane stress is denoted by  $\{\bar{S}\} = \bar{\nabla}_s\{\bar{u}\}$ , where  $\bar{\nabla}_s$  is the symmetric part of the gradient in the plane  $(x,y)$  and  $\{\bar{S}\} = [S_x \ S_y \ 2S_{xy}]^T$ . This vector can be expressed as  $\{\bar{S}\} = \{\bar{S}_0\} + z\{\kappa\}$ , in which  $\{\bar{S}_0\} = \bar{\nabla}_s\{\bar{u}_0\}$  and  $\{\kappa\} = \bar{\nabla}_s\{\beta\}$  are “generalised” strains. For layer  $\ell = 1,3$  the constitutive relation is given by:

$$\{\bar{T}\}_\ell = [\bar{c}]_\ell\{\bar{S}\} - \{\bar{e}\}_\ell E_{z\ell} \quad (\text{A.22})$$

$$D_{z\ell} = \{\bar{e}\}_\ell^T\{\bar{S}\} + \bar{e}_\ell E_{z\ell}. \quad (\text{A.23})$$

For the elastic central layer ( $\ell = 2$ ), the relation is simply  $\{\bar{T}\}_\ell = [\bar{c}]_\ell\{\bar{S}\}$ . When the evaluation of the first two terms in Eq. (A.4) is considered, the expressions of  $\{\bar{S}\}$  and  $\{\bar{E}\}$  (and of their variations) permit to take into account an integration in two steps: first in  $z$ , then in  $(x,y)$ :

$$\begin{aligned} \int_{z^-}^{z^+} \{\delta S\}^T\{T\} dz &= \{\delta\bar{S}_0\}^T \int_{z^-}^{z^+} \{\bar{T}\} dz + \{\delta\kappa\}^T \int_{z^-}^{z^+} z \{\bar{T}\} dz = \{\delta\bar{S}_0\}^T\{N\} + \{\delta\kappa\}^T\{M\} \\ \int_{z^-}^{z^+} \{\delta E\}^T\{D\} dz &= \delta E_{z1} \int_{z^-}^{h_2/2} D_{z1} dz + \delta E_{z3} \int_{h_2/2}^{z^+} D_{z3} dz = \{\delta\bar{E}\}^T\{\bar{D}\}. \end{aligned}$$

The integration over  $z$  of Eq. (A.22) and Eq. (A.23) (see (BATOZ; DHATT, 1990) for the mechanical part and (PREUMONT, 2002) for a simplified description of the piezoelectric part) leads to “generalised” stresses  $\{N\} = \int_{z^-}^{z^+} \{\bar{T}\} dz$ ,  $\{M\} = \int_{z^-}^{z^+} z\{\bar{T}\} dz$ , and  $\{\bar{D}\} = [\bar{D}_{z1} \ \bar{D}_{z3}]^T$ , considering  $\bar{D}_{z1} = \int_{z^-}^{h_2/2} D_{z1} dz$  and  $\bar{D}_{z3} = \int_{h_2/2}^{z^+} D_{z3} dz$ . This also leads to “global” constitutive relations:

$$\begin{aligned} \begin{Bmatrix} \{N\} \\ \{M\} \end{Bmatrix} &= \begin{bmatrix} [C_N] & [C_{NM}] \\ [C_{NM}]^T & [C_M] \end{bmatrix} \begin{Bmatrix} \{\bar{S}_0\} \\ \{\kappa\} \end{Bmatrix} - \begin{bmatrix} \{e_{N1}\} & \{e_{N3}\} \\ \{e_{M1}\} & \{e_{M3}\} \end{bmatrix} \begin{Bmatrix} E_{z1} \\ E_{z3} \end{Bmatrix} \\ &= \begin{bmatrix} [C_N] & [C_{NM}] \\ [C_{NM}]^T & [C_M] \end{bmatrix} \begin{Bmatrix} \{\bar{S}_0\} \\ \{\kappa\} \end{Bmatrix} - \begin{bmatrix} [e_N] \\ [e_M] \end{bmatrix} \{\bar{E}\} \end{aligned}$$

$$\begin{aligned} \begin{Bmatrix} \bar{D}_{z1} \\ \bar{D}_{z3} \end{Bmatrix} &= \begin{bmatrix} \{e_{N1}\}^T & \{e_{M1}\}^T \\ \{e_{N3}\}^T & \{e_{M3}\}^T \end{bmatrix} \begin{Bmatrix} \{\bar{S}_0\} \\ \{\kappa\} \end{Bmatrix} + \begin{bmatrix} h_1 \bar{e}_1 & 0 \\ 0 & h_3 \bar{e}_3 \end{bmatrix} \begin{Bmatrix} E_{z1} \\ E_{z3} \end{Bmatrix} \\ \{\bar{D}\} &= \begin{bmatrix} [e_N]^T & [e_M]^T \end{bmatrix} \begin{Bmatrix} \{\bar{S}_0\} \\ \{\kappa\} \end{Bmatrix} + [\bar{e}]\{\bar{E}\}, \end{aligned}$$

with:

$$\begin{bmatrix} [C_N] & [C_{NM}] \\ [C_{NM}] & [C_M] \end{bmatrix} = \int_{z^-}^{z^+} \begin{bmatrix} [\bar{c}] & z[\bar{c}] \\ z[\bar{c}] & z^2[\bar{c}] \end{bmatrix} dz,$$

$$[\bar{\epsilon}] = \begin{bmatrix} h_1 \bar{\epsilon}_1 & 0 \\ 0 & h_3 \bar{\epsilon}_3 \end{bmatrix} = \begin{bmatrix} \int_{z^-}^{h_2/2} \bar{\epsilon}_1 dz & 0 \\ 0 & \int_{h_2/2}^{z^+} \bar{\epsilon}_3 dz \end{bmatrix},$$

$$\begin{aligned} \{e_{N1}\} &= \int_{z^-}^{h_2/2} \{\bar{\epsilon}_1\} dz, & \{e_{N3}\} &= \int_{h_2/2}^{z^+} \{\bar{\epsilon}_3\} dz, & [e_N] &= \begin{bmatrix} \{e_{N1}\} & \{e_{N3}\} \end{bmatrix}, \\ \{e_{M1}\} &= \int_{z^-}^{h_2/2} z\{\bar{\epsilon}_1\} dz, & \{e_{M3}\} &= \int_{h_2/2}^{z^+} z\{\bar{\epsilon}_3\} dz, & [e_M] &= \begin{bmatrix} \{e_{M1}\} & \{e_{M3}\} \end{bmatrix}. \end{aligned}$$

It is important to notice that when the materials are isotropic in the plane  $(x,y)$  and the layers are symmetric with respect to the mid-plane,  $[C_{NM}] = [0]$ . In this case, membrane and transverse free vibrations are uncoupled if electric BC are free or if  $p_1 = p_3$  or  $p_1 = -p_3$  for each couple of ceramics. This can be verified by inspecting the content of  $[e_N]$  and  $[e_M]$  and this is assumed in remaining and adopted in the PLQP software.

### FE for plate bending

This section considers finite elements in the frame of a displacement approach and for plate bending for the sake of simplicity (BATOZ; DHATT, 1990). This supposes that the conditions for the uncoupling of membrane and transverse vibrations are satisfied. In this case,  $\{\bar{u}_0\}$  and  $u_z$  are uncoupled and  $\{\bar{u}_0\} = \{0\}$  corresponds to out-of-plane vibrations. Plate bending is implemented in PLQP software for triangular elements (DKT). In plate bending, when uncoupled with membrane, the constitutive relation is given as:

$$\{M\} = [C_M]\{\kappa\} - [e_M]\{\bar{E}\} \quad (\text{A.24a})$$

$$\{\bar{D}\} = [e_M]^T\{\kappa\} + [\bar{\epsilon}]\{\bar{E}\}. \quad (\text{A.24b})$$

At this stage, all integration in  $z$  is done in the frame of the shell model, therefore, nodes and elements are defined in the mid-plane of the plate. The volume  $V$  is described by a surface area  $\Sigma$  of the mid-plane and a thickness  $h(x,y)$ . Introducing  $z_- = -h/2$ ,  $z_+ = h/2$  simplifies the expression of integral bounds.  $\partial\Sigma$  denotes the boundary of  $\Sigma$ . Meshing  $\Sigma$  in triangular or



quadrangular elements leads to a set of elements and to a set of nodes. In a piezoelectric region  $V_c \subset V_P$  (three continuous and homogeneous layers), the FE approximation of  $u_z$  at  $r = (x, y)$  and time  $t$  can be written as:

$$\{\tilde{u}\} = [\tilde{N}_u]\{\tilde{U}_u\} \quad \text{i.e.} \quad \begin{Bmatrix} u_z(r, t) \\ \{\beta(r, t)\} \end{Bmatrix} = \begin{bmatrix} [\tilde{N}_{uz}(r)] \\ [\tilde{N}_\beta(r)] \end{bmatrix} \{\tilde{U}_u(t)\} \quad (\text{A.25})$$

$$\begin{aligned} \{\bar{\phi}\} &= [\tilde{N}_\phi]\{\tilde{U}_\phi\}, & \text{i.e.} & \quad \{\bar{\phi}(r, t)\} = [\tilde{N}_\phi(r)]\{\tilde{U}_\phi(t)\} \\ [\tilde{N}_\phi(r)] &= [\tilde{N}_c] \text{ constant on } V_c & \text{and} & \quad \{\bar{\phi}_c(t)\} = [\tilde{N}_c]\{\tilde{U}_\phi(t)\} \text{ on } V_c. \end{aligned} \quad (\text{A.26})$$

It must be noticed that to simplify the notation for the interpolation functions and for the vectors of DOFs, the same notation of Eq. (A.6a) and Eq. (A.6b) is adopted but matrices  $[\tilde{N}_u]$ ,  $[\tilde{N}_\phi]$ ,  $\{\tilde{U}_u\}$ , and  $\{\tilde{U}_\phi\}$  are completely different. In  $[\tilde{N}_u]$ , function  $u_z$  must be  $C_1$ , whereas  $[\tilde{N}_\beta]$  is  $C_0$  and  $[\tilde{N}_\phi]$  is piecewise constant.  $\{\tilde{U}_\phi\}$  contains electrode potentials and  $\{\tilde{U}_u\}$  contains rotations  $\theta_x = -\beta_y$ ,  $\theta_y = \beta_x$ , and the displacement  $u_z$  of the nodes.  $[\tilde{N}_\beta]$  is linked to  $[\tilde{N}_{uz}(r)]$  by the definition of  $\{\beta\}$ . Then,  $\{\kappa\}$  is obtained through its definition and the expression  $\{\bar{E}\}$  of the constant electric field in each of the two layers of a piezoelectric area  $V_c$  are simply given by Eq. (A.21):

$$\begin{aligned} \{\kappa\} &= [\tilde{B}_u]\{\tilde{U}_u\} & \text{with} & \quad [\tilde{B}_u] = \bar{\nabla}_s[\tilde{N}_\beta] \\ \{\bar{E}\} &= [\tilde{B}_\phi]\{\tilde{U}_\phi\} & \text{with} & \quad [\tilde{B}_\phi] = [\tilde{B}_c] = [\bar{b}_c][\tilde{N}_c] \text{ in } V_c. \end{aligned}$$

As previously, the partition “known/unknown” leads to:

$$\{\kappa\} = [\bar{B}_u]\{\bar{U}_u\} + [B_u]\{U_u\} \quad (\text{A.27a})$$

$$\{\bar{E}\} = -[\bar{B}_\phi]\{\bar{U}_\phi\} - [B_\phi]\{U_\phi\}, \quad (\text{A.27b})$$

where:

$$\{\tilde{U}_u\} = [\bar{N}_u]\{\bar{U}_u\} + [N_u]\{U_u\} \quad \text{with } [N_u] = [0] \text{ on } \partial_u \Sigma \quad (\text{A.28a})$$

$$\{\tilde{U}_\phi\} = [\bar{N}_\phi]\{\bar{U}_\phi\} + [N_\phi]\{U_\phi\} \quad \text{with } [N_\phi] = [0] \text{ on } \partial_\phi V_p \subset \partial V_p. \quad (\text{A.28b})$$

Let  $n_c$  be the number of areas  $V_c$ , where couples of piezoelectric ceramics define either a

sensor or an actuator, then:

$$\begin{aligned}
\int_{\partial V_p} \delta\phi \sigma \, d\Gamma &= \sum_{c=1}^{n_c} \left( \int_{\Gamma_{c1}^-} \delta\phi_{c1}^- \sigma_{c1}^- \, d\Gamma + \int_{\Gamma_{c1}^+} \delta\phi_{c1}^+ \sigma_{c1}^+ \, d\Gamma + \int_{\Gamma_{c3}^-} \delta\phi_{c3}^- \sigma_{c3}^- \, d\Gamma + \int_{\Gamma_{c3}^+} \delta\phi_{c3}^+ \sigma_{c3}^+ \, d\Gamma \right) \\
&= \sum_{c=1}^{n_c} \left( \delta\phi_{c1}^- \int_{\Gamma_{c1}^-} \sigma_{c1}^- \, d\Gamma + \delta\phi_{c1}^+ \int_{\Gamma_{c1}^+} \sigma_{c1}^+ \, d\Gamma + \delta\phi_{c3}^- \int_{\Gamma_{c3}^-} \sigma_{c3}^- \, d\Gamma + \delta\phi_{c3}^+ \int_{\Gamma_{c3}^+} \sigma_{c3}^+ \, d\Gamma \right) \\
&= \sum_{c=1}^{n_c} \{\delta\bar{\phi}_c\}^T \{\bar{\sigma}_c\},
\end{aligned}$$

where:

$$\{\bar{\sigma}_c\} = \left[ \int_{\Gamma_{c1}^-} \sigma_{c1}^- \, d\Gamma \quad \int_{\Gamma_{c1}^+} \sigma_{c1}^+ \, d\Gamma \quad \int_{\Gamma_{c3}^-} \sigma_{c3}^- \, d\Gamma \quad \int_{\Gamma_{c3}^+} \sigma_{c3}^+ \, d\Gamma \right]^T.$$

Introducing the assumed electric potential approximation and plate bending kinematics in Eq. (A.4) and making the required integrations, the variational form used for plate bending elements with two piezoelectric layers is obtained for free BC:

$$\begin{aligned}
\int_{\Sigma} \left( \{\delta\kappa\}^T \{M\} - \{\delta\bar{E}\}^T \{\bar{D}\} - \{\delta\tilde{u}\}^T \{\tilde{f}_d\} + \{\delta\tilde{u}\}^T [m] \{\ddot{u}\} \right) d\Gamma \\
- \int_{\partial\Sigma} \{\delta\tilde{u}\}^T \{\tilde{F}\} \, ds + \sum_{c=1}^{n_c} \{\delta\bar{\phi}_c\}^T \{\bar{\sigma}_c\} = 0, \quad (\text{A.29})
\end{aligned}$$

$$\text{where } [m] = \int_{z^-}^{z^+} \rho \begin{bmatrix} 1 & 0 & 0 \\ 0 & z^2 & 0 \\ 0 & 0 & z^2 \end{bmatrix} dz.$$

Now, introducing the constitutive relation Eq. (A.24) in Eq. (A.29), it gives:

$$\begin{aligned}
\int_{\Sigma} \left( \{\delta\kappa\}^T [C_M] \{\kappa\} - \{\delta\kappa\}^T [e_M] \{\bar{E}\} - \{\delta\bar{E}\}^T [e_M]^T \{\kappa\} - \{\delta\bar{E}\}^T [\bar{\epsilon}] \{\bar{E}\} \right. \\
\left. + \{\delta\tilde{u}\}^T [m] \{\ddot{u}\} - \{\delta\tilde{u}\}^T \{\tilde{f}_d\} \right) d\Gamma - \int_{\partial\Sigma} \{\delta\tilde{u}\}^T \{\tilde{F}\} \, ds + \{\delta\tilde{U}_\phi\}^T \left( \sum_{c=1}^{n_c} [\tilde{N}_c]^T \{\bar{\sigma}_c\} \right) ds = 0.
\end{aligned} \quad (\text{A.30})$$

The FE approximations Eq. (A.25) and Eq. (A.26), considering Eq. (A.28) with  $\{\delta u\} = [N_u] \{\delta U_u\}$  and  $\{\delta\phi\} = [N_\phi] \{\delta U_\phi\}$  in Eq. (A.30) for all  $\{\delta U_u\}$  and  $\{\delta U_\phi\}$ , lead to the FE matrix

equations:

$$\{\delta U_u\}^T \left( \int_{\Sigma} [N_u]^T [m] \{\ddot{u}\} d\Gamma + \int_{\Sigma} [B_u]^T [C_M] \{\kappa\} d\Gamma - \int_{\Sigma} [B_u]^T [e_M] \{\bar{E}\} d\Gamma - \int_{\Sigma} [N_u]^T \{\tilde{f}_d\} d\Gamma - \int_{\partial_F \Sigma} [N_u]^T \{\tilde{F}_d\} d\Gamma \right) = 0$$

$$\{\delta U_{\phi}\}^T \left( \int_{\Sigma} [B_{\phi}]^T [e_M]^T \{\kappa\} d\Gamma + \int_{\Sigma} [B_{\phi}]^T [\bar{\epsilon}] \{\bar{E}\} d\Gamma + \sum_{c=1}^{n_c} [N_c]^T \{\bar{\sigma}_c\} \right) = 0, \quad (\text{A.31a})$$

and thus:

$$\begin{aligned} \int_{\Sigma} [N_u]^T [m] \{\ddot{u}\} d\Gamma + \int_{\Sigma} [B_u]^T [C_M] \{\kappa\} d\Gamma - \int_{\Sigma} [B_u]^T [e_M] \{\bar{E}\} d\Gamma \\ = \int_{\Sigma} [N_u]^T \{\tilde{f}_d\} d\Gamma + \int_{\partial_F \Sigma} [N_u]^T \{\tilde{F}_d\} d\Gamma \end{aligned} \quad (\text{A.32a})$$

$$\int_{\Sigma} [B_{\phi}]^T [e_M]^T \{\kappa\} d\Gamma + \int_{\Sigma} [B_{\phi}]^T [\bar{\epsilon}] \{\bar{E}\} d\Gamma = - \sum_{c=1}^{n_c} [\tilde{N}_c]^T \{\bar{\sigma}_c\}. \quad (\text{A.32b})$$

Considering now  $V$  and  $V_p$  and introducing Eq. (A.27) into Eq. (A.32a), it gives:

$$\begin{aligned} \int_{\Sigma} [B_u]^T [C_M] \{\kappa\} d\Gamma &= \underbrace{\int_{\Sigma} [B_u]^T [C_M] [B_u] d\Gamma}_{[K_{uu}]} \{U_u\} + \underbrace{\int_{\Sigma} [B_u]^T [C_M] [\bar{B}_u] d\Gamma}_{-\{F_{1u}\} = -[Q_{1u}]} \{\bar{U}_u\} \\ - \int_{\Sigma} [B_u]^T [e_M] \{\bar{E}\} d\Gamma &= \underbrace{\int_{\Sigma_p} [B_u]^T [e_M] [B_{\phi}] d\Gamma}_{[K_{u\phi}]} \{U_{\phi}\} + \underbrace{\int_{\Sigma_p} [B_u]^T [e_M] [\bar{B}_{\phi}] d\Gamma}_{-\{F_{2u}\} = -[Q_{2u}]} \{\bar{U}_{\phi}\} \\ \int_{\Sigma} [N_u]^T [m] \{\ddot{u}\} d\Gamma &= \underbrace{\int_{\Sigma} [N_u]^T [m] [N_u] dV}_{[M] = [M_{uu}]} \{\ddot{U}_u\} + \underbrace{\int_{\Sigma} [N_u]^T [\bar{N}_u] dV}_{-\{F_{3u}\} = -[Q_{3u}]} \{\ddot{\bar{U}}_u\} \\ \int_{\Sigma} [N_u]^T \{\tilde{f}_d\} d\Gamma &= \{F_{4u}\} = [Q_{4u}] \{v\} \\ \int_{\partial_F \Sigma} [N_u]^T \{\tilde{F}_d\} d\Gamma &= \{F_{5u}\} = [Q_{5u}] \{v\}. \end{aligned}$$

Analogously, considering  $V$  and  $V_p$  and introducing Eq. (A.27) into Eq. (A.32b), it leads

to:

$$\begin{aligned}
\int_{\Sigma} [B_{\phi}]^T [e]^T \{S\} d\Gamma &= \underbrace{\int_{\Sigma_p} [B_{\phi}]^T [e_M]^T [B_u] d\Gamma}_{[K_{\phi u}] = [K_{u\phi}]^T} \{U_u\} + \underbrace{\int_{\Sigma_p} [B_{\phi}]^T [e_M]^T [\bar{B}_u] d\Gamma}_{-\{F_{1\phi}\} = -[Q_{1\phi}]\{v\}} \{\bar{U}_u\} \\
\int_{\Sigma} [B_{\phi}]^T [\bar{\epsilon}] \{E\} d\Gamma &= - \underbrace{\int_{\Sigma_p} [B_{\phi}]^T [\bar{\epsilon}] [B_{\phi}] d\Gamma}_{[K_{\phi\phi}]} \{U_{\phi}\} - \underbrace{\int_{\Sigma_p} [B_{\phi}]^T [\bar{\epsilon}] [\bar{B}_{\phi}] d\Gamma}_{\{F_{2\phi}\} = [Q_{2\phi}]\{v\}} \{\bar{U}_{\phi}\} \\
- \sum_{c=1}^{n_c} [N_c]^T \{\bar{\sigma}_c\} &= \{F_{3\phi}\} = [Q_{3\phi}]\{v\}.
\end{aligned}$$

Again, all the “known” quantities are linked to  $\{v\}$ . Due to the choice of same notation for the continuum approach, Eq. (A.12) and Eq. (A.15) are obtained from Eq. (A.32a) and Eq. (A.32b), considering different matrix contents, which do not represent the same model.

### Discrete Kirchhoff triangle element

When the Kirchhoff bending plate theory is considered, triangular plate elements have good properties and are able to follow the  $C_1$  continuity requirement. Usually, these elements are not numerous and are not complicated to implement and/or use. In PLQP software, a three-node discrete Kirchhoff element (DKT), with three DOFs per node ( $u_z, \theta_x = -\beta_y, \theta_y = \beta_x$ ) as described in (BATOZ; DHATT, 1990) is chosen. In this kind of element, Kirchhoff’s theory is not perfectly respected. The shear energy is zero and Eq. (A.19) states at the nodes but a zero shear strain  $S_{sz}$  is only imposed on the edges (curvilinear abscissa  $s$ ) of the triangle. In order to test DTAC or control methods, it allows to build a wide variety of active structure models, including several couples of piezoelectric material, restricted to flat geometries but with a complex dynamic behaviour.

### References

- ALLIK, H.; HUGHES, T. J. R. Finite element method for piezoelectric vibration. *International Journal for Numerical Methods in Engineering*, v. 2, p. 151-157, 1970.
- BATHE, K. J. *Finite Element Procedures in Engineering Analysis*. Prentice Hall, 1982.
- BATOZ, J. L.; DHATT, G. *Modélisation des structures par éléments finis: poutres et plaques*. Hermès, 1990.
- PREUMONT, A. *Vibration Control of Active Structures: An Introduction*. Kluwer Academic Publishers, 2002.

## ANNEXE B - RÉSUMÉ ÉTENDU EN FRANÇAIS

### B.1 Introduction

La réduction des vibrations (ou Active Vibration Control, AVC), le contrôle de forme et la surveillance in situ de l'état structural (ou Structural Health Monitoring, SHM) sont devenus des enjeux d'un intérêt essentiel dans de nombreux secteurs de l'industrie innovante, notamment dans les domaines des transports, du génie civil et du génie médical. Il peut s'agir d'adapter la forme d'un objet pour optimiser son fonctionnement dans un environnement donné, de limiter l'endommagement des structures en réduisant l'amplitude et la durée des vibrations, ou encore de détecter et d'identifier les défauts liés aux endommagements pour prédire et maîtriser la durée de vie des systèmes. Les technologies basées sur l'emploi de matériaux intelligents connaissent un essor important du fait de leur aptitude à répondre aux objectifs précédents grâce à leurs propriétés multi-physiques, ceci, de façon active ou réactive. Les matériaux piézoélectriques peuvent, par exemple, être intégrés aux structures et connectés à des circuits électriques dédiés pour dissiper l'énergie vibratoire ou pour véhiculer des informations sur l'état de la structure. Ces matériaux peuvent être aussi utilisés dans un cadre de contrôle actif, où ils sont connectés à un microprocesseur, avec une efficacité notable par rapport aux techniques passives, en contrepartie d'un coût énergétique parfois élevé et d'une complexité accrue.

Une structure intelligente est donc capable de rejeter les perturbations extérieures, mais l'est-elle toujours si un endommagement survient? Peut-on reconfigurer la loi de contrôle ou l'adapter à la présence du dommage? Peut-on contrôler ou limiter l'évolution de l'endommagement? Le contrôle actif tolérant aux dommages (ou DTAC pour Damage-Tolerant Active Control) est un nouveau champ de recherche qui intègre les concepts de la surveillance in situ de l'état structural, du contrôle actif des vibrations et de la commande tolérante aux défauts (ou Fault-Tolerant Control, FTC). La réduction des vibrations dans une structure en présence d'endommagement est un sujet de recherche récent. Très peu de travaux traitent des effets des dommages sur les vibrations et sur leur contrôle, en tenant compte des besoins industriels en termes de rejet de vibration et de maintenance des structures, et visant à améliorer la durée de vie opérationnelle. Cette thèse se situe dans ce contexte, et nous proposons des techniques modales pour réaliser un système de contrôle actif tolérant aux dommages.

## B.2 Objectifs

Dans un premier temps, nos travaux se sont focalisés sur l'élaboration d'une commande  $H_\infty$  modale permettant d'atténuer les vibrations associées à certains modes et en présence d'incertitudes et de dommages. Cette approche a été testée expérimentalement sur une poutre en aluminium sur laquelle un dommage a été introduit.

Nous avons aussi étudié et proposé une technique modale pour la détection de dommages, où l'effet des dommages sur chaque mode de vibration peut être quantifiée. Ainsi, nous utilisons une technique SHM modale pour repérer les modes de vibration qui sont les plus touchés. Avec cette information, le correcteur  $H_\infty$  modal est conçu pour distribuer l'énergie de commande de manière efficace entre les modes, même quand un dommage survient. Cependant, cette méthode nécessite de la connaissance a priori de la région critique de la structure où les dommages peuvent survenir. L'historique de maintenance ou une étude préliminaire sur les modes de vibrations les plus endommageants peuvent, par exemple, indiquer les zones critiques. Cette approche a été testée en réalisant une simulation par éléments finis sur une structure de type poutre-plaque (poutre large modélisée par la théorie des plaques).

La dernière technique proposée est basée sur une approche adaptative avec double boucle de commande pour faire face à des endommagements imprévisibles, tels que ceux provoqués par des impacts. Pour atteindre cet objectif, le premier correcteur  $H_\infty$  modal est conçu pour satisfaire les contraintes de performance et de robustesse sur la structure saine. Le second a pour objectif de détecter un dommage et de réagir de façon satisfaisante, même en présence d'endommagement. Cette loi de commande modale s'appuie sur une stratégie de reconfiguration en ligne du correcteur. Cette approche a également été testée avec une simulation par éléments finis sur la même structure de type poutre-plaque.

## B.3 Modèle modal d'une structure intelligente

Cette section présente un bref aperçu du modèle modal d'état pour décrire le comportement des structures flexibles, où une représentation canonique spécifique est adoptée. Une struc-

ture flexible générique avec plusieurs transducteurs PZT peut être modélisée par les équations linéaires du second ordre suivantes:

$$\begin{aligned} \mathbf{M}\ddot{\mathbf{p}}(t) + \mathbf{D}\dot{\mathbf{p}}(t) + \mathbf{K}\mathbf{p}(t) &= \mathbf{B}_w\mathbf{w}(t) + \mathbf{B}_u\mathbf{u}(t) \\ \mathbf{y}(t) &= \mathbf{C}_d\mathbf{p}(t) + \mathbf{C}_v\dot{\mathbf{p}}(t) + \mathbf{C}_w\mathbf{w}(t) + \mathbf{C}_u\mathbf{u}(t), \end{aligned} \quad (\text{B.1})$$

où  $\mathbf{p}(t)$  est le vecteur des déplacements des noeuds,  $\mathbf{M}$  est la matrice de masse,  $\mathbf{D}$  est la matrice d'amortissement,  $\mathbf{K}$  est la matrice de rigidité,  $\mathbf{B}_w$  et  $\mathbf{B}_u$  sont les matrices d'entrée, où  $\mathbf{w}(t)$  décrit perturbations et  $\mathbf{u}(t)$  la commande,  $\mathbf{y}(t)$  contient les signaux de sortie modelisés par les matrices  $\mathbf{C}_d$ ,  $\mathbf{C}_v$ ,  $\mathbf{C}_w$  et  $\mathbf{C}_u$ . En général, les modèles éléments finis génèrent des modèles d'ordre très élevé qui doivent être réduits pour des raisons pratiques, tout en représentant correctement la bande d'intérêt. Une procédure de troncature simple en respectant les modes qui présentent un niveau d'énergie important est assez souvent suffisante pour obtenir de bons résultats. En supposant que le nombre de modes adopté est  $m$ , la matrice modale est définie dans l'équation suivante:

$$\Phi = \begin{bmatrix} \phi_1 & \phi_2 & \dots & \phi_m \end{bmatrix}.$$

Une transformation en coordonnées modales est obtenue en utilisant  $\mathbf{p}(t) = \Phi\mathbf{q}(t)$ . Prémultipliant Eq. (B.1) par  $\Phi^T$ , cela conduit à:

$$\begin{aligned} \Phi^T\mathbf{M}\Phi\ddot{\mathbf{q}}(t) + \Phi^T\mathbf{D}\Phi\dot{\mathbf{q}}(t) + \Phi^T\mathbf{K}\Phi\mathbf{q}(t) &= \Phi^T\mathbf{B}_w\mathbf{w}(t) + \Phi^T\mathbf{B}_u\mathbf{u}(t) \\ \mathbf{y}(t) &= \mathbf{C}_d\Phi\mathbf{q}(t) + \mathbf{C}_v\Phi\dot{\mathbf{q}}(t) + \mathbf{C}_w\mathbf{w}(t) + \mathbf{C}_u\mathbf{u}(t), \end{aligned}$$

qui peut s'écrire:

$$\mathbf{M}_m\ddot{\mathbf{q}}(t) + \mathbf{D}_m\dot{\mathbf{q}}(t) + \mathbf{K}_m\mathbf{q}(t) = \mathbf{B}_{w_m}\mathbf{w}(t) + \mathbf{B}_{u_m}\mathbf{u}(t) \quad (\text{B.2})$$

$$\mathbf{y}(t) = \mathbf{C}_{d_m}\mathbf{q}(t) + \mathbf{C}_{v_m}\dot{\mathbf{q}}(t) + \mathbf{C}_w\mathbf{w}(t) + \mathbf{C}_u\mathbf{u}(t), \quad (\text{B.3})$$

où  $\mathbf{M}_m = \Phi^T\mathbf{M}\Phi$ ,  $\mathbf{D}_m = \Phi^T\mathbf{D}\Phi$ ,  $\mathbf{K}_m = \Phi^T\mathbf{K}\Phi$ ,  $\mathbf{B}_{w_m} = \Phi^T\mathbf{B}_w$ ,  $\mathbf{B}_{u_m} = \Phi^T\mathbf{B}_u$ ,  $\mathbf{C}_{d_m} = \mathbf{C}_d\Phi$  et  $\mathbf{C}_{v_m} = \mathbf{C}_v\Phi$ . Les matrices  $\mathbf{M}_m$  et  $\mathbf{K}_m$  sont diagonales tandis que  $\mathbf{D}_m$  n'est pas nécessairement diagonale. Pour faciliter l'analyse, la matrice d'amortissement généralement adoptée est une combinaison linéaire de la matrice de rigidité et la matrice de masse:  $\mathbf{D} = \alpha\mathbf{M} + \beta\mathbf{K}$  pour  $\alpha, \beta \geq 0$ . Cette hypothèse est raisonnable et habituelle du fait que les structures flexibles ont de petits facteurs d'amortissement (GAWRONSKI, 2004).

En supposant que la matrice  $M_m$  est inversible, Eq. (B.2) peut être écrite comme:

$$\ddot{\mathbf{q}}(t) + M_m^{-1} D_m \dot{\mathbf{q}}(t) + M_m^{-1} K_m \mathbf{q}(t) = M_m^{-1} B_{w_m} \mathbf{w}(t) + M_m^{-1} B_{u_m} \mathbf{u}(t), \quad (\text{B.4})$$

où le vecteur d'état restenu est:

$$\mathbf{x}(t) = \begin{bmatrix} \mathbf{x}_1(t) \\ \mathbf{x}_2(t) \end{bmatrix} = \begin{bmatrix} \mathbf{q}(t) \\ \dot{\mathbf{q}}(t) \end{bmatrix}.$$

Avec cette définition, Eq. (B.3) et Eq. (B.4) peuvent être transformés en:

$$\begin{aligned} \dot{\mathbf{x}}_1(t) &= \mathbf{x}_2(t) \\ \dot{\mathbf{x}}_2(t) &= -M_m^{-1} K_m \mathbf{x}_1(t) - M_m^{-1} D_m \mathbf{x}_2(t) + M_m^{-1} B_{w_m} \mathbf{w}(t) + M_m^{-1} B_{u_m} \mathbf{u}(t) \\ \mathbf{y}(t) &= C_{d_m} \mathbf{x}_1(t) + C_{v_m} \mathbf{x}_2(t) + C_w \mathbf{w}(t) + C_u \mathbf{u}(t), \end{aligned}$$

ce qui conduit à la représentation d'état:

$$\begin{aligned} \dot{\bar{\mathbf{x}}}(t) &= \bar{\mathbf{A}} \bar{\mathbf{x}}(t) + \bar{\mathbf{B}}_1 \mathbf{w}(t) + \bar{\mathbf{B}}_2 \mathbf{u}(t) \\ \mathbf{y}(t) &= \bar{\mathbf{C}}_2 \bar{\mathbf{x}}(t) + D_{21} \mathbf{w}(t) + D_{22} \mathbf{u}(t), \end{aligned}$$

où  $\bar{\mathbf{C}}_2 = [C_{d_m} \ C_{v_m}]$ ,  $D_{21} = C_w$  et  $D_{22} = C_u$ . Les matrices  $\bar{\mathbf{A}}$ ,  $\bar{\mathbf{B}}_1$  et  $\bar{\mathbf{B}}_2$  sont obtenues en utilisant:

$$\bar{\mathbf{A}} = \begin{bmatrix} \mathbf{0} & \mathbf{I} \\ -M_m^{-1} K_m & -M_m^{-1} D_m \end{bmatrix}, \bar{\mathbf{B}}_1 = \begin{bmatrix} \mathbf{0} \\ M_m^{-1} B_{w_m} \end{bmatrix}, \text{ and } \bar{\mathbf{B}}_2 = \begin{bmatrix} \mathbf{0} \\ M_m^{-1} B_{u_m} \end{bmatrix}.$$

Enfin, ce modèle peut être écrit sous diverses formes de représentations canoniques modales en utilisant des matrices de transformation. Dans ce travail de thèse, la configuration suivante est adoptée:

$$\mathbf{A} = \begin{bmatrix} \mathbf{A}_1 & \mathbf{0} & \cdots & \mathbf{0} \\ \mathbf{0} & \mathbf{A}_2 & \cdots & \mathbf{0} \\ \vdots & \vdots & \ddots & \vdots \\ \mathbf{0} & \mathbf{0} & \cdots & \mathbf{A}_m \end{bmatrix}, \mathbf{B}_1 = \begin{bmatrix} b_{11} \\ b_{12} \\ \vdots \\ b_{1m} \end{bmatrix}, \mathbf{B}_2 = \begin{bmatrix} b_{21} \\ b_{22} \\ \vdots \\ b_{2m} \end{bmatrix}, \text{ et } \mathbf{C}_2 = \begin{bmatrix} c_{21}^T \\ c_{22}^T \\ \vdots \\ c_{2m}^T \end{bmatrix}^T,$$

où  $\mathbf{A}_i$  est une matrice  $2 \times 2$  pour  $i = 1, \dots, m$ .



#### B.4 Commande $H_\infty$ modale

Le système à commander est donné Eq. (B.5), où un indicateur de performance est introduit sous la forme d'un vecteur de sortie  $\mathbf{z}(t)$ . Généralement, cet indice de performance dépend seulement du temps. Cependant, pour inclure les exigences modale, une transformation de cette sortie de performance est nécessaire. En considérant seulement le vecteur de performance en fonction du temps, les équations en l'espace d'états suivants sont utilisés pour concevoir des correcteurs  $H_\infty$  traditionnels:

$$\begin{aligned}\dot{\mathbf{x}}(t) &= \mathbf{A}\mathbf{x}(t) + \mathbf{B}_1\mathbf{w}(t) + \mathbf{B}_2\mathbf{u}(t) \\ \mathbf{z}(t) &= \mathbf{C}_1\mathbf{x}(t) + \mathbf{D}_{11}\mathbf{w}(t) + \mathbf{D}_{12}\mathbf{u}(t) \\ \mathbf{y}(t) &= \mathbf{C}_2\mathbf{x}(t) + \mathbf{D}_{21}\mathbf{w}(t) + \mathbf{D}_{22}\mathbf{u}(t),\end{aligned}\tag{B.5}$$

où les matrices  $\mathbf{C}_1$ ,  $\mathbf{D}_{11}$  et  $\mathbf{D}_{12}$  sont choisis pour définir le vecteur de performance désiré. Ce vecteur peut être décrit en termes de performance modale en notant :  $\mathbf{z}(t) = \sum_{i=1}^m \mathbf{z}_i(t)$ , où  $\mathbf{z}_i(t)$  représente les signaux de performance relatifs au mode  $i$ . En outre, le vecteur de perturbation  $\mathbf{w}(t)$ , avec  $\mathbf{w} \in \mathcal{L}_2]0, \infty[$ , peut être filtré en retenant  $m$  bandes de fréquences contiguës de façon à ce que  $\mathbf{w}(t) = \sum_{i=1}^m \mathbf{w}_i(t)$ , où chaque bande est choisie pour contenir un seul mode distinct. Pour le contrôleur  $\mathbf{K}_c$  suivant:

$$\begin{aligned}\dot{\mathbf{x}}_c(t) &= \mathbf{A}_c\mathbf{x}_c(t) + \mathbf{B}_c\mathbf{y}(t) \\ \mathbf{u}(t) &= \mathbf{C}_c\mathbf{x}_c(t) + \mathbf{D}_c\mathbf{y}(t),\end{aligned}\tag{B.6}$$

le problème de commande  $H_\infty$  standard consiste à rechercher les matrices de correcteur par la minimisation de la fonction objective suivante:

$$J_\infty = \frac{\int_0^\infty \mathbf{z}^T(t)\mathbf{z}(t)dt}{\int_0^\infty \mathbf{w}^T(t)\mathbf{w}(t)dt}.$$

Une norme  $H_\infty$  modale, qui est écrite en fonction des matrices de pondération modales, est introduite et minimisée pour trouver le contrôleur  $H_\infty$  modal dans Eq. (B.6), où le système en boucle fermée satisfait:

$$\underbrace{\inf}_{K_c \in V} \underbrace{\sup}_{\mathbf{w} \in \mathcal{L}_2]0, \infty[} J_m < \gamma^2,\tag{B.7}$$

où  $V$  représente l'ensemble de tous les contrôleurs qui stabilisent le système et:

$$J_m = \frac{\sum_{i=1}^m \int_0^\infty \mathbf{z}_i^T(t) \mathbf{Q}_i \mathbf{z}_i(t) dt}{\sum_{i=1}^m \int_0^\infty \mathbf{w}_i^T(t) \mathbf{w}_i(t) dt},$$

où la matrice diagonale  $Q_i > 0$  pondère le mode  $i$ , ce qui conduit à assurer la sélectivité modale.

Un nouvel indicateur de performance modale est défini par:

$$\mathbf{z}_p(t) = \mathbf{\Gamma} \mathbf{x}(t) + \mathbf{\Theta} \mathbf{w}(t) + \mathbf{\Lambda} \mathbf{u}(t),$$

avec:

$$\mathbf{\Gamma} = \begin{bmatrix} \mathbf{Q}_1^{\frac{1}{2}} \mathbf{C}_{1_1} & \mathbf{Q}_2^{\frac{1}{2}} \mathbf{C}_{1_2} & \cdots & \mathbf{Q}_m^{\frac{1}{2}} \mathbf{C}_{1_m} \end{bmatrix}, \quad \mathbf{\Theta} = (\mathbf{Q}_1^{\frac{1}{2}} \mathbf{D}_{11_1} + \cdots + \mathbf{Q}_m^{\frac{1}{2}} \mathbf{D}_{11_m}),$$

$$\mathbf{\Lambda} = (\mathbf{Q}_1^{\frac{1}{2}} \mathbf{D}_{12_1} + \cdots + \mathbf{Q}_m^{\frac{1}{2}} \mathbf{D}_{12_m}),$$

où  $\mathbf{C}_{1_i}$ ,  $\mathbf{D}_{11_i}$  et  $\mathbf{D}_{12_i}$  correspondent aux sous-matrices relatives au mode  $i$  en  $\mathbf{C}_1$ ,  $\mathbf{D}_{11}$  et  $\mathbf{D}_{12}$ .

Le problème modal donné en Eq. (B.7) peut être résolu de manière équivalente comme précisé dans:

$$J_\infty = \frac{\int_0^\infty \mathbf{z}_p^T(t) \mathbf{z}_p(t) dt}{\int_0^\infty \mathbf{w}^T(t) \mathbf{w}(t) dt},$$

Des outils classiques peuvent être appliqués pour résoudre ce problème. Par exemple, pour le correcteur dans Eq. (B.6) et le système dans Eq. (B.5), le système en boucle fermée avec correcteur est donné par:

$$\begin{aligned} \dot{\tilde{\mathbf{x}}}(t) &= \tilde{\mathbf{A}} \tilde{\mathbf{x}}(t) + \tilde{\mathbf{B}} \mathbf{w}(t) \\ \tilde{\mathbf{z}}(t) &= \tilde{\mathbf{C}} \tilde{\mathbf{x}}(t) + \tilde{\mathbf{D}} \mathbf{w}(t). \end{aligned}$$

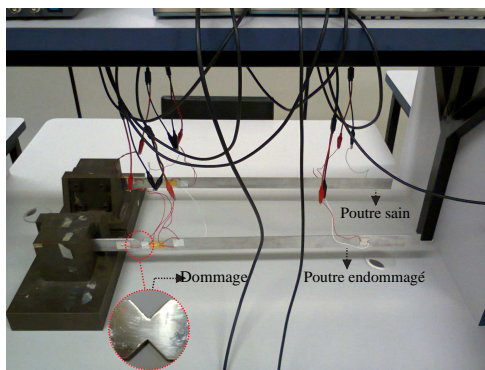
Basé sur le bounded real lemma,  $\tilde{\mathbf{A}}$  est stable et  $\|T_{\tilde{\mathbf{z}}\mathbf{w}}\|_\infty < \gamma$  si et seulement si il existe une matrice symétrique  $\tilde{\mathbf{P}}$  qui satisfait les inégalités matricielles suivantes (LMIs):

$$\begin{bmatrix} \tilde{\mathbf{A}}^T \tilde{\mathbf{P}} + \tilde{\mathbf{P}} \tilde{\mathbf{A}} & \tilde{\mathbf{P}} \tilde{\mathbf{B}} & \tilde{\mathbf{C}}^T \\ \tilde{\mathbf{B}}^T \tilde{\mathbf{P}} & -\mathbf{I} & \tilde{\mathbf{D}}^T \\ \tilde{\mathbf{C}} & \tilde{\mathbf{D}} & -\gamma \mathbf{I} \end{bmatrix} < 0$$

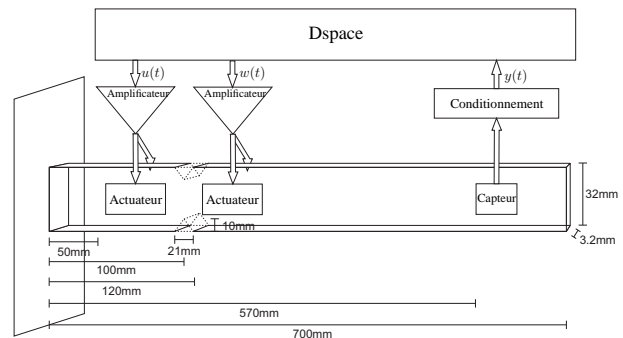
$$\tilde{\mathbf{P}} > 0. \tag{B.8}$$

### B.4.1 Résultats expérimentaux

Afin de valider et tester la commande modale, un dispositif expérimental spécifique a été réalisé (Fig. B.1(a)). Il est constitué de deux poutres encastrées identiques en aluminium munies de trois paires de céramiques PZT permettant d'appliquer la commande  $u(t)$  et la perturbation  $w(t)$  ainsi que de mesurer les vibrations  $y(t)$ . Dans les tests, la perturbation est un signal de type "chirp" qui possède une bande de fréquence comprise entre 78 Hz et 500 Hz, durée de 5.4 secondes et amplitude of 0.5 V est amplifiée par vingt et est considéré comme le perturbation. Afin de générer un dommage, nous avons réalisé deux encoches sur une des deux poutres. Les dimensions des poutres, du dommage ainsi que la position des PZTs sont illustrées à la Fig. B.1(b). Le dispositif est complété par une carte dSPACE®.



(a) Poutres en aluminium.



(b) Diagramme.

Figure B.1 - Dispositif expérimental.

Nous avons comparé le rejet de perturbation entre une commande  $H_\infty$  standard (RC, Regular  $H_\infty$  Controller) et la commande modale (MC, Modal  $H_\infty$  Controller) proposée. Les correcteurs ont été testés sur la poutre saine et endommagée. Pour les MCs plusieurs matrices de pondération ont été choisies:

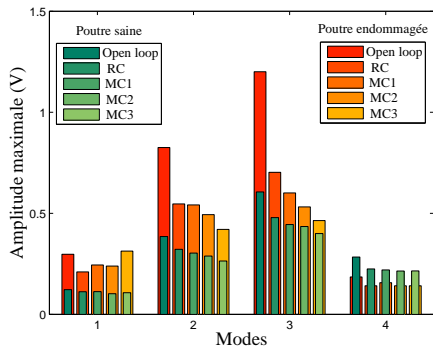
$$1.MC1: [Q_1^{1/2} \quad Q_2^{1/2} \quad Q_3^{1/2}] = [0.5 \quad 1.0 \quad 1.2];$$

$$2.MC2: [Q_1^{1/2} \quad Q_2^{1/2} \quad Q_3^{1/2}] = [0.5 \quad 1.2 \quad 1.4];$$

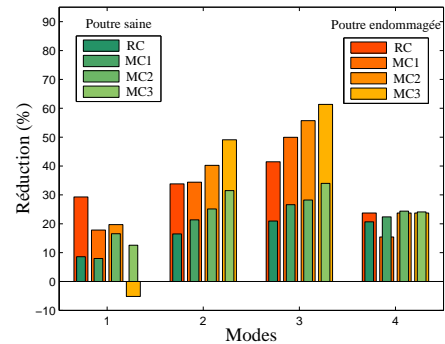
$$3.MC3: [Q_1^{1/2} \quad Q_2^{1/2} \quad Q_3^{1/2}] = [0.5 \quad 1.4 \quad 1.6].$$

Les résultats sont donnés à la Fig. B.2. Ils montrent que les 4 correcteurs fournissent un très bon taux de rejet dans le cas de la poutre saine. Cependant sur la poutre endommagée les correcteurs MC que nous proposons sont bien plus efficaces. On peut aussi noter comment la fonction de pondération permet d'atténuer un mode parmi les modes sélectionnés au détriment

des autres. La Fig. B.3(b) montre que l'augmentation de la pondération implique également une augmentation du signal de commande pour les poutres saine et endommagée.

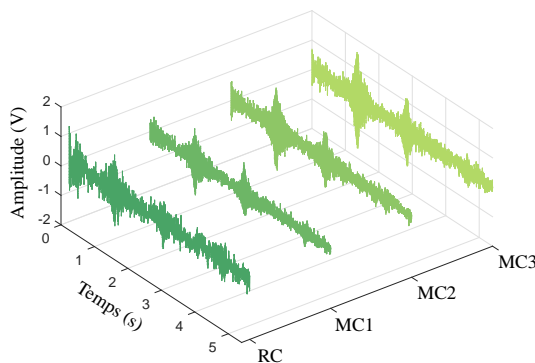


(a) Amplitude maximale de vibration.

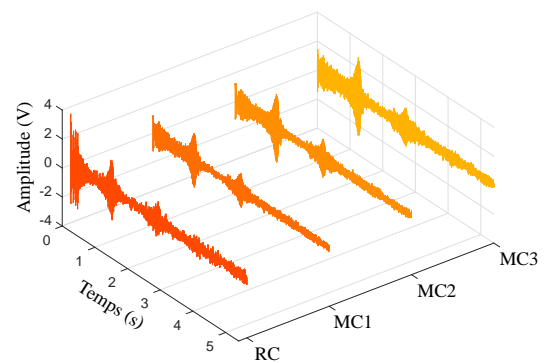


(b) Pourcentage de réduction de l'amplitude.

Figure B.2 - Amplitudes expérimentales maximales de vibration de chaque mode.



(a) Poutre saine.



(b) Poutre endommagée.

Figure B.3 - Signaux de commande expérimentaux pour les structures saine et endommagée.

## B.5 Prise en compte des effets des dommages dans la conception du correcteur modal

Une métrique pour quantifier les effets des dommages sur les modes de la structure est proposé ici. Elle permet de prendre en compte les effets des dommages dans la conception du correcteur  $H_\infty$  modal. La stratégie adoptée considère que les structures flexibles sont souvent soumises à des perturbations répétitives, où certaines régions sont plus touchées que d'autres. Ces régions critiques peuvent être identifiées par l'analyse de la structure, par des essais de fatigue et par l'histoire de la maintenance par exemple. Ainsi, il est possible de simuler des

dommages et d'inclure cette étude dans la conception du correcteur. Pour atteindre cet objectif, une technique de SHM est appliquée pour évaluer la sévérité du dommage sur chaque mode. En utilisant cette information, nous avons conçu un correcteur qui permet d'atténuer les vibrations en tenant compte de cette sévérité.

### B.5.1 Métrique modale pour détecter les dommages et identifier leur sévérité.

La matrice d'observabilité infinie pour la structure flexible  $\mathbf{M}$  décrite par Eq. (B.5) est:

$$\mathcal{O}_\infty(\mathbf{M}) = \left[ (\mathbf{C}_2)^T \quad (\mathbf{C}_2\mathbf{A})^T \quad (\mathbf{C}_2\mathbf{A}^2)^T \quad \dots \right]^T.$$

Le modèle  $\mathbf{M}$  peut être décomposé en  $m$  sous-modèles modaux. Par conséquent, la matrice d'observabilité infinie d'un sous-modèle modal  $\mathbf{M}_i$  est défini par:

$$\mathcal{O}_\infty(\mathbf{M}_i) = \left[ (\mathbf{C}_{2_i})^T \quad (\mathbf{C}_{2_i}\mathbf{A}_i)^T \quad (\mathbf{C}_{2_i}\mathbf{A}_i^2)^T \quad \dots \right]^T,$$

où  $\mathbf{C}_{2_i}$  et  $\mathbf{A}_i$  représentent respectivement les éléments de  $\mathbf{C}_2$  et  $\mathbf{A}$  relatif au mode  $i$ . Pour deux modèles  $\mathbf{M}^{(1)}$  et  $\mathbf{M}^{(2)}$  stables, les matrices d'observabilité infinie relatives au mode  $i$  sont  $\mathcal{O}_\infty(\mathbf{M}_i^{(1)})$  et  $\mathcal{O}_\infty(\mathbf{M}_i^{(2)})$ . La distance entre  $\mathbf{M}_i^{(1)}$  et  $\mathbf{M}_i^{(2)}$  pour le mode  $i$  est proposée comme:

$$\Delta_i(\mathbf{M}_i^{(1)}, \mathbf{M}_i^{(2)})^2 = \log \left( \prod_{j=1}^2 \frac{1}{\cos^2 \theta_j} \right),$$

où  $\theta_j$  est l'angle principal  $j$  entre les sous-espaces  $\mathcal{O}_\infty(\mathbf{M}^{(1)})$  et  $\mathcal{O}_\infty(\mathbf{M}^{(2)})$ .

### B.5.2 Détermination des matrices de pondération modale

Cette sous-section présente une approche originale qui permet de tenir compte des informations sur le dommage (mode, sévérité...) lors de l'élaboration du correcteur  $H_\infty$  modal. L'algorithme SHM présenté plus haut permet d'évaluer les effets des dommages sur les modes,

mais il n'est pas capable de distinguer si l'amplitude de vibration augmente ou se réduit. Pour surmonter cette limitation, la méthode proposée évalue l'effet d'un correcteur  $H_\infty$  standard sur la structure saine. L'idée est d'utiliser pour chaque mode de la structure saine son atténuation en boucle fermée et ses valeurs de crête respectives. L'association de ces deux valeurs aux effets des dommages sur chaque mode donne une indication sur la variation d'amplitude et aussi sur sa sévérité.

Considérant  $p$  signaux de performance différents, la Fig. B.4 montre la réponse en fréquence, entre le signal de performance  $z_l(t)$  pour  $l = 1, \dots, p$  et la perturbation  $w(t)$ , en boucle ouverte de la structure saine ainsi qu'en boucle fermée avec un correcteur  $H_\infty$  standard. Un indicateur  $\bar{q}_l$  est introduit pour équilibrer la réduction des vibrations réalisée par le correcteur  $H_\infty$  standard et l'effet relatif des dommages pour chaque mode:

$$\bar{\mathbf{q}}_l = \left[ \left( \frac{\alpha_{l1} \Delta_1}{\phi_{l1}} \right) \quad \left( \frac{\alpha_{l2} \Delta_2}{\phi_{l2}} \right) \quad \dots \quad \left( \frac{\alpha_{lm} \Delta_m}{\phi_{lm}} \right) \right], \quad (\text{B.9})$$

où  $\Delta_i$  est la distance modale calculée,  $\alpha_{li}$  est l'amplitude de crête pour la structure contrôlée et  $\phi_{li}$  est la réduction de l'amplitude de crête modale, pour  $i = 1, \dots, m$ .

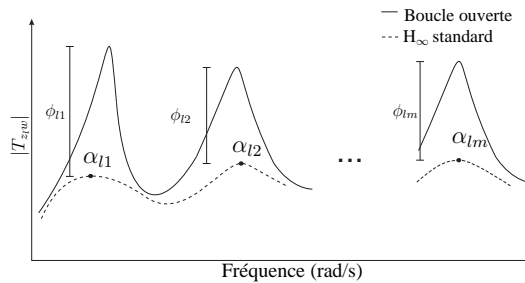


Figure B.4 - Atténuation de  $T_{z_l, w}$  et les amplitudes de crête respectives.

On peut remarquer que chaque facteur dans Eq. (B.9) doit correspondre à un élément dans la matrices de pondération modale. Cependant, ces paramètres peuvent être très petits ou très grands. Pour limiter ces valeurs, il convient d'établir une transformation d'amplitude, en tenant compte des valeurs maximales et minimales dans Eq. (B.9). En attribuant deux nouvelles valeurs pour ces indicateurs, la transformation adoptée est l'équation de la droite formée par ces deux points dans un plan. Les nouvelles valeurs doivent conserver les paramètres dans un intervalle raisonnable, choisi en fonction des aspects pratiques, comme par exemple la tension de sortie maximale. Le nouveau vecteur est alors:

$$\mathbf{q}_l = \left[ \beta_{l1} \quad \beta_{l2} \quad \dots \quad \beta_{lm} \right],$$

et conduit aux matrices suivantes de pondération modale, qui distribuent l'énergie de commande entre les modes:

$$\mathbf{Q}_1^{\frac{1}{2}} = \begin{bmatrix} \beta_{11} & 0 & 0 & 0 \\ 0 & \beta_{21} & 0 & 0 \\ \vdots & \vdots & \ddots & \vdots \\ 0 & 0 & 0 & \beta_{p1} \end{bmatrix}, \dots, \mathbf{Q}_m^{\frac{1}{2}} = \begin{bmatrix} \beta_{1m} & 0 & 0 & 0 \\ 0 & \beta_{2m} & 0 & 0 \\ \vdots & \vdots & \ddots & \vdots \\ 0 & 0 & 0 & \beta_{pm} \end{bmatrix}. \quad (\text{B.10})$$

### B.5.3 Résultats simulés

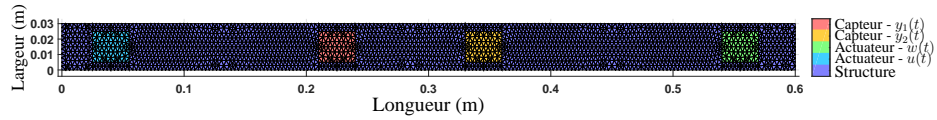
La structure utilisée pour tester la technique est représenté Fig. B.5(a). C'est une poutre bi-encastree (clamped-clamped) en aluminium avec une section transversale rectangulaire de 30 mm × 3.2 mm. Quatre paires d'éléments en céramique piézoélectrique sont symétriquement fixés de chaque côté de la poutre, conformément aux schémas présentés Fig. B.5(b) et Fig. B.5(c). Le modèle nominal utilisé pour concevoir les correcteurs est réduit à quatre modes. Un modèle avec dix modes, appelé ici modèle complet, est utilisé pour la boucle fermée afin de vérifier que le correcteur est suffisamment efficace pour éviter le spillover.

Le dommage est simulé par un encastrement partiel à  $x = 600$  mm comme montré Fig. B.5(d). La longueur  $h$  de la frontière libre caractérise la sévérité de ce dommage. Ceci peut être interprété comme le modèle d'une fissure de longueur  $h$  dans la liaison de la poutre au cadre rigide. Dans ce contexte, trois longueurs différentes de la fissure sont considérées:

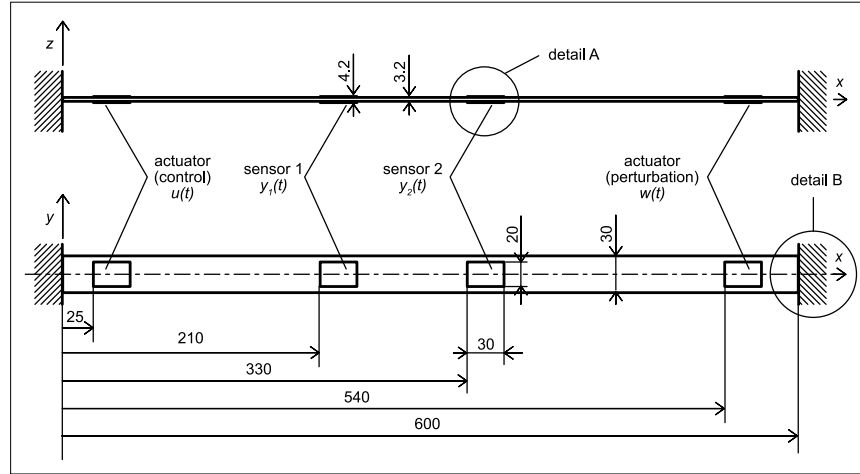
- Structure saine:  $h = 0$ ;
- Dommage 1:  $h = 10$  mm;
- Dommage 2:  $h = 15$  mm;
- Dommage 3:  $h = 20$  mm.

La figure B.6 présente les distances modales pour les trois cas de dommages, où l'on observe clairement que ces distances augmentent avec la sévérité des dommages. Les matrices de pondération sont calculées pour ce problème à partir de Eq. (B.10). La valeur de pondération minimale est 0.6 et la valeur maximale est 4.5. Ainsi, les matrices de pondération sont:

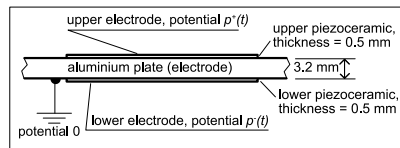
$$\mathbf{Q}_1^{\frac{1}{2}} = \begin{bmatrix} 0.6 & 0 \\ 0 & 0.6 \end{bmatrix}, \mathbf{Q}_2^{\frac{1}{2}} = \begin{bmatrix} 0.7 & 0 \\ 0 & 0.6 \end{bmatrix}, \mathbf{Q}_3^{\frac{1}{2}} = \begin{bmatrix} 0.7 & 0 \\ 0 & 0.7 \end{bmatrix} \text{ et } \mathbf{Q}_4^{\frac{1}{2}} = \begin{bmatrix} 4.5 & 0 \\ 0 & 4.5 \end{bmatrix}.$$



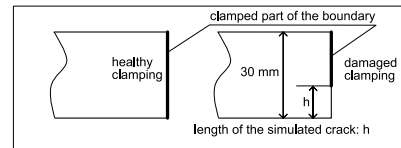
(a) Maillage éléments finis de la structure flexible.



(b) Schéma du dispositif (dimensions en mm).



(c) Détail A.



(d) Détail B.

Figure B.5 - Structure en aluminium possédant des éléments actifs, modélisée par éléments finis et maillée avec des éléments plaque triangulaires (éléments DKT)

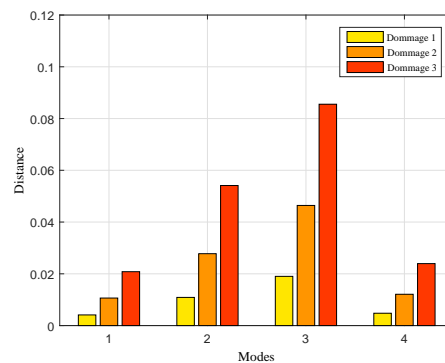


Figure B.6 - Distances modales en fonction du dommage.

La stratégie adoptée vise à concentrer l'action de contrôle sur les modes qui sont plus touchés pour les dommages. La perturbation est simulée par un signal de type chirp avec une bande de fréquence comprise entre 0 Hz et 500 Hz, d'une durée de 20 secondes et d'amplitude 4 V. Les réponses de la boucle fermée avec le correcteur  $H_\infty$  modal (MC) et avec le correcteur  $H_\infty$  standard (RC) sont comparées avec la structure endommagée (dommage 3) en boucle



ouverte et avec celle de la structure saine avec RC (performance de référence en boucle fermée) en Fig. B.7. Les modes 1, 2 et 3 en boucle fermée sont légèrement affectés par les dommages, mais les deux correcteurs présentent des performances similaires et proches de la référence. Pour le mode 4, les correcteurs ont les performances différentes. La vibration augmente considérablement avec le RC, qui conduit à des amplitudes maximales plus élevées que pour la boucle ouverte. Avec le MC, l'amplitude maximale du mode 4 proche de la référence et significativement plus petit que pour le comportement en boucle ouverte.

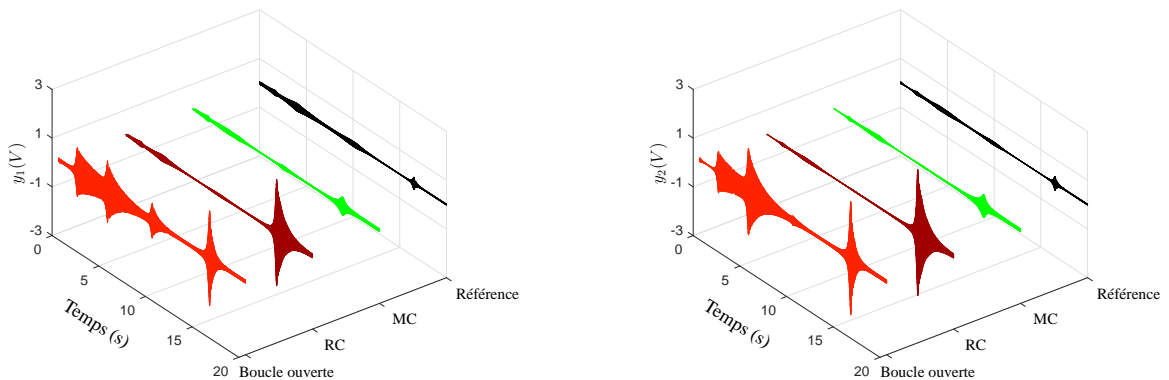


Figure B.7 - Structure soumise au dommage 3: comparaison des réponses.

La figure B.8 montre le comportement des signaux de commande pour les deux correcteurs testés. La superposition des couleurs permet de montrer les amplitudes relatives des deux signaux. Pour les modes 1 et 3, les signaux de commande des deux correcteurs ont des amplitudes similaires. Pour le mode 2, l'amplitude (tension en Volt) du MC est inférieure à l'amplitude du RC. L'amplitude du signal de commande pour le MC relatif au mode 4 est beaucoup plus grande que celle du RC, et conduit à la forte atténuation de la vibration modale causée par le dommage.

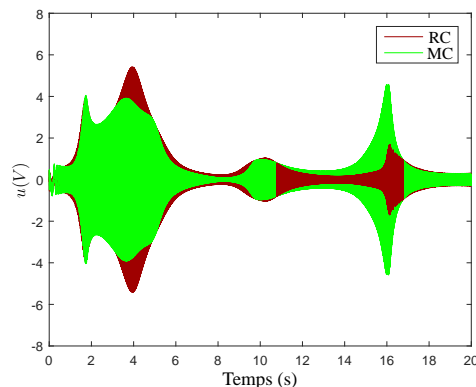


Figure B.8 - Comparaison de signaux de commande.

## B.6 Double boucle de commande

Les stratégies discutées précédemment offrent de très bonnes performances de robustesse grâce aux propriétés inhérentes à l'utilisation de la norme  $H_\infty$ . Ainsi les correcteurs seront robuste vis-à-vis des incertitudes de modèles et des dommages dans les effets sont connues a priori. Pour lorsqu'il est possible de les insérer comme contraintes de conception lorsque la zone endommagée est connue. Cependant, souvent les dommages sont imprévisibles, par exemple, les dommages de type impact. Cette section présente une technique de commande originale qui s'adapte automatiquement à un endommagement inconnu. La figure B.9 montre le bloc-diagramme détaillé du système de DTAC proposé, où sont montrés la structure et les cinq sous-systèmes constitutifs, respectivement le correcteur nominal, l'observateur modal, le modèle de référence, le compensateur de dommage et le mécanisme de reconfiguration. Le correcteur nominal génère le signal de commande  $\mathbf{u}_1(t)$  et il est basé sur commande  $H_\infty$  modale. Le compensateur de dommage génère le signal de commande  $\mathbf{u}_2(t)$ , où les paramètres du correcteur sont actualisés par le mécanisme de reconfiguration. Le module de SHM comprend un observateur d'état modal et un modèle de référence, dont la sortie  $\mathbf{x}_r(t)$  est comparée à l'état observé  $\hat{\mathbf{x}}(t)$  pour générer le résidu  $\mathbf{e}_x(t) = \hat{\mathbf{x}}(t) - \mathbf{x}_r(t)$ . Le résidu est essentiel pour la configuration des paramètres. Ces modules sont détaillés ci-dessous.

### B.6.1 Observateur modal

Le vecteur d'état  $\mathbf{x}(t)$  du modèle est estimé en ligne à partir du signal de sortie mesuré  $\mathbf{y}(t)$  et du signal de commande  $\mathbf{u}(t)$ . La représentation suivante est adoptée pour inclure les dommages dans le modèle d'état:

$$\begin{aligned}\dot{\mathbf{x}}(t) &= \mathbf{A}\mathbf{x}(t) + \mathbf{B}_1\mathbf{w}(t) + \mathbf{B}_2(\mathbf{u}(t) + \varphi(t)) \\ \mathbf{y}(t) &= \mathbf{C}_2\mathbf{x}(t) + \mathbf{D}_{21}\mathbf{w}(t),\end{aligned}$$

où  $\varphi(t)$  représente le vecteur de dommage inconnu. En outre, il est supposé que  $\varphi \in \mathcal{L}_2$ , la paire  $(\mathbf{A}, \mathbf{C}_2)$  est observable et  $\mathbf{D}_{22} = \mathbf{0}$ .

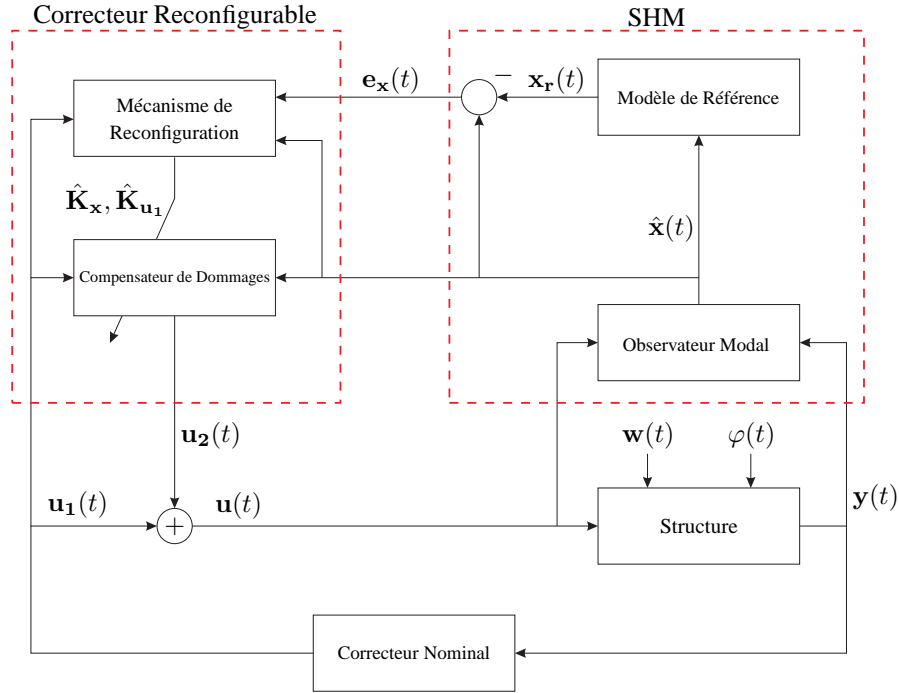


Figure B.9 - Le bloc-diagramme détaillé du système de DTAC.

L'observateur traditionnel de Luenberger suivant est adopté pour estimer le vecteur d'état:

$$\begin{aligned}\dot{\hat{\mathbf{x}}}(t) &= \mathbf{A}\hat{\mathbf{x}}(t) + \mathbf{B}_2\mathbf{u}(t) + \mathbf{L}(\mathbf{y}(t) - \hat{\mathbf{y}}(t)) \\ \hat{\mathbf{y}}(t) &= \mathbf{C}_2\hat{\mathbf{x}}(t),\end{aligned}$$

où  $\hat{\mathbf{x}}(t)$  et  $\hat{\mathbf{y}}(t)$  sont les estimations du vecteur d'état et du vecteur de sortie. Le gain  $\mathbf{L}$  est choisi de façon que  $\hat{\mathbf{x}}(t)$  converge asymptotiquement vers  $\mathbf{x}(t)$ .

La dynamique d'erreur d'estimation  $\dot{\mathbf{e}}(t)$  est donné par:

$$\begin{aligned}\dot{\mathbf{e}}(t) &= \dot{\mathbf{x}}(t) - \dot{\hat{\mathbf{x}}}(t) \\ &= (\mathbf{A} - \mathbf{L}\mathbf{C}_2)\mathbf{e}(t) + (\mathbf{B}_1 - \mathbf{L}\mathbf{D}_{21})\mathbf{w}(t) + \mathbf{B}_2\varphi(t),\end{aligned}$$

où cette dynamique est globalement stable s'il existe des matrices  $\bar{\mathbf{P}} = \bar{\mathbf{P}}^T \geq 0$ ,  $\Theta$  et scalaires  $\rho, \nu, \alpha > 0$  qui satisfont  $\|\mathbf{e}(t)\|_2 \leq \rho\|\varphi(t)\|_2$ ,  $\|\mathbf{w}(t)\|_2 \leq \nu$  et l'inégalité matricielle suivante:

$$\begin{bmatrix} \mathbf{A}^T\bar{\mathbf{P}} - \mathbf{C}_2^T\Theta^T + \bar{\mathbf{P}}\mathbf{A} - \Theta\mathbf{C}_2 + \mathbf{I} + \alpha\mathbf{I} & \bar{\mathbf{P}}\mathbf{B}_2 & \bar{\mathbf{P}}\mathbf{B}_1 - \Theta\mathbf{D}_{21} \\ \mathbf{B}_2^T\bar{\mathbf{P}} & -\mu\mathbf{I} & \mathbf{0} \\ \mathbf{B}_1^T\bar{\mathbf{P}} - \mathbf{D}_{21}^T\Theta^T & \mathbf{0} & -\frac{1}{\beta}\mathbf{I} \end{bmatrix} < 0, \quad (\text{B.11})$$

où  $\mu = \rho^2$ ,  $\beta = \alpha^{-1}\nu^2$  et le gain d'observateur est calculé en utilisant  $\mathbf{L} = \bar{\mathbf{P}}^{-1}\Theta$ .

### B.6.2 Modèle de référence

Le modèle de référence est le modèle de la structure saine en boucle fermée, avec le correcteur nominal. Ainsi, l'entrée de perturbation doit être connue pour être utilisée pour exciter le modèle de référence. Habituellement, il est difficile d'estimer en ligne les forces de perturbation agissant sur les structures réelles. Ici pour pouvoir adapter en ligne la commande nous avons choisi d'utiliser une approche basée sur l'estimation de la perturbation dans le pire des cas. Cette dernière est définie par:

$$\mathbf{w}^*(t) = (\gamma^2 \mathbf{I} - \tilde{\mathbf{D}}^T \tilde{\mathbf{D}})^{-1} (\tilde{\mathbf{B}}^T \tilde{\mathbf{P}} + \tilde{\mathbf{D}}^T \tilde{\mathbf{C}}) \hat{\mathbf{x}}(t),$$

où cette équation est basée sur la solution du problème de commande nominal, représentée ici par l'ensemble des LMIs (B.8).

### B.6.3 Compensation de dommage

Le sous-système de compensation des dommages est conçu pour minimiser le vecteur de résidu  $\mathbf{e}_x(t)$ , basé sur la stratégie d'adaptation modale. En considérant le modèle donné dans Eq (B.5) et le signal de commande  $\mathbf{u}(t)$  formé par les signaux de sortie des deux correcteurs, nous pouvons écrire l'équation suivante:

$$\dot{\mathbf{x}}(t) = \mathbf{A}\mathbf{x}(t) + \mathbf{B}_1 \mathbf{w}(t) + \mathbf{B}_2 \mathbf{u}_1(t) + \mathbf{B}_2 \mathbf{u}_2(t),$$

où la paire  $(\mathbf{A}, \mathbf{B}_2)$  est considéré comme contrôlable.

Pour une loi idéale de commande avec gain fixe pour les dommages comme:

$$u_2(t) = \mathbf{K}_x^T \mathbf{x}(t) + \mathbf{K}_{u_1}^T \mathbf{u}_1(t), \quad (\text{B.12})$$

où  $\mathbf{K}_i$  est le vecteur de gains et  $\mathbf{X}_i(t)$  est le vecteur d'état, les deux relatives dans mode  $i$ . Alors,

le système en boucle fermée avec ce correcteur est donnée par:

$$\dot{\mathbf{x}}(t) = (\mathbf{A} + \mathbf{B}_2 \mathbf{K}_x^T) \mathbf{x}(t) + \mathbf{B}_1 \mathbf{w}(t) + (\mathbf{B}_2 + \mathbf{B}_2 \mathbf{K}_{u_1}^T) \mathbf{u}_1(t). \quad (\text{B.13})$$

L'objectif du compensateur de dommages est de suivre asymptotiquement l'état du modèle de référence pour atténuer les effets des dommages. Le modèle de la structure saine est défini par:

$$\dot{\mathbf{x}}_r(t) = \mathbf{A}_r \mathbf{x}_r(t) + \mathbf{B}_{1r} \mathbf{w}(t) + \mathbf{B}_{2r} \mathbf{u}_1(t), \quad (\text{B.14})$$

avec les conditions suivantes (matching conditions) obtenues en comparant Eq. (B.13) à Eq. (B.14):

$$\mathbf{A}_r = \mathbf{A} + \mathbf{B}_2 \mathbf{K}_x^T, \mathbf{B}_{1r} = \mathbf{B}_1, \text{ et } \mathbf{B}_{2r} = \mathbf{B}_2 + \mathbf{B}_2 \mathbf{K}_{u_1}^T. \quad (\text{B.15})$$

Basé sur Eq. (B.12) et sur les résultats de l'estimation, la loi de commande réelle suivante est proposée:

$$\mathbf{u}_2(t) = \hat{\mathbf{K}}_x^T(t) \hat{\mathbf{x}}(t) + \hat{\mathbf{K}}_{u_1}^T(t) \mathbf{u}_1(t), \quad (\text{B.16})$$

où  $\hat{\mathbf{K}}_x(t)$ ,  $\hat{\mathbf{K}}_{u_1}(t)$  et  $\hat{\mathbf{x}}(t)$  sont respectivement les estimations en ligne de  $\mathbf{K}_x$ ,  $\mathbf{K}_{u_1}$  et  $\mathbf{x}(t)$ . Ainsi, la boucle fermée avec ces nouveaux gains est donnée par:

$$\dot{\mathbf{x}}(t) = (\mathbf{A} + \mathbf{B}_2 \hat{\mathbf{K}}_x^T(t)) \hat{\mathbf{x}}(t) + \mathbf{B}_1 \mathbf{w}(t) + (\mathbf{B}_2 + \mathbf{B}_2 \hat{\mathbf{K}}_{u_1}^T(t)) \mathbf{u}_1(t). \quad (\text{B.17})$$

#### B.6.4 Mécanisme de reconfiguration

Le but du mécanisme de reconfiguration est fournir l'estimation de  $\hat{\mathbf{K}}_x(t)$  et  $\hat{\mathbf{K}}_{u_1}(t)$ . La dynamique de l'erreur d'estimation du vecteur d'état est définie par  $\dot{\mathbf{e}}_x(t) = \dot{\hat{\mathbf{x}}}(t) - \dot{\mathbf{x}}_r(t)$ . En considérant Eq. (B.14), Eq. (B.17) et en utilisant les conditions données par Eq. (B.15), nous pouvons écrire:

$$\dot{\mathbf{e}}_x(t) = \mathbf{A}_r \mathbf{e}_x(t) + \mathbf{B}_2 \Delta \mathbf{K}_x^T(t) \hat{\mathbf{x}}(t) + \mathbf{B}_2 \Delta \mathbf{K}_{u_1}^T(t) \mathbf{u}_1(t), \quad (\text{B.18})$$

où  $\Delta \mathbf{K}_x^T(t) = (\hat{\mathbf{K}}_x^T(t) - \mathbf{K}_x^T)$  et  $\Delta \mathbf{K}_{u_1}^T(t) = (\hat{\mathbf{K}}_{u_1}^T(t) - \mathbf{K}_{u_1}^T)$  sont les erreurs d'estimation des gains.

Les gains adaptatifs  $\hat{\mathbf{K}}_{\mathbf{x}}(t)$  et  $\hat{\mathbf{K}}_{\mathbf{u}_1}(t)$  doivent être estimés de manière adéquate afin d'assurer la stabilité de la dynamique de l'erreur de suivi. Ainsi, Eq. (B.18) est stable pour les lois d'adaptation suivantes:

$$\dot{\hat{\mathbf{K}}}_{\mathbf{x}}(t) = -\mathbf{T}_{\mathbf{x}}\hat{\mathbf{x}}(t)\mathbf{e}_{\mathbf{x}}^T(t)\mathbf{P}\mathbf{B}_2 \text{ et } \dot{\hat{\mathbf{K}}}_{\mathbf{u}_1}(t) = -\mathbf{T}_{\mathbf{u}_1}\mathbf{u}_1(t)\mathbf{e}_{\mathbf{x}}^T(t)\mathbf{P}\mathbf{B}_2,$$

où pour  $\mathbf{R} = \mathbf{R}^T > 0$ ,  $\mathbf{P} = \mathbf{P}^T > 0$  satisfait l'équation algébrique de Lyapunov suivante:

$$\mathbf{P}\mathbf{A}_r + \mathbf{A}_r^T\mathbf{P} = -\mathbf{R}. \quad (\text{B.19})$$

En outre,  $\mathbf{T}_{\mathbf{x}} > 0$  et  $\mathbf{T}_{\mathbf{u}_1} > 0$  sont les matrices diagonales qui déterminent les taux d'adaptation. La matrice  $\mathbf{T}_{\mathbf{x}}$  est une fonction des sous-matrices modales:

$$\mathbf{T}_{\mathbf{x}} = \text{diag}(\mathbf{T}_1, \mathbf{T}_2, \dots, \mathbf{T}_m), \quad (\text{B.20})$$

où la matrice  $\mathbf{T}_i$   $2 \times 2$  détermine le taux d'adaptation du mode  $i$ .

### B.6.5 Résultats simulés

La structure utilisée pour tester la technique est la même structure représentée Fig. B.5(a), où seul les dommages 2 et 3 sont considérés. Pour concevoir le correcteur nominal, nous utilisons les matrices de pondération suivantes:

$$\mathbf{Q}_1^{\frac{1}{2}} = \begin{bmatrix} 0.7 & 0 \\ 0 & 0.7 \end{bmatrix}, \mathbf{Q}_2^{\frac{1}{2}} = \begin{bmatrix} 0.7 & 0 \\ 0 & 0.7 \end{bmatrix}, \mathbf{Q}_3^{\frac{1}{2}} = \begin{bmatrix} 0.9 & 0 \\ 0 & 0.9 \end{bmatrix} \text{ et } \mathbf{Q}_4^{\frac{1}{2}} = \begin{bmatrix} 1.6 & 0 \\ 0 & 1.6 \end{bmatrix}.$$

Pour concevoir le compensateur de dommages, le problème LMI (B.11) est résolu pour  $\nu = 5$  et  $\alpha = 5$ . Les matrices de taux d'adaptation sont choisis comme:

$$\mathbf{T}_1 = \mathbf{T}_2 = \begin{bmatrix} 50 & 0 \\ 0 & 50 \end{bmatrix}, \mathbf{T}_3 = \begin{bmatrix} 500 & 0 \\ 0 & 500 \end{bmatrix}, \mathbf{T}_4 = \begin{bmatrix} 2000 & 0 \\ 0 & 2000 \end{bmatrix} \text{ et } \mathbf{T}_{u_1} = 0.001.$$

Le même signal chirp que précédemment est utilisé pour simuler la perturbation pendant

trois cycles de 12 répétitions. Chaque cycle correspond à une condition de la structure: dispositif sain, dispositif avec le dommage 2 et dispositif avec le dommage 3. Trois méthodes de commande sont examinées dans ces différentes situations: RC avec boucle simple, MC avec boucle simple et double boucle de commande (ou modal double-loop framework, MDLF) avec l'association du MC avec le compensateur de dommage.

La Figure B.10 montre le comportement de chaque mode dans 12 graphes séparés. Les amplitudes modales maximales des réponses en boucle ouverte et également la réponse en boucle fermée pour les signaux de sortie  $y_1(t)$  et  $y_2(t)$  et le signal de commande respectives  $u(t)$  peuvent y être observés. Le dommage ne change pas les performances des compensateurs pour les modes 1 à 3. En ce qui concerne les signaux de commande, les amplitudes maximales sont similaires à tous les compensateurs pour les modes 1 et 3. Pour le mode 2, on peut voir que l'amplitude du signal de commande pour le RC est supérieure à celles des deux compensateurs modaux. En ce qui concerne le mode 4, les vibrations modales augmentent de manière significative dans le RC. Le MC présente une meilleure performance que le RC, mais les vibrations modales augmentent également avec la sévérité du dommage. Pour le dommage 1, le MDLF répond initialement de façon similaire au MC, mais l'ajustement adaptatif de ses paramètres réduit progressivement l'amplitude de crête. Pour le dommage 2, la réponse est bien meilleure dès le début de l'apparition des dommages. Les amplitudes du signal de commande augmentent pour tous les correcteurs pour faire face aux dommages, mais l'amplitude du MDLF est plus élevée, ce qui conduit à une atténuation efficace du mode.

## B.7 Conclusion

Le contrôle actif tolérant aux dommages (DTAC) est un nouveau champ de recherche qui vient répondre à l'exigence de maintien dans le temps de la qualité et la santé des structures. En adaptant la loi de rejet de perturbation pour contenir l'évolution d'un dommage, détecté par un dispositif SHM, DTAC participe à la prolongation de la durée de vie de la structure. Il est le vis-à-vis pour les structures, des dispositifs FTC devenus incontournables dans la commande des systèmes.

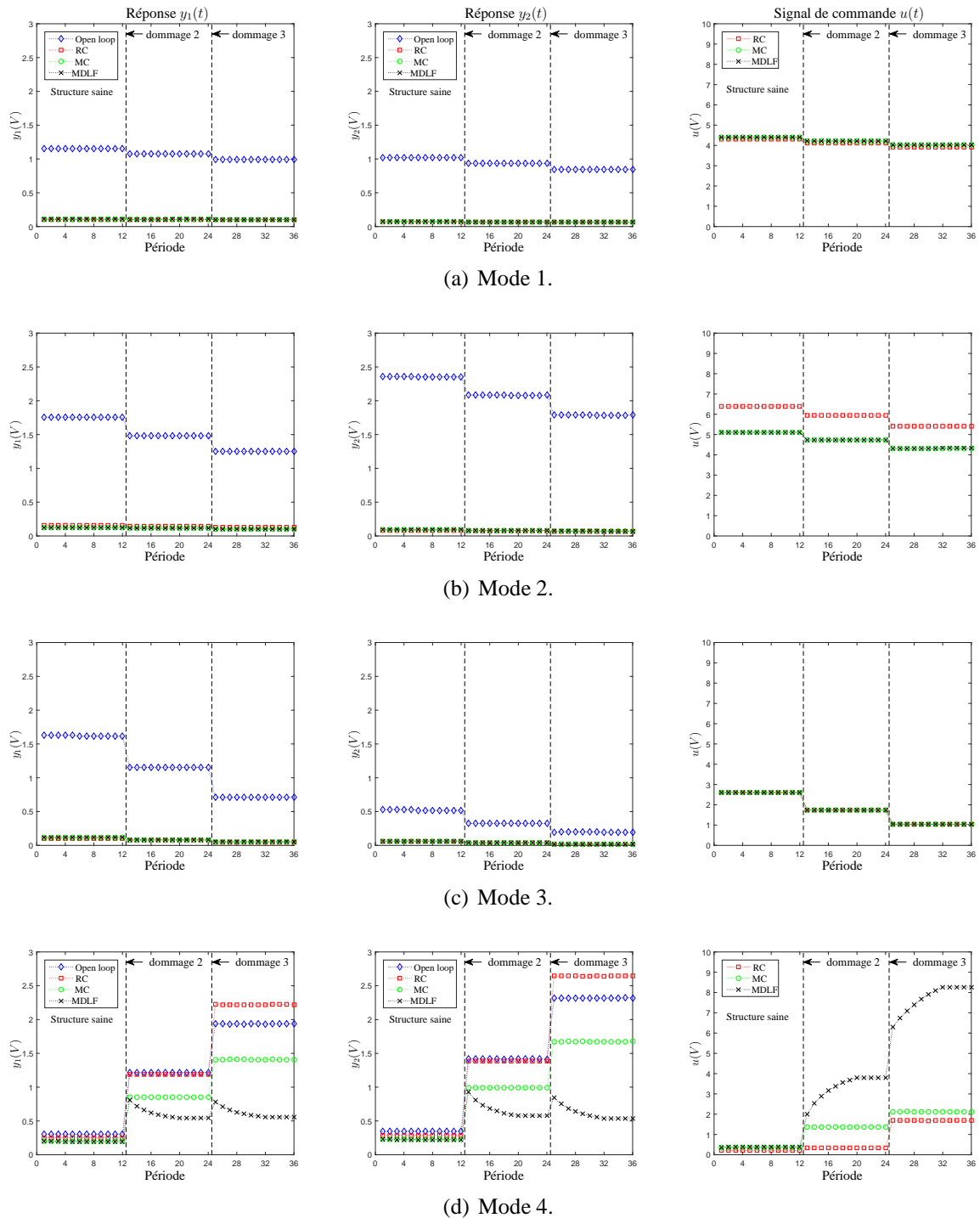


Figure B.10 - Comparaison des amplitudes maximales des modes de la structure contrôlée.

Cette thèse présente trois différentes techniques originales de lois de rejets de perturbation en présence d'endommagements. En premier lieu, nous avons proposé une technique de commande  $H_\infty$  modale qui présente un bon compromis entre la robustesse et la performance. Nous avons testé expérimentalement cette technique, où elle a montré de bien meilleurs résultats qu'une commande  $H_\infty$  standard principalement en raison de la sélection modale. Ensuite, nous avons développé une méthode qui utilise des informations sur les zones critiques de



la structure pour concevoir un correcteur  $H_\infty$  modal tolérant aux dommages. Cette méthode a été validée par des simulations EF d'une structure de type poutre-plaque munie d'actionneurs et capteurs PZT. Les simulations ont permis d'étudier les performances de l'approche vis-à-vis de différentes sévérités de dommages. Les résultats ont montré que la méthodologie est très efficace pour atténuer les effets des dommages dans les zones critiques. Pour finir, nous avons proposé une technique pour faire face aux dommages imprévisibles, par exemple, des dommages de type impact. Cette technique s'appuie sur une double boucle de commande, où le premier correcteur ( $H_\infty$  modal) est conçu pour satisfaire les contraintes de performance et de robustesse sur la structure saine. Le second a pour objectif d'assurer de façon satisfaisante le cahier des charges du système bouclé en considérant une stratégie de reconfiguration en ligne du correcteur, quand un dommage survient. Cette stratégie a été testée en utilisant les mêmes modèles éléments finis, mais sans aucune considération a priori sur le dommage. Les résultats ont montré que les deux correcteurs coopèrent pour une meilleure atténuation des vibrations, et ceci en présence de dommages inconnus.

## Contrôle Actif Modal de Structures Tolérant aux Dommages

**RESUME:** Les structures intelligentes sont de plus en plus présentes dans différentes industries et notamment dans les domaines de l'aéronautique et du génie civil. Ces structures sont dotées de fonctions qui leur permettent d'interagir avec leur environnement, d'adapter leurs caractéristiques structurelles (raideur, amortissement, viscosité, etc.) selon les besoins ou de surveiller leur état de santé ou « SHM » (Structural Health Monitoring). Aujourd'hui, les performances des méthodes de contrôle actif peuvent être considérablement dégradées lors de l'apparition d'endommagement. Le contrôle actif tolérant aux dommages ou « DTAC » (Damage Tolerant Active Control) est un champ de recherche récent qui s'intéresse à l'élaboration d'approches intégrées pour réduire les vibrations tout en surveillant l'intégrité de la structure, en identifiant les éventuels dommages, et en reconfigurant la loi de commande.

Cette thèse apporte une contribution au DTAC en proposant une approche originale basée sur la norme  $H_{\infty}$  modale. Les méthodes proposées se focalisent principalement sur le cas où plusieurs actionneurs et capteurs piézoélectriques non-colocalisés sont utilisés pour atténuer les vibrations des structures endommagées. Le manuscrit comprend quatre parties principales. Le chapitre 2 présente des rappels sur la commande  $H_{\infty}$  et sur sa solution sous optimale obtenue par une approche par inégalité matricielle linéaire ou « LMI » (Linear Matrix Inequality), sur laquelle s'appuient les développements proposés dans ce travail. Le chapitre 3 décrit la norme  $H_{\infty}$  modale introduite pour le contrôle actif des vibrations. Cette commande présente une sélectivité modale élevée, permettant ainsi de se concentrer sur les effets du dommage tout en bénéficiant des propriétés de robustesse qu'offre la commande  $H_{\infty}$  vis-à-vis du spillover et des variations de paramètres. Une nouvelle stratégie de rejet des vibrations est proposée au chapitre 4. C'est une approche dite préventive où une prise en compte lors de l'élaboration de la commande  $H_{\infty}$  modale, des zones fortement contraintes de la structure, où le risque d'endommagement est élevé est réalisée. Un algorithme SHM est proposé afin d'évaluer la sévérité du dommage pour chaque mode. Le chapitre 5 propose une nouvelle approche modale à double boucle de commande pour faire face à des endommagements imprévisibles. Un premier correcteur est conçu dans ce but pour satisfaire les contraintes de performance et de robustesse sur la structure saine, tandis que le second a pour objectif de conserver un contrôle satisfaisant quand un dommage survient. La loi de commande s'appuie sur un observateur d'état et d'un algorithme SHM pour reconfigurer en ligne le correcteur. Toutes les approches DTAC proposées sont testées en utilisant des simulations (analytiques et éléments finis) et/ou des expérimentations sur des structures intelligentes.

**Mots clés:** Contrôle actif tolérant au dommage, structures intelligentes, contrôle actif des vibrations, contrôle santé des structures, commande modal  $H_{\infty}$ , commande adaptative, robustesse, céramiques piézoélectriques.

## Damage-Tolerant Modal Control Methods for Flexible Structures

**ABSTRACT:** Smart structures have increasingly become present in different industry applications and particularly in the fields of aeronautics and civil engineering. These structures have features that allow interactions with the environment, adapting their characteristics according to the needs (stiffness, damping, viscosity, etc.), monitoring their health or controlling their vibrations. Today, smart structure active control methods do not respond appropriately to damage, despite the capability of good rejection of external disturbances. Damage-tolerant active control (DTAC) is a recent research area that aims to develop integrated approaches to reduce vibrations while monitoring the structure integrity, identifying damage occurrence, and reconfiguring the control law of the adopted active vibration control method.

This thesis contributes to the DTAC area by proposing a novel modal control framework and some application strategies. The developed methods focus on noncollocated flexible structures, where multiple piezoelectric sensors and actuators are used to attenuate damaged structure vibration. The chapters present four main topics and the conclusions. Chapter 2 reviews the regular suboptimal  $H_{\infty}$  problem and its respective solution based on the linear matrix inequality approach, which is a fundamental tool for the development of subsequent topics. Chapter 3 introduces the modal  $H_{\infty}$ -norm-based method for vibration control, which reveals high modal selectivity, allowing control energy concentration on damage effects and presenting robustness to spillover and parameter variation. A new control strategy is developed in Chapter 4, taking into account existing knowledge about the structure stressed regions with high probability of damage occurrence, leading to specific requirements in the modal  $H_{\infty}$ -controller design. A structural health monitoring (SHM) technique assesses each damaged mode behaviour, which is used to design a preventive controller. Chapter 5 presents a novel modal double-loop control methodology to deal with the unpredictability of damage, nevertheless ensuring a good compromise between robustness and performance to both healthy and damaged structures. For this purpose, the first-loop modal controller is designed to comply with regular requirements for the healthy structure behaviour and the second-loop controller is reconfigured aiming to ensure satisfactory performance and robustness when and if damage occurs, based on a state observer and an SHM technique to adapt the controller online. In all these chapters, simulated (analytical- and finite-element-based) and/or experimental smart structures are used to examine the proposed methodology under the respective control strategies. The last chapter summarises the achieved results for each different approach described in the previous chapters.

**Keywords:** Damage-tolerant active control, smart structures, active vibration control, modal  $H_{\infty}$  control, structural health monitoring, modal double-loop control, robustness, piezoelectric patches.